# Recent decades and future hydrological changes related to glacier shrinkage in the Andes (11°N-55°S)

Dennys Alexis Caro Paredes

THÈSE

Pour obtenir le grade de

**DOCTEUR DE L'UNIVERSITÉ GRENOBLE ALPES**

École doctorale : STEP - Sciences de la Terre de l'Environnement et des Planètes
Spécialité : Sciences de la Terre et de l'Environnement
Unité de recherche : Institut des Géosciences de l'Environnement

# Changements hydrologiques des dernières décennies et futurs liés au retrait des glaciers des Andes (11°N-55°S)

# Recent decades and future hydrological changes related to glacier shrinkage in the Andes (11°N-55°S)


Présentée par :

Dennys Alexis CARO PAREDES

Direction de thèse :

| | |
|---|---|
| **Thomas CONDOM**<br>CHARGE DE RECHERCHE, Université Grenoble Alpes | Directeur de thèse |
| **Antoine RABATEL**<br>PHYSICIEN, Université Grenoble Alpes | Co-directeur de thèse |

Rapporteurs :

**Fabien MAUSSION**
ASSOCIATE PROFESSOR, Universitat Innsbruck
**Andrés RIVERA**
FULL PROFESSOR, Universidad de Chile


Thèse soutenue publiquement le **20 octobre 2023.** devant le jury composé de :

| | |
|---|---|
| **Thomas CONDOM**<br>CHARGE DE RECHERCHE HDR, IRD délégation Sud-Est | Directeur de thèse |
| **Antoine RABATEL**<br>PHYSICIEN, Université Grenoble Alpes | Co-directeur de thèse |
| **Isabelle GOUTIEVIN**<br>INGENIEURE DES PONTS ET CHAUSSEES, Météo France | Examinatrice |
| **Fabien MAUSSION**<br>ASSOCIATE PROFESSOR, Universitat Innsbruck | Rapporteur |
| **Andrés RIVERA**<br>FULL PROFESSOR, Universidad de Chile | Rapporteur |
| **Anne-Catherine FAVRE**<br>PROFESSEURE DES UNIVERSITES, Grenoble INP | Présidente |

# Preamble

This Ph.D. thesis is a contribution to the regional knowledge of the glaciers' state across the Andes, their relationship with the climate and their water contribution to the Andean rivers, during the historical and future periods.

The results were achieved thanks to the award of research funding and the development of the project in France. This project was funded by the government of the Republic of Chile through the Agencia Nacional de Investigación y Desarrollo (ANID) / Scholarship Program / DOCTORADO BECAS CHILE / 2019-72200174, and developed in the *Institut des Géosciences de l'Environnement* (IGE) of the *Université Grenoble Alpes* (UGA). Three other international collaboration projects contributed to the realization of this PhD thesis: Andesnow (CLIMAT-AmSud) project funded in France by the CNRS, the GLASI project funded by LabEx OSUG@2020 (UGA) and the IRN-ANDES C2H national project (IRD).

This doctoral thesis consists of four main parts:

- Part I: Synopsis

  It provides an overview, presenting the main glaciological processes and the current knowledge across the Andean glaciers and their water contribution to catchments (chapter 1). Followed by the data and methodologies used in the doctoral project (chapter 2). Finally, a summary of the main results and conclusions based on three research publications, one in progress and results not published yet are presented (chapter 3).

- Part II: Research publications

  This part contains the main body of this thesis given by three research publications led by me as the first author and one research draft in progress.

  **Article n°1**. Caro et al. (2020). Glacier Clusters identification across Chilean Andes using Topo-Climatic variables. Investigaciones Geográficas, (60), 119-133.
  https://doi.org/10.5354/0719-5370.2020.59009

  **Article n°2**. Caro et al. (2021). Climatic and Morphometric Explanatory Variables of Glacier Changes in the Andes (8–55°S): New Insights From Machine Learning Approaches. Front. Earth Sci. 9:713011.
  https://doi.org/10.3389/feart.2021.713011

**Article n°3**. Caro et al. (2023). Andean Catchments Hydrological Response to Recent Glacier Mass Loss. [*submitted to The Cryosphere]*. https://doi.org/10.5194/egusphere-2023-888

**Article 4**. Caro et al.. Glacio-hydrological changes along the Andes over the first half of the 21st Century. [*in progress*]

- Part III: Glaciological and climate data

  Data generated in the research publications is available for download.

- Part IV: Appendix

  Academic activities like participation in congresses, workshops, summer schools, classes and related projects are described.

# Acknowledgements

This thesis was developed with the invaluable assistance of my advisors, the thesis monitoring committee, and my colleagues at the University of Chile. I am deeply grateful to Dr. Thomas Condom and Dr. Antoine Rabatel for generously sharing their knowledge and research experience with me. Their guidance and support have been fundamental throughout this thesis. I would also like to thank Dr. Isabelle Gouttevin, Dr. Théo Vischel and Dr. Nicolas Champollion for their meticulous review of my findings and their valuable advice. Their thoroughness has greatly contributed to the quality of my work.

I am immensely indebted to the Chilean government and the Agencia Nacional de Investigación y Desarrollo (ANID) for awarding me the doctoral scholarship abroad, which has made this project possible. I sincerely thank to Dr. Antoine Rabatel and Dr. Thomas Condom for their assistance in the scholarship application process. I am grateful to Dr. Shelley MacDonell and Dr. James McPhee for recommending my application, and I am grateful to my colleagues Dr. David Farías, Dr. Álvaro Ayala, Dr. Pablo Mendoza, and Dr. Thomas Shaw for their support, which increased my chances of receiving the scholarship.

Finally, I would like to express my profound gratitude to all those mentioned above for their invaluable contributions, which have played a pivotal role in the successful completion of this doctoral thesis.

Sincerely,

Alexis Caro

Grenoble, France

# Contents

# Abstract

The implications of the accelerated retreat of Andean glaciers over recent decades on runoff patterns remain incompletely understood. In addition, projections of glacier runoff in the 21st century exhibit significant uncertainties due to climate projections and model structure. These uncertainties give rise to concerns about the future water availability for both communities and ecosystems at the catchment scale. To enhance our understanding of the relationship between glaciers, climate, and morphometry, conventional statistical techniques, machine learning, and glacio-hydrological simulations were used. This thesis aims to elucidate these intricate connections and estimate the changes in glacier runoff within the Andean catchments (11°N-55°S) from 1980 to 2100. Seven findings stand out from this work, which are compiled into four scientific articles: (1) glacier changes (mass balance and area) between 1980 and 2018 are primarily explained by precipitation in the Outer Tropics to the Dry Andes (8-37°S), while temperature is the dominant explanatory variable in the Wet Andes (40-55°S); (2) based on the most significant variables explaining glacier changes, a proposal for 12 glaciological zones across the Andes has been made, considering 32000 glaciers; (3) simulation results indicate that between 2000-2009 and 2010-2019, 93% of catchments experienced reductions in glacier volume (-8.3%) and surface area (-2.2%), which was accompanied by an increase of 12% in mean annual glacier melt and 2% in rainfall on glaciers; (4) a regional pattern of melt factors for the simulations of snow/ice melt is found, with decreasing values from the Tropical to Wet Andes; (5) analysis of GCMs and their use in simulations highlight the importance of studying temperature and precipitation during both historical and future periods (1990 to 2049) because GCMs identified with lower scores predict higher glacier runoff at the catchment scale; (6) cumulative glacier runoff shows that the most significant reductions between 2000-2019 and 2030-2049 are expected in the Tropical Andes (-43%), followed by the Dry Andes (-37%), and the Wet Andes (-32%), where catchments in the Dry Andes exhibit the most pronounced variations in glacier runoff; and (7) glacier runoff projections throughout the 21st century indicate that a majority of catchments reach their peak water before the first half of the century; however, the timing of this peak water varies by catchment and glaciological region. This thesis underlines the significance of exploring and evaluating climate variables impacting glacier surfaces. It also emphasizes the importance of utilizing local and regional climate, hydrological, and glaciological data through statistical techniques and simulations to advance our comprehension of glacier changes and their runoff across the Andes, both historically and in the future.

# Résumé

Les implications du retrait accéléré des glaciers Andins au cours des dernières décennies sur les régimes hydrologiques restent partiellement comprises. De plus, les projections d'évolution de la ressource en eau d'origine glaciaire au 21e siècle présentent des incertitudes significatives, notamment en raison des projections climatiques. Ces incertitudes suscitent des préoccupations concernant la disponibilité future en eau pour les communautés et les écosystèmes à l'échelle du bassin versant. Afin d'améliorer la compréhension de la relation entre le glacier, le climat et la morphométrie, ainsi que de son impact sur les écoulements d'eau d'origine glaciaire, des techniques statistiques conventionnelles, l'apprentissage automatique et des simulations glacio-hydrologiques sont utilisées. Cette thèse vise à mieux comprendre ces connexions complexes et à estimer les changements de l'écoulement d'eau des glaciers dans les bassins versants andins (11°N-55°S) de 1980 à 2100. Sept résultats ressortent de ce travail, qui sont compilés dans quatre articles scientifiques: (1) les changements des glaciers (bilan de masse et superficie) entre 1980-2018 sont principalement expliqués par les précipitations des Tropiques externes jusqu'aux Andes arides (8-37°S), tandis que la température est la variable explicative dominante dans les Andes humides (40-55°S) ; (2) en se basant sur les variables expliquant les changements des glaciers, une proposition de 12 zones glaciologiques à travers les Andes a été formulée ; (3) les résultats des simulations indiquent qu'entre 2000-2009 et 2010-2019, 93 % des bassins versants ont connu des réductions du volume des glaciers (-8,3 %) et de la superficie (-2,2 %), ce qui a été accompagné d'une augmentation de 12 % de la fonte annuelle moyenne des glaciers et de 2 % des précipitations sur les glaciers ; (4) la nécessité d'une paramétrisation régionale du facteur de fonte pour les simulations de fonte de neige/glace est identifiée, avec des valeurs décroissantes des Tropiques aux Andes humides ; (5) l'analyse des GCMs et leur utilisation dans les simulations mettent en évidence l'importance de l'étude de la température et des précipitations pendant les périodes historiques et futures (1990-2049), car les GCMs identifiés avec de faibles scores prédisent un écoulement d'eau des glaciers plus élevé à l'échelle du bassin versant ; (6) l'écoulement d'eau cumulé provenant des glaciers montre que les réductions les plus significatives entre 2000-2019 et 2030-2049 sont attendues dans les Andes tropicales (-43 %), suivies des Andes arides (-37 %) et des Andes humides (-32 %), où les bassins versants des Andes arides présentent les variations les plus marquées de l'écoulement d'eau provenant des glaciers ; et (7) les projections de l'évolution de la production d'eau des glaciers au long du 21e siècle indiquent que la majorité des bassins versants atteindront leur pic de production d'eau avant la première moitié du siècle. Cependant, la période pendant laquelle ce pic sera atteint varie selon le bassin versant. Ce travail de thèse souligne l'importance d'explorer et d'évaluer les variables climatiques impactant les surfaces et volumes des glaciers. Elle met également en avant l'importance de l'utilisation de données climatiques, hydrologiques et glaciologiques locales et

régionales à travers des méthodes d'apprentissage automatique et des simulations hydro-glaciologiques pour avancer dans notre compréhension des changements des glaciers et de leur production d'eau à travers les Andes dans le futur.

# Resumen

Las implicancias del retroceso acelerado de los glaciares andinos en la escorrentía siguen sin entenderse por completo. En este aspecto, las proyecciones de la escorrentía glaciar durante el siglo XXI muestran una alta incertidumbre proveniente de las proyecciones climáticas pero también de la estructura para llevar a cabo la simulación. Estas incertidumbres generan preocupaciones sobre la futura disponibilidad de agua tanto para las comunidades como para los ecosistemas. Para mejorar la comprensión de la relación entre glaciar, clima y morfometría y su impacto en la escorrentía glaciar, en esta tesis se emplean técnicas estadísticas convencionales, aprendizaje automático y simulaciones glacio-hidrológicas. Esta tesis tiene como objetivo dilucidar estas relaciones y estimar los cambios en la escorrentía glaciar en las cuencas Andinas (11°N-55°S) entre 1980 y 2100. Destacan siete resultados que han sido compilados en cuatro artículos científicos: (1) los cambios glaciares (balance de masa y área) entre 1980 y 2018 se explican principalmente por la precipitación en los trópicos exteriores y los Andes secos (8-37°S), mientras que la temperatura es la variable explicativa dominante en los Andes húmedos (40-55°S); (2) en base a las variables explicativas de los cambios glaciares, se proponen 12 zonas glaciológicas a lo largo de los Andes usando 32000 glaciares; (3) los resultados de la simulación indican que entre 2000-2009 y 2010-2019, el 93 % de las cuencas experimentaron reducciones en el volumen glaciar (-8,3 %) y en la superficie (-2,2 %), lo que estuvo acompañado de un aumento del 12 % en el promedio annual de derretimiento glaciar y 2% en la lluvia sobre glaciares; (4) se encuentra un patrón regional en los factores de derretimiento utilizados para simular derretimiento de nieve/hielo, con valores decrecientes desde los Andes tropicales hasta los húmedos; (5) en el análisis de los GCMs y en su aplicación en simulaciones, destaca la importancia de estudiar la temperatura y la precipitación durante períodos histórico y futuro (1990 a 2049), debido a que los GCMs identificados con menor desempeño predicen una mayor escorrentía glaciar a escala de cuenca; (6) la escorrentía glaciar acumulada muestra que las reducciones más significativas entre 2000-2019 y 2030-2049 ocurren en los Andes tropicales (-43 %), seguido de los Andes secos (-37 %) y los Andes húmedos (-32 %), donde las cuencas de los Andes Secos exhiben las variaciones más pronunciadas en la escorrentía glaciar; y (7) las proyecciones de escorrentía glaciar durante el siglo XXI indican que la mayoría de las cuencas alcanzan la mayor contribución glaciar (peak water) antes de la primera mitad del siglo, sin embargo, el periodo en que ocurre este máximo varía según la cuenca y la región glaciológica. Esta tesis subraya la importancia de explorar y evaluar las variables climáticas que afectan las superficies de los glaciares. También enfatiza la importancia de utilizar datos climáticos, hidrológicos y glaciológicos locales y regionales a través de técnicas estadísticas y simulaciones para avanzar en nuestra comprensión de los cambios en los glaciares y de su escorrentía a través de los Andes, tanto en el pasado reciente como en el futuro.

# Part I: Synopsis

# 1. Introduction and State of the Art

## 1.1 Glaciers as water reservoirs in the Andean catchments

The Andes cordillera in South America stretches over 8000 km, extending from Colombia-Venezuela to southern Chile-Argentina (11°N-55°S). This vast mountain range encompasses diverse climatic and topographic conditions. Along its length, the Andes intercept Low Level Jets, which transport significant moisture along the mountain chain, except in the western subtropical latitudes. This moisture transport plays a crucial role in modulating temperature variability and precipitation patterns (Espinoza et al., 2020). The Andes boasts the largest glacierized surface area in both the tropical region and the southern hemisphere outside of Antarctica (Kaser and Osmaston, 2002; RGI Consortium, 2017). However, Andean glaciers have experienced a persistent negative mass balance and consecutive shrinkage, with particularly pronounced effects since the late 1970s (Rabatel et al., 2013; Zemp et al., 2019; Masiokas et al., 2020). As a result, some catchments northward of 37°S have shown an increase in glacier runoff (Huss and Hock, 2018). Studies estimating glacier contributions to rivers in these catchments range from 3% to 23% (e.g., Mark and Seltzer, 2003; Gascoin et al., 2011; Ragettli and Pellicciotti, 2012; Soruco et al., 2015; Ayala et al., 2020). In contrast, catchments southward of 37°S exhibit more variable signals, with some showing an increase in glacier runoff while others experience a reduction (Huss and Hock, 2018). Despite various studies focusing on glacier changes and their hydrological impacts in specific catchments such as Antisana (Ecuador), Río Santa (Perú), Zongo glacier and La Paz (Bolivia), and Yeso and Maipo basins (Chile), the changes in glacier runoff in most Andean catchments remain unknown. Therefore, there is a need for further research to assess the impacts of glacier changes on the hydrology of these catchments and enhance our understanding of the broader implications for water resources in the Andes.

Local studies on glacier processes in the Andes have utilized various databases, methodologies, spatial scales, and temporal scales to gain a better understanding of these processes or simulate them. On the other hand, regional studies have primarily focused on certain glaciological variables such as glacier surface area, geodetic mass balance, or glacier volume, which typically have a lower temporal resolution (Barcaza et al., 2017; Meier et al., 2018; Braun et al., 2019; Dussaillant et al., 2019; Farinotti et al., 2019; Seehaus et al., 2019, 2020; Zalazar et al., 2020; Hugonnet et al., 2021; Millan et al., 2022). Therefore, these local and global data sets can be processed through machine learning methods and global models to perform an analysis of climate and morphometric variables that explain the recent glacier changes, as well as, to calibrated simulations of glacier surface mass balance and dynamics, to

correct/evaluate inputs and to evaluate output simulations, considering historical and future periods of simulation across the Andes.

## 1.2 Research goals

Considering previous reports of recent and future changes in glaciers (e.g., area variation, mass balance, ice volume) and glacier runoff at local and regional scales in the Andes and their relations with the climate, as well as many glaciological and climate datasets available, the following questions that define the goals of this research arose:

a) How different are the climate conditions across the Andean glaciers since 1980?

b) Can climate and morphometric conditions of glaciers help to understand their recent changes in the different zones across the Andes?

c) Which glaciological regions and catchments (11°N-55°S) show the largest differences in glacier runoff (snow/ice melt and rainfall on glaciers) throughout the 21st century regarding the historical period?

d) Can we find regional patterns of the parameters used to estimate glacier mass balance between 2000-2019?

e) Can we estimate using a hydro-glaciological model the year when the maximum contribution of glaciers (peak water) will occur throughout the 21st century?

These questions allowed me formulating the following goals:

To classify the climatic and morphometric variables that explain recent glacier changes in area and volume across the Andes, using machine learning tools [allow answering a and b].

To simulate the recent mass balance and dynamics of the Andean glaciers and their runoff by using a calibrated and validated modeling approach [allow answering c and d]

To simulate future Andean glacier changes during the 21st century based on a modeling approach validated in the historical period [allow answering e]

# 1.3 The role of glaciers in the hydrological cycle

Glaciers play a crucial role in the hydrological cycle, which encompasses the movement of water in different physical states through the atmosphere, surface, and subsurface. Several key processes are associated with glaciers, including precipitation in the form of snow and rainfall, ice and snowmelt, runoff, evaporation, and sublimation (the transition of solid ice directly to water vapor) (Cuffey and Paterson, 2010; Daanen et al., 2011). These processes, along with others, are discussed in detail in Section 1.3.1 of the thesis, focusing on glacier surface mass balance.

A glacier is defined by Cogley et al. (2011) as “perennial mass of ice, and possibly firn and snow, originating on the land surface by the recrystallization of snow or other forms of solid precipitation and showing evidence of past or present flow”.

In this context, I will describe the role of glaciers in the hydrological cycle throughout a hydrological year, which typically spans from April to March in the mid-latitudes of the southern hemisphere, and from October to September in the northern hemisphere. Additionally, I will focus on the seasons when glaciers experience the most significant mass loss. However, due to the extensive range of the Andes, stretching from 11°N to 55°S, the timing of hydrological cycle processes varies across different regions of the Andes. Furthermore, the liquid output from glaciers, which comprises the meltwater from ice, firn, and snow, as well as rainfall on glaciers, will be referred to as glacier runoff. Glacier runoff plays a critical role in modifying catchment flow in terms of both quantity and timing, ranging from hourly to annual scales. This is particularly important during dry seasons when glacier runoff compensates for low streamflows in catchments, acting as a modulating factor (Radic and Hock, 2014). Additionally, the annual amount of glacier runoff is closely linked to the glacier's negative and positive mass balance.

## 1.3.1 Tropical Andes (11°N-18°S)

The tropical Andes exhibit distinct climate patterns influenced by various factors. In the eastern and western slopes of the equatorial Andes (Ecuador and Colombia), precipitation is primarily driven by convective storms that develop over the mountains, with a 0°C isotherm at approximately 4800 m a.s.l. (Garreaud et al., 2009). The eastern slopes receive increased rainfall due to the influence of moist air from the Amazon basin and the Gulf of Panama, resulting in higher rainfall on the eastern side of the Andes. On the other hand, the Altiplano region experiences low temperatures, high radiation levels, and dry conditions throughout the year (e.g., Aceituno, 1993), with interruptions during the austral summer (November to March) when intense convective storms bring significant precipitation. The northern areas, around Lake Titicaca, receive more summer precipitation compared to the southern areas around Uyuni dry lake (Garreaud et al., 2009).

The influence of tropical Pacific sea surface temperatures (SST) and the El Niño-Southern Oscillation (ENSO) phenomenon on glacier mass balance has been observed in many studies, indicating their significant role in modulating interannual variations in glacier mass balance (e.g., Rabatel et al., 2013; Masiokas et al., 2020).

In terms of the regional division of the tropical Andes, Troll (1941) classified the region into two zones: the inner tropics and the outer tropics. The inner tropics extend approximately from 11°N to 5°S (Colombia and Ecuador), while the outer tropics span from 5°S to 17.5°S (Peru and Bolivia) (Rabatel et al., 2013). Tropical glaciers in these regions exhibit a strong vertical mass balance gradient, meaning that the mass balance varies significantly with elevation. This gradient is attributed to continuous ablation near the glacier fronts throughout the year and frequent changes in snow cover during the ablation season across the ablation area. The frequency and intensity of year-round snowfall also play a role in modulating the melt processes (Sicart et al., 2011). In Ecuador, ablation rates remain relatively constant year-round, whereas in the outer tropics, the melt rate is higher during the transition season (Favier et al., 2004; Autin et al., 2022).

The Inner tropics contain the smaller glacierized surface area of the tropical Andes, presenting monthly homogeneous precipitation and temperature year-round (Rabatel et al., 2013). Because of that, a small temperature variation can onset the melt by determining the phase of precipitation, changing the ablation zone albedo (Kaser, 1999; Francou et al., 2004; Masiokas et al., 2020). Figure 1A illustrates the principal component of gain and loss in the Antisana glacier, which is situated in the inner tropics. Favier et al. (2004) estimated that in one year, 74% of the precipitation received by the glacier comes from snowfall (715 mm $yr^{-1}$) and 26% from rainfall (255 mm $yr^{-1}$, which occurs mainly in the ablation zone). Ablation, on the other hand, is predominantly dominated by melting, accounting for 95% of the total ablation (6350 mm $yr^{-1}$), with sublimation contributing 5% (300 mm $yr^{-1}$). In a study by Gualco et al. (2022) focused on the Antisana glacier, it was found that the ablation zone of the glacier received 74% of the precipitation as rainfall and 33% as snow during the period from 2011 to 2013. Figure 2, represents a smaller glacierized catchment within the Antisana volcano in the inner tropics, it shows low mean monthly temperature and precipitation variations. The runoff from this catchment exhibits a lower monthly variation, with the maximum occurring in the months of January to March (JFM) and April to June (AMJ) (Gualco et al., 2022).

In the Outer tropics, where the largest surface area of tropical glaciers can be found (71% in Perú and 20% in Bolivia in 1970 and 1980, respectively, Kaser, 1999), Sicart et al. (2011) described three seasons related to the processes observed in a glacier surface:

- the transition season (September-December) with low accumulation of snow and melt ice progressively increasing to reach its maximum in November (Figure 1B),
- the wet season (January-April) with a high accumulation of snow (Kaser, 2001),
- the dry season (May-August) when ablation is limited but largest losses occur through sublimation.

Figure 1B shows the main processes on the glacier surface during the transition season, where the largest ablation occurs each year, being melting the main process of mass loss. Nearly 20% of the annual precipitation occurs during the transition season (Ramallo, 2013), where approximately 90% is related to snowfall (Zongo glacier at 5050 m a.s.l., Valex, 2015). Sicart et al. (2005) found that the main sources of melt are shortwave radiation followed by incoming longwave radiation, where the sublimation is 13% during the transition season (Zongo glacier, 4900 to 6000 m a.s.l., 1998-2000). In the Zongo glacier located in the outer tropics, the annual mass balance is conditioned by the beginning of the wet season, which interrupts the high ice melt occurring in the transition season (Sicart et al., 2011), where a possible precipitation delay can lead to very negative ablation rates. This season shows the largest ablation considering 27 years of records with a maximum in November (Autin et al., 2022), when the largest increases in glacier runoff are also observed (Frans et al., 2015). Because of that, the surface mass balance is correlated to the total amount and the seasonal distribution of precipitation (Francou et al., 2003; Sicart et al., 2005; Autin et al., 2022). Figure 2 (outer tropics) presents the mean monthly runoff in the Zongo catchment, with the maximum during the transition and wet season (October to March) related to larger mean monthly temperature and precipitations (Frans et al., 2015; Autin et al., 2022).

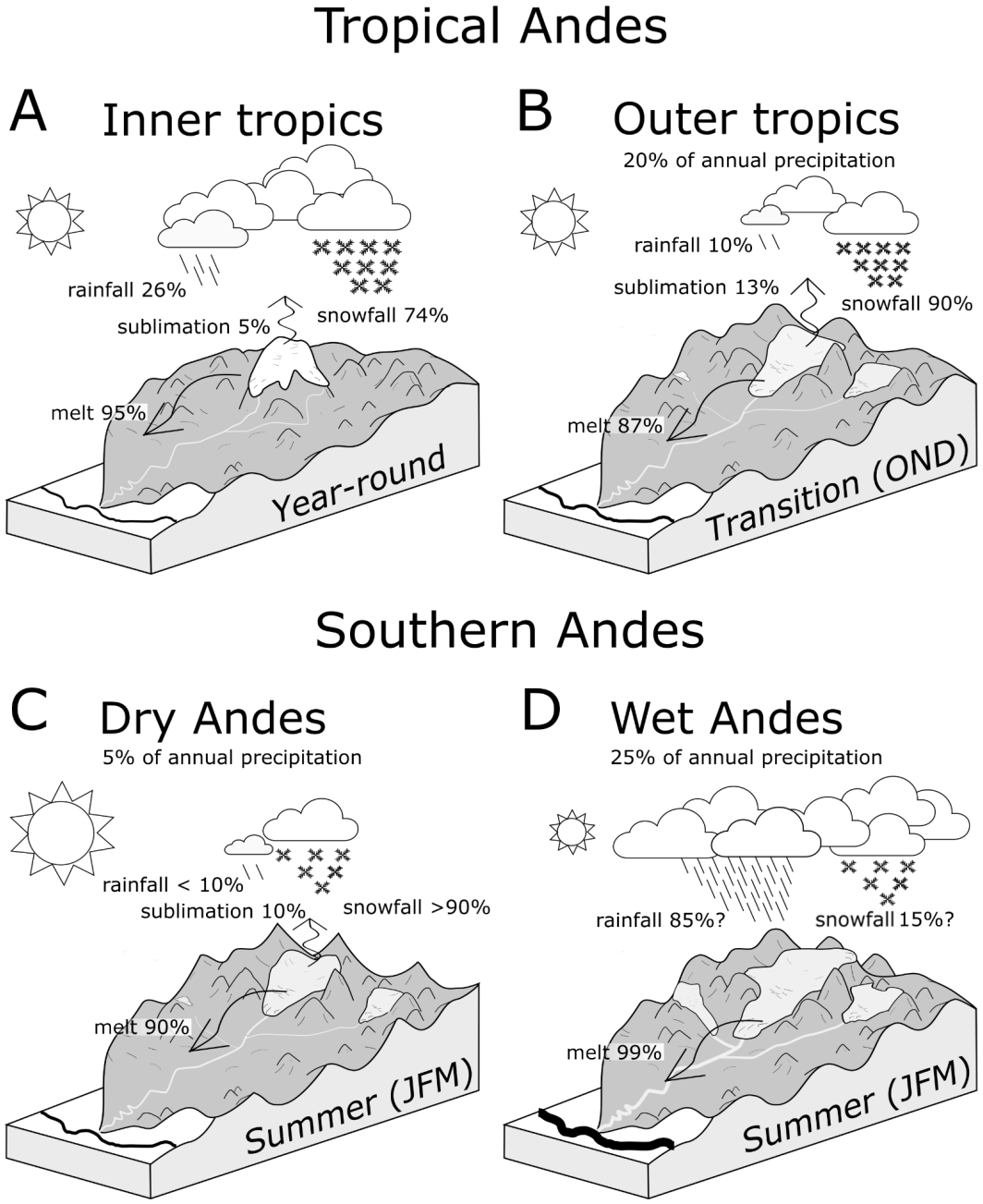


Figure 1. Relevant processes on glacier surfaces (% are given over various periods depending on the references for (i) glacier gains: rainfall + snowfall; (ii) glacier losses: melt + sublimation), during the seasons where the largest ablation occurs in the Andes. Each glaciological region shows the largest surface mass losses related to one season except (A) the Inner tropics (11°N to 5°S), where ablation occurs year-round. These seasons are the transition season in (B) the Outer tropics (5°S to 17.5°S) and the summer season in (C) the Dry (17.5°S to 35°S) and (D) Wet Andes (35°S to 55°S). The term "% of annual precipitation" pertains to the cumulative precipitation within each of the previously mentioned seasons in relation to the total annual precipitation.

The relevance of the processes in each glaciological region was related to specific locations: Inner tropics in Antisana glacier (0.3°S, 5753 m a.s.l.) and related catchment (Kaser, 1999; Favier et al., 2004; Rabatel et al., 2013; Gualco et al., 2022).

Outer tropics in Zongo glacier (16°S, 4900-6000 m a.s.l.) (Sicart et al., 2005; Sicart et al., 2011; Ramallo, 2013; Valex, 2015; Autin et al., 2022).

Dry Andes in the Maipo basin (33°S), Echaurren Norte (3650-3900 m a.s.l) and Juncal Norte (2904-5896 m a.s.l.) glaciers (DGA, 2015; Masiokas et al., 2016; Farías-Barahona et al., 2019; Ayala et al., 2017; 2020).

Wet Andes in San Rafael glacier (0-4000 m a.s.l.) and catchments of west side of NPI (47°S) (Ohata et al. 1985; Fujiyoshi et al., 1987; Kondo and Yamada, 1988; Koppes et al., 2011; Dussaillant et al., 2012; Krogh et al., 2014; Schaefer et al.,

2015; Lo Vecchio et al., 2019).

### 1.3.2 Southern Andes (18-55°S)

The Southern Andes stretch for over 4500 km, spanning from northern Chile to Tierra del Fuego. The elevation at which the 0°C isotherm can be found varies from approximately 4000 m a.s.l. in the north to around 500 m a.s.l. at the southern tip of the continent. As a result, snowfall occurs at higher elevations in northern Chile and persists throughout the winter in the south (Garreaud et al., 2009). During the winter months from April to September, solid precipitation, in the form of snow, is predominant when the air temperature is below freezing (< 0°C). In contrast, during the summer months from October to March, warmer temperatures lead to the release of water stored as snow through meltwater. This snowmelt serves as a significant water supply, particularly during the early summer, while ice melt becomes more dominant in the late summer. Lliboutry (1998) proposed two climatological regions in the Southern Andes: the Dry Andes (17.5-35°S) and the Wet Andes (35-55°S).

In the Dry Andes, the descending air motion associated with the subtropical anticyclone over the southeastern Pacific Ocean leads to arid conditions in the western side of the Andes (Houston and Hartley, 2003; Garreaud et al., 2009). The region between 18-23°S on both sides of the Andes experiences the most pronounced contrast in precipitation. In the northern area of the Dry Andes, known as the Desert Andes, mean monthly temperatures remain negative throughout the year, and precipitation is concentrated in the winter season from May to August (Nicholson et al., 2009). Observations taken at Frontera station (29°S) located at 4927 m a.s.l. (between 2002-2008) near the elevation of glacier fronts show mean monthly temperatures ranging from -0.6°C to -10.9°C. Precipitation in this region mostly occurs in the form of solid precipitation, with less than 900 mm per year at 3800 m a.s.l. (2001-2009). Around 90% of the precipitation occurs during winter (May-August), while the remainder can occur at higher elevations in summer (February-March) due to convective activity (Rabatel et al., 2011). In high-elevation glaciers of the Dry Andes, mass balance variability is primarily driven by annual precipitation (Rabatel et al., 2011; Masiokas et al., 2016). Ablation, on the other hand, is dominated by sublimation, reaching 81% in the Desert Andes (Guanaco glacier, 29°S, 2008-2011, MacDonell et al., 2013). However, sublimation is lower in the Central Andes, accounting for approximately 7% of the glacier-wide ablation in Juncal Norte glacier at 33°S during the summer of 2009 (Ayala et al., 2017).

Figure 1C illustrates the processes studied in the Maipo basin and the Echaurren Norte and Bello glaciers located in the Central Andes. During the strong ablation season (summer, JFM), precipitation comprises only 5% of the total annual precipitation (mostly snowfall) (Masiokas et al., 2016), and the

maximum annual amount of glacier runoff is estimated (Ayala et al., 2020). Glacier ablation in this region is primarily composed of glacier melting (snow and ice) accounting for 90%, while sublimation contributes 10%, as simulated in the Bello glacier (33°S, 2013-2016, DGA, 2015). Figure 2 (Dry Andes) displays the observed mean monthly temperature and precipitation near the Echaurren Norte glacier (Masiokas et al., 2016) and the glacier runoff related to the Maipo basin, where the maximum glacier runoff occurs during the summer season (JFM) under warm and dry conditions (Ayala et al., 2020). Glacier runoff contributions to the Huasco (29°S), Aconcagua (33°S), and Maipo basins (34°S) have been estimated to range from 3% to 23% considering catchment sizes between 241 to 4843 $km^2$ (Gascoin et al., 2011; Ragettli and Pellicciotti, 2012; Ayala et al., 2020).

In the Wet Andes, the western side receives abundant precipitation due to frontal systems moving eastward from the Pacific Ocean, resulting in a high precipitation gradient from west to east. Annual total precipitation in this region ranges from 3000-7000 mm per year near 45°S, and maximum precipitation can reach up to 10000 mm per year (Garreaud et al., 2009; Schaeffer et al., 2017; Yamada, 1987). Conversely, in the eastern Andes, far from the icefields, the annual mean precipitation decreases to less than 100 mm per year, creating a cold and windy steppe environment (Garreaud et al., 2009). The Southern and Northern Patagonian icefields, located in the Wet Andes, host numerous glaciers, most of which have their equilibrium-line altitude (ELA) below the mean annual 0°C isotherm (Masiokas et al., 2020). In the icefields, seasonal variations in precipitation and temperature are small, with wet and windy summers (Fujiyoshi et al., 1987; Koppes et al., 2011). In the Northern Patagonian Icefield, simultaneous rainfall and snowfall can occur (Fujiyoshi et al., 1987; Koppes et al., 2011). Kondo and Yamada (1988), on San Rafael glacier, estimated that snowfall can occur even if the air temperature is above 0°C, and both solid and liquid precipitation occur in summer (December-January), with considerable accumulation in early summer. For instance, over the 1985-1986 summer season, Kondo and Yamada (1988) showed that snowfall composed 15% of precipitation at 1034 m a.s.l. and decreased to 5% at lower elevations (426 m a.s.l.). However, the annual snowfall has been estimated at 49% between 1975-2011 in the Northern Patagonian Icefield (Schaefer et al., 2015). Regarding surface ablation, Ohata et al. (1985) estimated that calving and melting contributed equally to the total mass loss in the San Rafael glacier.

Figure 1D depicts these processes on a glacier in the Wet Andes during the summer season, where glaciers with inland fronts experience ablation primarily through melting, and rainfall amounts can be significant. Cloud cover is present for over 50% of the time during summer (Lo Vecchio et al., 2019), leading to a reduction in incoming shortwave radiation (Schaefer et al., 2015). Meteorological records on the east side of the Northern Patagonian Icefield indicate that 25% of the annual precipitation (Lago Vargas station, at low 1000 m a.s.l.) occurs during the summer season (Dussaillant et al., 2012). In

catchments located on the east side of the icefield, Krogh et al. (2014) estimated a high contribution of rainfall to the annual precipitation, with rainfall accounting for 68% of the total in the León and Delta catchments. Maximum streamflows are recorded during summer in the Baker River (Bertrand Lake), and they are not solely correlated with precipitation, suggesting a high contribution from snow in the basin and glacier melt (snow/ice melt). The climograph and hydrograph of the Baker basin can be observed in Figure 2 (Wet Andes). Mean monthly temperatures range from -3 to 6°C, with precipitation occurring year-round but concentrated in the winter season from April to September. Flow discharges at the Ñadis gauging station exhibit large monthly river flows, with maximums occurring during the summer season (JFM) (Dussaillant et al., 2012).

Recent studies have observed that glacier mass loss through calving (both ocean and lake-terminating) is significant in the total mass loss in the Wet Andes. The most substantial mass loss by calving was estimated in the Southern Patagonian Icefield, accounting for nearly half of the total loss during the period 2000-2019, where calving is the main factor of mass loss of glaciers like Jorge Montt (Minowa et al., 2021; Bown et al., 2019). However, mass loss by calving constitutes only a minor fraction (lower than 20%) for most glaciers in the Northern Patagonian Icefield (Minowa et al., 2021).

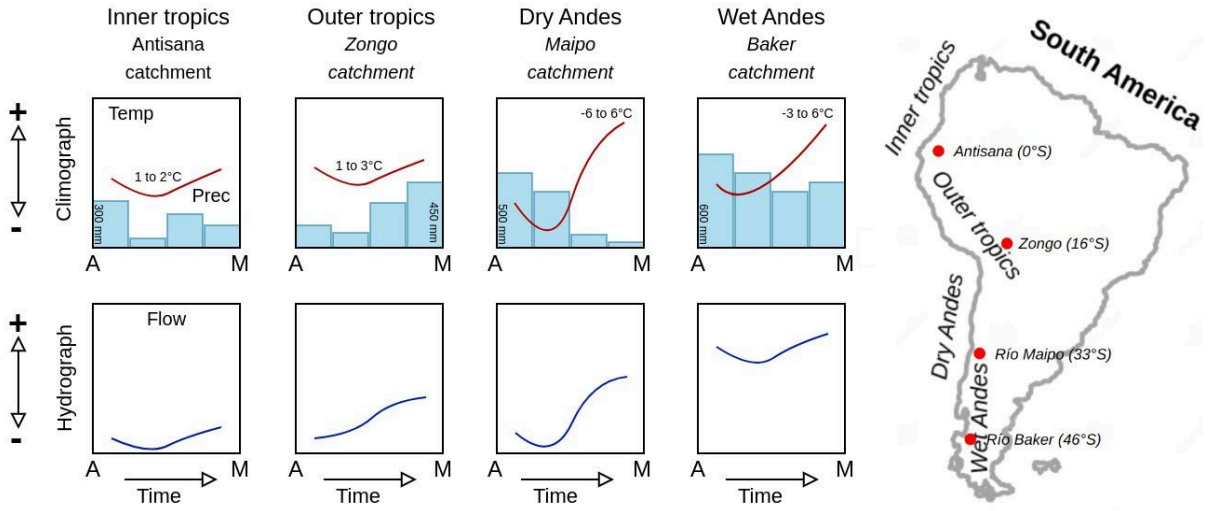


Figure 2. Seasonal schematic seasonal climographs and hydrographs of glacierized catchments in the glaciological regions of the Andes from April (A) to March (M). Seasonal distribution of temperature and precipitation exhibit an increase southward. The seasonal variability of temperature reaches its maximum in the Dry Andes, where all regions show maximum temperature during the summer (JFM). Variability of monthly precipitation is lower in the inner tropics (lowest amount) and the Wet Andes (largest amount), and higher in the outer tropics and the Dry Andes, showing these latter opposite wet and dry seasons. The catchment flows also show high differences across the Andes, with an increase from the inner tropic to Wet Andes and a larger seasonal response (maximum in summer) in the outer tropics and Dry Andes. Axis x represents the hydrological year from April to March. The climate and hydrological variables in each region were related to specific locations:

- Inner tropics in the Antisana catchment (Gualco et al., 2022).
- Outer tropics in the Zongo catchment and Zongo glacier (Frans et al., 2015; Autin et al., 2022).
- Dry Andes in the Maipo basin and Echaurren Norte glaciers (Masiokas et al., 2016; Ayala et al., 2020).-
- Wet Andes in Baker basin (Dussaillant et al., 2012).

# 1.4 Glacier mass balance and flow of ice

## 1.4.1 Glacier surface mass balance

For mass balance estimations glaciers could be considered just as frozen water, where sediments and meltwater in transit or in storage are considered outside the glacier (Cogley et al., 2011). Annually, glaciers gain (mostly by snowfall) and lose surface mass (mostly by melt) causing changes in their size over time, involving processes that can transfer mass in the glacier and its surroundings or between ice and liquid water within the glacier (Cuffey and Paterson, 2010). The rates of these processes over time determine the glacier mass balance, Overall, mass exchanges are related to elevation. Because of that, an increase in specific balances (gain of mass) will thicken and steepen the glacier increasing the ice flow. These processes related to glacier dynamics are also influenced by the regional climate (Cuffey and Paterson, 2010) which allows considering the glacier mass balance as a climate indicator (Francou and Vincent, 2015). The specific mass balance represents a change of mass per unit area in one year ($\dot{b}$, in kg $m^{-2}$ $yr^{-1}$) which can be divided into sub-periods. In most cases, the surface balance ($\dot{b}_s$) dominates over basal balance ($\dot{b} = \dot{b}_s$), although the basal balance could be important in some glaciers (Cuffey and Paterson, 2010). Due to the above, changes in glacier mass can be conceptualized in terms of a budget, in which processes of gain (positive $\dot{b}$) and loss (negative $\dot{b}$) can be estimated. The areas on a glacier where the mass gain exceeds ablation are called the accumulation zone, whereas the areas where a deficit is greater are known as the ablation zone. In one year, the net change determines whether a glacier grows or shrinks from one year to the next (Cuffey and Paterson, 2010).

In the surface balance rate ($\dot{b}_s$, Equation 1) at a point, several processes are related: snowfall ($\dot{a}_s$), avalanche deposition ($\dot{a}_a$), melt ($\dot{m}_s$), refreezing of water ($\dot{a}_r$), sublimation ($\dot{s}$) and wind-blown snow ($\dot{a}_w$). However, snowfall and melt dominate the surface balance.

$$\dot{b}_s = \dot{a}_s + \dot{a}_a - \dot{m}_s + \dot{a}_r - \dot{s} \pm \dot{a}_w , \qquad \text{Equation 1}$$

Where wind-blown snow can be positive (windborne snow) or negative (wind scour) (Cogley et al., 2011). Although refreezing is related mostly to melt water, rain and runoff from adjacent hillslopes can be considered (Cuffey and Paterson, 2010).

In surface accumulation processes, snowfall varies widely and controls accumulation. Three factors are identified: snowfall increases with the atmospheric water vapor, precipitation reaches to the ground as snow when the air temperature is subfreezing (precipitation partitioning in rain or snow) and high snowfall rates occur where air masses rapidly cool (Cuffey and Paterson, 2010). Meanwhile, in surface

ablation processes, a glacier surface loses mass mostly by melt, sublimation and calving. Melt and sublimation are driven by the flux of energy from the atmosphere to the surface: radiation and turbulent fluxes. If the temperature of the surface snow/ice is at melting point, the rate of melt increases proportionally to the net energy flux, however, melting can occur with subfreezing air temperatures (Cuffey and Paterson, 2010). Meanwhile, sublimation can occur at all temperatures year-round and is the dominant ablation mechanism in cold and windy environments (MacDonell et al., 2013). Sublimation converts radiant and sensible energy fluxes to latent heat, thereby reducing the energy available for melting (Cuffey and Paterson, 2010). Strong sublimation can suppress surface melting even if overlying air temperatures are several degrees above the freezing point (Kuhn 1987). In accumulation and ablation processes the snowfall is another important factor, because lower winter precipitation exposes earlier firn/ice in the ablation season (with lower albedo), conversely a snowfall in summer reduces total melt (with high albedo) (Cuffey and Paerson, 2010).

Figure 3 from Cuffey and Paterson (2010) depicts an idealized annual cycle of glacier surface mass balance for mid-latitude glaciers. According to the diagram, the mass of the glacier increases during winter due to snowfall events, and gradually decreases throughout the summer season, reaching its maximum value at the end of each season. The times of two successive minimums are denoted as t1 and t2, while tm represents the time of the intermediate maximum. These time intervals are used to define the annual balance of the glacier. Furthermore, the annual balance can be further subdivided into winter mass balance (from t1 to tm, when snow accumulates) and summer mass balance (from tm to t2, when ablation processes dominate). This change in mass per unit area relative to the previous summer surface (accumulation less ablation from the start of the balance year) is defined as the specific balance ($b$). This specific balance defines the net balance for the year or mass balance ($b_n$).

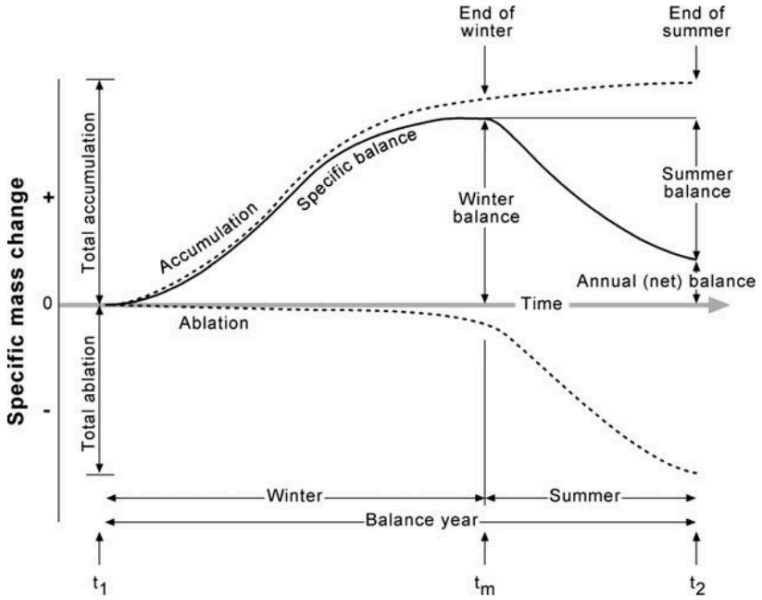


Figure 3. Definition of specific surface mass balance or specific balance by Cuffey and Paterson (2010)

Thus, the annual glacier mass balance ($B_n$, Equation 2) is getting integrating the annual specific balance over the total area of a glacier ($\Omega$), which quantifies the change of mass per unit area or equivalent thickness of ice or water from the entire glacier in one year.

$$B_n = \int_{\Omega} b_n \, d\Omega \quad , \qquad \text{Equation 2}$$

Other concepts like ELA and AAR are relevant to understand the glacier-wide gain and loss. Cuffey and Paterson (2010) define the ELA as the elevation of the boundary between accumulation and ablation zones, where accumulation equals ablation for the year (at the end of the ablation season), and the accumulation-area ratio (AAR) as the ratio of the accumulation zone regarding the total glacier area.

Glaciers in the Andes exhibit distinct patterns of accumulation and ablation depending on their location within different glacio-climatological regions. Figure 4 provides an idealized representation of the annual cycle of glacier surface mass balance during a balanced-budget year ($B_n = 0$) in the main glaciological regions of the Andes. In the inner tropics, based on observations from the Antisana glacier (located at 0°S in Ecuador) spanning a period of 10 years, both ablation and accumulation processes occur throughout the year. The largest amounts of accumulation are typically observed in April and February (Rabatel, 2015). In the outer tropics, glaciers such as the Zongo glacier (situated at 16°S in Bolivia) exhibit greater accumulation during the wet season (JFM). Measurements spanning 27 years indicate

year-round ablation, with significant accumulation occurring in April, August, and from January to March (Autin et al., 2022). In the Dry Andes, short-term measurements, particularly related to albedo, provide insights into year-round ablation and accumulation. Ablation is most pronounced during the summer months, while accumulation is largest in winter (DGA, 2015). Within the Wet Andes, simulations and observations of mass balance over a span of 9 years in the Mocho-Choshuenco glacier demonstrate year-round accumulation, with the period from June to January exhibiting the highest concentration of accumulation. Ablation, on the other hand, primarily occurs from April to June and in February and March (Schaefer et al., 2017).

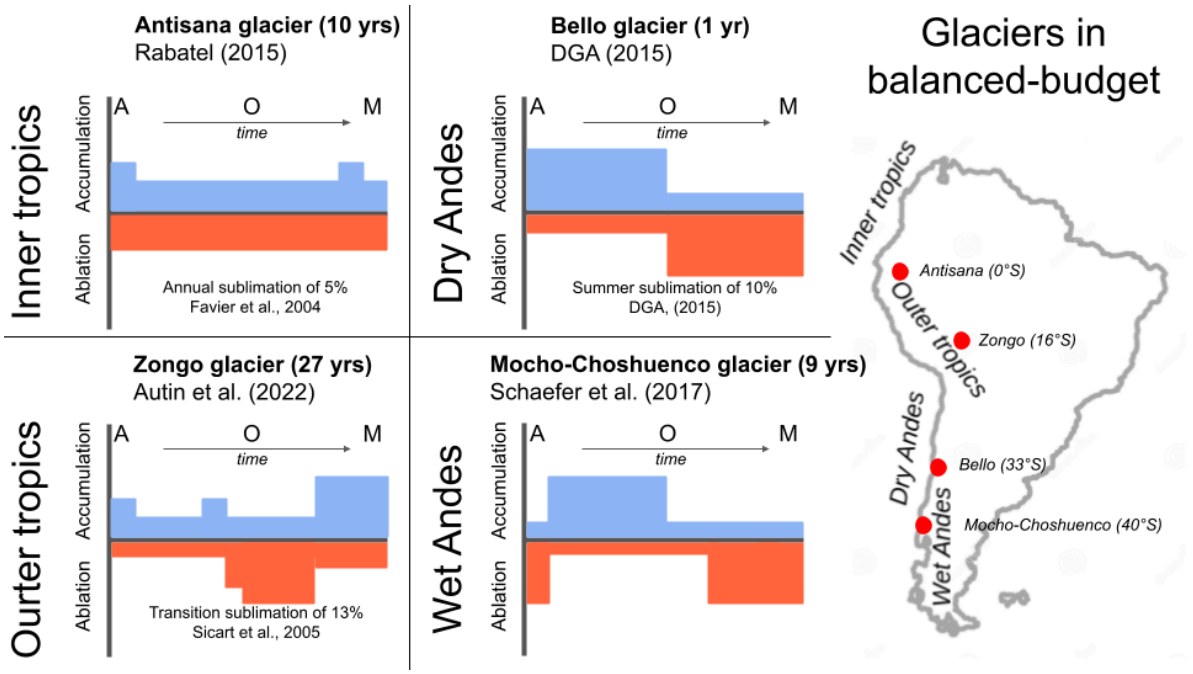


Figure 4. The diagrams show the accumulation and ablation of four Andean glaciers throughout one year considering balance-budget ($B_n = 0$). Figures are inspired in Kaser (1995), taken the observation and simulation of the Antisana (Rabatel, 2015), Zongo (Autin et al., 2022), Bello (DGA, 2015) and Mocho-Choshuenco glaciers (Schaefer et al., 2017). A, O and M, refer to April, October and March.

## 1.4.2 Measurements and simulations of glacier surface mass balance

The glacier surface changes are estimated from elevation differences related to snow/ice densities, getting the specific balance associated to the representative area and then used to estimate the annual glacier surface mass balance. For that, several *in situ* and remote sensing methods have been applied, which will be described briefly considering that the relevant methods for this thesis are described in sessions of methodology. The *in situ* method used stakes to estimate surface elevation changes on the glacier (snow and/or ice) and snow density measurements are performed through the use of density

cutters (box, cylinder and wedge) (Proksch et al., 2016; Caro, 2014), Mount Rose snow cylinder, or snow penetrometer (Mössner et al., 2013), between other techniques. However, accessible *in situ* measurements of elevation change are usually not representative of the whole glacier. The remote sensing measurements used also to estimate surface elevation changes can cover the entire glacier surface. However, some limitations are related to spatial resolution, atmospheric conditions and to passive or active sensors, these latter are related to the reception of natural or emitted signals. The remote sensing measurements could be split into three approaches: close, aerial and orbital ranges. In the first one is implicated the terrestrial (TLS) and aerial transported laser scanners (ALS) better known as LiDAR (Laser imaging, detection, and ranging) and the unmanned aerial vehicles (UAV) implemented with active or passive sensors. The second one is related to aerial photographs. The last one, orbital range, is related to satellite data, which comprise active or passive measurements. Recent studies have estimated the recent glacier surface elevation changes using active (e.g., Braun, 2018) and passive sensors (e.g., Dussaillant et al., 2019, Hugonnet et al., 2021) across the Andes. In addition, in the annual glacier mass balance estimation of large areas, the glacier surface area is extracted from local and/or global glacier inventories (glacier outline).

The surface mass balance simulation is performed usually through the energy balance or temperature-index methods. The surface energy balance applied in snow/ice melt calculation (e.g., Rothlisberger and Lang, 1987) was tested and improved with several measurements (e.g., Hay and Fitzharris, 1988; Braithwaite and Olesen, 1990; Munro, 1990; Brock et al., 2000). The principal components of energy balance to estimate surface melt rate ($Q_M$, Equation 3) are described by Arnold et al. (1996) like the summation of the net radiation fluxes in shortwave ($Q$ *) and longwave ($I$ *), and the turbulent fluxes of sensible ($Q_S$) and latent heat ($Q_L$) (Brock et al., 2000). However, later studies incorporated the energy supplied by rain in this balance (e.g., Hock and Holmgren, 2005; Kinnard et al., 2022).

$$Q_M = + Q^* + I^* + Q_S + Q_L, \qquad \text{Equation 3}$$

The temperature-index methods cover the degree-day model related to the degree-day factor (DDF) and enhanced temperature-index model (ETI) (Hock, 2003; Pellicciotti et al., 2005). Daily and other time intervals as hourly or monthly can be used for determining DDF (Hock, 2003). The main difference between both models is the incorporation of incoming shortwave radiation and albedo in ETI, which improve the temperature-index models performance in glaciers in which the shortwave dominates the energy available for melt at the hourly time step (Pellicciotti et al., 2005).

Hock (2003) through the degree-day model estimated ice/snow melt (M, in mm, Equation 4) during a period of n time intervals ($\Delta t$) to the sum of positive air temperatures of each time interval ($T^+$) during the same period like:

$$\sum_{i=1}^{n} M = DDF \sum_{i=1}^{n} T^+ \Delta t \ , \qquad \text{Equation 4}$$

Where the degree-day factor (DDF) is expressed in mm $d^{-1}$ $k^{-1}$ for $\Delta t$ in days and temperature in °C (Braithwaite, 1995). This model through the DDF is influenced by all terms of the energy balance (Hock, 2003). The simulations of snow/ice melt performed in this thesis are based in Hock (2003).

## 1.4.3 Glacier dynamics

In glaciers that have distinct accumulation (upper zone with gain in mass) and ablation zones (lower zone with loss of mass), the ice is transferred from higher to lower elevations through a process known as ice flow (Jiskoot, 2011). This redistribution of ice within a glacier is governed by the concept of force balance, where the gravitational driving stress is balanced by resistive stresses, such as basal sliding and bed deformation. Understanding these dynamics is crucial for describing the dynamic of the glacier (Cuffey and Paterson, 2010).

The gravitational driving stress is influenced by gravitational acceleration, ice density, ice thickness, and surface slope. The resistive stresses primarily act at the base of the glacier in the form of basal drag, although lateral drag and dynamic resistance due to longitudinal stress gradients within the ice can also play a role (Jiskoot, 2011). Among these resistive forces, basal drag is generally the most significant (Cuffey and Paterson, 2010). In Figure 5, the basal shear stress ($\tau_b$, from 10 kPa for ice streams to 100 kPa for valley glaciers, Cuffey and Paterson, 2010) is related to glacier thickness, the surface slope, and the shape of the glacier valley, which for a section can be defined like

$$\tau_b = fpgh \sin \alpha \ , \qquad \text{Equation 5}$$

$pgh \sin \alpha$ represents the weight of the ice column parallel to the plane, where $p$ is the ice density (kg $m^{-3}$), $g$ is the gravitational acceleration (9.81 m $s^{-2}$), $h$ in the ice thickness (m), $\alpha$ is the ice thickness gradient ($dh/dx$) (equals the ice surface slope on a horizontal bed), and $f$ a shape factor related to the glacier profile and valley shape (glacier geometry) (Cuffey and Paterson, 2010). $f$ represents friction along the bed as a fraction of the basal/lateral drag, which can be expressed as the ratio between the hydraulic radius (defined as the cross-sectional area of the glacier divided by the wetted perimeter) and

the centerline ice thickness (Nye, 1965; Jiskoot, 2011) (values between 0.5 and 1.5 from Cuffey and Paterson, 2010). Equation 5 is similar to the shallow ice approximation (SIA) where basal shear stress is calculated from ice thickness and surface slopes over distances equal or larger than the ice thickness (Jiskoot, 2011), whereas, for shorter distances the longitudinal stresses need to be included because if this stress is unbalanced (i.e. the ice mass is pushing or pulling) the basal shear stress can be very different in Equation 5 (Jiskoot, 2011).

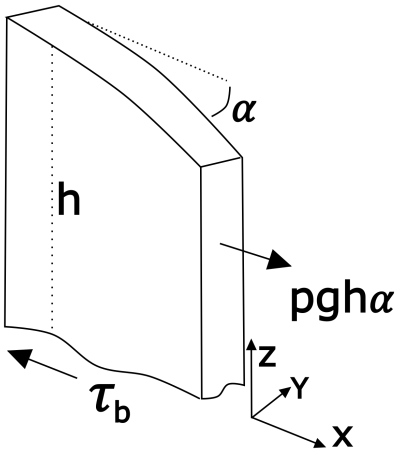


Figure 5. Diagram of an ice flow line showing the main stress terms acting on ice columns. The term $\tau_b$ represents the stress acting on the base of the ice in direction x. Adapted from Cuffey and Paterson, 2010.

### 1.4.3.1 The three major components of ice flow

The generalized flow law for the creep (internal deformation) of glacier ice, the Glen's flow law, was developed by Nye (1951, 1957) and Glen (1952, 1955), where a sliding law was developed by Weertman (1957) and Lliboutry (1958) who recognized the two main processes of basal sliding (regelation and enhanced creep). Subsequently, the roles of water pressure and cavitation in the process of sliding were identified by Lliboutry (1968), which led to theories on how switches in the subglacial drainage system control sliding speed (Kamb, 1987; Jiskoot 2011).

In response to the driving stress, glaciers can move due to three independent ice flow processes which could contribute ensemble: (1) internal deformation (creep), (2) basal sliding, and (3) soft bed deformation. All glaciers move due to creep flow, but basal sliding is the major component in glaciers that do not have a frozen bed (temperate and polythermal glaciers), meanwhile, glaciers that are underlain by soft deformable substrate (till) experience bed deformation. Where sliding and/or bed

deformation are present, these processes can contribute to more than 50% of the total velocity of the glacier surface (e.g., Boulton and Hindmarsh, 1987 in Jiskoot 2011).

The ice flow measured at the glacier surface (U) can be described as the sum of deformation velocity (Uc, creep velocity), sliding velocity (Us), and bed deformation velocity (Ud), where the last two terms can be combined as basal motion (Ub) (see Figure 6A). When glaciers move mostly by internal deformation, the velocity decreases as a fourth order polynomial with depth (with maximum velocity at the surface to minimum at the base) (in Figure 6A see Uc), where the transverse velocity profile (across the glacier) shows a parabolic distribution with a maximum in the center. Whereas, glaciers dominated by basal motion have a uniform transverse velocity profile (plug flow, Sharp, 1988) (in Figure 6B). The flow processes described as follows will explain these differences in velocity.

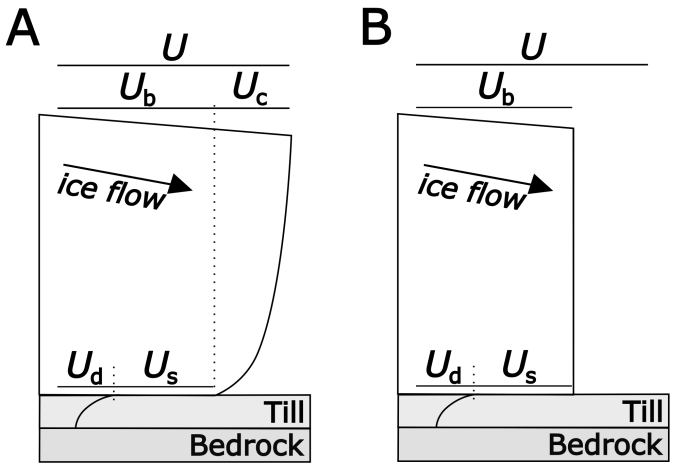


Figure 6. Vertical and transversal glacier ice flow. A) Cross section of vertical velocity and surface velocity (U) of a glacier with the three components of ice flow active: internal deformation (Uc), basal sliding (Us) and bed deformation (Ud). The basal motion (Ub) is composed by Us and Ud. B) Cross section of vertical velocity with high basal velocity (Ub). Adapted from Jiskoot (2011).

### 1.4.3.2 1st ice flow process: Internal deformation

The ice deformation rate (shear strain rate) under a constant shear stress rate is initially high but then decreases to a constant value (secondary strain rate). The value of the constant shear strain rate is dependent on the amount of stress applied, ice temperature, stress history, and on impurities within the ice. Glen (1955) derived the constitutive relationship of glacier ice, given by the relation between secondary shear strain rate ($\varepsilon$) and applied stress ($\tau$). His empirical flow law for ice creep in steady state (Glen's flow law, Equation 6) is expressed as:

$$\varepsilon = A\tau^{n}, \qquad \text{Equation 6}$$

where *A* is the ice creep parameter depending on ice temperature (Glen, 1955), which is not affected by hydrostatic pressure (Rigsby, 1958). Cuffey and Paterson (2010) propose a value of $2.4 \times 10^{-24}$ $s^{-1}$ $Pa^{-3}$, which decreases log-linearly with temperature below the freezing point. The exponent $n$ is a constant that depends on applied stress (range 1.5 to 4.2, usually equal to 3 for valley glaciers) (Cuffey and Paterson, 2010). Thus, for temperate valley glaciers the deformation rate is proportional to the vertical shear stress cubed, which is a function of the ice thickness (Jiskoot 2011). Strain rate profiles can be constructed by adding shear stresses across the glacier thickness. The sum of all deforming ice layers is expressed as glacier surface velocity. The mean flow velocity resulting from the horizontal deformation (creep) in an ice column (Uc, Equation 7) can be described as (Jiskoot 2011):

$$U_c = c_I h \tau^n, \qquad \text{Equation 7}$$

where the constant $c_I$ depends on the values for *A* and $n$ from Glen's flow law (Equation 6), $h$ is ice thickness and $\tau$ is basal shear stress (Kamb and Echelmeyer, 1986). From Equation 7, the geometric controls in this relationship are clear: steeper and thicker glaciers have a larger internal deformation rate than thin ones with shallow slopes (Jiskoot 2011).

### 1.4.3.3 2nd ice flow process: Basal sliding

If glaciers are not frozen to the substrate (bedrock or sediments) glacier displacement can occur through glaciers sliding over their beds, where cavitation (empty space in contact substrate/ice) plays an important role (Jiskoot, 2011). The basal shear stress ($\tau$) and the effective pressure ($N_e$) are the basal boundary conditions for the sliding velocity ($U_s$). The effective pressure is estimated from ice overburden pressure ($p_i = \rho g h$) and water pressure ($p_w$) differences. When water pressures exceed the ice overburden pressure the glacier bed can start decoupling from the bedrock. The sliding velocity flow law (Equation 8) can be understood like (Jiskoot 2011):

$$U_s = \frac{k \tau^m}{N_e}, \qquad \text{Equation 8}$$

where constants $k$ is function of bed roughness (between 0.5/13 and 0.5*13, Cuffey and Paterson, 2010) and $m >= n$ (Bindschadler, 1983; Cuffey and Paterson, 2010). Jiskoot (2011) mentions that this approach ignores the effects of frictional forces between rock particles frozen in the basal ice and the

underlying bedrock and the effects of chemical reactions in bedrock or in basal ice impurities by melting/refreezing.

#### 1.4.3.4 3rd ice flow process: Soft bed deformation

Ice flow over a soft bed is a combination of basal sliding and bed deformation (Jiskoot 2011). The type and amount of bed deformation is dependent on till thickness and composition and water pressure, where soft bed deformation flow can be expressed as (Jiskoot 2011):

$$\dot{\varepsilon} = A_2 e^{\frac{\tau}{b\tau_0}} , \qquad \text{Equation 9}$$

where $A_2$ is a constant related to a reference strain rate, $b$ a constant that is dependent on pre-consolidation stresses and texture of the till, and $\tau_0$ the stress taken at a reference shear strain rate (Hooke, 2005). This relationship implies that small increases in shear stress should result in large increases in till deformation, which is related to an unstable runaway flow of glaciers which in extreme cases could result in surges (Jiskoot 2011).

### 1.4.4 Simulation of glacier dynamics

Accurate knowledge of glacier ice thickness and the processes governing ice flow is essential for initializing future estimations of glacier changes (Goelzer et al., 2018). The estimation of glacier ice thickness can be achieved through two main approaches: i) the inversion of mass conservation; and ii) the inversion of momentum conservation based on Glen's flow law. These methods utilize different types of input data and equations (Jouvet, 2022). The inversion of mass conservation, as described by various studies (Paterson, 1971; Haeberli and Hoelzle, 1995; Farinotti et al., 2009; Maussion et al., 2019), estimates ice fluxes by analyzing changes in surface mass balance and infers ice thickness using the shallow ice approximation (SIA). On the other hand, methods based on the conservation of momentum employ varying levels of complexity, ranging from SIA (e.g., Gantayat et al., 2014; Michel-Griessera et al., 2014) and shallow shelf approximation (Goldberg and Heimbach, 2013) to high-order models, including full-Stokes models that consider wall drag and longitudinal drag (Blatter, 1995; Perego et al., 2014; Jouvet, 2022). These advanced methods have proven effective in determining optimal basal friction conditions (e.g., Gagliardini et al., 2013; Morlighem et al., 2013; Mosbeux et al., 2016) and simultaneously optimizing ice thickness and sliding parameterization (Goldberg and Heimbach, 2013; Perego et al., 2014; Jouvet, 2022).

Currently, many models rely on the simplified SIA, which does not account for longitudinal or transverse stress gradients or other complex mechanisms (Le Meur et al., 2004). One limitation of these models is that they assume an almost immediate response of glaciers to climate forcing, whereas full-Stokes models offer a more realistic, delayed, response (Oerlemans, 2008; Jiskoot, 2011). However, developing the adjoint problem in full-Stokes models is challenging and computationally expensive. As a result, glaciologists have started exploring the application of deep learning approaches to overcome these difficulties (Jouvet, 2022).

In the glacier dynamics simulation, I used the inversion of mass conservation method which deduces the ice thickness from the SIA implemented in Open Global Glacier Model (OGGM) (Maussion et al., 2019). In this model, the mass conservation approach was inspired from Farinotti et al. (2009), which is described below.

The method proposed by Farinotti et al. (2009) provides an estimation of the ice thickness distribution by combining the principles of mass conservation and ice flow mechanics. The flux is converted into ice thickness using Glen's flow law (Glen, 1955), taking into account the apparent mass balance gradient derived from the difference between surface mass balance and the rate of ice thickness change. This method requires specific input data, including the glacier surface topography, glacier outline, flowlines, ice flow subcatchments, three parameters that define the distribution of the apparent mass balance, and two parameters that describe the ice flow dynamics.

In agreement to the principle of mass conservation, the mass balance distribution should be balanced by the divergence of the ice flow and the resulting change in surface elevation, then the ice thickness can be inferred from the ice fluxes. In the mass conservation (Equation 10) are considers a length $(dx)$ and height $(h)$ of an ice column in a longitudinal glacier profile (Figure 7), with a constant ice density $(p)$ and a plane strain. (Farinotti et al., 2009).

$$\frac{\partial h}{\partial t} = \dot{b} + \dot{b}' - \frac{\partial q}{\partial x'} , \qquad \text{Equation 10}$$

where $\partial h/\partial t$ is the rate of ice thickness change, $\dot{b}$ is surface mass balance and $\dot{b}'$ is bed mass balance (considered equal zero), and $q$ is the specific mass flux. In three-dimensional case, the mass conservation equation can be written (Farinotti et al., 2009):

$$\frac{\partial h}{\partial t} = \dot{b} - \nabla_{xy} \vec{q} , \qquad \text{Equation 11}$$

where $\nabla_{xy}\,\vec{q}$ is the ice flux divergence. Integrating Equation 11 over the glacier area (Ω) leads to using the Gauss's law:

$$\int_{\Omega} \frac{\partial h}{\partial t}\, d\Omega = \int_{\Omega} \dot{b}\, d\Omega \ , \qquad \text{Equation 12}$$

Then, Farinotti et al. (2009) propose:

$$\int_{\Omega} \nabla_{xy}\, \vec{q} = \int_{\partial\Omega} \vec{q}\, d\vec{n} = 0 \, , \qquad \text{Equation 13}$$

where $\vec{n}$ is the normal vector to the glacier outline ∂Ω. Because, the spatial distributions of surface mass balance ($\dot{b}$) and the rate of ice thickness change (∂h/∂t) are unknown, Farinotti et al. (2009) introduce the apparent mass balance variable ($\overline{b}$, m w.e. $a^{-1}$), which varies linearly with elevation and satisfies:

$$\int_{\Omega} \overline{b}\, d\Omega = \int_{\Omega} \dot{b}\, d\Omega - \int_{\Omega} \frac{\partial h}{\partial t} d\Omega = \int_{\Omega} \left( \dot{b} - \frac{\partial h}{\partial t} \right) d\Omega = 0 \, , \qquad \text{Equation 14}$$

Being the main advantage of estimating $\overline{b}$ and not $\dot{b}$ and ∂h/∂t separately is that, under the condition in Equation (14), the integrated mass conservation equation (Equation 12) is fulfilled without the need for information about the distribution of the surface mass balance and the spatial and temporal variation of the glacier surface elevation (Farinotti et al., 2009). If the given geometry corresponds to steady state, $\overline{b}$ is the actual glacier surface mass balance (i.e. observable).

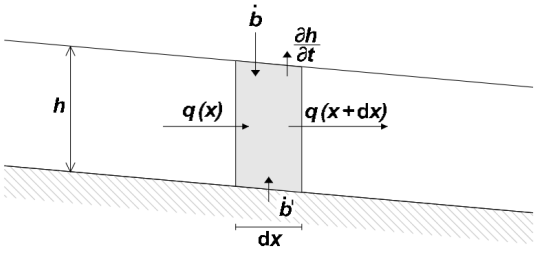


Figure 7. Diagram of the concept of mass balance conservation for an ice column in a longitudinal glacier profile. From Farinotti et al. (2009).

# 1.5 Recent and future changes of Andean glaciers

## 1.5.1 Andean glacier characteristics

The Andes cordillera presents different topographic and climatic conditions, which allows a diverse cryosphere, containing the largest extension of global tropical glaciers (Kaser and Osmaston, 2002), cold glaciers in the semi-arid region and, in Patagonia and Tierra del Fuego, the largest temperate glacier extension in the southern hemisphere outside Antarctica (Masiokas et al., 2020).

Because the glacier surface mass balance response to the climate (Francou and Vincent, 2015), its variability through the El Niño-Southern Oscillation (ENSO) and the Southern Annular Mode (SAM) plays an important role in glacier mass balance. The ENSO generates the major source of precipitation interannual variability from the tropical to central Andes. This coupled ocean-atmosphere phenomenon is characterized by irregular fluctuations (2-7 year periodicity) between warm (El Niño) and cold (La Niña) (Garreaud et al., 2009). The El Niño episodes are associated with:

- below average precipitation over tropical South America,
- above average precipitation over subtropical South America,
- warmer than the normal air temperature in all latitudes ranges.

Opposite conditions prevail during La Niña episodes (Garreaud et al., 2009). Because of that, in the tropical Andes, the precipitation deficit and atmospheric warming during El Niño events results in a strongly negative mass balance (Francou et al., 2003, 2004), while in the Dry Andes during the Niño event (precipitation increase) glaciers showed a more soft negative mass balance or even positive mass balance (Rabatel et al., 2011; Ayala et al., 2020). Southward, in the Austral Andes, there is no clear ENSO signal in precipitation or temperature (Garreaud et al., 2009). In contrast, the Southern Annular Mode (SAM, e.g., Thompson and Wallace 2000) appears to modulate the air temperature (Gillet et al., 2006; Garreaud et al., 2009). This region is the only continental surface that intersects the Southern Westerly Winds (SWW) which is an important wind belt with its core between 50-55°S during summer (Moreno et al., 2018). The SAM or Antarctic Oscillation describes the movement of the SWW over a timescale of decades to centuries. During a SAM positive phase there is a poleward expansion of the band of stronger westerlies weakened at mid-latitudes (between 40 and 50°S) (Moreno et al., 2018a), presenting warm and dry conditions, whereas a negative phase is related to cold and wet conditions (Moreno et al., 2018b; Davies et al., 2020).

Considering the extensive glaciological study compilation made by Rabatel et al. (2013) and Masiokas et al. (2020) in the Andes, they will be the principal references to describe the recent glaciological

behavior in tropical and extratropical glaciers. The Andean monitored glaciers have been the base to understand the relationship between the surface mass balance and climate (See Figure 8) in South America.

#### 1.5.1.1 Tropical glaciers

Over recent decades, observed glacier changes in the inner tropics show a glacierized area reduction in Venezuela of -87% (1952-2003, - 2 $km^2$, Morris et al., 2006), followed by Colombia with an overall glacier reduction of -36% (1990-2016) (Rabatel et al., 2018). In Ecuador, the results of Jordan et al. (2005) in the Cotopaxi Volcano (5897 ma.s.l.) showed a decrease of -30% between 1976-1997. While the surface area of the glaciers on Chimborazo (6268 m a.s.l.) decreased by -57% from 27.7 to 11.8 $km^2$ (1962-1997) (Caceres, 2010). In Cotopaxi and Antisana volcanoes (5753 m a.s.l.), the loss in surface area was -37% and -33% (1979-2007), respectively (Caceres, 2010). Recently, a reduction of -42% (1956-2016, 13.84 $km^2$ in 2016) was estimated in the Antisana ice cap, founding the strongest mass loss during 1979–1997 (−0.82 m w.e. $yr^{-1}$) in contrast to recent years (1998–2016, −0.26 m w.e. $yr^{-1}$) (Basantes-Serrano et al., 2022). In the outer tropics, glaciers in Perú, inventoried since 1962/1975 (2399 $km^2$; INAIGEM, 2018) show a glacierized area of 1114 $km^2$ in 2016, losing -54% between 1962-2016 (INAIGEM, 2018). The northern cordilleras (Blanca, Huallanca, Huayhuash, and Raura) lost -40% in the same period, whereas the central cordilleras (Huagoruncho, La Viuda, Central, Huaytapallana and Chonta) showed much larger glacier shrinkage reaching up to -70% surfaces. At last, in the southern cordilleras (Ampato, Vilcabamba, Urubamba, Huanzo, Chila, La Raya, Vilcanota, Carabaya and Apolobamba) the glacier surface area loss was -60% (INAIGEM, 2018; Masiokas et al., 2020). Two recent publications by Seehaus et al. (2019; 2020) estimated a strong glacier area reduction in Perú and Bolivia of -29% (2000-2016).

Previous reports show that glaciers experienced highly negative mass balance rates from the late 1970s to the early 2000s (Rabatel et al., 2013), which has continued during the last two decades. Dussaillant et al. (2019) estimated a geodetic mass balance of -0.42 ± 0.23 m w.e. $yr^{-1}$ (2001-2017) for the Outer tropics (5°S to 17.5°S), where the negative mass balance was observed in the period 2001-2008 (-0.44 ± 0.25 m w.e. $yr^{-1}$) was less negative during the second period (-0.38 ± 0.24 m w.e. $yr^{-1}$ between 2009 and 2017). Dussaillant et al. (2019) estimated a geodetic mass balance of -0.37 ± 0.25 m w.e. $yr^{-1}$ (2001-2016) in the Inner tropics (11°N to 5°S).

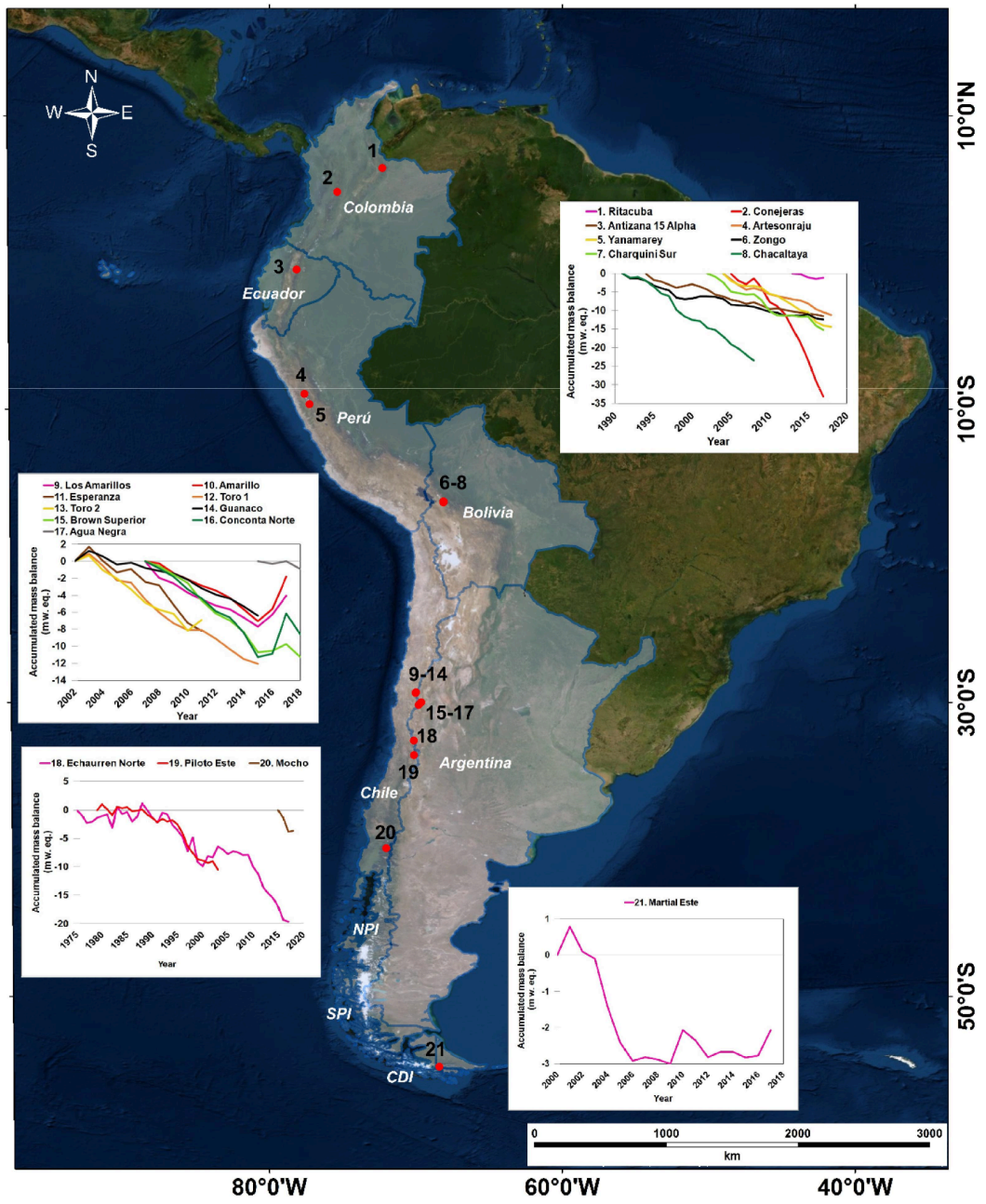


Figure 8. Location and mass balance observations of the Andean monitored glacier from Colombia to Tierra del Fuego. Glaciers with a long time series of mass balance measurements (>5 years) are presented. Figure published in Masiokas et al. (2020).

### 1.5.1.2 Southern Andes glaciers

The climatic differences between the west and east Andes are also reflected in glacier distribution and size. On the western drier Andes, glaciers cover a total area of 71 km$^2$ (Barcaza et al., 2017), whereas the eastern wet Andes exhibit a larger glacierized surface area (217 km$^2$; IANIGLA-Conicet, 2018; Masiokas et al., 2020). In these glaciers found at high elevations, mass balance variability is driven by the annual precipitation (Rabatel et al., 2011; Masiokas et al., 2016). In the Central Andes, mountains host a large variety of glaciers (e.g., snowfields/glacierets, mountain glaciers, debris-covered, and rock glaciers) (Barcaza et al., 2017). This region also includes glaciers that start as clean-ice at high

elevations and gradually turn into debris-covered surfaces further down, and finally end as rock glaciers at the lowest zones (Monnier and Kinnard, 2015, 2017; Zalazar et al., 2017; Masiokas et al., 2020). The glacierized surface area in this region (~1700 $km^2$) is concentrated between 3600 and 4000 m a.s.l. and presents a dominant southeastern orientation (Barcaza et al., 2017; IANIGLA-Conicet and Mayds, 2018).

Glaciers in the Desert Andes show a glacier area reduction of -29% (1955-2007) (Rabatel et al., 2011), a similar observation was made in the Central Andes by Malmros et al. (2016) in the Olivares basin (-30 ± 3%, 1955-2014). However, this glacier reduction is lower in the Aconcagua basin (-20%, 1955-2003, Bown et al., 2008). In comparison, a detailed analysis of the Juncal Norte glacier presented a smaller reduction of -14% (1955-2006) (Bown et al., 2008), which could be related to the size of the studied ice bodies because a smaller one presents an accelerated reduction in comparison to larger one (Rabatel et al., 2011). In general, glaciers in the Dry Andes have shown a thinning and area reduction during the last century (Masiokas et al., 2020). The reconstruction of the annual mass balance in Echaurren Norte glacier shows some periods with positive mass balances and minor glacier advances around the first decade of the 21st century (Masiokas et al., 2016), where the glacier mass loss pattern is related to the recent decreasing in precipitation observed in the subtropical region clearly intensified since 2010 (Masiokas et al., 2016; Hugonnet et al., 2021). This phenomenon is called megadrought (Garreaud et al., 2017). Dussaillant et al. (2019) estimated that over the period 2000/2001-2017 glaciers in the Desert and Central Andes have experienced moderate thinning rates of -0.12 ± 0.17 and -0.31 ± 0.19 m w.e. $yr^{-1}$, respectively. However, during the periods 2000-2008 and 2009-2017 the mass balance rate remained similar in the Desert Andes, but increased during the second period in the Central Andes (-0.17±0.23 m w.e. $yr^{-1}$ related with -0.40±0.21 m w.e. $yr^{-1}$) (Dussaillant et al., 2019; Masiokas et al., 2020). In addition, MacDonell et al. (2013) estimated in the Desert Andes an ablation by sublimation of 81% (Guanaco glacier, 29°S, 2008-2011).

In the North Patagonian Andes (total glacierized area ~1800 $km^2$; Barcaza et al., 2017, Masiokas et al., 2020), glaciers do not descend below 3000 m a.s.l. at 35°S and their fronts can reach 700 m a.s.l. at 45°S (Barcaza et al., 2017; Zalazar et al., 2017). Here, glaciers are comparatively smaller than those located further south and are located in volcanoes and high peaks (Masiokas et al., 2020). The South Patagonian Andes contains a large number of glaciers, outlet glaciers, and icefields, including the Northern and Southern Patagonian Icefields, and the icefield of Cordillera Darwin located in Tierra del Fuego. From Masiokas et al. (2020), the Southern Patagonian Icefield covers an area of 12200 $km^2$ (De Angelis, 2014; Meier et al., 2018), meanwhile, the Northern Patagonian Icefield 3700 $km^2$ (Dussaillant et al., 2018), followed by the Cordillera Darwin 2300 $km^2$ (Bown et al., 2014). Millan et al. (2022) estimated an ice volume of 4756 ± 923 $km^3$ in Northern and Southern Patagonian Icefields. Small ice caps can be

found at Mount San Lorenzo (140 $km^2$; Falaschi et al., 2013) and Gran Campo Nevado (200 $km^2$; Schneider et al., 2007; Weidemann et al., 2013).

The glacier area changes were estimated by many studies considering different latitudes, methods and periods of time. However, the results agree that generalized glacier growth and frontal advances culminated in the 19th century (Masiokas et al., 2020). Paul and Moelg (2014) found a total glacier area reduction of -25% in the North Patagonian Andes (1985-2011, 40.5-44.5°S). Meanwhile, southward 45°S Meier et al. (2018) estimated a mean glacier area reduction of -9 ± 5% (1986-2016). Some specific large glaciers presented a high frontal retreat between 1945-2005 like the San Rafael glacier (-5.7 km), the O'Higgins glacier (-11.6 km) and the Marinelli glacier (-12.2 km) (Lopez et al., 2010). It has to be noted some advancing trends in the Pío XI glacier (Hata and Sugiyama, 2021) and Garibaldi glacier (Melkonian et al., 2013), showing the Perito Moreno glacier a stable frontal position with short-term advances and retreats during the last century (Minowa et al., 2015). In general, the recent acceleration of mass loss since the Little Ice Age was confirmed by Meier et al. (2018), because the glacier area loss southward 45°S was -0.10 ± 0.04% $yr^{-1}$ until 1986, increasing to -0.33 ± 0.28% $yr^{-1}$ between 1986-2005 and to -0.25±0.50% $yr^{-1}$ for the period 2005-2016. Recent global estimates suggest that Southern Andes contributed 8% (2000-2019) of the global mass loss (Hugonnet et al., 2021). For this region, Dussaillant et al. (2019) estimated a mass balance of -0.75 ± 0.23 m w.e. $yr^{-1}$ (2000-2016), where the negative mass balance was reduced between the first to the second decades from the 2000s (-0.72 ± 0.26 m w.e. $yr^{-1}$ in the period 2000-2008 and -0.69 ± 0.25 m w.e. $yr^{-1}$ in the period 2010-2017). These increase in negative mass balance during the second period is observed between the Desert Andes to North Patagonia.

Schaefer et al. (2015) modeled the surface mass balance for the entire Southern Patagonian Icefield estimating an average annual accumulation of 67.7 $km^3$ and a mean ice surface melt of 36.5 $km^3$ (1975-2011), with a strong increase in annual ice mass losses due to calving between 1975-2000 and 2000-2011 (changing from 44.4 to 61.3 $km^3$ of ice). However, Collao-Barrios et al. (2018) applied a physically based model to estimate the glacier dynamic of the San Rafael glacier (Northern Patagonian Icefield) founding a slightly positive mass balance (0.08 ± 0.06 Gt $yr^{-1}$) between 2000-2012, suggesting that previous mass balance estimations over the entire glacier were higher due to an overestimation in the accumulation area (e.g. Schaefer et al., 2013 and Koppes et al., 2011). In a recent study by Minowa et al. (2021), the largest glaciers in the Northern and Southern Patagonian Icefields were investigated. Their findings indicate that ablation due to calving constitutes approximately one-fifth of the total mass loss in the Northern Patagonian Icefield (NPI), while in the Southern Patagonian Icefield (SPI), the mass loss by calving is half of the total mass loss. In this region, limitations in glacier dynamic and mass

balance estimations are due to in situ data lack (e.g., precipitation/accumulation in the upper zones, temperature/melt patterns, and calving fluxes and dynamics) (Masiokas et al., 2020).

### 1.5.2 Projections of Andean glaciers throughout the 21st century

The majority of knowledge regarding future glacier changes in the Andes is derived from global simulations that provide estimations of glacier volume changes throughout the 21st century (e.g., Marzeion et al., 2012; Radic and Hock, 2014; Huss and Hock, 2015; Rounce et al., 2023). These studies demonstrate consistent estimates of mass loss in the Tropical Andes (approximately -98 ± 13% for RCP 8.5, CMIP5 models). However, there is a wider range of results for the southern Andes, which encompasses the largest glacierized area. Mass loss in this region varies from -44 ± 14% to -68 ± 20% (Table 1) (Huss and Hock, 2015; Rounce et al., 2023).

In addition to global simulations, there are also local studies that simulate future glacier changes across specific regions of the Andes. These studies focus on glaciers in countries such as Colombia, Ecuador, Peru, Bolivia, and Chile (e.g., Frans et al., 2015; Réveillet et al., 2015; Yarleque et al., 2018; Vuille et al., 2018; Rabatel et al., 2018; Scheiter et al., 2021). Furthermore, investigations have been conducted on glaciers in the Patagonian icefields (e.g., Schaefer et al., 2013; Bravo et al., 2021). In the tropical Andes, Vuille et al. (2018) found that the Antizana Glacier (located at 0°S in the inner tropics) is more susceptible to warming throughout the 21st century compared to the Zongo Glacier (16°S in the outer tropics). Projections for the Zongo Glacier indicate volume losses ranging from -40 ± 7% to -89 ± 4% between 2010 and 2100, depending on the selected Representative Concentration Pathway (RCP) (Réveillet et al., 2015). However, no studies have been conducted in the Dry Andes. For the Wet Andes, Scheiter et al. (2021) projected an ice volume loss between -56% and -97%, depending on the RCP, in the Mocho Choshuenco glacier until 2100. Regarding the Patagonian icefields, Schaefer et al. (2013) reported a significant increase in ablation from 2050 onwards in the Northern Patagonian Icefield, accompanied by a reduction in solid precipitation from 2080 onwards due to higher temperatures. In a comparison of simulations for the period 2005-2050 with the historical period 1976-2005, Bravo et al. (2021) estimated a larger reduction in mass balance ranging from -1.5 to -1.9 m w.e. $yr^{-1}$ for the Northern Patagonian Icefield, in contrast to the Southern Patagonian Icefield (-1.1 to -1.5 m w.e. $yr^{-1}$).

Table 1 Summary of the global estimations of glacier volume change from 2010 to 2100 in the Tropical and Southern Andes.

| References | Period | RCP | Tropical Andes (low latitudes) | Southern Andes |
|---|---|---|---|---|
| Huss and Hock, 2015 | 2010-2100 | 2.6 | -78 ± 9% | -10 ± 8% |
| | | 8.5 | -98 ± 0% | -44 ± 14%. |
| Marzeion et al. (2012) from Huss et al., 2017 | 2010-2100 | 4.5 | -94 ± 7% | - |
| Giesen and Oerlemans (2013) from Huss et al., 2017 | 2010-2100 | 4.5 | -66 ± 18% | - |
| Radic et al. (2014) from Huss et al., 2017 | 2010-2100 | 4.5 | -82 ± 5% | - |
| Huss and Hock (2015) from Huss et al., 2017 | 2010-2100 | 4.5 | -79 ± 9% | - |
| Rounce et al. (2023) | 2015-2100 | 2.6 | -69 ± 25% | -38 ± 15% |
| | | 8.5 | -98 ± 13% | -68 ± 20% |

## 1.6 Historical and future glacier runoff contribution to the Andean catchments

During the dry season, the melting of glaciers in the region spanning from Peru-Bolivia to central Chile-Argentina plays a vital role as a freshwater source for various purposes such as human consumption, ecosystems, industrial activities and hydropower generation (Masiokas et al., 2013; Soruco et al., 2015; Dangles et al., 2017; Schoolmeester et al., 2018; Ayala et al., 2020). Notably, the hydrological significance of glaciers in the Dry Andes is higher compared to the Wet Andes, which receives abundant precipitation (Masiokas et al., 2019).

Although the estimation of glacier runoff and glacier contributions (volume of streamflow from glaciers related to the total catchment streamflow) has been limited to a few catchments across the Andes, a global study conducted by Huss and Hock (2018) focused on 12 Andean catchments during the period from 1980 to 2099. Until 2020, Huss and Hock (2018) estimated an increase in glacier runoff in the Tropical and Dry Andes. However, in the Wet Andes, some catchments showed no change in glacier runoff, while others experienced either a reduction or an increase. Future projections indicate that glacier runoff (including ice and snow melt as well as rainfall on glaciers) during the austral summer will generally increase in most catchments until 2050, followed by a subsequent reduction in all catchments except the Santa Cruz catchment. Figure 9 shows Peak Water (PW) estimations in 12 catchments. Huss and Hock (2018) identified past PW in the Inner tropics (2 catchments), with a PW between 2011-2046 in the Outer tropics (4 catchments). In the Dry Andes, PW is near 2010 ± 24 (in 2 catchments in western side of Andes), whereas in the Wet Andes, the PW is between 2003 ± 11 to

2096 ± 24 (in 4 catchments). In the Wet Andes the PW occurs in the past across the northern area of this region on both sides of the Andes.

In the Tropical Andes, the annual glacier contribution was estimated to be approximately 12% in the Río Santa catchment (9°S) (Mark and Seltzer, 2003) and around 15% in the La Paz catchment (16°S) (Soruco et al., 2015). In the glacier Zongo catchment, a projected reduction in discharges of about 25% annually and 57% during the dry season under the RCP4.5 scenario is estimated by 2100 (Frans et al., 2015). Moving to the Dry Andes, the Huasco (29°S), Aconcagua (33°S), and Maipo (34°S) catchments exhibited glacier contributions ranging from 3% to 23%, depending on the catchment size (241-4843 $km^2$) (Gascoin et al., 2011; Ragettli and Pellicciotti, 2012; Ayala et al., 2020). In the Wet Andes, larger glaciers have been found to contribute a significant amount of meltwater to the Baker catchment (Dussaillant et al., 2012). However, Huss and Hock (2018) did not observe any significant changes in glacier runoff in this basin between 1980 and 2000.

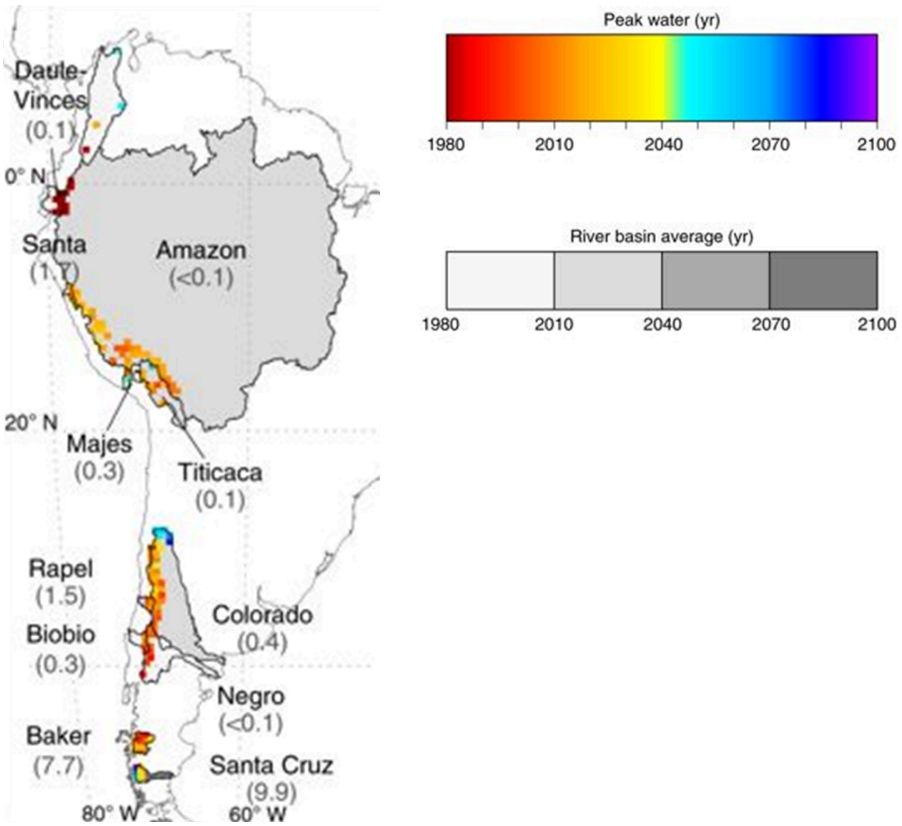


Figure 9. Peak water in 12 Andean glacierized basins throughout the 21st century. Colors show the modeled year of peak water (0.5 × 0.5° grid cells) computed from 11-year moving averages of annual glacier runoff (snow/ice melt and rainfall on glaciers). Peak water is also shown with grey scales for all basins. The results refer to runoff from the initially glacierized area based on a mean of 14 GCMs (RCP4.5). The glacierized surface area in percentage by basin is below the basin names. The figure is taken from Huss and Hock (2018).

# 2. Materials and Methods

This section describes the data, procedure, statistical analysis and simulations carried out during my thesis and used in the three published Articles, a 4th Article in progress to be published (see sections 3.5 and 5.4) and lastly the analysis of geodetic mass balance and glacier area variation, as well as, simulations using the HBV-IANIGLA tool (not considered to be published). The results that are not considered in any of the Articles will be described in more detail in this section (2.1.2.2 and 2.3.2) in comparison with published articles and the last one in progress, because the Articles can be found in Part II.

The subsections are detailed as follows and summarized in Figure 10: i) data and preprocessing: climate, glaciological and hydrological data; ii) statistical methods and data analysis: traditional and machine learning models; and iii) glaciological and hydrological models.

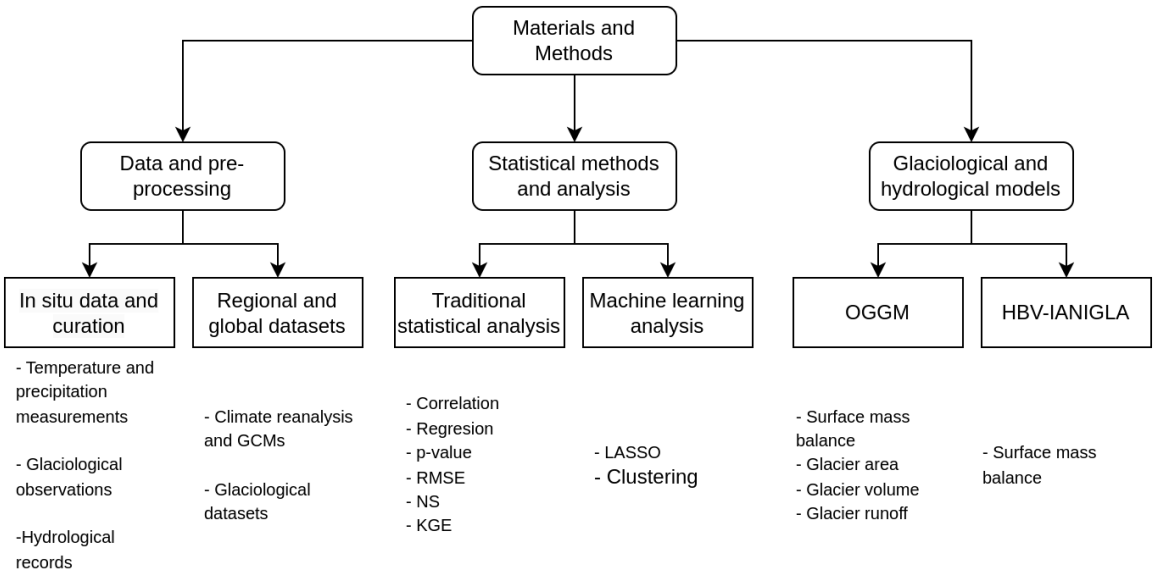


Figure 10. Brief description of materials and methods used in this Thesis to analyze the change in glaciers and glacier runoff across the Andes between 1980 to 2099.

# 2.1 Data and preprocessing

Table 2 exhibits the main data used to analyze and to run the models to know the changes in glaciers and glacier runoff across the Andes. The data and preprocessing are described below.

## 2.1.1 In situ data and curation

### 2.1.1.1 Temperature and precipitation measurements

In situ measurements from 35 meteorological stations were used (Rabatel et al., 2011; MacDonell et al., 2013; Schaefer et al., 2017; CECs, 2018; Shaw et al., 2020; Hernández et al., 2021; CEAZA, 2022; DGA, 2022; GLACIOCLIM, 2022; IANIGLA, 2022; Mateo et al., 2022; Senamhi, 2022). Mean monthly air temperature and precipitation variables were measured in locations near or on glaciers (see Table S1 in Article n°3). These data were used to quantify local vertical annual temperature lapse rates across the Andes, correct the TerraClimate temperature and to evaluate the corrected TerraClimate data of temperature (see Table S2 and Figure S2 in Article n°3). The algorithm was written in the R programming language.

### 2.1.1.2 Glaciological observations

In situ measurements of surface mass balance from 15 monitored glaciers since 2000 were compiled (e.g., Marangunic et al., 2021; WGMS, 2021) (see Table S4 in Article n°3). These data were used to evaluate the simulated mass balance. On the other hand, accumulation data from 10 glaciers (between 5°N to 55°S) were used to correct the precipitation variable from TerraClimate (see datails in Table S4 of Supplementary Information of Article n°3). The precipitation correction considered a match between the standard deviation of the simulated annual mass balance and the standard deviation of the observed mass balance (see Tables S3, S4 and S5 in Article n°3). The algorithm was written in the R programming language.

### 2.1.1.3 Hydrological records

River discharge records were compiled for the La Paz (Soruco et al., 2015), Maipo and Baker catchments (Alvarez-Garreton et al., 2018) located in Bolivia and Chile, respectively. In Article n°3, these records were used to estimate the glacier contribution, considering the glacier runoff simulation only.

## 2.1.2 Regional and global datasets

### 2.1.2.1 Climate reanalysis and global circulation models

TerraClimate dataset

The TerraClimate dataset (TC) (Abatzoglou et al., 2018) were used in all the Articles related to this Ph.D. Thesis. The variables such as mean, maximum, minimum temperatures, precipitation and solar radiation were processed at annual and monthly time-steps for the period 1980-2019 for the Article n°1. For Article n°2, the TC dataset considered monthly variables of mean temperature, maximum temperature, minimum temperature and precipitation (snowfall and rainfall are considered together). The mean temperature and total precipitation were corrected and evaluated (only temperature) in the Article n°3 using in situ data.

Climate reanalysis datasets

Global climate data such as CHIRPS, ERA5-Land and CRU Ts4.0 and regional data like CR2met 2.0 and SENAMHI HSR PISCO were explored and some of them were used to run the glaciological models. However, some dataset were discarded considering following criteria: Latitudinal range, spatial resolution and variables values. For instance, the CR2met 2.0 (Chile and Andean Argentina) and SENAMHI HSR PISCO (Perú) do not extend across the entire Andes, and CHIRPS reaches 50°S (only precipitation). ERA5-Land (0.08°x0.08° lat long) and CRU Ts4.0 (0.5°x0.5° lat long) have an intermean spatial resolution. A quick comparison of the absolute values of the variables (temperature and precipitation) between ERA5-Land and Terraclimate with in situ data in the Dry and Wet Andes, allowed us to choose the TerraClimate data set, since the annual precipitation is better represented than in ERA5-Land, mainly near the Patagonian icefields. In addition, TerraClimate has a high spatial resolution (1/24° lat long, ~4 km).

Global circulation models (GCMs)

Temperature and precipitation in two scenarios of eight GCMs simulations from CMIP6 (see Table S1 in Article n°3) were analyzed, considering the Almazroui et al. (2021) assessment for TerraClimate in South America and the global evaluation of warmer models from Hausfather et al. (2022) and Tokarska et al. (2020). The climate models are: CESM2, FGOALS-f3-L, NorESM2-MM, MPI-ESM1-2-HR, INM-CM4-8, INM-CM5-0, CAMS-CSM1-0 and GFDL-ESM4. The analysis comprises three steps: 1) perform a statistical downscaling of GCMs data for the historical period using the corrected TerraClimate data as a reference; 2) calculate annual, seasonal and monthly metrics to compare the GCMs data and the corrected TerraClimate data for the historical period; and 3) identify the changes in climate variables

between the historical and future periods (Details can be seen in section Data and Methodology of Article n°4 found in section 5.4). The GCMs output data were gathered for each glacier, however, the analysis was performed at the glaciological region scale, where climate characteristics vary substantially (Caro et al., 2021). Details can be seen in Article n°3.

### 2.1.2.2 Glaciological datasets

Glacier inventories

Three types of glacier inventories were used: national glacier inventories, global inventories and multitemporal glacier inventories. In Article n°1, the national glacier inventory version 2015 between 17.6-55.4°S of Chile (DGA, 2015). In Article n°2, the national glacier inventories made by the Andean countries were collected from Perú, Bolivia, Chile and Argentina (ANA, 2014; DGA, 2014; IANIGLA-CONICET and Mayds, 2018). Other inventories were compiled from published studies and the international GLIMS initiative (all inventories are described in Table 1 of Article n°2 found in section 5.2). From the most recent glacier inventories in the Andean countries and the Seehaus et al. (2020) glacier inventory in Bolivia, I merged the national glacier inventories (NGIs) which do not consider rock glaciers and glaciers considered fully debris-covered. In Article n°3, I used the NGIs and the Randolph Glacier Inventory version 6.0 (RGI Consortium, 2017). The RGI v6.0 was filtered using the NGIs, getting a total glacierized surface area of 30943 $km^2$ (filtering 633 $km^2$), and excluding the calving glaciers. Glacier extent in the RGI v6.0 is representative of the early 2000s.

Glacier area variations (GAV) dataset

A multi-temporal glacier surface area dataset was created using the glacier surface area information obtained from the inventories compiled in Article n°2 (see in section 5.2). For each glacier identified in the National Glacier Inventories (NGIs), the linear variation in area between 1980 and 2019 was calculated. The specific criteria used for selecting the glaciers on which this approach was applied can be found in Article n°2, which covers 4865 glaciers across the Andes spanning from 8°S to 55°S for the period from 1950 to 2019.

Following the subsequent procedures, the glacier area variation data (GAV), which is available for some glaciers, was extrapolated to the entire number of glaciers identified in the NGIs based on their glacier area by glaciological zones. Here are the steps involved: i) The glaciers from the NGIs, which encompass all glaciers, were grouped according to their areas into five quintiles (each quintile representing 20% of the glaciers). Within each quintile, the minimum and maximum areas were determined, along with the median area. ii) Glaciers with available GAV data were also grouped based on the area quintiles determined in the previous step. For each quintile of glacier area, the minimum and

maximum areas, as well as the median area, were identified. iii) By considering the distribution of glacier areas across quintiles for all glaciers in the NGIs and the subset of glaciers with GAV data (which represents a smaller number of glaciers), the distribution of area was assessed for each glaciological zone. This evaluation was conducted using Pearson's correlation and mean differences of area (bias). iv) Finally, the GAV data obtained from a subset of glaciers were extrapolated to all glaciers within each glaciological zone, based on the area quintile ranges. This allowed for the estimation of glacier area variations at a broader scale. The algorithms used for these procedures were implemented in the R programming language. For a more comprehensive understanding of the evaluation of GAV at the cluster scale, please refer to section 3.5.

Glacier mass balance (GMB) from elevation differences

The change in glacier surface elevation was collected from Dussaillant et al. (2019) and Hugonnet et al., (2021). In Article n°2, the average glacier-wide annual mass balance for each glacier was recalculated for the period 2000-2018 from Dussaillant et al. (2019). The NGIs (8-55°S) were used to estimate the geodetic mass balance per glacier, considering a cell size ~30×30 m and a glacier ice density of 900 kg $m^3$ (Cuffey and Paterson, 2010). Meanwhile, the Hugonnet et al. (2021) dataset was used in Article n°3 and for the analysis that has not been published to run the HBV-IANIGLA tool. In Article n°3, the Hugonnet et al. (2021) data was used to calibrate the simulated mass balance in the OGGM model. For the analysis that has not been published, the geodetic mass balance to calibrate the surface mass balance simulated in the HBV-IANIGLA tool (GMB, Equation 15) was estimated. This estimation, considering glacier outlines from NGIs, comprises the period January 2000 to December 2019, a weighted surface area of each grid ~100x100 m and a glacier ice density of 900 kg $m^3$ (Cuffey & Paterson, 2010).

$$GMB = \sum_{i=1}^{n} mb_i , \qquad \text{Equation 15}$$

where $mb_i$ is the mass balance in a grid. The GMB uncertainty per glacier was estimated using the random error methodology (Brun et al., 2017), where a 300 m buffer from glacier outlines was considered to estimate the uncertainty on the elevation change related with off glacier ground. The uncertainty on the density is 50 kg $m^{-3}$ (Results in section 3.5). The algorithms were written in the R programming language.

Glacier volume

The global glacier ice thickness product by Farinotti et al. (2019) and based on the mass conservation and shallow ice approximation was used for each glacier of the RGI v6.0. This product ensembled the outputs of five different models to get ice thickness distribution on 215000 glaciers outside the Greenland and Antarctic ice sheets. Farinotti et al. (2019) data allow us to calibrate the parameters of the simulated ice thickness in the OGGM model (see section 2.3.1).

### 2.1.2.3 Glaciological, Meteorological, Hydrological products

For Article n°3 (see section 5.3), the HydroSHEDS catchments level 9 data (Lehner et al., 2006) were compiled. We considered catchments representing >= 0.01 % of glacierized surface area (3236-20 km$^2$, 11°N-55°S). This data was used to compile the simulation of the glacier mass balance, glacier dynamic and glacier runoff at the catchment scale. In addition, these catchments were associated with the glaciological zones described in Article n°2.

Table 2 Summary of in situ and regional/global datasets as well as preprocessing data.

| Name/acronym of data | | Description | Reference |
|---|---|---|---|
| In situ data | Temperature and precipitation | Point measurements in meteorological stations. Monthly mean temperature and total precipitation. Data from 35 meteorological stations located between 9°S to 51°S and 220 to 5300 m a.s.l. | Rabatel et al., 2011; MacDonell et al., 2013; Schaefer et al., 2017; CECs, 2018; Shaw et al., 2020; Hernández et al., 2021; CEAZA, 2022; DGA, 2022; GLACIOCLIM, 2022; IANIGLA, 2022; Mateo et al., 2022; Senamhi, 2022 |
| | Glacier surface mass balance | Measurements in 15 glaciers considering hydrological years since 2000. Glaciers located between 5°N and 55°S | Marangunic et al., 2021; WGMS, 2021 |
| | River discharge records | Point measurements from hydrological stations at monthly time step. Data related to La Paz (16°S), Maipo (33°S) and Baker basin (47°S) between 1990 and 2019 | Soruco et al., 2015; Alvarez-Garreton et al., 2018 |
| Regional and global data | Corrected TerraClimate temperature (cTCp) and precipitation (cTCp) and data without correction | Spatial resolution of 1/24° lat long (~4 km) at a monthly time step. Global data of precipitation and maximum and minimum temperature | Abatzoglou et al., 2018 https://www.climatologylab.org/terraclimate.html |
| | CHIRPS | Spatial resolution of 0.05 lat long at 6-hourly to 3-monthly aggregates time step. Data of precipitation northward 50°S | https://data.chc.ucsb.edu/products/CHIRPS-2.0/ |
| | ERA5-Land | Spatial resolution of 0.1° lat long (~9 km) and monthly time step. Global data of precipitation and mean temperature | https://cds.climate.copernicus.eu/cdsapp#!/dataset/reanalysis-era5-land-monthly-means?tab=form |
| | CRU Ts4.0 | Spatial resolution of 0.5° lat long and monthly time step. Global data of precipitation and mean temperature | https://catalogue.ceda.ac.uk/uuid/edf8febfdaad48abb2cbaf7d7e846a86 |
| | CR2met 2.0 | Spatial resolution of 0.05° lat long (~5 km) at monthly time step. Data of precipitation and mean temperature across the Chile | https://www.cr2.cl/downloads/cr2met/ |
| | SENAMHI HSR PISCO | Spatial resolution of 0.05° lat long (~5 km) at monthly time step. Data of precipitation across the Perú | https://iridl.ldeo.columbia.edu/SOURCES/.SENAMHI/.HSR/.PISCO/index.html?Set-Language=es#info |
| | GCMs from CMIP6 | Different spatial resolutions at monthly time step Global data of precipitation and mean temperature. CESM2, FGOALS-f3-L, NorESM2-MM, MPI-ESM1-2-HR, INM-CM4-8, INM-CM5-0, CAMS-CSM1-0 and GFDL-ESM4 models | https://cds.climate.copernicus.eu/cdsapp#!/dataset/projections-cmip6?tab=form |

| | | | |
|---|---|---|---|
| | National glacier inventories of the Andean countries (NGIs) | Inventories from Perú, Bolivia, Argentina and Chile with information between 2000 to 2015 | ANA 2014; Seehaus et al., 2020; DGA 2014; IANIGLA-CONICET 2018; Zalazar et al., 2020 |
| | Multitemporal glacier inventories | Regional, national and global inventories from Perú, Bolivia, Argentina and Chile with information between 1955 to 2018 | Hidrandina S.A., 1989; INAIGEM, 2018; Soruco et al., 2009; Marangunic, 1979; Caviedes, 1979; Valdivia, 1984; Garín, 1987; Casassa et al., 2002; Möller et al., 2007; Vivero, 2008; DGA, 2011; Rivera & Bown, 2013; Barcaza et al., 2017; García et al., 2017; Malmros et al., 2016; AMTC, 2019; Meier et al., 2018; GLIMS, Raup et al., 2007 |
| | Randolph glacier inventory v6.0 (RGIv6.0) | Global glacier inventory with information close to years 2000-2003 in the Andes | https://www.glims.org/RGI/ |
| | Glacier surface elevation changes and Glacier mass balance | Surface changes in period 2000-2018 (~30×30 m) from Dussaillant et al. (2019) and in period 2000-2019 (~100x100 m) from Hugonnet et al. (2021) | Dussaillant et al., 2019; Hugonnet et al., 2021 |
| | Glacier ice thickness | Data for 215000 glaciers outside the Greenland and Antarctic ice sheets considering glaciers from the RGIv6.0 | Farinotti et al., 2019 |
| | Catchments | Global data from HydroSHEDS level 9 | Lehner et al., 2006 https://www.hydrosheds.org/products/hydrobasins |

# 2.2 Statistical methods and analysis

## 2.2.1 Traditional statistical analysis

Pearson's correlation coefficient and linear regressions were used to estimate the strength and the sign of the relationship between two variables and to predict the value of a variable (or multiple) based on another variable. The variance was used to determine how far each value is from the mean and from every other value of the variable. The statistical significance was checked through the p-value and the data dispersion was estimated using the standard deviation. The ability to predict the target value in linear models (accuracy) was estimated using the root mean squared error (RMSE), and the mean differences between variable values was estimated using the bias. In the glacier runoff, the Nash-Sutcliffe (NS) and Kling-Gupta efficiency scores (KGE) were estimated (Nash and Sutcliffe, 1970; Gupta et al., 2009).

## 2.2.2 Machine learning analysis

This section describes the machine learning method used to identify the explanatory variables of the glacier change and to a group of catchments with similar morphometric and climate variables. The algorithms were written in the R programming language.

#### 2.2.2.1 LASSO

The Least Absolute Shrinkage and Selection Operator algorithm (LASSO) (Tibshirani, 1996) was used in the Article n°2, using as inputs the morphometric (e.g., area and elevation) and climate variables (e.g., monthly precipitation and temperature) by glacier extracted from the national glacier inventories, the TerraClimate dataset, the glacier area variation (GAV, 1980-2019) and the glacier mass balance (GMB, 2000-2018). The LASSO algorithm discarded morphometric and climate variables that do not explain a sufficient amount of variance of the GAV and GMB inside each watershed (n = 274). Here, the root mean square error (RMSE) was used to evaluate the results and the p-value test from the multiple linear regression method to evaluate the statistical significance of the selected variables by the LASSO algorithm.

#### 2.2.2.2 Clustering

The cluster analysis was performed in Article n°1 and n°2 by means of the k-medoids technique using the Partitioning Around Medoids (PAM) algorithm (Kaufman and Rousseeuw, 2008). In Article n°1, the glacier cluster analysis was applied at the glacier scale considering climate and topographical variables of the glaciers, whereas in Article n°2 the clusters were performed using climate and morphometric variables relevant to the glacier change at the catchment scale. In addition, the sensitivity of the watersheds to cluster assignment by the PAM algorithm was evaluated by removing variables (by unit and groups) and by changing the variable values.

## 2.3 Glaciological and hydrological models

Two numerical models were tested to simulate glacier mass balance as well as glacier runoff. We tested the implemented OGGM model (Maussion et al., 2019 ) and the modular HBV-IANIGLA tool (Toum et al., 2021). The principal differences between these models are their modular structure and simulated process. For example, the OGGM model is completely implemented, where calibration procedures are included, conversely, the HBV-IANIGLA tool does not have a modular structure implemented. Regarding the process, OGGM is a glaciological model that simulates mass balance and dynamics, whereas the HBV-IANIGLA is a hydrological tool with a glaciological module that simulates the mass balance only. Despite these differences, due to the hydrological objectives that each model looks to simulate, both models were implemented at the Andes scale, but only the results from OGGM were published (see Article n°3 and n°4 in sections 5.3 and 5.4 respectively).

## 2.3.1 OGGM

The OGGM is a modular and open-source numerical workflow that contains enough input data to simulate glacier mass balance and ice dynamics using calibrated parameter values for each glacier (Maussion et al., 2019). Its temporal configuration is a monthly time step. The required input data are: air temperature and precipitation time series, glacier outlines and surface topography for specific years. From these inputs, annual output like the surface mass balance, glacier volume and area and monthly glacier melt (snow and ice) and rainfall on the glacier can be obtained (Figure 1 in Article n°3 in section 5.1). The workflow consists in using a glacier outline and topography to estimate flow lines and catchments per glacier. Mass balance is estimated using a precipitation phase partitioning and a temperature index approach (Braun and Renner, 1992; Hock, 2003; Marzeion et al., 2012). Assuming a bed shape, it estimates the ice thickness based on mass conservation and shallow ice approximation (Farinotti et al., 2009) per glacier. Then, area, volume and glacier runoff per glacier can be determined. The calibration of mass balance and volume are performed using the Hugonnet et al. (2021) and Farinotti et al. (2019) datasets.

In the Articles n°3 and n°4 the corrected TerraClimate (temperature and precipitation) were implemented, the calibration of simulated mass balance was made for the period 2000-2019 and the evaluations of the simulated mass balance in 15 monitored glaciers (Methodological details can be found in sections 5.3 and 5.4). During the historical period, the OGGM performance was observed and evaluated in several places across the Andes and specifically in the La Paz, Maipo and Baker catchments. In addition, the OGGM performance was tested using the CRU, ERA 5 and CR2met 2.5 as climate forcings in Chilean catchments and specific Andean glaciers. I edited the original OGGM algorithms associated with historical and future climate using the Python programming language, whereas the analysis was performed using the R and Python programming languages.

### 2.3.1.1 Surface mass balance simulation

The mass balance is implemented using a precipitation phase partitioning and a temperature index approach (Braun and Renner, 1992; Hock, 2003; Marzeion et al., 2012). The monthly mass balance ($mb_i$) at an elevation z is calculated as follows:

$$mb_i(z) = TC_{pi}^{snow}(z) * P_f - M_f * max(cTC_{ti}(z) - T_{melt}, 0), \qquad \text{Equation 16}$$

Where $cTC_{pi}^{snow}$ is the TerraClimate solid precipitation before being scaled by the precipitation correction factor ($P_f$), $M_f$ is the temperature of ice/snow melt factor, $cTC_{ti}$ is the monthly corrected

TerraClimate temperature, and $T_{melt}$ is the monthly air temperature above which ice melt is assumed to occur (from 0°C to 2.1 °C). $TC_{pi}^{snow}$ is calculated as a fraction of the total precipitation ($TC_{pi}$) where 100% is obtained if $cTC_{ti}$ <= $T_i^{snow}$ (defined 0°C in the Dry and Wet Andes and 2.1°C in the Tropical Andes) and 0% if $cTC_{ti}$ <= $T_i^{rain}$ (defined 2°C in the Dry and Wet Andes and 4.1°C in the Tropical Andes), using a linear regression between these temperature thresholds to obtain the solid/liquid precipitation fraction. Here, $M_f$ was calibrated for each glacier individually using the previously described glacier volume change datasets (Hugonnet et al., 2021).

### 2.3.1.2 Glacier volume simulation

Here, I describe the ice thickness simulation. The way OGGM estimates the glacier thickness was inspired from Farinotti et al. (2009), where the ice creep parameter (*A or Glen A parameter*) was calibrated using the data of glacier volume provided by Farinotti et al. (2017). OGGM comprises explicitly just the 1st ice process internal deformation, which was described in section 1.4.3.2. In OGGM, the flux of ice ($q$, m$^3$ s$^{-1}$) through a cross section of area $S$ (m$^2$) is estimated like (Maussion et al., 2019):

$$q = uS, \qquad \text{Equation 17}$$

where $u$ is the average velocity (m s$^{-1}$). Using an estimate for $u$ and $q$ obtained from the physics of ice flow and the mass balance, $S$ and the local ice thickness $h$ (m) can be computed relying on some assumptions about the bed geometry. $S$ can be assumed with a parabolic ($S = \frac{2}{3} hw$, where $w$ is the glacier width) or rectangular ($S = hw$) bed shape. Here, a parabolic bed shape is used (Figure 11).

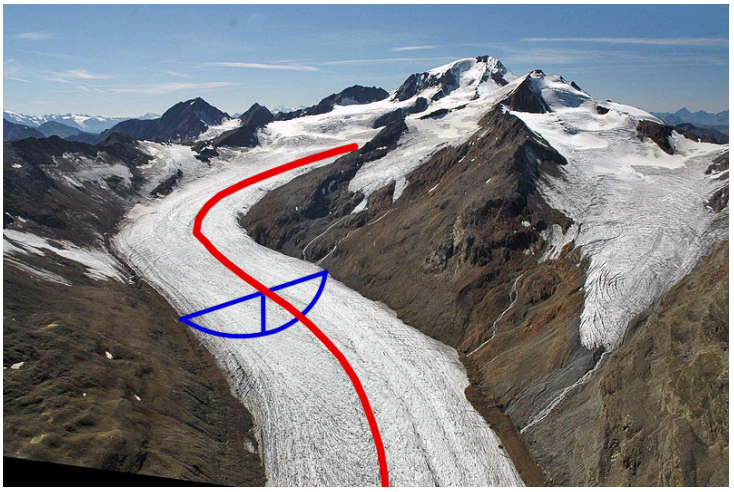

Figure 11. Example of a cross section area and lowline along the Hinereisferner glacier. Reference from OGGM project in Ice dynamics flowline model (default) — OGGM 1.6.1.dev1+ge3eedfe.d20230310 documentation

The depth-integrated ice velocity is estimated using the SIA (Hutter, 1981, 1983) as a function of the basal shear stress ($\tau$):

$$u = u_d + u_s = f_d h\tau^n + f_s \frac{\tau^n}{h}, \quad \text{Equation 18}$$

where $u_d$ and $u_s$ are the ice velocity for ice deformation and basal sliding, respectively, and $n$ is the exponent of Glen's flow law ($n$ = 3). $f_d = \frac{2A}{n+2}$ comprise the shape factor or deformation parameter that represents a fraction of the basal/lateral drag ($c_I$ in Equation 7) and is related to Glen's $A$ parameter (Oerlemans, 1997). Meanwhile, the sliding parameter ($f_d$) which represent the effect of basal water on sliding is not modeled explicitly (Equation 8). $A$ is the ice creep parameter ($s^{-1}$ $Pa^{-3}$) and $\tau$ is the basal shear stress

$$\tau = pgh\alpha, \quad \text{Equation 19}$$

where $p$ is the ice density (900 kg $m^{-3}$), $g$ is the gravitational acceleration (9.81 m $s^{-2}$), and $\alpha$ is the surface slope along the flow line (Maussion et al., 2019).

If it is consider a point on the flow line and the catchment area $\Omega$ upstream of this point, mass conservation implies:

$$q = \int_{\Omega} \left( ḃ - p\frac{\partial h}{\partial t} \right) dA = \int_{\Omega} \bar{b}\, dA, \quad \text{Equation 20}$$

where ḃ is the mass balance (kg $m^{-2}$ $s^{-1}$) and $\bar{b} = p\partial h/\partial t$ is the apparent mass balance from Farinotti et al. (2009). If the glacier is in steady state, the apparent mass balance is equivalent to the actual mass balance (observable). In the non steady state case ∂h/∂t is unknown, it is necessary to integrate (and delay) mass balance $\int_{\Omega} ḃ$ responsible for the flux of ice through a section of the glacier at a certain time (Maussion et al., 2019).

OGGM cannot resolve the transient problem, because of that, a steady state is assumed ($\bar{b} = ḃ$), allowing a direct use of the equilibrium mass balance $\bar{b}\,(t^*)$ satisfying $\int \bar{b} = 0$ (Maussion et al., 2019). Then, the ice flux ($q$) is done by integrating the equilibrium mass balance along the flow line of the glacier. In this process, the tributaries contribute positively to the flux at the last point on their flow

lines, which is then transferred downstream. In the model configuration, $q$ starts at zero and gradually increases along the main flow line, reaching its maximum at the ELA. From there, it decreases towards zero at the glacier tongue (Maussion et al., 2019).

The OGGM is capable of reproducing the volume and related thickness of glaciers, which are sensitive to the value of the creep parameter $A$. Smaller values of $A$ are expected for colder glaciers, as the ice becomes stiffer and the glacier tends to be thicker. Conversely, larger values of $A$ are associated with temperate glaciers, where the ice is softer and the glacier tends to be thinner. A numerical experiment demonstrated that including sliding in the model leads to a significant reduction in thickness because both sliding and the ice rheology parameter ($A$) control the computed ice flux ($q$). On the other hand, incorporating lateral bed stresses in the model results in a decrease in ice velocity and an increase in ice volume (Maussion et al., 2019).

#### 2.3.1.3 Calibration of surface mass balance in OGGM

Surface mass balance is calibrated on a glacier-by-glacier basis using average geodetic observations from January 1 of 2000 to January 1 of 2020, as reported by Hugonnet et al., 2021. Prior to this calibration step, parameters such as precipitation factor, temperature lapse rate, thresholds for solid or liquid precipitation, and temperature for the onset of melting are determined (more details in section Data and methods of Article n°3 in section 5.3). Just the melt factor parameter (Equation 16) is calibrated with the average geodetic observations over the reference period.

The iterative procedure involves the following steps: i) The monthly specific mass balance along the glacier flowlines is estimated, resulting in an annual modeled mass balance. This allows for the determination of specific mass balance at various elevations. ii) The average mass balance is then computed for the entire reference period using the annual mass balance values obtained in the previous step. iii) The average modeled mass balance is compared with the observed mass balance during the reference period. If they match, the melt factor parameter is saved. If they do not match, the monthly specific mass balance is recalculated with a new melt factor parameter value.

#### 2.3.1.4 Calibration of glacier ice thickness in OGGM

Considering Equation 20, when a glacier is in a steady state, the apparent mass balance is equal to the actual mass balance. However, in reality, glaciers are often not in a steady state, and the actual mass balance is not known. To overcome this limitation and continue the analysis, it is common to make the assumption that the glacier geometry is in equilibrium (Maussion et al., 2019). This assumption implies that the glacier is neither advancing nor retreating because the input (accumulation) and output (ablation) of mass are balanced.

To address the challenge of estimating the mass balance when the actual values are not known, OGGM employs a method of creating an artificial mass balance profile. OGGM achieves this by introducing a bias to the mass balance profile observed between 2000 and 2020. The bias is applied in such a way that the specific mass balance becomes zero, aligning with the equilibrium assumption. This approach ensures that the artificial mass balance profile remains physically consistent with the original profile and maintains the overall mass turnover characteristics of the glacier (Maussion et al., 2019).

The inversion factor $f_{inv}$ is a parameter used in the bed inversion procedure, and it represents the only free parameter that requires calibration. Prior to the inversion, several climate and glacier-related parameters are fixed, meaning they are predetermined and not subject to calibration.

$$A = f_{inv} A_0 \qquad \text{Equation 21}$$

Where $A_0$ es the standard creep parameter ($2.4^{-24}$ $s^{-1}$ $Pa^{-3}$). However, the parameter $f_{inv}$, lacks a defined optimum value in the model. There is considerable uncertainty surrounding the true value of $f_{inv}$ and other factors affecting ice thickness. While global sensitivity analyses suggest the default value is reasonable (Maussion et al., 2019), it may lead to overestimated ice volume (Farinotti et al., 2019).

## 2.3.2 HBV-IANIGLA

The HBV.IANIGLA tool developed by Toum et al. (2021) provides a modular and extended implementation of the HBV (Hydrologiska Byråns Vattenbalansavdelning) model (Bergström and Lindström, 2015). Such as HBV, HBV.IANIGLA tool applied to glaciers requires few data inputs (here, air temperature and precipitation). This tool incorporates the glacier mass balance simulation considering accumulation and melting of snow/ice. The modular feature allows an extensive configuration of the spatial and temporal resolution of the simulation, where the first is defined by the modeler and the second by the climate forcing.

The glacier mass balance is estimated using a glacier surface where the precipitation phase partitioning and a temperature-index approach are estimated (Hock, 2003; Braun and Renner, 1992). Precipitation is considered to be snow or rain depending of a temperature threshold ($T_r$ in °C), then its fit through a precipitation factor ($P_f$ , -).,

$$P_{rain/snow} = P * P_f \qquad if \quad T_{air} > T_r \ , \qquad \text{Equation 22}$$

Glacier melting for snow ($M_{snow}$) or ice ($M_{ice}$) in mm $mth^{-1}$, takes into account air temperature ($T_{air}$ in °C), melting temperature threshold for snow and ice ($T_{melt}$ in °C, and melting factors for snow ($M_{f\,snow}$) and ice

($M_{f\ ice}$). If the air temperature is above the threshold ($T_{melt}$), melting occurs at a rate proportional to the melting factor.

$$M_{snow/ice} = (T_{air} - T_{melt}) * M_{f\ snow/ice} \quad \text{if} \quad T_{air} > T_{melt}\ , \qquad \text{Equation 23}$$

These processes allow to obtain the following model output: Liquid and solid precipitation, snow water equivalent, and snow and ice melt.

The implementation of the model involved several steps, starting with the preprocessing of precipitation and temperature variables, as well as glacier area data. Climate variables were collected for each TerraClimate grid cell where a glacier was present, focusing on the centroid of those glaciers. Glacier area data was obtained from Caro et al. (2021). Detailed information on glacier area variation can be found in section 2.1.2.2. The model's time step depended on the input data, which consisted of monthly variables from the TerraClimate dataset. Precipitation phase partitioning and temperature-index parameters were calibrated using random sampling.

The calibration procedure was carried out using the geodetic mass balance (GMB) with mean values of 20 yrs by glacier, as described in section 2.1.2.2. This involved running the model 50000 times with a random combination of melting values for snow/ice parameters ranging from 0 to 600 mm $mth^{-1}$ $°C^{-1}$ and precipitation factor values ranging between 0.5 and 4. The objective was to find a match between the mean simulated mass balance and the mean GMB for each glacier. The match was achieved by minimizing the difference between the mean annual simulated mass balance and the GMB from January 2000 to January 2019. This process resulted in obtaining an optimal simulation and a set of parameter values for mass balance for each glacier. The five calibrated parameters were: precipitation factor ($P_f$), temperature threshold ($T_r$), melting temperature ($T_{melt}$), and melting factors for snow or ice ($M_{f\ snow}$, $M_{f\ ice}$). The procedure consisted of calibrating all the parameters through a Monte Carlo approximation (Shaw et al., 2020), setting the minimum and maximum limits from previously values reported on Andean glaciers (e.g., Fukami & Naruse, 1987; Stuefer et al., 1999; Takeuchi et al., 1995; Rivera, 2004; Condom et al., 2011; Caro, 2014; Huss and Hock, 2015; Bravo et al., 2017). Nevertheless, these investigations took into account various scales, encompassing spatial dimensions ranging from small stakes to larger catchment areas, and temporal aspects ranging from hourly observations to monthly data. Additionally, they utilized different values for the melt factor, both from in situ measurements and fixed values reported in the literature, to characterize the snow and ice melt factor. The workflow algorithm, calibration, and analysis were implemented using the R programming language.

# 3. Results

The four research Articles aim to address the research questions that guide this thesis, specifically investigating the relationship between climate/morphometric variables and glacier changes. These Articles are summarized in Figure 12. Furthermore, the objective is to understand how climate will impact the historical and future changes in Andean glaciers, including their glacier runoff. To achieve this, a variety of datasets (ranging from in situ observations to regional/global products) and methodologies (including machine learning techniques and glaciological-hydrological models) were employed across the Andes region (11°N-55°S). Notably, the study initially explored the capacity of climate and topographic variables to group glaciers in Chile. The findings underscored the importance of considering longitudinal differences among glaciers in the Wet Andes when conducting regional studies. It was further revealed that the monitored glaciers may not serve as representative examples of a larger number of glaciers within the same basin. Subsequently, the analysis was scaled up to encompass the entirety of the Andes, investigating how these climate and morphometric variables are associated with glacier changes during the historical period. This analysis ultimately resulted in the clustering of glacier zones based on the observed relationship between these variables. Subsequently, armed with the knowledge of variables influencing glacier changes in specific glaciological zones in the Andes, I proceeded to simulate glacier changes in historical and future periods. The simulation procedures involved the calibration and evaluation of model parameters and climate inputs during the historical period (2000-2019). In the simulation of future glacier changes, utilizing a calibrated and validated model, I assessed the climate variables derived from various climate models and scenarios of climate change spanning both historical and future periods. Notably, significant disparities in the hydrological response of glaciers were observed when employing climate models that exhibited lower scores.

This section comprises five subsections, corresponding to the main results presented in three published research Articles where I was the first author (sections 3.1, 3.2, and 3.3). Additionally, a fourth section (3.4) is currently being prepared for publication, with me as the primary author. Finally, the results related with the analysis of glacier area variation extrapolation and geodetic mass balance using the NGIs, as well as, the simulation of glacier mass balance using the HBV.IANIGLA tool are presented in the fifth section (3.5).

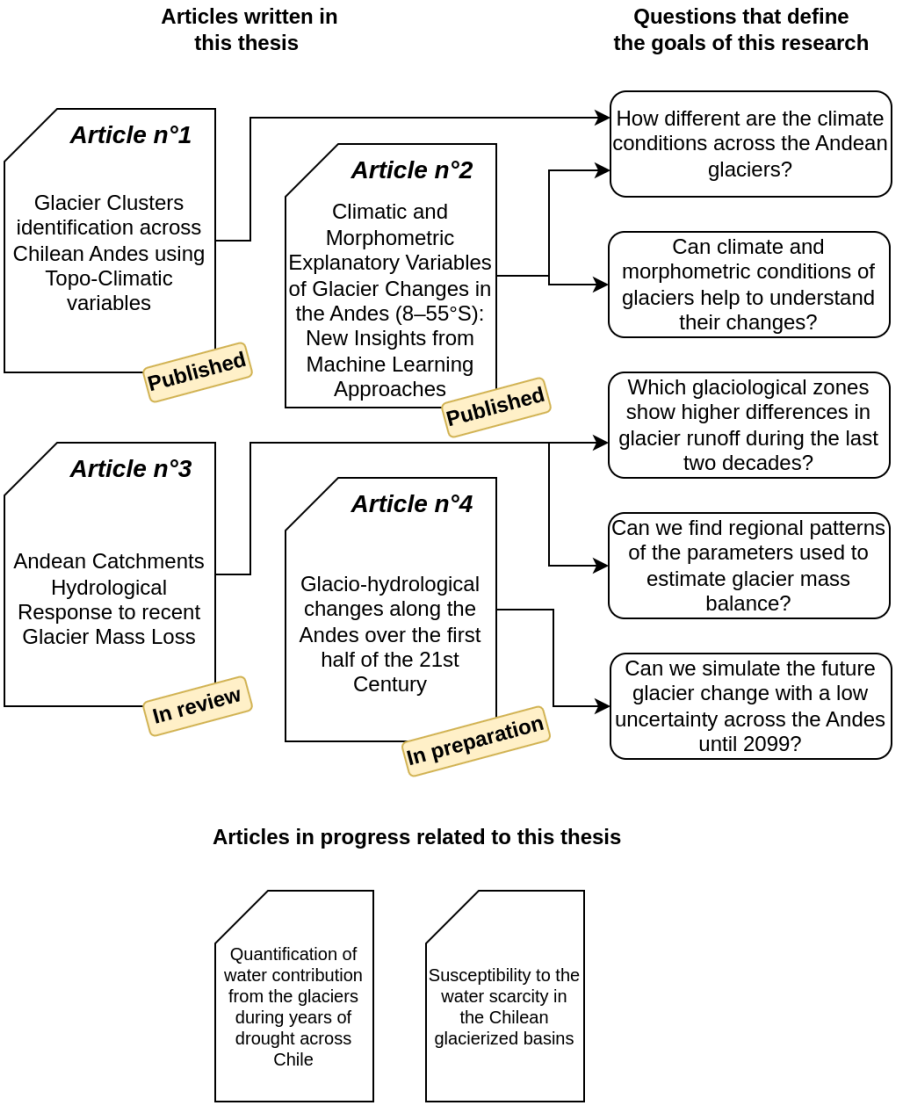


Figure 12. Summary of Articles in this thesis and their relation to the guiding research questions

# 3.1 Glacier Clusters identification across Chilean Andes using Topo-Climatic variables

## *Entire Article n°1 in section 5.1*

### 3.1.1 Abstract of Article n°1

Using topographic and climatic variables, we employed the Partitioning Around Medoids (PAM) unsupervised machine learning algorithm to identify clusters of glaciers in the Chilean Andes (17.6-55.4°S). The analysis yielded 23974 glaciers classified into thirteen distinct clusters, each

exhibiting specific conditions related to annual and monthly precipitation, temperature, and solar radiation. Within the Dry Andes region, the average annual values of precipitation and temperature exhibited notable differences among the five glacier clusters (C1-C5), with variations of up to 400 mm $yr^{-1}$ (between 29 and 33°S) and 8°C (at 33°S), respectively. Additionally, there was an average elevation contrast of 1800 m between glaciers in the C1 and C5 clusters, spanning from 18 to 34°S. In the Wet Andes, the most significant discrepancies were observed around the latitude of the Southern Patagonia Icefield (50°S). In this area, the mean annual precipitation values ranged from above 3700 mm $yr^{-1}$ (C12) in the western, more influenced by maritime air masses, to below 1000 mm $yr^{-1}$ in the eastern side of the Southern Patagonia Icefield (C10). These clusters exhibited temperature variations of approximately 4°C and a mean elevation contrast of 500 m. This classification underscores the fact that Chilean glaciers cannot be solely categorized based on latitude. These findings contribute to a better understanding of recent regional-scale changes in glacier volumes.

### 3.1.2 Glacier cluster identification

The Chilean Andes, spanning from 17.6 to 55.4°S, contain 23974 glaciers with distinct climatic and topographic characteristics. Moving southwards, there is an increase in mean annual temperature and precipitation, accompanied by a decrease in elevation and expansion of the glacier surface area. The Dry Andes (north of 35°S) (Lliboutry, 1998) exhibit colder and drier conditions with higher elevations, while the Wet Andes (south of 35°S) experience higher temperatures, greater precipitation, and lower elevations.

By employing the PAM method and Silhouettes cluster optimization, thirteen glacier clusters were identified based on topo-climatic variables. In the Dry Andes (C1-C5) and Wet Andes (C6-C13), five and eight glacier clusters were identified, respectively, with a boundary near 37°S. The results revealed that the first two Principal Component Analysis (PCA) explain 84% of the shared variance among the variables (PCA1: 67.2%, PCA2: 16.6%). The first PCA component showed a strong correlation with mean elevation ($r = -0.86$) across all variables, followed by the maximum mean annual temperature ($r = 0.76$) and mean maximum temperature of January ($r = 0.60$).

Regarding the glacier surface areas within the identified glacier clusters, the C1-C4 zone (18.1-34.2°S; Desert Andes and part of the Central Andes) exhibited a strong relationship with precipitation (95.3%) and minimum elevation (4.7%), explaining 98% of the variance. In contrast, for the C6-C9 zone (41.9-48.2°S; Lakes District to South Patagonia), 95% of the variance was explained by latitude (90%) and solar radiation (10%). The glacier surface area variance within the C11-C13 zone (49.2-54.6°S; South Patagonia) could be attributed to precipitation (99%). The C5 and C10 glacier clusters, located

between these three zones (C1-C4, C6-C9, and C11-C13), are considered transitional zones as they do not fit well within the other clusters.

### 3.1.3 Glacier cluster overlaps

Figure 13 exhibits the distribution of the thirteen glacier clusters at the glacier scale showing both latitudinal and longitudinal overlaps. By analyzing the number of glacier bodies associated with the latitude quartiles (25-75%) for each cluster, it is possible to identify a latitudinal distribution of glaciers with topo-climatic similarities that do not overlap northward of 31°S. Previous studies have utilized these topo-climatic similarities to define glaciological zones across Chile (Barcaza et al., 2017; Dussaillant et al., 2019; Lliboutry, 1998; Masiokas et al., 2009; Sagredo & Lowell, 2012). However, the differentiation of glacier clusters based on latitude becomes less clear southward of 31°S. In general, these studies identified between four to seven glaciological zones across Chile, with an aggregation into the Dry and Wet Andes and a boundary between 35-36°S. For instance, Lliboutry (1998) established the initial identification of glaciological zones in Chile, while Sagredo and Lowell (2012) identified zones based on climatic characteristics using a smaller number of glaciers (<234 glacier bodies). From north to south, they distinguished the following zones: Desert Andes (17 to 27-32°S), Central Andes (27-32 to 35-36°S), Lakes District (35-36 to 41-46°S), North Patagonia (41-43 to 44-48°S), South Patagonia (46-48 to 52-53°S), and Tierra del Fuego (52-53 to 56°S).

### 3.1.4 Utility of cluster-based spatial analysis

The Echaurren Norte glacier (33.6°S, 70.1°W) in Central Chile is a reference glacier due to its extensive record of mass balance measurements in the Southern Hemisphere since 1976 (Masiokas et al., 2016; Zemp et al., 2019). Over the years, it has exhibited a negative cumulative mass balance since 1955. However, this mass loss appears to be greater than that observed in other glaciers within the watershed, which could be attributed to the heterogeneity of climate conditions and of glacier size encountered within the Maipo watershed (Ayala et al., 2020; Farías-Barahona et al., 2019, 2020b). In our analysis, the glaciers within the Maipo watershed are divided into three clusters (C3, C4, and C5) and demonstrate significant variations in precipitation and temperature. The Echaurren Norte glacier is located in the C5 cluster (mean elevation 3259 m a.s.l.), characterized by the smallest glacierized surface area (5%), the warmest and wettest climate conditions (mean temperature of 3.1°C and annual precipitation of 574 mm), and the highest proportion of rock glaciers within the Maipo basin (68%). These findings indicate that the Echaurren Norte glacier does not represent the typical characteristics of the glaciers within the Maipo watershed.

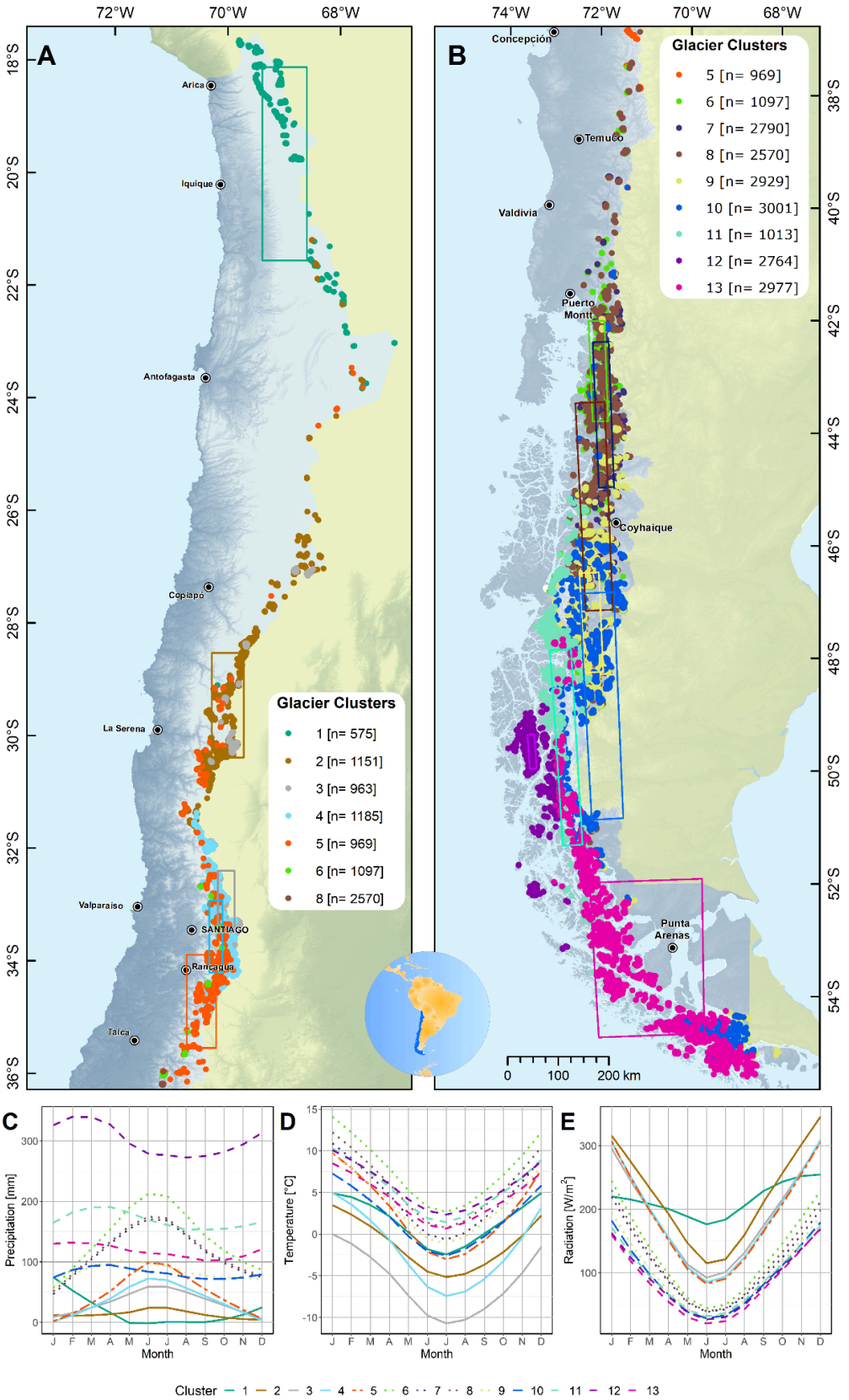


Figure 13. Glacier clustering distribution across Chile and climograms. The Chilean glacier's location is associated with a cluster through points (color palette), where the concentration in latitude and longitude ranges (Q1-Q3) of these is represented by rectangles in the Dry Andes (A) and the Wet Andes (B). The three plots below show from left to right the average monthly distribution between 1980-2019 of precipitation (C), temperature (D) and solar radiation (E) associated with each cluster.

### 3.1.5 Conclusions of Article n°1

The utilization of topo-climatic variables derived from 23974 glaciers in the Chilean Andes (17.6-55.4°S) has facilitated the identification of thirteen distinct glacier clusters characterized by unique climatological conditions. These clusters exhibit variations in annual mean temperature, precipitation, and solar radiation from north to south, showcasing diverse annual regimes. This novel classification of glacierized zones in Chile, utilizing the globally validated TerraClimate dataset and comparing it with previous national studies, has revealed that a purely latitudinal classification based on a limited number of glaciers does not accurately represent the diversity of Chilean glaciers. This is primarily due to a substantial overlap of climate regimes along the latitudinal gradient. For instance, in the Central Andes, multiple glacier clusters are associated with variations in elevation, while in the Patagonian region, glacier clusters are distributed longitudinally, where the wet Western air plays a key role in the maritime to continental precipitation regimes. The identification of these glacier clusters contributes to a regional understanding of the dominant meteorological factors influencing glacier mass balance. Furthermore, it highlights the potential association of monitored glaciers with others found within the same cluster, in contrast to the observed low representativeness of the Echaurren Norte glacier in the Maipo basin. This improved understanding of glacier distribution and climatic influences will be useful in the implementation of studies in glacierized watersheds.

## 3.2 Climatic and Morphometric Explanatory Variables of Glacier Changes in the Andes (8–55°S): New Insights from Machine Learning Approaches

## *Entire Article n°2 in section 5.2*

### 3.2.1 Abstract of Article n°2

In recent decades, glaciers in the Andes have experienced significant mass loss, posing risks of water scarcity for the local population and ecosystems. However, there is limited documentation regarding the factors influencing glacier changes at a watershed scale across the Andes. To address this gap, we utilized machine learning techniques, specifically the Least Absolute Shrinkage and Selection Operator (LASSO), to examine the climatic and morphometric variables that explain spatial variations in glacier surface area and mass balances. Our study analyzed data from 2500 to 21000 glaciers distributed between 8 and 55°S, encompassing 35 watersheds for surface area variations (1980-2019) and 110 watersheds for mass balance variations (2000-2018). Through the application of the Partitioning Around

Medoids (PAM) algorithm, we also identified new glacier zones (clusters). Our findings highlight the dominant role of climatic variables in explaining spatial variances in glacier changes, with precipitation variability exhibiting a stronger explanatory power than morphometric variables from the Outer Tropics to the Dry Andes (8-37°S), accounting for 49 to 93% of the variances. Conversely, in the Wet Andes (40-55°S), temperature variability emerges as the most important climatic variable, explaining 29 to 73% of glacier changes' spatial variance. However, it is worth noting that morphometric variables, such as glacier surface area, exhibit significant explanatory power for spatial variances in glacier mass loss in certain watersheds, such as Achacachi in the Outer Tropics ($r^2$ = 0.6) and Río del Carmen in the Dry Andes ($r^2$ = 0.7). As a result of our clustering analysis, we propose a novel spatial framework for hydro-glaciological analysis consisting of 12 glaciological zones. This framework incorporates the diverse seasonal climate and morphometric characteristics of glaciers and encompasses 274 watersheds with 32000 glaciers. Our study underscores the utility of exploring variables controlling glacier changes and utilizing the derived glaciological zones for hydro-glaciological modeling across the Andes (8-55°S). These insights contribute to a better understanding of the complex dynamics of Andean glaciers and their implications for water resources in the region.

### 3.2.2 Glacier changes in the Andes between 8-55°S

At the regional scale, our study estimated the mean glacier mass balance (GMB) as -0.82 ± 0.12 m w.e. $yr^{-1}$ (2000-2018) and the glacier area variation (GAV) as -31.2 ± 2% (1980-2019). Our GMB estimation aligns closely with the findings of Dussaillant et al. (2019), who reported a GMB of -0.72 ± 0.22 m w.e. $yr^{-1}$ (2000-2018) for the entire Andes. However, our estimate is more negative compared to the estimate of Braun et al. (2019) at -0.61 ± 0.07 m w.e. $yr^{-1}$ (2000-2015). These differences can be attributed to variations in the glacier inventories used for quantifying mass balance through elevation differencing and calculations. Based on the recent study by Minowa et al. (2021), it has become evident that we have underestimated the mass balance, particularly in the Southern Patagonian Icefield. In this region, calving contributes to nearly half of the total mass loss (Minowa et al., 2021).

Regarding GAV, the Desert Andes (-53 ± 0.002%) and the Lakes District (-52 ± 0.1%), which encompass smaller glacierized areas, exhibited the highest levels of glacier shrinkage. Our estimates of glacier shrinkage surpass those reported by Rabatel et al. (2011) at -29% over the 1955-2007 period in the Desert Andes and Paul and Mölg (2014) at -25% over the 1985-2011 period in the Lakes District. However, it is important to note that the differences can be attributed to variations in the study periods, and our inclusion of the decade 2010-2020, during which glacier loss in these regions intensified (Dussaillant et al., 2019).

South of 42°S, the mean GAV estimated in our study (-24 ± 0.4% to -32 ± 1.3%) exceeded the observations of Meier et al. (2018) at -9 ± 5% over the period 1986-2016. This divergence can be attributed to differences in study periods and our exclusion of large calving glaciers in the Patagonian icefields, where we encountered inconsistencies in glacier outlines, particularly in the accumulation zones. These calving glaciers constitute up to 13% of the total glacier area in South Patagonia and 20% in North Patagonia. While we acknowledge methodological limitations that precluded the assessment of glacier growth, the impact of this exclusion is expected to be minimal given the numerous studies documenting a general trend of glacier retreat across the Andes. Only a few exceptions, reporting glacier growth, have been documented (Hata and Sugiyama, 2021; Rivera and Casassa, 1999; Wilson et al., 2016) in comparison to the wealth of studies describing glacier shrinkage (e.g., Malmros et al., 2016; Meier et al., 2018; Paul & Mölg, 2014; Rabatel et al., 2011; Rivera and Bown, 2013; Seehaus et al., 2019, 2020).

### 3.2.3 Main controls of glacier changes

Figure 14 presents the explanatory variables of glacier changes across the Andes (8–55°S) since 1980. At the watershed scale, we found that climate variables have the highest explanatory power for the spatial variances of glacier area variation (GAV, $r^2$ = 0.5) and glacier mass balance (GMB, $r^2$ = 0.4) in the Andes (8-55°S). On average for the entire study region, climate variables account for more than 65% of the spatial variances in GAV and GMB (> 35% for temperature), while surface area is the most relevant morphometric variable (> 16%). There is a latitudinal boundary between 37.5°S (DA3 in Argentina) and 39.9°S (WA2 in Chile), where precipitation and temperature exhibit differential explanatory capacity for GAV and GMB spatial variances across the Andes. Precipitation plays a significant role in explaining GAV and GMB spatial variances (ranging from 49% to 93% depending on the clusters) in the Outer Tropics and the Dry Andes (8-37°S), while the temperature becomes the most relevant climate variable (explaining between 29% and 73% of spatial variance depending on the cluster) in the Wet Andes (40-55°S).

The influence of precipitation on GMB variability has been observed in previous studies based on in situ glacier monitoring, such as Favier et al. (2004) and Wagnon et al. (2001) in the Outer Tropics. Sicart et al. (2003, 2011) have highlighted the importance of precipitation frequency and intensity in modulating ablation during the transition season, which impacts glacier surface albedo. In the Dry Andes, studies by Rabatel et al. (2011), Masiokas et al. (2016), and Kinnard et al. (2020) have emphasized the sensitivity of GMB to precipitation. Our findings also indicate that glacier surface area significantly contributes to the variance in GMB (49% in DA1) in agreement with Rabatel et al. (2011), who demonstrated a more negative GMB for smaller glaciers in the Desert Andes compared to moderate mass loss for larger

glaciers. In the Wet Andes, specifically in the Patagonian icefields, temperature emerges as the main controlling factor for spatial variances in glacier changes (WA3 to WA6). This is consistent with the findings of Abdel Jaber et al. (2019), who attributed the mass loss in the Northern Patagonia Icefield to higher temperatures. In areas outside the Patagonian icefields to the east (WA4), glacier shrinkage can be attributed to temperature increase, as no significant change in precipitation was observed from 1979 to 2002 (Masiokas et al., 2015). Additionally, Falaschi et al. (2019) identified a strong correlation between GMB and temperature in Monte San Lorenzo from 1958 to 2018, particularly during the October to March period (r = -0.86).

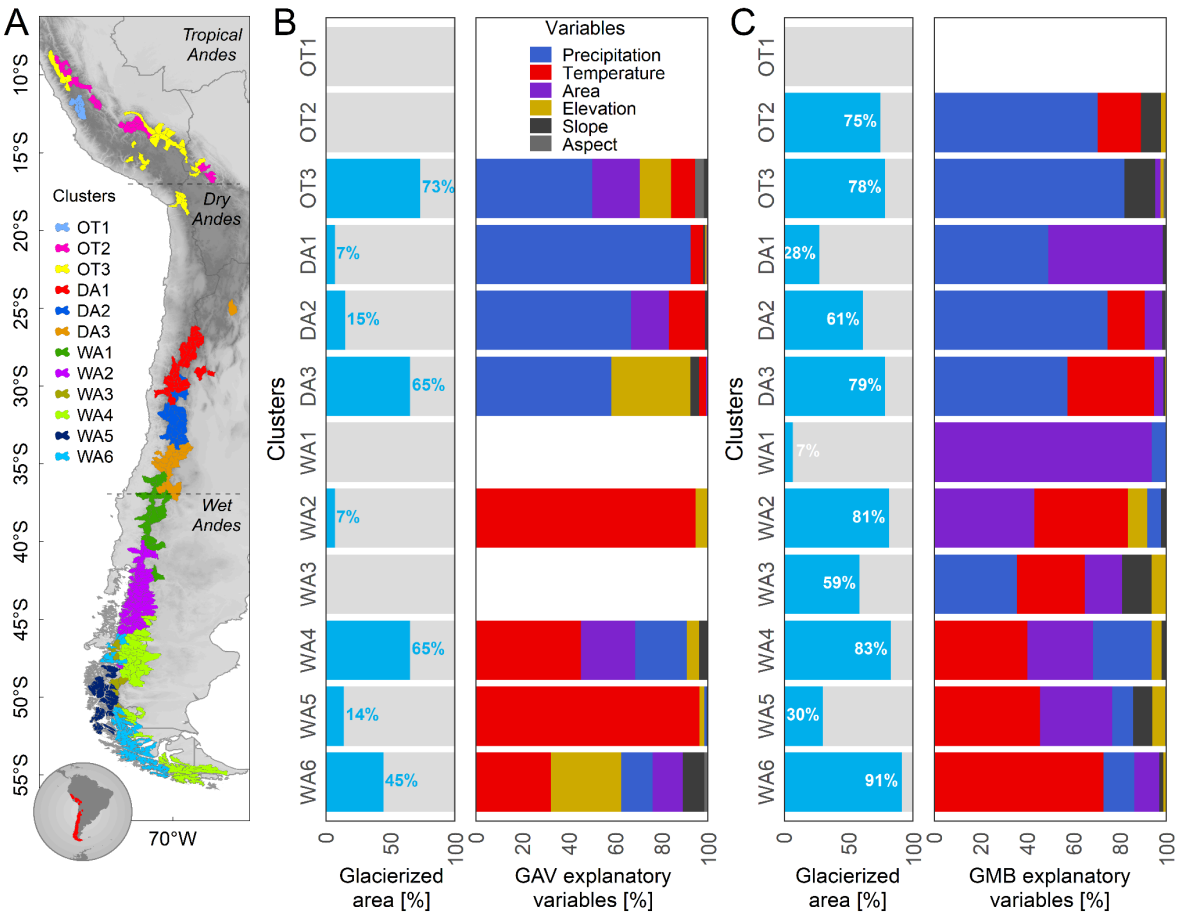


Figure 14. Explanatory variables of glacier changes across the Andes (8–55°S) since 1980 at watershed scale. (A) The 274 glacierized watersheds inside 12 clusters are shown on the map of South America. The glacierized area considered in estimates of the (B) GAV (1980–2019) and (C) GMB (2000–2018) explanatory variables (light blue bars) are shown with regard to the percentage of explanatory variables for the GAV and GMB spatial variances (blank spaces are due to a lack of data in that cluster).

## 3.2.4 Clusters without a latitudinal distribution across the Andes

We utilized morphometric and climatic variables associated with GMB data for 20740 glaciers and GAV data for 2484 glaciers to propose a new classification comprising 12 clusters, encompassing a total of 274 watersheds and 31963 glaciers between 8 and 55°S (Figure 15). This regional identification was

based on the primary explanatory variables of glacier changes (GAV and GMB). Previously, only one type of classification for glacier environments based on latitudinal ranges had been employed, initially by Troll (1941) and Lliboutry (1998), followed by recent studies (e.g., Barcaza et al., 2017; Dussaillant et al., 2019; Masiokas et al., 2009, 2020; Zalazar et al., 2020). Sagredo & Lowell (2012) proposed another glaciological classification with nine zones between 8 and 55°S, which was solely based on climate variables and encompassed a small number of glaciers (n < 234). In this study, the clusters provide a more detailed classification, allowing for better consideration of regional-scale diversity in glacier characteristics and evolution. For instance, glaciers on volcanoes in northern Chile and western Bolivia are no longer associated with the Dry Andes but are clustered with those of the Outer Tropics (OT3). Moreover, watersheds located at the same latitude sometimes belong to different clusters. These findings are consistent with Ayala et al. (2020), who observed significant differences (GMB, runoff contribution, and glacier elevation) between the southern (DA2) and northern (DA3) watersheds within the Río Maipo basin. Our results also indicate that a latitudinal classification is not feasible for the Outer Tropics and the Wet Andes, which aligns with previous studies (e.g., Caro et al., 2020; Sagredo and Lowell, 2012). Southward of 46°S, we identified distinct clusters from west to east, reflecting the pronounced contrast in precipitation and temperature (WA3 to WA6), which are associated with the moist air masses originating from the Pacific Ocean (Langhamer et al., 2018). Studies on the Patagonian icefields have demonstrated this substantial difference in precipitation between the western and eastern sides of the cordillera (Barcaza et al., 2017; Bravo et al., 2019; Warren, 1993).

The sensitivity analysis revealed that the exclusion of the variables Tmax and precipitation led to a reconfiguration of cluster assignments for each watershed. However, the removal of morphometric variables and Tmin did not result in significant changes in these assignments.

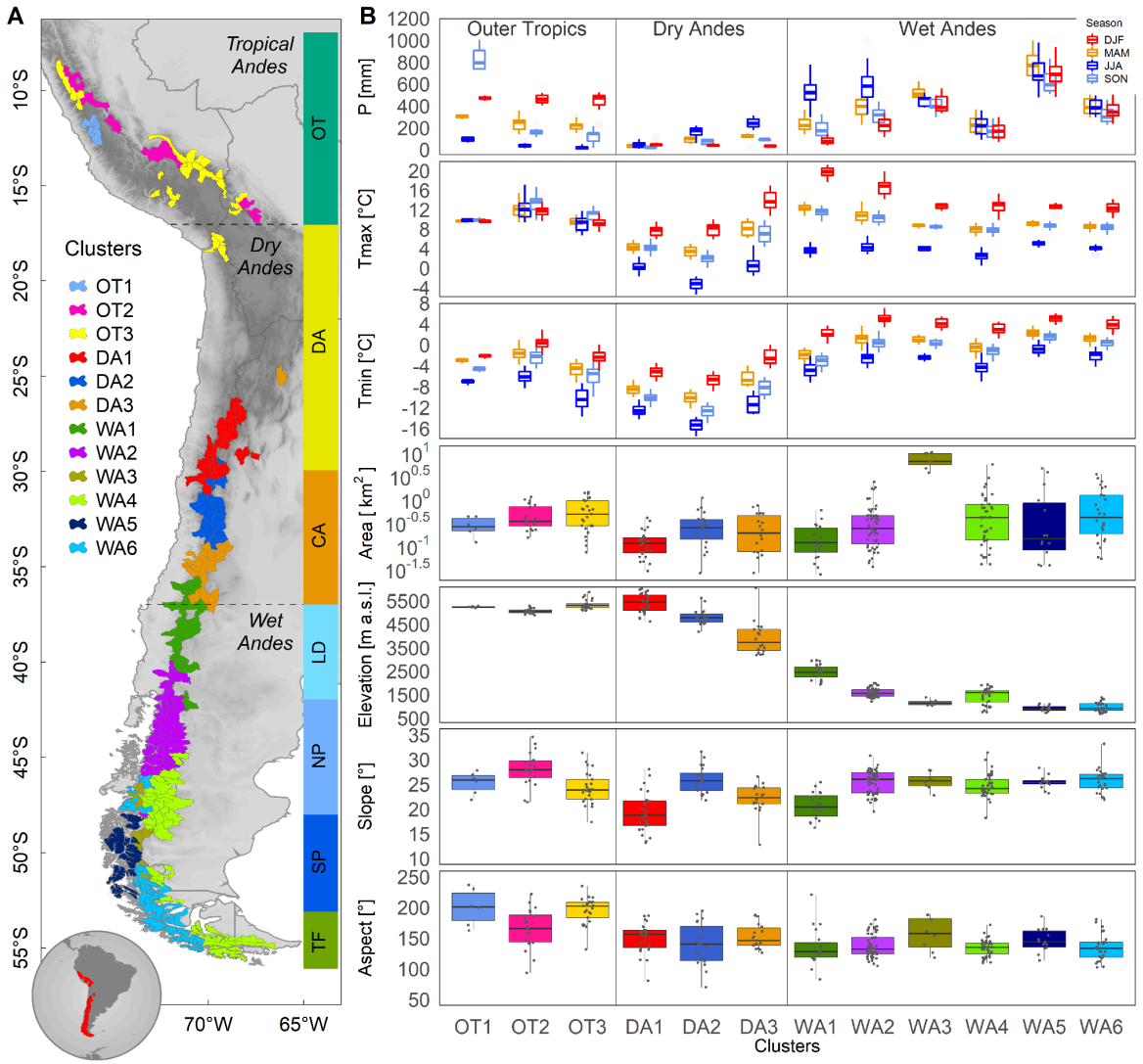


Figure 15. The 12 clusters of the glacierized watersheds across the Andes (8–55°S) and the behavior of climatic and morphometric variables. The average values of variables (for 274 watersheds and using 31963 glaciers) are presented for the 12 clusters identified (through PAM algorithm) using the GAV and GMB explanatory variables (through LASSO algorithm). These clusters are found in three regions: Outer Tropics (OT; 8–17°S), Dry Andes (DA; 17–37°S) and Wet Andes (WA; 37–55°S). (A) shows the cluster distribution across the Andes and the classic zones, from north to south are: Outer Tropics (OT; 8–17°S), Desert Andes (DA; 17–30°S), Central Andes (CA; 30–37°S), Lakes District (LD; 37–42°S), North Patagonia (NP; 42–48°S), South Patagonia (SP; 48–53°S) and Tierra del Fuego (TF; 53–55°S). (B) presents the climatic variables (1980–2019) which are grouped into the summer (DJF), autumn (MAM), winter (JJA), and spring (SON) seasons for the Southern Hemisphere. The total precipitation and the mean extreme temperatures are shown here. Additionally, morphometric variables associate with the glacierized area are shown (i.e., surface area, elevation, slope, and aspect). In blox plots the 25th, 50th and 75th percentiles are estimated.

## 3.2.5 Conclusions of Article n°2

This study represents the first attempt to investigate the relationship between climatic and morphometric variables and the spatial distribution of glacier changes across the Andes (8-55°S) using a machine learning approach. Specifically, we examined variations in glacier surface area since 1980 and surface mass balance changes since 2000. Employing a linear machine learning method, our findings indicate

that the primary factors influencing the spatial variability of glacier changes are precipitation patterns from the Outer Tropics to the Dry Andes (8-37°S) and temperature variations in the Wet Andes (40-55°S).

Our analysis, conducted at the watershed scale, has enabled us to identify 12 distinct glaciological zones through a clustering analysis. This approach provides more detailed information compared to the traditional zones based solely on latitude ranges.

Based on the observed increase in temperature-driven glacier changes and the decrease in precipitation-driven glacier changes from the Outer Tropics to the Wet Andes, we draw the following conclusions:

- The reduction in annual precipitation and alterations in monthly distribution are expected to have a more pronounced impact on glacier mass loss in the Outer Tropics and the Dry Andes, as compared to the Wet Andes. Conversely, changes in monthly temperature are likely to play a more significant role in simulating glacier mass loss in the Wet Andes.

- The newly established glaciological zones provide valuable guidance for conducting glacier change simulations, taking into account the key variables that govern Glacier Area Variations (GAV) and Glacier Mass Balance (GMB) across the Andes. For instance, in regional studies spanning from the Dry Andes to the Wet Andes, the precipitation and temperature relevance identified in this study can be effectively utilized to estimate mass balance. This can be achieved by incorporating precipitation and ice melt factors derived from various studies (e.g., Ayala et al., 2020; Bravo et al., 2017; Caro, 2014; Farías-Barahona et al., 2020; Huss and Hock, 2018; Masiokas et al., 2016). By employing our results, future regional hydro-glaciological simulations at the watershed and zones spatial scales across the Andes can be guided appropriately.

## 3.3 Andean Catchments Hydrological Response to recent Glacier Mass Loss

## *Entire Article n°3 in section 5.3*

### 3.3.1 Abstract of Article n°3

The impacts of the accelerated glacier retreat in recent decades on glacier runoff changes are still unknown in most Andean catchments, increasing uncertainties in estimating water availability. This

particularly affects the Outer Tropics and Dry Andes, heavily impacted by prolonged droughts. Current global estimates overlook climatic and morphometric disparities among Andean glaciers, which significantly influence simulation parameters. Meanwhile, local studies have used different approaches to estimate glacier runoff (sum of the melting snow/ice and rainfall on the glacier) in a few catchments. Improving the accuracy in 21$^{st}$ century glacier runoff projections hinges on our ability to calibrate and validate the models on the basis of corrected historical climate inputs and calibrated parameters across diverse glaciological zones. Here, we simulate glacier evolution and related glacier runoff changes between 2000 and 2019 in 786 Andean catchments from Colombia to Tierra del Fuego (11,282 km$^2$ of glacierized area, 11°N-55°S) using the Open Global Glacier Model (OGGM). We also emphasize on climate correction, parameters calibration, and results evaluation within the workflow simulation. Our homogeneous methodological framework across the Andes considers the diverse glaciological zones in the Andes. The atmospheric variables from the TerraClimate product were corrected using *in situ* measurements, underlining the use of local temperature lapse rates. Meanwhile, the glacier mass balance and volume were calibrated glacier-by-glacier. Furthermore, procedures by glaciological zones allow us to correct mean temperature bias up to 2.1°C and increase the amount of monthly precipitation. The related calibrated parameters, such as melt factor (for mass balance) and Glen A (for ice thickness), show strong alignment with cold/warm and dry/wet environmental conditions. The simulation results were evaluated with *in situ* data in three documented catchments (glacierized surface area > 8%) and on monitored glaciers. Our results at the Andes scale show that the glacier volume and surface area were reduced by 8.3% and 2.2%, respectively, between the periods 2000-2009 and 2010-2019. The glacier loss during these periods is associated with a decrease in precipitation (9%) and an increase in temperature (0.4 ± 0.1°C). Comparing these two periods, glacier and climate variations have led to a 12% increase in mean annual glacier melt (86.5 m$^3$/s) and a decrease in mean annual rainfall on glaciers of -2% (-7.6 m$^3$/s) across the Andes, both variables compose the glacier runoff. The results at the catchment scale indicate glacier runoff contribution in agreement with previous studies in the Maipo catchment (34°S, Chile). However, we suggest that the largest glacier runoff contribution in the La Paz catchment (16°S, Bolivia) is found during the transition season. Additionally, we calculated for the first time the glacier runoff contribution in the Baker catchment (47°S, Chile). In summary, our calibrated and validated modeling approach, organized by glaciological zones and based on our local understanding, utilizing the same methodological approach, stands as a crucial requirement for simulating future glacier runoff in the Andes.

### 3.3.2 Climate and simulated mass balance evaluation

Our evaluation of the corrected TerraClimate dataset demonstrates statistical significance (p-value < 0.01) at 32 meteorological stations. The mean temperature bias is 0.4°C, indicating a slight overestimation, and the mean correlation is 0.96, indicating a strong agreement with observed data. However, it is important to note that in the Tropical Andes, there is a larger bias with a mean of 2.1°C observed at four stations. In contrast, the Wet Andes and Dry Andes exhibit the lowest bias of 0.2°C, with the mean monthly temperature amplitudes well reproduced in most stations. Regarding the evaluation of simulated mass balance, we compared it to in situ data from 15 monitored glaciers. The in situ data indicate a mean negative mass balance of -832 ± 795 mm w.e. $yr^{-1}$ between 2000 and 2019, which is greater than our mean simulated mass balance of -647 ± 713 mm w.e. $yr^{-1}$ for the same glaciers. The evaluation results yield a mean correlation of 0.67, indicating a moderate correlation, and the mean simulated mass balance underestimates the observed values by 185 mm w.e. $yr^{-1}$ (bias). However, it is worth noting that 40% of the glaciers exhibit a correlation equal to or greater than 0.7, indicating a stronger agreement between simulated and observed mass balance for these specific glaciers.

### 3.3.3 Glaciological and glacier runoff changes across the Andes during the period 2000-2019

In our study, we focused on 36% of the total glacierized surface area across the Andes, which encompasses 85% in the Dry Andes, 79% in the Tropical Andes, and 29% in the Wet Andes (excluding calving glaciers). We conducted simulations at a monthly time scale to assess annual mass balance, glacier dynamics, glacier area, glacier volume, and glacier runoff (including glacier melting from snow and ice, as well as rainfall on glaciers).

Analyzing climate change between the periods 2000-2009 and 2010-2019 across the Andes, we observed a cumulative decrease in precipitation of -9% (-234 mm $yr^{-1}$) and a mean annual temperature increase of 0.4 ± 0.1°C. Specifically, precipitation showed a significant decline in the Dry Andes (-256 mm $yr^{-1}$; -23%) and Wet Andes (-337 mm $yr^{-1}$; -9%), while it increased in the Tropical Andes (44 mm $yr^{-1}$; 5%). The temperature experienced an increase ranging from 0.3 to 0.4°C across all regions. During the same time period, the Andean catchments exhibited a reduction in glacier volume by -8.3% (-59.1 $km^3$) and a decrease in glacier area by -2.2% (-245 $km^2$), accompanied by a negative mean annual mass balance of -0.5 ± 0.3 m w.e. $yr^{-1}$. In Figure 16 are shown the largest loss in glacier volume (-47.8 $km^3$, -9%) occurred in the Wet Andes, followed by the Tropical Andes (-5.9 $km^3$, -7%) and the Dry Andes (-5.4 $km^3$, -6%). Similarly, the greatest decrease in glacier surface area was observed in

the Wet Andes (-144.4 km$^2$, -2%), followed by the Tropical Andes (-55.5 km$^2$, -4%), and finally the Dry Andes (-45.2 km$^2$, -3%). As expected, there was a positive correlation (r = 0.9) between changes in glacier area and volume at the zonal scale.

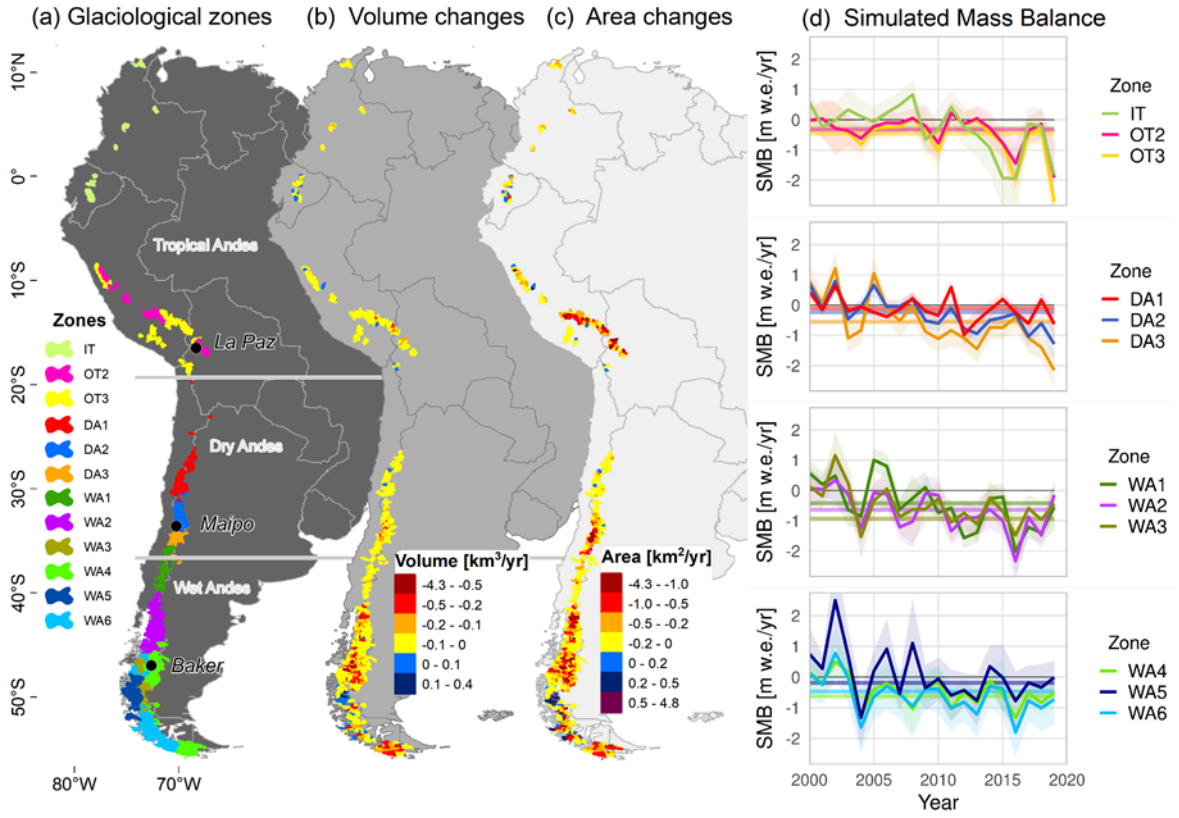


Figure 16. Recent glacier changes across the Andes. The glacier changes are comprised of the mean annual differences between the periods 2000-2009 and 2010-2019 per catchment (n = 786). (a) It shows the distribution of the glaciological zones (11°N-55°S), followed by the (b) volume and (c) area changes at the catchment scale. The (d) annual simulated mass balances are presented in each glaciological zone (the shaded areas are the standard deviation), where the straight lines correspond to the mean geodetic mass balance (2000-2019) estimated by Hugonnet et al. (2021).

Figure 17 shows the changes of the glacier runoff, resulting from glacier melt and rainfall on glaciers, displaying significant variations between the periods 2000-2009 and 2010-2019 across the Andes. Mean annual glacier melt exhibited an increase in 12% (86.5 m$^3$ s$^{-1}$) across the Andes, with 84% (n = 661) of catchments experiencing an increase and 12% (n = 95) showing a decrease. The increase in glacier melt was predominantly observed in catchments with higher glacier elevations, larger glacier sizes, lower mean temperatures, and higher mean precipitation, compared to catchments with decreased or unchanged glacier melt. The latter catchments also experienced the largest decrease in precipitation (-10 to -14%). The highest percentage increase in mean annual glacier melt was observed in the Tropical Andes (40%, 21 m$^3$ s$^{-1}$), followed by the Dry Andes (36%, 21.7 m$^3$ s$^{-1}$), and the Wet Andes (8%, 4.8 m$^3$ s$^{-1}$).

Our analysis reveals that the mean annual rainfall on glaciers across the Andes exhibited a decrease in -2% (-7.6 $m^3$ $s^{-1}$) between the periods 2000-2009 and 2010-2019. This decrease was observed in 41% of the catchments (n = 322). On the other hand, the majority of catchments (51%, n = 403) showed an increase in rainfall on glaciers. Notably, the catchments with an increased rainfall on glaciers were concentrated in the same latitude range as those experiencing an increase in glacier melt. These catchments shared similar glacier elevations and sizes. It is worth mentioning that catchments in the Dry Andes region, where rainfall contributes less to the overall glacier runoff volume, did not exhibit significant changes in rainfall on glaciers. At the glaciological region scale, the mean annual rainfall on glaciers displayed a decrease in the Wet Andes (-3%, 10.1 $m^3$ $s^{-1}$), while showing an increase in the Tropical Andes (23%, 2.4 $m^3$ $s^{-1}$) and the Dry Andes (3%, 0.1 $m^3$ $s^{-1}$). These regional patterns further highlight the diverse impacts of climate change on rainfall distribution across the Andes.

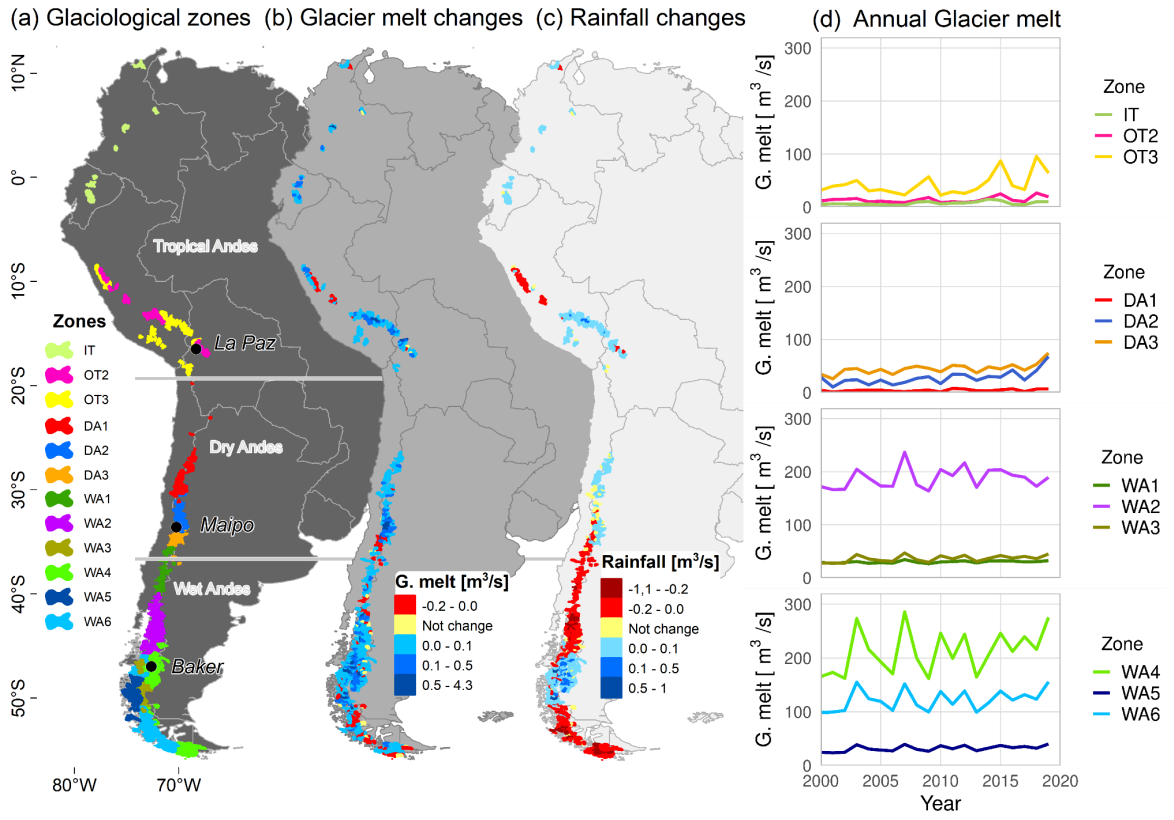


Figure 17. Recent changes in glacier runoff components across the Andes between the periods 2010-2019 and 2000-2009. The mean differences of total glacier melt and rainfall on glaciers per catchment (n = 786) are presented. (a) It shows the distribution of the glaciological zones (11°N-55°S), followed by (b) glacier melt and (c) rainfall on glaciers at the catchment scale. The (d) total annual glacier melt is presented in each glaciological zone.

## 3.3.4 Conclusions of Article n°3

In this study, we present a detailed quantification of the glacio-hydrological evolution across the Andes (11°N-55°S) over the period 2000-2019 using OGGM. Our simulations rely on a glacier-by-glacier

calibration of the changes in glacier volume. Simulations cover 11,282 $km^2$ of the glacierized surface area across the Andes, taking out account that calving glaciers (mostly in the Patagonian icefields and Cordillera Darwin) were not considering because calving is not accounted for in the version of glaciological model used here. The simulations were performed for the first time employing the same methodological approach, a corrected climate forcing and parameters calibration at the glaciological zone scale throughout the Andes. Evaluation of our simulation outputs spanned glacier-specific and catchment-scale, integrating in situ observations -which is uncommon in regional studies. From our results, we can conclude the following:

- In relation to glacier runoff composed by glacier melt and rainfall on glacier at the catchment scale; the largest percentage of studied Andean catchments encompassing 84% of total (661 catchments) presented an increase in 12% of the mean annual glacier melt (ice and snowmelt) between the periods 2000-2009 and 2010-2019. These catchments present glaciers with higher elevation, larger size and also a lower mean annual temperature and higher mean annual precipitation compared with glaciers located in catchments that showed a decrease in glacier melt in the same period which comprise just 12% of studied catchments. Additionally, the mean annual rainfall on glacier between the periods 2000-2009 and 2010-2019 exhibited a reduction of -2%.
- Special attention must be directed towards the Tropical and Dry Andes regions, as they exhibited the most significant percentage increase in glacier runoff between the periods 2000-2009 and 2010-2019, reaching up to 40% due to glacier melt, and 3% due to increased rainfall on glacier over the past decade. Specifically, the Dry Andes 1 (DA1) showcased a remarkable 62% increase, while the Inner Tropic zone exhibited a 73% rise in glacier runoff in the same periods. Notably, these particular glaciological zones displayed the smallest absolute quantities of glacier runoff across the entire Andes region. The DA1 zone emerges as the most vulnerable glaciological zone to glacier runoff water scarcity in the Andes.
- Three catchments (La Paz, Maipo and Baker) located in contrasted climatic and morphometric zones (glaciological zones) are used to evaluate the simulations. Our results show consistency with previous studies and *in situ* observations. The larger glacier runoff contributions to the catchment water flows during the period 2000-2019 are quantified for the Baker (43%) and Maipo (36%) catchments during the summer season (January-March). On the other hand, the larger glacier runoff contribution to the La Paz catchment (45%) was estimated during the transition season (September to November).
- The correction of temperature and precipitation data, coupled with parameter calibration conducted at the glaciological zone scale, notably enhanced the accuracy of mass balance simulations and glacier runoff estimations. Highlighting the estimation of annual temperature lapse rates and variability in glacier mass balance through measurements to correct climate data across distinct

glaciological zones. This improvement not only ensures better alignment with local observations but also establishes a more robust tool for forecasting future glacier runoff patterns in the Andes. This method stands apart from global models by specifically addressing the local climate and parameter values inherent to the Andean region.

Lastly, our results help to improve knowledge about the hydrological responses of glacierized catchments across the Andes through the correction of inputs, calibration by glaciers and validation of our simulations considering different glaciological zones. The implementation of this model during the historical period is a prerequisite for simulating the future evolution of the Andean glaciers.

# 3.4 Glacio-hydrological changes along the Andes over the first half of the 21st Century

## *Entire Article n°4 in section 5.4*

### 3.4.1 Abstract of Article n°4

This study examines the future changes in glacier runoff and their implications across the Andes during the 21st century, adopting a catchment perspective and employing a validated and calibrated model integrating mass balance and glacier dynamics as well as glacier runoff (snow and ice melt). Focusing on a glacierized area of 27669 $km^2$, we investigate the future change in glacier runoff using eight Global Circulation Models (GCMs) from CMIP6 during the period 1990-2049. Additionally, glacier runoff simulations are performed individually by glacier, thanks to a validated and calibrated version of the Open Global Glacier Model (OGGM). The study delves into the future glacier runoff projections in 778 catchments throughout the 21st century, specifically for the period 2030-2049, considering two climate scenarios (SSP1-2.6 and SSP5-8.5). Our results reveal differences in GCMs performance, with specific models showing more accuracy scores in different glaciological regions. Between 1990-2019 and 2020-2049 warming trends are observed in the Andes, with the most significant mean annual temperature increase expected in the Tropical Andes (above 0.7°C on average between the two 30-yr periods). Conversely, precipitation is anticipated to change in a lower amount, decreasing in all regions (-1 to -3%) except the Tropical Andes (+0.6%). These variables are key in glacier mass loss. Glacier runoff estimations demonstrate most significant cumulative loss in terms of percentage regarding the historical period, with a reduction of -43% (25.8 $m^3 s^{-1}$ in SSP1-2.6) in the Tropical Andes, followed by the Dry Andes with a reduction of -37% (-14.4 $m^3 s^{-1}$ in SSP1-2.6), and the Wet Andes, with a cumulative loss of -32% (177.2 $m^3 s^{-1}$ in SSP1-2.6). Notably, some catchments in the Dry Andes exhibit the largest changes in reduction (e.g., Atuel catchment with -62%, decrease of 2.4 $m^3 s^{-1}$) and increase

(e.g., Tupungato catchment with 32%, increase of 0.9 $m^3 s^{-1}$) of mean annual glacier runoff in the Andes, leading to complex spatial patterns of Andean glacier behavior. The majority of catchments are expected to reach a peak water before the first half of the 21st century (percentiles 25-75 in 2010 and 2028), albeit with variations dependent on the glaciological region. The study underscores the critical importance of considering seasonal variations when analyzing GCMs in glaciological simulations and emphasizes regional disparities in glacier runoff across the Andes for future water resources management.

### 3.4.2 Changes in glacier runoff for the period 2030-2049

This section focuses on analyzing the mean annual change of glacier runoff between two distinct 20-yr periods: 2000-2019 and 2030-2049. To estimate these changes, we employ an ensemble of GCMs that exclude GCMs with low scores (when data are compared for the historical period) as well as those exhibiting significant deviations in temperature and precipitation patterns (hot/cold and/or dry/wet GCMs). This refined ensemble is referred to as the filtered ensemble. The analysis is conducted at both the glaciological region and catchment scales, taking into consideration the cumulative volumes of glacier runoff by catchment. Additionally, we have computed the changes in mean annual glacier runoff using an ensemble consisting of eight GCMs. This alternative ensemble is referred to as the complete ensemble. Detailed information is available in the Supplementary Information in the article (Tables S5 and S6, and Figure S4).

Figure 18 illustrates the mean annual changes in glacier runoff in comparison with the historical and future periods for each of the 778 catchments analyzed in the Andes. Within the glaciological regions, the filtered ensemble reveals a median reduction in glacier runoff of -0.1 $m^3 s^{-1}$ for both scenarios in the Tropical Andes. This reduction is observed in the majority of catchments up to the 90th percentile. In the Dry Andes, variations in glacier runoff are observed between the two scenarios. The SSP1-2.6 scenario displays the highest number of catchments with reduced glacier runoff (median = -0.01 $m^3 s^{-1}$), indicating a decrease in overall melt rates. Conversely, the SSP5-8.5 scenario shows that a significant number of catchments exhibit minimal changes in glacier runoff (median = -0.003 $m^3 s^{-1}$). However, until the 90th percentile of these catchments, an increase in glacier runoff (+0.72 $m^3 s^{-1}$) is observed in the SSP5-8.5 scenario. For the Wet Andes, both scenarios indicate a median reduction in glacier runoff of -0.2 $m^3 s^{-1}$, suggesting decreased glacier runoff rates. Negative values persist until the 90th percentile of catchments, indicating a consistent reduction in glacier runoff for this region.

At the regional scale, the glacier runoff changes using the filtered ensemble show similar amounts that simulations from the complete ensemble, whereas, at the catchment scale more conservative changes are estimated from the filtered ensemble.

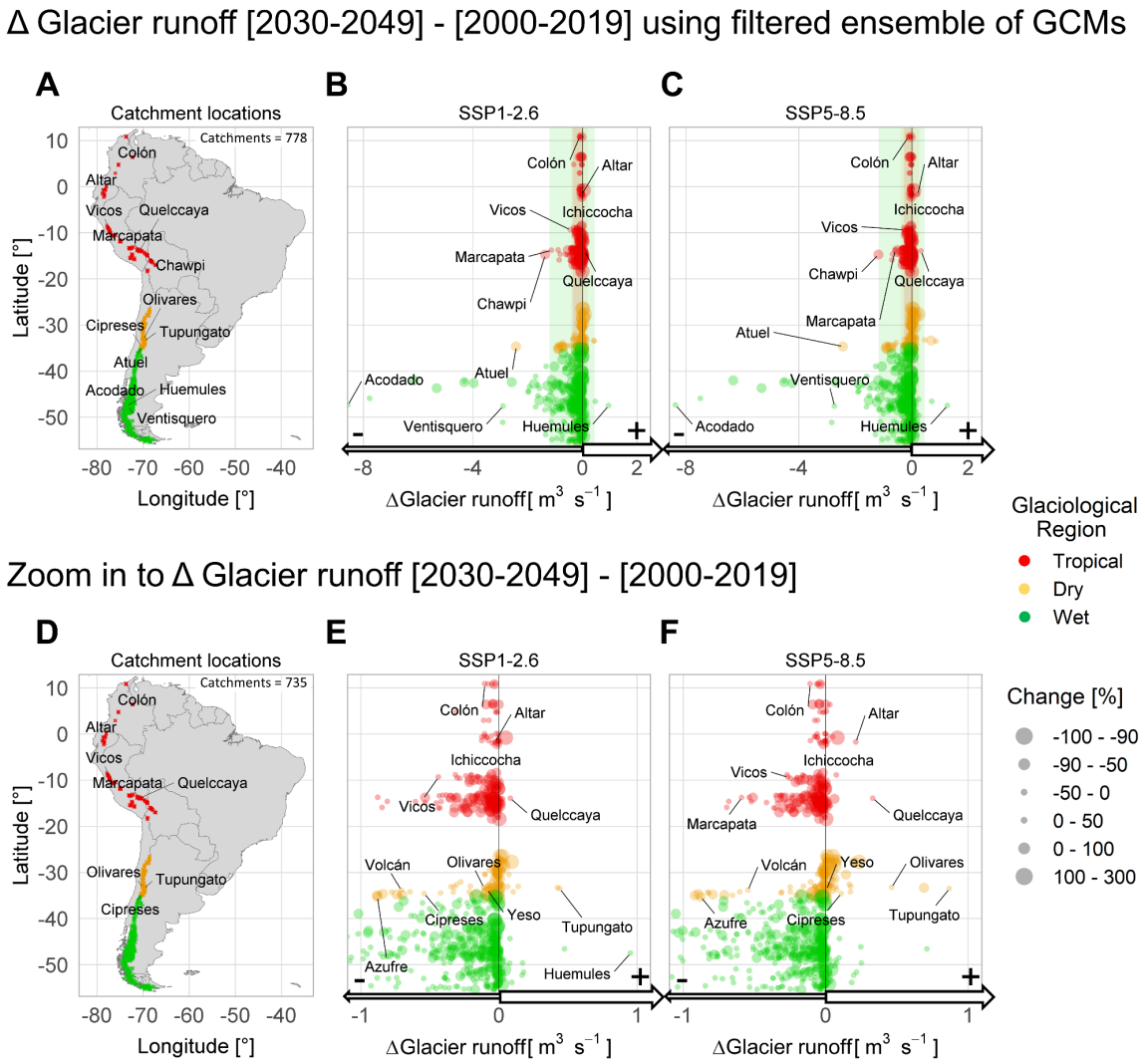


Figure 18. Mean annual changes in glacier runoff between the periods 2000-2019 and 2030-2049 at the catchment scale using the filtered ensemble of GCMs. In the period 2000-2019 is considered the corrected TerraClimate running whereas in the period 2030-2049 is an ensemble of evaluated GCMs. A) and D) show the location of all catchments and the other ones considered in the zoom in, respectively. In B) the glacier runoff differences are present in percentage across the Andes (778 catchments) and in absolute values of changes ($m^3 s^{-1}$) in the SSP1-2.6 and C) SSP5-8.5 scenarios. E) and F) represent catchments in a zoom in between glacier runoff changes of -0.15 and 0.15 $m^3 s^{-1}$. Shadows in B and C display the standard deviation of glacier runoff changes by the Tropical, Dry and Wet Andes.

Three distinct types of behavior observed in glacier runoff changes across catchments, considering the SSP1-2.6 and SSP5-8.5 scenarios. These behaviors include positive changes, negative changes, and catchments that exhibit positive changes under SSP5-8.5 and negative changes under SSP1-2.6. The largest volume changes in glacier runoff are consistently negative across all regions and time periods

(2000-2019 and 2030-2049) for both scenarios. The Tropical Andes exhibit the most significant cumulative loss in terms of percentage regarding the historical period, with a reduction of 43% (25.8 $m^3 s^{-1}$ in SSP1-2.6). This is followed by the Dry Andes, which experience a cumulative loss of 37% (-14.4 $m^3 s^{-1}$ in SSP1-2.6), and the Wet Andes, with a cumulative loss of 32% (177.2 $m^3 s^{-1}$ in SSP1-2.6). However, a smaller number of catchments (n = 22) show an increase in glacier runoff, predominantly in the Dry Andes. These catchments experience a 38% increase (3.5 $m^3 s^{-1}$ in SSP5-8.5). Additionally, some catchments exhibit both increases and reductions in glacier runoff depending on the scenario. Specifically, in the Dry Andes, these catchments demonstrate a 6% increase (1.1 $m^3 s^{-1}$) in the SSP5-8.5 scenario and a 7% reduction (-1.4 $m^3 s^{-1}$) in the SSP1-2.6 scenario. Notably, the Olivares (id = 6090889690) and Cipreses catchment (id = 6090897370) in Chile are among these catchments showing contrasting behavior. Regarding the spatial distribution of catchments, positive changes are predominantly observed in Argentine catchments, such as the Tupungato catchment (id = 6090891240). Conversely, the negative changes, which constitute the majority of the volume changes, are distributed evenly between Chile and Argentina. Noteworthy catchments in this category include the Azufre (id = 6090904960) and Atuel catchment (id = 6090900470).

### 3.4.3 Peak water throughout 21st century along the Andes

The maximum annual contribution of glacier runoff to river discharge is expected to occur before the first half of the 21st century across the Andes. Figure 19 presents the peak water (PW) estimation for 778 Andes catchments, considering the filtered ensemble of GCMs. Across the Andes, the distribution of PW years (percentiles 25 and 75 in both scenarios) is concentrated between 2010 and 2028. The PW years closest to the present occur first in the Wet Andes (2010-2024, n = 465 catchments), followed by the Tropical Andes (2014-2030, n = 183 catchments), and finally in the Dry Andes (2021-2046, n = 130 catchments). Additionally, we observed PW years occurring only in the past period (2000-2025), where all three regions show similar peak water years between 2010 and 2022. In the future period (2026-2099), the PW years are concentrated between 2026 and 2049. First, the Tropical Andes experience PW years (2026-2040, 50 to 86 catchments), followed by the Wet Andes (2030-2038, 40 to 30 catchments), and finally the Dry Andes (2030-2048, 82 to 110 catchments). In the Dry Andes, most catchments show PW years in the future (2026-2099) when the SSP5-8.5 scenario is employed, which can be compared with the results obtained using the SSP1-2.6 scenario. Note that the calving glaciers are excluded from this study, which could be very relevant in the peak water estimation in some catchments of the Wet Andes.

Specific locations in Figure 19 and Table 2 provide a detailed view of the changes in peak water year and the associated amounts of glacier runoff. These details allow for an examination of glacier runoff at the catchment scale within the SSP5-8.5 scenario.

In the Tropical Andes, the Pico Cristóbal Colón catchments in Colombia exhibit PW years between 2020-2028, with a maximum glacier runoff of 0.3 ± 0.02 $m^3 s^{-1}$. In Ecuador, the PW years are delayed until the second half of the 21st century (2022-2084). Notably, the Altar catchment in Ecuador stands out, with a PW year of 2052 ± 10 and a glacier runoff of 1.0 ± 0.04 $m^3 s^{-1}$. In Perú, the principal glacierized cordilleras experience their PW year before the first half of the 21st century. The Cordillera Blanca demonstrates PW years between 2018-2064, while the Cordillera Vilcanota shows PW years between 2024-2050. The largest estimated glacier runoff volume in the Tropical Andes is found in the Marcapata catchment (3.0 ± 0.1 $m^3 s^{-1}$, PW year in 2030 ± 10) located in the Cordillera Vilcanota. However, this maximum glacier runoff is one-third of the maximum identified in the central zone of Chile and Argentina (CL-AR box) in the Dry Andes. The Dry Andes region demonstrates a PW year range between 2010-2062. The largest glacier runoff contributions are simulated in the Cipreses (9.3 ± 0.2 $m^3 s^{-1}$), followed by the Volcán (4.0 ± 0.1 $m^3 s^{-1}$), and the Olivares catchment (3.6 ± 0.2 $m^3 s^{-1}$). For PW years simulated after 2049, larger glacier runoff volumes are observed in the Tupungato catchment (4.0 ± 0.1 $m^3 s^{-1}$) and the Yeso catchment (1.2 ± 0.02 $m^3 s^{-1}$). Compared to the Tropical and Dry Andes, the Wet Andes region exhibits substantial amounts of glacier runoff. Catchments in the Wet Andes, specifically in the latitudinal range of 46-48°S (including the Northern Patagonian Icefield and surrounding glaciers), demonstrate a PW year range before the first half of the 21st century (2010-2048). The maximum glacier runoff is observed in the Acodado catchment (17.8 ± 0.4 $m^3 s^{-1}$) with a PW year of 2010 ± 10, which flows to the west side of the Andes. On the eastern side of the Northern Patagonian Icefield, in the catchments related to the Baker basin, PW years are estimated to occur before 2030. Among these catchments, the Soler catchment (in the NPI) exhibits a larger PW volume of 8.5 ± 0.24 $m^3 s^{-1}$ compared to those found east of the NPI (Maitén, 0.9 ± 0.1 $m^3 s^{-1}$).

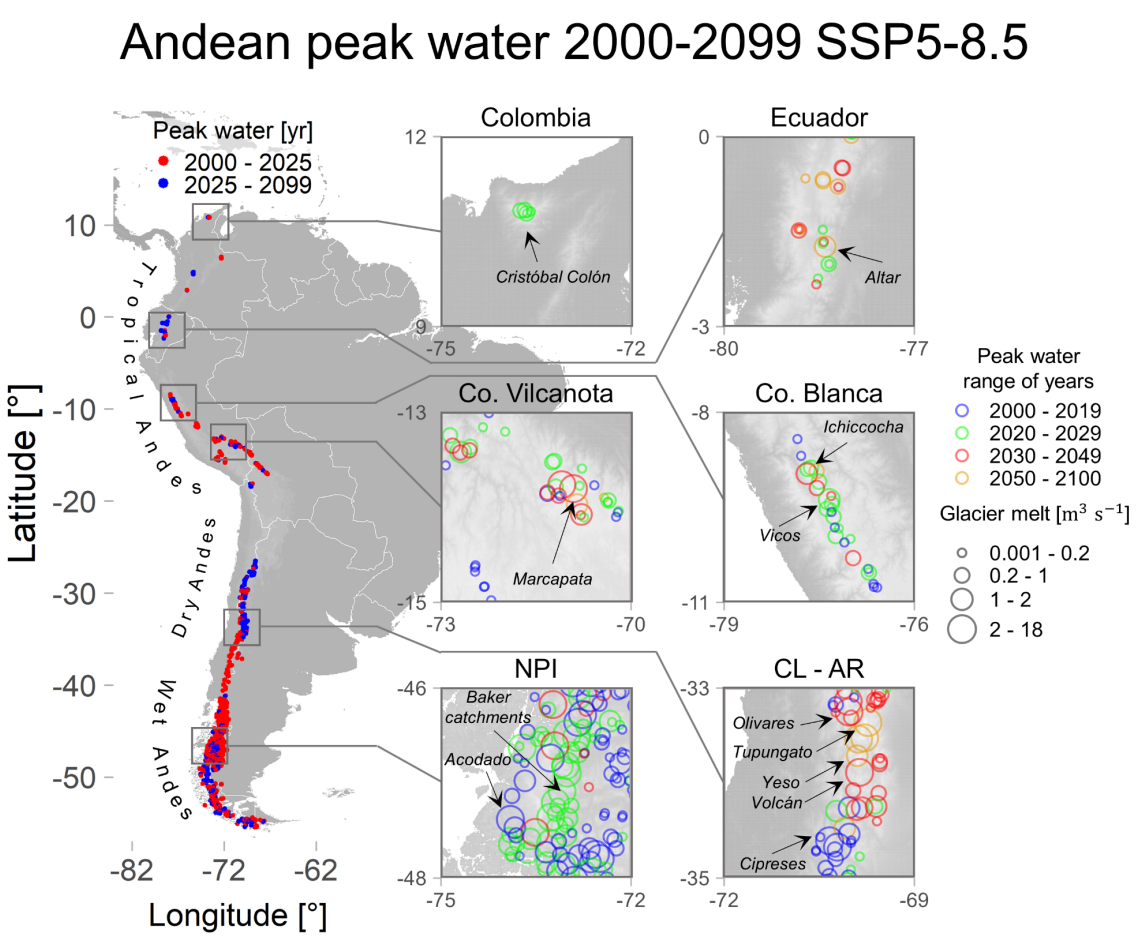


Figure 19. Peak water year and related mean annual glacier runoff across the Andes for the SSP5-8.5 scenario throughout the 21st century. In the South American maps, the peak waters per catchment are exhibited before (2000-2025) and after today (2026-2099), using simulations forced by the filtered ensemble of GCMs. Details can be seen in six locations from Colombia to NPI (Northern Patagonian Icefield). The CL-AR location shows central Chile and Argentina.

Table 2. Catchments highlighted by glacier runoff during the identified peak water year between 2000-2099 across the Andes

| Catchment name | PW year | PW glacier runoff [$m^3$ $s^{-1}$] | Location | Country | Catchment id |
|---|---|---|---|---|---|
| Pico Cristóbal Colón | 2024 ± 10 | 0.3 ± 0.02 | Colombia | Colombia | 6090000970 |
| Altar | 2052 ± 10 | 1.0 ± 0.04 | Ecuador | Ecuador | 6090249220 |
| Vicos | 2020 ± 10 | 1.5 ± 0.05 | Co. Blanca | Perú | 6090461650 |
| Ichiccocha | 2030 ± 10 | 1.2 ± 0.06 | Co. Blanca | Perú | 6090449220 |
| Marcapata | 2030 ± 10 | 3.0 ± 0.09 | Co.Vilcanota | Perú | 6090571030 |
| Cipreses | 2010 ± 10 | 9.3 ± 0.23 | CL-AR box | Chile and Argentina | 6090897370 |
| Volcán | 2040 ± 10 | 4.0 ± 0.06 | CL-AR box | Chile and Argentina | 6090892940 |
| Olivares | 2040 ± 10 | 3.6 ± 0.18 | CL-AR box | Chile and Argentina | 6090889690 |
| Tupungato | 2058 ± 10 | 4.0 ± 0.09 | CL-AR box | Chile and Argentina | 6090891240 |
| Yeso | 2054 ± 10 | 1.2 ± 0.02 | CL-AR box | Chile and Argentina | 6090892710 |
| Acodado | 2010 ± 10 | 17.8 ± 0.39 | NPI | Chile | 6090024320 |
| Soler | 2026 ± 10 | 8.5 ± 0.24 | NPI | Chile | 6090963530 |
| Maitén | 2010± 10 | 0.9 ± 0.05 | East of NPI | Chile | 6090962900 |

## 3.4.4 Conclusions of Article n°4

In this article, we conducted an analysis of eight GCMs from CMIP6 to determine the climate models that demonstrate the highest performance in reproducing the corrected TerraClimate data for the period 1990-2019 and between them in the period 2020-2049 across the Andes, covering a total glacierized surface of 27669 $km^2$. These results were used to run the Open Global Glacier Model (OGGM) and to estimate the changes in glacier runoff throughout the 21st century from Colombia and Tierra del Fuego (11°N-55°S).

- Among the GCMs analyzed, we identified those that exhibit the best scores in the Andes, specifically for the Tropical Andes (CAMS, FGOALS, GFDL, INM-CM5, and NorESM2), in the Dry Andes (GFDL, INM-CM5, MPI, and NorESM2) and for the Wet Andes (CAMS, INM-CM4, and NorESM2). With these models (filtered ensemble), as well as, all analyzed GCMs (complete ensemble), we were able to analyze the changes in glacier runoff.
- For the first time, we conducted a comprehensive simulation of glacier dynamics and glacier runoff in 778 Andean catchments, utilizing a calibrated and validated model with a specific focus on the Andes region. Our findings revealed a notable reduction in glacier runoff across the Andes during the periods 2000-2019 and 2030-2049, particularly when considering the filtered ensemble of GCMs. In the Tropical and Wet Andes regions, we observed a negative median change in glacier runoff (-0.1 $m^3 s^{-1}$ and -0.2 $m^3 s^{-1}$, respectively), while the Dry Andes exhibited a relatively lower median reduction in glacier runoff (-0.003 $m^3 s^{-1}$). Interestingly, within these regions, we identified certain catchments that displayed significant increases in glacier runoff, notably Tupungato and Olivares in the Dry Andes, exceeding 16%. The Dry Andes region demonstrated a cumulative increase of 38% in glacier runoff compared to the historical period (3.5 $m^3 s^{-1}$ for SSP5-8.5 in 34 catchments). Conversely, the Chawpi Urqu catchment in the Tropical Andes, situated on the Bolivia-Peru border, experienced a substantial reduction of 45% in glacier runoff. Overall, the Tropical Andes experienced the most significant cumulative loss, with a reduction of 43% compared to the historical period.
- The projection indicates that peak water from glacier runoff will occur across the Andes before the first half of the 21st century, specifically between 2010 and 2028. Nevertheless, the distribution of peak water years exhibits significant variations along the Andes and locally at the mountain range scale. The Wet Andes region is expected to experience the earliest peak water years (2010 to 2024), followed by the Tropical Andes (2014 to 2030). In contrast, the Dry Andes region is projected to experience peak water years later, primarily in 130 catchments, occurring between 2021 and 2046. During the future period of 2026-2099, the occurrence of peak water years is anticipated to be lower in number across the Andes. Notably, the Dry Andes region

comprises the largest number of catchments, ranging from 82 to 110 (2030 to 2048). Within this region, specific attention should be given to catchments that contribute the highest amounts of glacier runoff, such as the Cipreses (peak water in 2010 ± 10 with 9.3 $m^3$ $s^{-1}$), Volcán (peak water in 2040 ± 10 with 4.0 $m^3$ $s^{-1}$), and the Olivares catchment (peak water in 2040 ± 10 with 3.6 $m^3$ $s^{-1}$). However, the estimation of peak water in the Wet Andes could present a larger uncertainty. This uncertainty arises from the exclusion of calving glaciers and frontal evolution, transitioning from land-terminating glaciers to lake or ocean-terminating glaciers.

This simulation approach provides a comprehensive understanding of the variations in glacier runoff using the GCMs with coherent behavior in the historical and future periods. We highlight the temporal and spatial variations in peak water from glacier runoff across the Andes, emphasizing the importance of considering regional and catchment differences in water resource adaptation strategies, especially in the most affected region by a long drought in the Andes as the central zone of Chile and Argentina.

## 3.5 Statistical glacier change analysis, glacier mass balance modeling using HBV-IANIGLA tool and comparison with the OGGM model

At the outset of this project, I contemplated comparing two glacier evolution approaches: one incorporating a basic statistical formulation of the glacier change (area and volume) and the glacier runoff quantification (HBV-IANIGLA model [hydrological model]), while the other is focusing on glacier volume simulation and related glacier runoff (OGGM [glaciological model]). The disparities between these glacier simulation implementations are presented in Table 3. Notably, the discrepancies lie in OGGM's simulation of glacier dynamics (simulation of glacier area and volume). HBV-IANIGLA does not take into account the glacier dynamics (glacier area is an input). Another difference between the two models is the HBV-IANIGLA's melting partitioning between snow and ice melt on the glacier surface (two different melting factors), this is not the case for OGGM. Finally, the simulation and calibration workflow implementation in OGGM is more complete. These distinctions make the simulation of glacier changes and related runoff using the HBV-IANIGLA tool more challenging at regional scale. For these reasons, it is imperative to spend more time in the implementation and calibration workflows of the HBV-IANIGLA tool.

Table 3. Differences in simulated processes on glacier between the Open Global Glacier Model (OGGM) and HBV-IANIGLA

| Simulated processes | | OGGM | HBV-IANIGLA |
|---|---|---|---|
| Mass balance | Snow accumulation | Yes | Yes |
| | Snow melt | Simulation together | Simulation separately |
| | Ice melt | | |
| Glacier dynamics | Glacier surface area | Yes | No |

| | | | |
|---|---|---|---|
| | Ice thickness | Yes | No |
| | Glacier volume | Yes | No |
| Glacier runoff | From rainfall | Yes | Yes |
| | From snowmelt | Simulation together | Simulation separately |
| | From ice melt | | |
| Calibration implementation | Mass balance | Yes | No |
| | Ice thickness | Yes | No |
| Model Structure | Spatial distribution | Ice flow lines | semi-distributed |
| | Simulated processes | Only glacier | Glacier and whole basin |

In this section, I will present the outcomes of the geodetic glacier mass balance estimated to be used in the calibration of the mass balance simulated (section 3.5.1), the estimation of the glacier area variation (section 3.5.2) and the mass balance simulations utilizing the HBV-IANIGLA tool (section 3.5.3) and their limitations and advantages in the glacier runoff simulation (section 3.5.4). These results have not been published to date.

## 3.5.1 Glacier mass balance estimated for calibration procedure

According to the National Glacier Inventories (NGIs), a total of 27676 glaciers covering an area of 28777 $km^2$ were identified in the Andes. Among these, 26805 glaciers with a total area of 28272 $km^2$ were classified as debris-free glaciers, while 871 glaciers with an area of 504.7 $km^2$ were classified as debris-covered glaciers. The geodetic mass balance of these glaciers was estimated using the surface elevation changes provided by Hugonnet et al. (2021), which yielded a value of -0.74 ± 0.1 m w.e. $yr^{-1}$. However, it was found that the geodetic mass balance estimation for these glaciers had large errors. To address this issue and calibrate the simulated mass balance using HBV-IANIGLA tools for the period 2000-2019, glaciers with errors of mass balance greater than the error 97th percentile were filtered out. By applying this filtering procedure, the maximum mean error per glacier was reduced from 151 to 2.5 m w.e. $yr^{-1}$. This resulted in a mean error in mass balance of 0.1 m w.e. $yr^{-1}$, while maintaining the mean mass balance of -0.74 ± 0.1 m w.e. $yr^{-1}$. However, the number of glaciers was reduced to 25343, covering an area of 28215 $km^2$.

These adjustments by filtering out glaciers with larger errors in the geodetic mass balance ensure that the calibrated model provides a more reliable representation of the mass balance at the catchment scale in the Andes during the selected period.

In Table 4 and Figure 20, the filtered debris-free glaciers exhibit a larger negative mass balance of -0.75 ± 0.1 m w.e. $yr^{-1}$ compared to the debris-covered glaciers, which have a negative mass balance of -0.25 ± 0.02 m w.e. $yr^{-1}$. It is worth noting that the debris-covered glaciers cover a total glacierized area of 495 $km^2$ across the Andes region (8-55°S), which is relatively small in comparison to the vast area covered by the debris-free glaciers, spanning 27720 $km^2$.

| Table 4. Geodetic mass balance for covered and free of debris glaciers between 2000-2019 identified in NGIs between 8-55°S | | |
|---|---|---|
| | Debris-covered | Free of debris cover |
| Mass balance in glacier with elevation change data | -0.25±0.02 | -0.75±0.10 |
| Glacier surface area covered by elevation change data | 493.9 km$^2$ | 26241.9 km$^2$ |
| Glacier surface area of glaciers with elevation change data from the NGIs | 494.9 km$^2$ | 27719.9 km$^2$ |
| Number of glaciers with elevation change data from the NGIs | 839 | 24504 |
| Percentage of glacier surface data regarding to total area without filter | 98 | 98 |

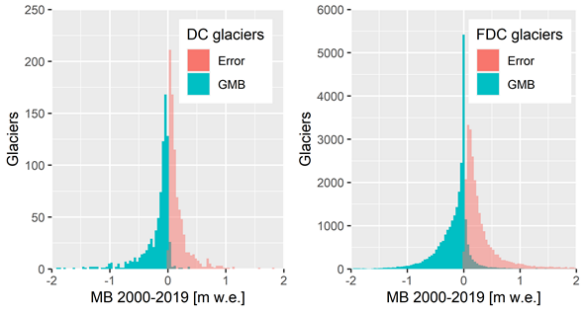


Figure 20. Mass balance and error frequency for the debris-covered (DC) and free of debris-cover (FDC) glaciers described in Table 4.

In Figure 21, the glacier mass balance distribution estimated from Hugonnet et al. (2021) and the NGIs between 2000-2019 shows the debris-covered glaciers identified southward 28°S to the Wet Andes (brown columns), the latter being identified in the glacier inventory of Argentina, with a larger loss in mass also in the Wet Andes. Similarly, the free of debris-cover glaciers exhibit larger mass loss in the Wet Andes, which agrees with the results reported by Dussaillant et al. (2019).

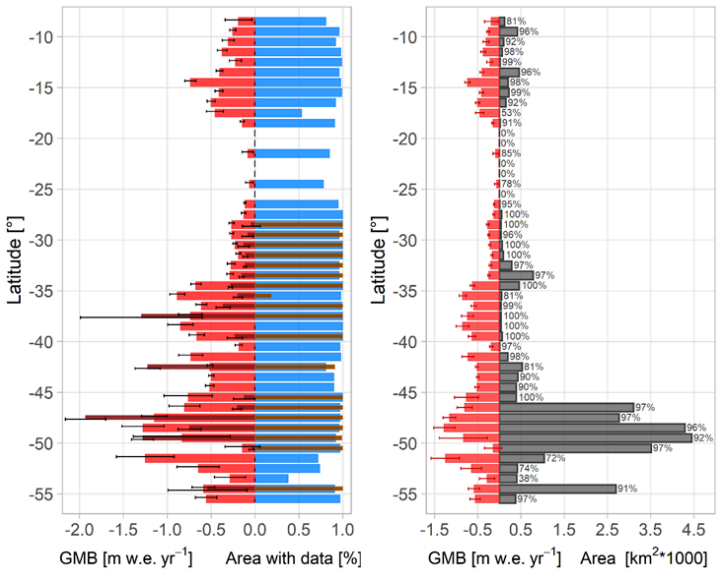

Figure 21. Surface mass balance and glacierized surface area of the debris-covered and the free of debris-cover glaciers by latitudinal range are exhibited across the Andes (8-55°S). In A) the debris-covered (brown columns) and free of debris-cover glaciers (red and blue columns) are different, whereas in b) these are considered in an ensemble. Percentages in b) refer to the proportion of surface with glacier mass balance data regarding the total. Geodetic mass balance estimated from the glacier elevation changes in Hugonnet et al. (2021) and glacier outlines from the GNIs. Glacier surfaces and glacier area were extracted from the NGIs.

## 3.5.2 Glacier area variation extrapolation

The glacier area variation data (GAV) was extrapolated to the glaciers for which this data was not available by considering the distribution of glacier area by quintile in each glaciological zone, as shown in Table 5. It was observed that the maximum glacier areas were underrepresented in the glaciers with GAV data. However, there is a strong correlation in the area quintiles from NGIs regarding glaciers with GAV data, indicating a consistent pattern across different glacier sizes. The mean difference between the observed areas and the mean areas (bias) is relatively low, with a maximum difference of -0.6 $km^2$ observed in the DA 2 zone.

Table 5. Results from GAV and GNIs glacier area per quintile in each glaciological zone across the Andes

| GAV data | | | | | GAV and NGIs comparison | | | |
|---|---|---|---|---|---|---|---|---|
| zones | Glacier surface area with data regarding the total [%] | N° of glaciers with data | Median surface area of glaciers with data [$km^2$] | Mean GAV 1980-2000 [%] | Min and max glacier area NGIs [$km^2$] | Min and max glacier area GAV [$km^2$] | Pearson's correlation | Glacier area bias [$km^2$] |
| OT1 | 35.8 | 61 | 0.17 | 63.8 ± 21 | 0.01 - 2.8 | 0.01 - 2.2 | 1 | -0.04 |
| OT2 | 40.2 | 383 | 0.23 | 66.5 ± 24 | 0.01 - 14.8 | 0.01 - 5.7 | 1 | 0 |
| OT3 | 37.6 | 613 | 0.29 | 55.7 ± 25 | 0.01 - 10.8 | 0.01 - 6.9 | 1 | 0.01 |
| DA1 | 21.8 | 150 | 0.06 | 59.9 ± 25 | 0.01 - 9.8 | 0.01 - 2.8 | 0.99 | 0.03 |
| DA2 | 5.2 | 58 | 0.40 | 43.5 ± 27 | 0.01 - 22.9 | 0.01 - 21.4 | 1 | -0.06 |
| DA3 | 20.1 | 176 | 0.33 | 43.9 ± 26 | 0.01 - 27.6 | 0.02 - 15.6 | 1 | -0.05 |
| WA1 | 8.5 | 17 | 0.30 | 64.3 ± 19 | 0.02 - 11.9 | 0.03 - 5.9 | 1 | 0 |
| WA2 | 8.2 | 320 | 0.38 | 66.3 ± 25 | 0.02 - 67.9 | 0.02 - 25.7 | 1 | -0.03 |
| WA3 | 8.8 | 96 | 0.15 | 42.1 ± 25 | 0.01 - 1241.2 | 0.01 - 31.6 | 1 | 0.02 |
| WA4 | 17.8 | 1375 | 0.25 | 41.9 ± 24 | 0.01 - 283.4 | 0.01 - 78.7 | 1 | 0.01 |
| WA5 | 8.7 | 284 | 0.17 | 48.5 ± 25 | 0.01 - 498.5 | 0.01 - 13.4 | 1 | -0.01 |
| WA6 | 16.1 | 727 | 0.17 | 41.8 ± 26 | 0.01 - 244.7 | 0.01 - 41.9 | 1 | 0.04 |

In Figure 22, a comparison is presented between data from the National Glacier Inventories (NGIs) and glaciers with glacier area variation (GAV) estimations. Figure 22A illustrates that the distribution of area per quintile in NGIs is well represented by the area quintiles from glaciers with GAV data. Figure 22B shows that larger GAV percentages are found in the Tropical Andes and DA 1 zones. Figures 22C and 20D demonstrate that the extrapolated GAV from glaciers with data to glaciers without data in the NGIs exhibit a very similar distribution per area quintile. Overall, the relationship between small glaciers and

higher area losses is observed in the OT1, OT2, OT3, WA1 zones (high slope), and DA1, DA3, WA4, WA5, WA6 zones (low slope). Conversely, the relationship between small glaciers and lower area loss is estimated in the DA2, WA2, and WA3 zones (low slope). These relationships can be attributed to several factors. First, the glaciers with GAV data are not representative of the glacier area in these zones, as the percentage of glaciers with data is lower (DA2 = 5% of the total). Second, the maximum areas are not adequately represented, such as in the case of WA3, which has an area of 31.6 $km^2$ compared to the total area of 1241 $km^2$. Last, the mean glacier areas of glaciers with GAV data are underrepresented, with biases observed in DA2 (-0.06 $km^2$) and WA2 (-0.03 $km^2$).

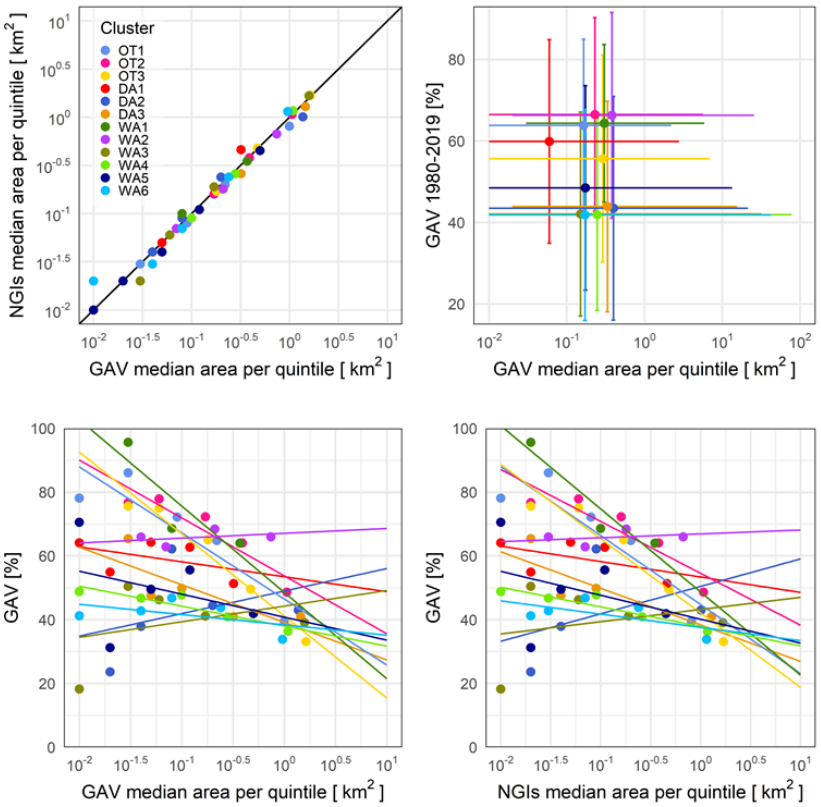


Figure 22. Glacier area quintiles from the NGIs and glaciers with GAV data in the Andes. Upper left, show the correlation between quintiles of the median glacier area in the NGIs (n = 25825) and GAV data (n = 4263). Upper right, the GAV median area per quintile showing maximum and minimum areas with GAV data, while in the GAV percentage is considered the GAV standard deviation. Figures below show correlations between GAV (%) and area per quintiles from glaciers with GAV data (left) and from GAV data extrapolated to the NGIs (right).

Figure 23 displays the glacier area distribution per quintile for glaciers with GAV data (n = 4263) and for the extrapolated glaciers in the NGIs (n = 20275). The figure allows comparing the distribution of glaciers in each quintile based on their area.

Furthermore, after the extrapolation, a total of 25825 glaciers with GAV data are available (i.e. incorporating the additional data from the extrapolated glaciers). This increased dataset provides a more comprehensive representation of the glacier area distribution across the Andes and allows for a more accurate analysis of glacier characteristics and trends in comparison with the small number of glaciers

with the original GAV data. This data by glacier is an input in the HBV-IANIGLA tool used to simulate the glacier mass balance and consequent volume of glacier runoff.

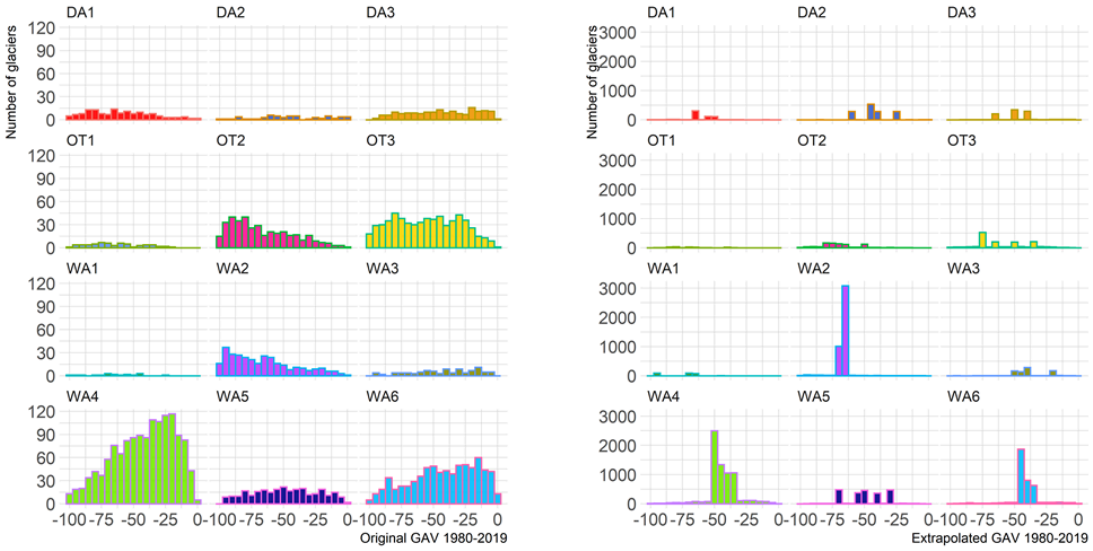


Figure 23. Number of glaciers with original GAV data (left) and with the extrapolated GAV data to the NGIs (right) by glaciological zones in the Andes. Note that the scale of the number of glaciers (axis Y) larger for the extrapolated GAV data.

## 3.5.3 Results of mass balance simulation using HBV-IANIGLA tool

The procedure to simulate mass balance with HBV-IANIGLA and how the parameters were calibrated are explained in section 2.3.2 HBV.IANIGLA. The preprocessing of data for the HBV-IANIGLA tool, along with the workflow and calibration procedure, was implemented in the R programming language. However, it is acknowledged that the calibration procedure needs improvement to identify the optimal calibration parameters for each glacier. Currently, the algorithm requires a significant amount of computational time to perform these tasks. Due to this limitation, the results presented in this study consider the calibration of the mean simulated mass balance between 2000-2019, taking into account the error range of the geodetic mass balance estimated per glacier during the same period. It should be noted that the calibration procedure does not aim to match the mean geodetic mass balance estimated in this study, which only represents 94% of the glacierized area (as shown in Table 6).

Table 6. HBV simulation with fixed glacier area and parameter random calibration based on Hugonnet et al. (2021) at cluster scale.

| Total cluster NGIs | NGIs | | Calibrated glaciers | | Calibrated glaciers % | |
|---|---|---|---|---|---|---|
| | Number of glacier | Glacierized surface [km$^2$] | Number of glacier | Glacierized surface [km$^2$] | Number of glacier [%] | Glacierized surface [%] |
| OT1 | 186 | 52.5 | 181 | 52.5 | 97.3 | 99.9 |
| OT2 | 958 | 442.8 | 581 | 351.0 | 60.6 | 79.3 |
| OT3 | 1617 | 1024.9 | 1493 | 1009.7 | 92.3 | 98.5 |
| DA1 | 646 | 139.3 | 602 | 124.2 | 93.2 | 89.2 |
| DA2 | 1427 | 752.4 | 1250 | 606.8 | 87.6 | 80.7 |

| | | | | | | |
|---|---|---|---|---|---|---|
| DA3 | 989 | 508.2 | 951 | 493.3 | 96.2 | 97.1 |
| WA1 | 459 | 97.7 | 404 | 82.9 | 88.0 | 84.8 |
| WA2 | 5473 | 1775.9 | 4611 | 1511.6 | 84.2 | 85.1 |
| WA3 | 839 | 7409.7 | 725 | 7318.4 | 86.4 | 98.8 |
| WA4 | 6957 | 6121.8 | 6368 | 5720.9 | 91.5 | 93.5 |
| WA5 | 2364 | 2231.3 | 1817 | 2146.5 | 76.9 | 96.2 |
| WA6 | 3910 | 3680.6 | 2881 | 3256.8 | 73.7 | 88.5 |
| Total | 25825 | 24237 | 21864 | 22675 | 84.7 | 93.6 |

The calibration of the simulated mass balance using the geodetic mass balance data ensures that the simulated mass balance closely reflects the observed changes in glacier mass. The simulated mass balances by region and zones can be observed in Figure 24 over the period 1960-2019. In terms of regional patterns, larger mass losses are observed in the Wet Andes, followed by the Tropical and Dry Andes. The annual mass balance changes are also evident when considering the glaciological zones. For instance, the WA5 zone shows small mass gains, suggesting that glaciers in this area are close to an equilibrium over the periode 1960-2020. On the other hand, the WA1 zone exhibits the highest mass losses, indicating a significant decline in glacier mass within this particular zone.

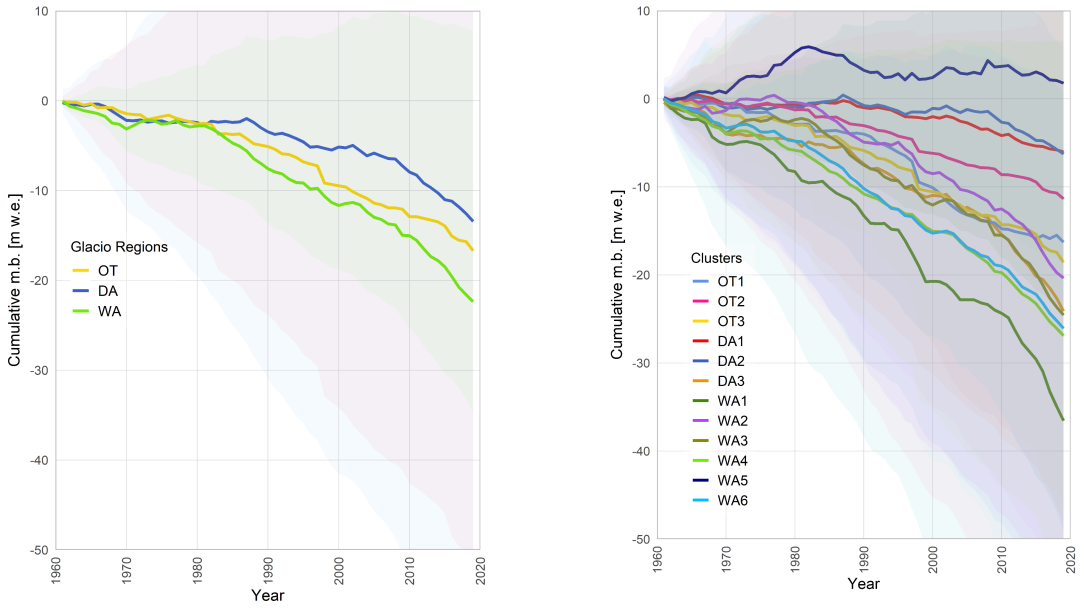


Figure 24. Cumulative simulated mass balance using the HBV-IANIGLA tool in the Andes (8-55°S) between 1960-2019. Results per glacier are compiled by glaciological regions (A) and clusters (B).

Because the values of calibrated parameters to determine the mass balance come from the period 2000-2019, the glaciers' response to temperature and precipitation variation in years before 2000 could be very different. For example, if a melting parameter factor of 200 mm $mth^{-1}$ $°C^{-1}$ is calibrated based on a year with only three months experiencing temperatures up to the snow/ice melt onset (0°C) until 2°C, and no consideration of precipitation variations is made in this example, the resulting melting would be estimated at 1200 mm $yr^{-1}$. However, in the decades before 2000, temperatures have generally been colder, resulting in lower rates of melting. This highlights the need to account for changing temperature

conditions when calibrating models. Models like OGGM often incorporate a spin-up procedure to simulate the historical dynamics of glaciers prior to the calibration period. This procedure involves applying a second melting factor, which is calibrated by running the model multiple times until the simulated historical glacier area or volume matches the observed area or volume from recent data. The spin-up procedure helps account for the glacier's response to climate conditions over a longer time period and ensures that the model captures the historical glacier dynamics.

### 3.5.4 Advantages and disadvantages in the use of HBV-IANIGLA for glacier runoff simulation

The main advantage of HBV-IANIGLA for estimated glacier runoff is their capacity of differentiated snow melting from ice melting, followed by their easy and quick implementation in the R programming language. However, the primary limitations encountered while attempting to obtain consistent results using the HBV-IANIGLA tool were twofold:

i) The need to develop a workflow of algorithms. Although the HBV-IANIGLA tool was designed to be flexible and adaptable, creating the workflow proved to be a time-consuming and demanding task.

ii) The glacier mass balance calibration procedure. Applying the mass balance calibration algorithm to all Andean glaciers at the entire glacier scale, without considering a glacier partitioning approach (such as elevation bands) resulted in an exceedingly long computational time.

These challenges underline the importance of addressing the workflow complexity and refining the calibration process to enhance the HBV-IANIGLA usability and efficiency for future glaciological studies to be applied over large regions. Added to the above is the procedure to obtain the minimum necessary inputs to simulate the glacier mass balance, including glacier surface area, temperature and precipitation.

# 4. General conclusions and outlooks

The findings of this work contribute to our understanding of glacier changes and glacier runoff in the Andes region, taking into account a comprehensive regional perspective and evaluating simulated processes at both the catchment and glacier scales. Machine learning techniques have been employed to establish relationships between glacier changes and climate as well as morphometric variables since 1980. Furthermore, glacier dynamics and associated glacier runoff were simulated from 2000 throughout the 21st century, with a specific focus on catchments with water scarcity.

From the exhibited results, I conclude:

**I)** For the first time, this study utilized a large dataset encompassing the entire Andes region to establish the relationships between climate/morphometric variables and changes in glacier area and glacier surface mass balance. These results provide a regional-scale understanding that extends beyond the observations made on a few specific glaciers. In the Dry Andes, it was found that precipitation played a more significant role in recent glacier changes than air temperature, whereas in the Wet Andes, temperature exhibited a greater influence. These analyses involved estimating linear changes (1980-2018 and 2000-2018) between climate/morphometric variables and glacier changes on a catchment level (Article n°2). These findings were further supported by calculating the linear correlation between annual climate variables (such as precipitation and temperature) and annual simulated mass balance time series on a catchment level (Article n°3).

**II)** Additionally, this study employed a calibrated, corrected, and evaluated OGGM model to estimate mass balance, dynamics, and glacier runoff (including ice and snow melt as well as rainfall on glaciers) across the entire Andes region (11°N to 55°S). These estimates are now available at both the glacier and catchment scale, totaling 786 catchments, for the scientific community and stakeholders (Article n°3). As expected, during the historical period (2000-2019), the highest volume of glacier runoff was estimated in the Wet Andes, followed by the Tropical and Dry Andes. However, the largest percentage increase in glacier runoff between the periods 2000-2009 and 2010-2019 was observed in the Dry Andes, a region highly sensitive to water scarcity since 2010 because of the precipitation reduction observed, particularly since the early 2010 (megadrought).

**III)** We evidenced a spatial pattern for the melting factor of the temperature-index model throughout the Andes region. This pattern was derived by calibrating the model on a glacier-by-glacier basis, while also accounting for a corrected and evaluated reanalysis climate dataset. Ensuring realistic and seasonally distributed parameter values is crucial for accurately simulating future glacier changes, particularly given the significant uncertainty associated with climate inputs throughout the 21st century. This control over

parameter values becomes especially important when considering periods encompassing both very wet and dry years.

**IV)** The glacier runoff changes were simulated across the Andes during the 21st century (Article n°4). To achieve this, eight Global Climate Models (GCMs) from CMIP6 (SSP1-2.6 and SSP5-8.5) were analyzed on a total glacierized area of 27669 $km^2$ during two periods: 1990-2019 and 2020-2049. Different GCMs exhibited the most accurate results for each region within the Andes. For the Tropical Andes, the selected GCMs were CAMS, FGOALS, GFDL, INM-CM5, and NorESM2. In the Dry Andes, the GCMs with the best scores were GFDL, INM-CM5, MPI, and NorESM2. Finally, for the Wet Andes, the CAMS, INM-CM4, and NorESM2 models provided the most reliable results.

**V)** Using the calibrated and evaluated model OGGM in the period 2000-2019 (Article n°3) and the best scored GCMs by glaciological region, we simulated the glacier dynamics in 778 catchments (Article n°4). Simulations showed an overall reduction in glacier runoff (snow/ice melt) across the Andes during the periods 2000-2019 and 2030-2049. The Dry Andes experienced relatively smaller reductions and even some increases, while the Tropical Andes faced the most substantial losses in terms of percentage reduction. In the Tropical (-0.1 $m^3\ s^{-1}$) and Wet Andes regions (-0.2 $m^3\ s^{-1}$) the median annual glacier runoff was negative, ranging up to the 90th percentile of catchments. However, the Dry Andes region exhibited a lower median reduction in annual glacier runoff (-0.003 $m^3\ s^{-1}$) with a 90th percentile of catchments that show an increase in annual glacier runoff (0.72 $m^3\ s^{-1}$).

**VI)** In the context of glacier shrinkage, it was projected that the peak water from glacier runoff will occur before the first half of the 21st century across the Andes, specifically between the years 2010 and 2028. However, the temporal distribution of peak water years varies significantly along the Andes. The Wet Andes region is expected to experience the earliest peak water years (2010 to 2024 in percentile 25-75), followed by the Tropical Andes (2014 to 2030 in percentile 25-75). The Dry Andes region is projected to experience peak water years later (2021 to 2046 in percentile 25-75). However, the estimation of peak water in the Wet Andes could present a larger uncertainty than estimated here. This uncertainty arises from the exclusion of calving glaciers and frontal evolution, transitioning from land-terminating glaciers to lake-terminating, or ocean-terminating to land-terminating glaciers.

**VII)** Throughout the 21st century, simulations have significantly contributed to a comprehension of changes in glaciers, glacier runoff and glacier melt. These simulations shed light on temporal and spatial variations in peak water derived from glacier runoff across the Andes. Notably, it underlines the crucial significance of incorporating regional and catchment disparities into water resource adaptation strategies, particularly in the severely impacted region of the central zone of Chile and Argentina, which has endured prolonged droughts.

Possible outlooks to improve our knowledge of future glacier mass balance, glacier dynamic and glacier runoff could be the next:

**Outlook 1-** In regional glaciological studies, it is imperative to evaluate the climate inputs, such as the seasonal distribution and annual precipitation and air temperature, as well as the products utilized in the calibration process. Failing to perform this evaluation could lead to incomplete assessments of variables like surface mass balance and glacier volume. When examining the historical period, it is insufficient to solely rely on different climatic products or their ensemble to simulate mass balance or conduct comparisons among them. Instead, it is crucial to evaluate these variables from each climate dataset in comparison to spatially distributed observations that encompass diverse regional climates. By doing so, it becomes possible to determine which climatic product most accurately reproduces climatic variability in different glaciological regions during the model calibration period.

**Outlook 2-** To accurately assess the geodetic mass balance and glacier volume data in the Andes, it is crucial to evaluate global products and determine their uncertainties in glaciological zones. By doing so, it becomes possible to correct the largest inaccuracies that may arise. For instance, the glacier volume product by Farinotti et al. (2019) was only evaluated on 38 Andean glaciers, including less than 4 in the tropics and 38 in the southern glaciers. The evaluation revealed an average difference of 20% compared to ice thickness measurements. However, considering here the total glacierized area in the Andes (30943 $km^2$), the error estimated by Farinotti et al. (2019) could be larger. Therefore, it is important to evaluate the simulations in selected glaciers across different glaciological zones to validate the glacier volume data and ensure accuracy in the simulated glacier volume.

**Outlook 3-** The temperature-index model plays a significant role in representing the energy available for snow/ice melting on glacier surfaces, particularly since the largest glacierized areas are located in the southern Andes. This model has shown improvements when incorporating factors like solar radiation and albedo. While the monthly time step application of OGGM demonstrates good performance at the scale of the entire Andes region, it is important to incorporate a daily time step in catchment-specific applications (e.g. water management). This ensures a more accurate representation of the relationship between precipitation and temperature in the melting process. Another crucial process to consider in ablation is sublimation. The regional-scale assessment of surface mass loss due to sublimation in the Andes has not been extensively addressed. It is worth noting that sublimation is not significant in the Wet Andes region, and only small percentages of sublimation have been measured during seasons with the highest surface mass loss in the Tropical and Dry Andes. Only the Desert Andes, which encompass the smallest glacierized area within the Dry Andes, have exhibited larger amounts of sublimation at the glaciers' surface.

**Outlook 4-** The simulation of glacier dynamics using the mass conservation approximation implemented in OGGM does not account for different glaciological processes, for example the thermomechanical processes that can be highly relevant in temperate and polythermal glaciers and the basal stress. To address this limitation, models such as the Parallel Ice Sheet Model (PISM with thermomechanical processes) (Winkelmann et al., 2011) and Instructed Glacier Model (IGM with emulation of with thermomechanical and basal processes) (Jouvet et al., 2022) demonstrate great potential for regional applications in the Andes. However, these models need to be implemented at the regional scale. However, before starting improved simulations across the Andes throughout the 21st century, it is recommended to run these models in catchments that exhibit minimum and maximum changes in glacier runoff towards 2049 (identified in Article n°4). By incorporating models that account for thermomechanical processes or emulate them, researchers can gain a more comprehensive understanding of glacier behavior allowing them to know if improved models show a better performance that the simpler approximations.

**Outlook 5-** To mitigate the uncertainty associated with glacier runoff changes, I implemented correction, calibration, and evaluation procedures in both historical and future periods. This approach allowed me to determine the historical glacier contribution in monitored catchments by calculating the ratio between glacier runoff and observed streamflow. However, forecasting future catchment streamflow poses another challenge, as variables like land use and soil properties can undergo abrupt changes due to political decision-making, leading to increased uncertainty in streamflow estimations. These processes occurring outside of the glacierized surface areas were not included in this Thesis. To address this, I propose utilizing an ensemble of glaciological and hydrological simulations within the catchment. This ensemble should consider extreme catchment conditions, including potential changes in land use, to gain a better understanding of the range of possible streamflow conditions in the future. By incorporating these simulations, we can assess the impacts of various land use scenarios on streamflow, thus helping us anticipate and comprehend extreme streamflow conditions in glacierized catchments.

# Part II: Publications

# 5. Research publications

## 5.1 Article n°1

This Article is available at: https://doi.org/10.5354/0719-5370.2020.59009

Revista
Investigaciones
Geográficas

UNIVERSIDAD DE CHILE
FACULTAD DE ARQUITECTURA Y URBANISMO
DEPARTAMENTO DE GEOGRAFÍA

### Glacier Clusters identification across Chilean Andes using Topo-Climatic variables

Identificación de clústeres glaciares a lo largo de los Andes chilenos usando variables topoclimáticas

**Historial del artículo**
**Recibido:**
15 de octubre de 2020
**Revisado**
30 de octubre de 2020
**Aceptado:**
05 de noviembre de 2020

Alexis Caro[a]; Fernando Gimeno[b]; Antoine Rabatel[a]; Thomas Condom[a]; Jean Carlos Ruiz[c]

[a] Université Grenoble Alpes, CNRS, IRD, Grenoble-INP, Institut des Géosciences de l'Environnement (UMR 5001), Grenoble, France.
[b] Department of Environmental Science and Renewable Natural Resources, University of Chile, Santiago, Chile.
[c] Sorbonne Université, Paris, France.

**Keywords**
Chilean Andes, climatology, glacier clusters, topography

**Abstract**

Using topographic and climatic variables, we present glacier clusters in the Chilean Andes (17.6-55.4°S), where the Partitioning Around Medoids (PAM) unsupervised machine learning algorithm was utilized. The results classified 23,974 glaciers inside thirteen clusters, which show specific conditions in terms of annual and monthly amounts of precipitation, temperature, and solar radiation. In the Dry Andes, the mean annual values of the five glacier clusters (C1-C5) display precipitation and temperature difference until 400 mm (29 and 33°S) and 8°C (33°S), with mean elevation contrast of 1800 m between glaciers in C1 and C5 clusters (18 to 34°S). While in the Wet Andes the highest differences were observed at the Southern Patagonia Icefield latitude (50°S), were the mean annual values for precipitation and temperature show maritime precipitation above 3700 mm/yr (C12), where the wet Western air plays a key role, and below 1000 mm/yr in the east of Southern Patagonia Icefield (C10), with differences temperature near of 4°C and mean elevation contrast of 500 m. This classification confirms that Chilean glaciers cannot be grouped only latitudinally, hence contributing to a better understanding of recent glacier volume changes at a regional scale.

**Palabras clave**
Andes chilenos, clústeres glaciares, climatología, topografía.

**Resumen**

Utilizando variables topográficas y climáticas, presentamos clústeres glaciares en los Andes chilenos (17.6-55.4°S), donde se ejecutó el algoritmo de aprendizaje automático no supervisado Partitioning Around Medoids (PAM). Los resultados clasificaron 23,974 glaciares dentro de trece clústeres, que muestran condiciones específicas en términos de cantidades anuales y mensuales de precipitación, temperatura y radiación solar. En los Andes secos, los valores medios anuales de cinco clústeres glaciares (C1-C5) muestran una diferencia de precipitación y temperatura de hasta 400 mm (29 y 33°S) y 8°C (33°S), con una resta de elevación promedio de 1800 m entre glaciares clústeres C1 y C5 (18 a 34°S). Mientras que en los Andes húmedos las mayores diferencias se observaron en la latitud del Campo de Hielo Patagónico Sur (50°S), donde los valores medios anuales de precipitación y temperatura muestran una precipitación marítima por encima de 3700 mm/año (C12), donde el aire húmedo occidental juega un papel importante, y por debajo de 1000 mm/año al este del Campo de Hielo Patagónico Sur (C10), con diferencias de temperatura cercanas a 4°C y una resta de elevación promedio de 500 m. Esta clasificación confirma que los glaciares chilenos no pueden agruparse solo latitudinalmente, contribuyendo a una mejor comprensión de los cambios recientes en el volumen de los glaciares a escala regional.

Cómo citar: Caro, A., Gimeno, F., Rabatel, A., Condom, T., & Ruiz, J C. (2020). Identificación de clústeres glaciares a lo largo de los Andes chilenos usando variables topoclimáticas. *Investigaciones Geográficas*, 60, 119-133. https://doi.org/10.5354/0719-5370.2020.59009

## Introduction

The glacier behaviours are linked to the regional climate variability (Braithwaite & Hughes, 2020; Fujita & Ageta, 2000; Gerbaux et al., 2005; Huss & Fischer, 2016; Ohmura et al., 1992; Sakai & Fujita, 2017), showing in wetter conditions to be more sensitive to atmospheric warming than those found in dry regions (Ohmura et al., 1992; Radić & Hock, 2011). Conversely, glaciers located in arid regions are more sensitive to precipitation fluctuations (Fujita, 2008; Kinnard et al., 2020). However, it was observed that glacier behaviours not only respond to the climatic variability; for instance, exposure of the glacier and geometry (e.g. slope, hypsometry) proved to be relevant to explain glacier behaviours (Rabatel et al., 2013). In the Alps and Asia this relationship between topo-climatic and glacier behaviours was observed, where the temperature and precipitation were the most important predictors of the glacier area variation and its mass balance (Abermann et al., 2011; Bolibar et al., 2020; Davaze et al., 2020; Liu et al., 2016; Wang et al., 2019), explaining up to 79% of the glacier mass balances variance (Bolibar et al., 2020). On the other hand, the glacier slopes and elevations explained the 36% of the variance in this region (Davaze et al., 2020).

In the Andes, the glaciers cover a broad range of latitudes and elevations, showing an accelerated shrinkage from mid-20th century in Chile (e.g. Bown et al., 2008, 2013; Farías-Barahona et al., 2020a; Malmros et al., 2016; Masiokas et al., 2020; Meier et al., 2018; Rabatel et al., 2011; Rivera et al., 2000,2012; Rivera & Bown, 2013; Seehaus et al., 2019). In the Extratropical Andes in Chile, the glacier mass lost was explained mostly by climatic variables like precipitation, temperature, and solar radiation (Ayala et al., 2016; Falaschi et al., 2019; Kinnard et al., 2020; Macdonell et al., 2013; Masiokas et al., 2016; Rabatel et al., 2011; Ragettli & Pellicciotti, 2012; Schaefer et al., 2017; Weidemann et al., 2018). In turn, these variables have been fundamental to know the glacier runoff contribution in central Chile watersheds (Ayala et al., 2020; Bravo et al., 2017; Burger et al., 2019; Shaw et al., 2020). On the other hand, topographic variables of glaciers showed to be relevant in the glacier behaviours across the Andes (Fuchs et al., 2016; Rivera et al., 2005; Seehaus et al., 2019), but have not been quantitatively associated with the glacier behaviours in Chile.

In this context, the glacier topo-climatic characteristics (i.e. topographic and climatological variables) have not been studied across the Chilean Andes considering its high heterogeneity (Barcaza et al., 2017; Lliboutry, 1998; Masiokas et al., 2009; Sagredo & Lowell, 2012). Indeed, two main zones, the Dry and Wet Andes (with a limit between 35-36°S) have been considered, identifying between four to seven zones with glaciological similarities where their limits do not coincide and respond to latitudinal ranges across Chile (Barcaza et al., 2017; Dussaillant et al., 2019; Lliboutry, 1998; Masiokas et al., 2009; Sagredo & Lowell, 2012). In addition, the study that considers the largest number of glaciers does not exceed 234 glacier bodies along the 4000 km considering than only Chile have near of 24,000 glaciers identified (DGA, 2015a; Sagredo & Lowell, 2012). An identification of glaciers with topo-climatic similarities could contribute to understanding the mass losses observed at a regional scale, as it has been observed in the reference glacier Echaurren Norte (ECH; 33.6°S,70.1°W) in Central Chile, which has the longest time series of mass balance records in the Southern Hemisphere (DGA, 2009; Masiokas et al., 2016; Peña et al., 1987; Zemp et al., 2019). However, its negative mass balance from 1955 is greater compared with other glaciers of the same watershed (Ayala et al., 2020; Farías-Barahona et al., 2019, 2020b).

In order to identify the glacier similarities, we present a glacier cluster classification across the Chilean Andes using topo-climatic variables from the glacier national inventory of Chile and TerraClimate datasets, for 23,974 glaciers during the period 1980-2019 (Abatzoglou et al., 2018; DGA, 2015a). Goal in which the gridded data allows documenting the climate in poorly monitored regions (Condom et al., 2020; Manz et al., 2016; Schumacher et al., 2020). These glacier clusters will be calculated using the Partitioning Around Medoids (PAM) algorithm (Kaufman & Rousseeuw, 2008) and will allow identifying representative glaciers of zones with topo-climatic similarities.

## Materials and methods

a) Topographic variables from the GNI of Chile

The location and topographical characteristics of the Chilean glaciers were obtained from the Glacier National Inventory version 2015 (GNI), available from the Dirección General de Aguas of Chile (DGA, 2015a). For the western side of the Andes in the latitude range 17.6-55.4°S, this inventory presents higher accuracy compared to global inventories such as the Randolph Glacier Inventory v6.0 (RGI Consortium, 2017). From the GNI we identified 23,974 glacier bodies, with a total surface area of 22,130 km$^2$. The GNI provides eight topographic variables such as area (km$^2$), elevation (mean, maximum, minimum),

aspect, slope, latitude and longitude. We selected four topographic variables to estimate glacier clusters: elevation (mean, maximum, minimum) and aspect (four variables).

b) Climate variables from the TerraClimate dataset

The climatic variables were extracted from the TerraClimate (TC) product. TC comprises a global climate dataset based on reanalysis data since 1958, with a 4 km grid size of spatial resolution at monthly time series. This dataset was validated with the Global Historical Climatology Network using 3,230 stations for temperature (r = 0.95; MAE 0.32°C) and 6,102 stations for precipitation (r = 0.90; MAE 9.1%) (Abatzoglou et al., 2018). The variables such as mean, maximum, minimum temperatures, precipitation and solar radiation were processed. From these five variables, we calculated annual (five variables) and monthly (sixty variables) values for the period 1980-2019, obtained sixty-five climate variables in total. The annual values were estimated considering the mean of the annual sum (precipitation) or the mean of the annual mean (temperature and solar radiation), while the monthly values were calculated with the monthly mean in forty years. Regarding to the mean temperature, this was estimated from the maximum and minimum monthly temperatures.

c) Glacier clusters analysis from the Partitioning Around Medoids (PAM) algorithm

The topographic and climatic variables were grouped to make a Topo-Climatic variables matrix (TCM). The TCM with 23,974 glacier bodies and with sixty-nine topo-climatic variables, considered all glacier types. This clustering was developed by means of the k-medoids technique using the Partitioning Around Medoids (PAM) algorithm. The PAM algorithm divides the data set into groups where each one is represented by one of the data points in the group. These points are called a medoids cluster, which is an object within a cluster for which the average difference between it and all other cluster members is minimal (Kaufman & Rousseeuw, 2008). Similar methodologies have been used previously for glaciological studies (Dowson et al., 2020; Sagredo & Lowell, 2012; Sevestre & Benn, 2015). The cluster numbers were optimized using the Silhouette method which consists in running the PAM algorithm using different cluster numbers. The PAM results and Silhouette optimisation are compared through a Principal Component Analysis (PCA) to identify dominant explanatory variables in the glacier clusters. (Maćkiewicz & Ratajczak, 1993; Sagredo & Lowell, 2012).

## Results

The 23,984 glaciers found across the Chilean Andes (17.6 to 55.4°S) show great differences regarding climatic and topographic variables. Figure 1 displays, from north to south, an increase in mean annual temperature and mean annual total precipitation, which is associated with a decrease in elevation and an increase in the total glacier surface area. Considering the limit between the Dry and Wet Andes at 35°S (Lliboutry, 1998), the north shows colder and drier conditions (annual for average in $T < 4°C$ and $P<0.8$ m/yr) and above 1500 m a.s.l., with a small surface if compared to the Wet Andes which have higher temperatures and precipitations (annual for average in $T > 4°C$ and $P > 0.8$ m/yr) with elevations below the 1500 m a.s.l. These topo-climatic variables among others, allowed identifying thirteen glacier clusters through the PAM method and Silhouettes cluster optimisation. The results are presented in figure 2 using Principal Components Analysis (PC). The first two PCs explain 84.1% of the variance shared between the variables (PC1 67.2%, PC2 16.6%). The Pearson linear correlation between variables in PC1 shows high adjustment of the mean elevation (r = -0.86), followed by the maximum annual mean temperature (r = 0.76) and maximum mean temperature of January (r = 0.60). Topographic variables, like aspect, showed low correlation (r = -0.18).

Regarding the glacier surface areas in the identified glacier clusters, the C1-C4 zone (18.1-34.2°S) presents high adjustment with respect to the precipitation (95.3%) and minimum elevation (4.7%) explaining 98% of the variance. Meanwhile, in the C6-C9 zone (41.9-48.2°S) the 95% of the variance is explained by the latitude (90.5%) and solar radiation (9.5%). The variance of glacier surface areas in the C11-C13 zone (49.2-54.6°S) can be explained by the precipitation in 99%. Between these three zones (C1-C4, C6-C9 and C11-C13), the C5 and C10 glacier clusters are considered as transition clusters, as they do not fit well within the other clusters. These thirteen glacier clusters are presented in table 1 and figure 3.

The first zone C1-C4 mainly distributed between the latitude range 18.1-34.2°S (Q1-Q3) include glaciers from the Desert Andes to part of the Central Andes, covering watersheds from the río Lluta (17.6°S) to río Rapel (34.7°S). This zone has a glacier surface area of 976.5 $km^2$ (3874 glacier bodies) with a mean elevation of about 4500 m a.s.l. The climate shows an annual mean temperature of -1.4°C, an annual mean precipitation amount of 292 mm/yr and solar radiation of 207 $W/m^2$. In the north of this zone, the C1 cluster (18.1-21.6°S)

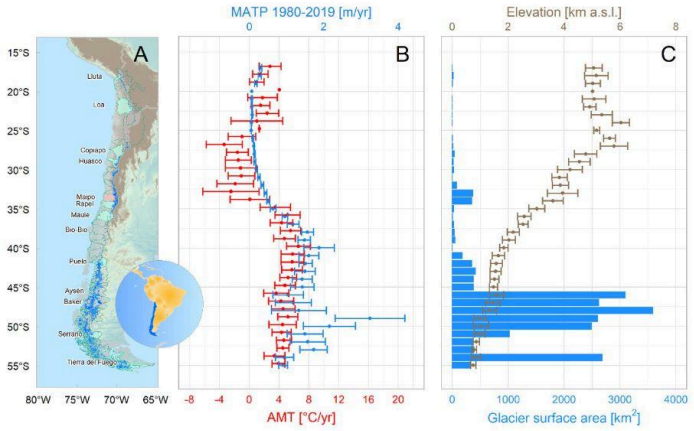


**Figure 1.** Chilean glacier locations and its topo-climatic variables distribution across the Andes. (A) The glacier distribution extracted from the Chilean GNI is presented (blue) as well the partial glacierized watersheds (green polygons), followed by (B) annual mean temperature (AMT) (red) and mean total annual precipitation (MATP) (blue) distribution between 1980-2019, and (C) the latitudinal total glacier surface area (blue bars) associated with the mean elevation (brown) observed in the Chilean Andes. *Source*: self-made.

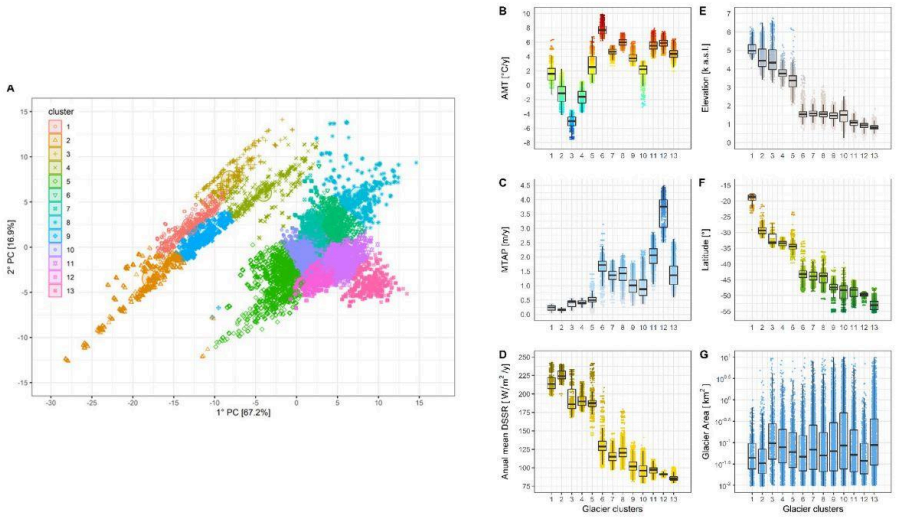


**Figure 2.** Relevance of the thirteen clusters in the first two CPs (A) and the behaviour of the climatic (B, C, D) and topographic (E, F, G) variables in each glacier cluster across Chilean Andes between 1980-2019. The annual mean temperature (AMT), mean total annual precipitation (MATP) and the annual mean downward surface shortwave radiation (DSSR) are presented. *Source*: self-made.

shows the highest glacier mean elevation (5119 m a.s.l.), the smallest glacial surface (45 km$^2$) and the warmest climate in the C1:C4 zone (1.7°C). In the río Copiapó watershed (27.2°S), C1, C2 and C3 are overlapped. The C2 cluster (28.5-30.4°S) and C3 (32.4-33.5°S) present a similar elevation, but the glacial surface is almost five times higher in C3 (490 km$^2$) in comparison with C2 (101 km$^2$), and a similar situation is observed in the annual mean precipitations (382 and 158 mm/yr). The solar radiation shows a significant change from C1, C2 to C3, as well as the temperature. The C3 cluster presents the lowest annual mean temperature (-5°C) of the C1-C4 zone. C4 cluster (32.9-34.2°S) shows a total glacier surface area of 341 km$^2$ with the highest amounts of annual mean precipitation (421 mm/yr) and the lowest average elevation at 3732 m a.s.l. for this region. With respect to the monthly climatology, the annual mean precipitation in C1 is concentrated in summer (November to March), with February showing the highest amount (70 mm) and the temperature is generally above 0°C except in the winter season (June to August) with a monthly minimum of -2.5°C (July). The solar radiation shows greater values from September to March, being interrupted in February due to summer precipitations. Between C2 to C4 the winter precipitation displays higher amounts from May to August (78 mm in July for C4), but these are less relevant in C2, where the summer precipitations are more important than in C3-C4. The temperature is below 0°C between May to October in C2 and C4, while C3 has low temperatures all year long, showing the higher temperatures during summer months (December to March). The amplitude of the monthly solar radiation is similar from C2 to C4, concentrating from October to March, where the highest radiation amounts are seen in C2 (335 w/m$^2$, December).

The C5 cluster is located in the Central Andes and Lakes District zones. C5 gathers glaciers found between latitudes 33.9-35.6°S (Q1-Q3), however, its limits extend from the río Huasco (29.1°S) to río Bio-Bio (37.5°S) watersheds and shares latitudinal range with C3 and C4 clusters. Unlike the C1-C4 zone, C5 presents a smaller glacier area than close clusters with 176 km$^2$ (969 glacier bodies) and a lower elevation (3259 m a.s.l.). On the other hand, the annual mean temperature and precipitation are higher than for all clusters to the north. At monthly scale, the highest precipitation occurs in the winter season (June, 104 mm) and the annual mean temperature reaches values below 0°C from June to September. The solar radiation is dominant from October to March, with highest value in December (297 w/m$^2$).

The third zone comprises four glacier clusters from C6 to C9, concentrated between latitude 42-48.2°S (Q1-Q3), distributed between río Maule (36.6°S) and río Serrano (50.9°S) watersheds and covering from Lakes District to South Patagonia, with a total glacierized area of 3,336 km$^2$ (9386 glacier bodies) and an average elevation above 1535 m a.s.l. The climate is warmer and wetter than for the previously described clusters (5.7°C; 1344 mm/yr), and shows a lower level of solar radiation with an annual mean of 118 w/m$^2$. In this zone there is an important latitudinal overlap between glacier clusters, as was seen in the zone C1-C4. The C6 cluster (42-43.8°S) contains a smaller glacier surface area (227 km$^2$), but the greatest amounts in the climatic variables (7.9°C, 1651 mm/yr, and 133 W/m$^2$) of the C6-C9 zone. To the south, the C7 cluster (42.3-44.9°S) gathers the second largest glacierized area with 859 km$^2$ and the highest elevation (1612 m a.s.l.) of the zone. It is followed by the C8 cluster (43.4-47.1°S) and the C9 cluster (46.4-48.2°S), which have the largest glacier area in the C6-C9 zone with 1670 km$^2$ and the lowest elevation (1450 m a.s.l.). The climate in C9 shows the lowest annual mean temperatures (3.9°C), precipitation (1026 mm) and solar radiation (103 W/m$^2$) of this zone. From C6-C8, the monthly precipitation is concentrated in the winter season, with highest values in June where C6 has the most important monthly value (218 mm). The precipitation in C9 occurs mainly between the months of March to August, with a maximum in June (105 mm), showing lower monthly variation with respect to C6-C8. The annual mean temperature in C6 and C8 does not present values below 0°C, while C7 and C9 show monthly mean temperatures of -1°C and -1.2C° in July. The radiation decreases in winter months with lowest value in June (C9, 28 W/m$^2$).

The C10 cluster, similarly to C5, does not have the same characteristics as the adjacent glacier clusters. C10 is located between latitudes 46.8-50.8°S (Q1-Q3) from río Puelo watershed (42.1°S) to the southern islands at Tierra del Fuego (55°S), associated with the North Patagonia and Tierra del Fuego glacier zones. It comprises the largest glacier surface area in Chile with 14031 km$^2$ (3001 glacier bodies) and an average elevation of 1462 m a.s.l. The climate shows values well below those observed in the C6-C9 zone, with which it shares a latitudinal range, and has an annual mean temperature of 2°C, an annual mean precipitation of 983 mm/yr, and an average solar radiation of 98 w/m$^2$. This zone includes a large part of the Southern Patagonia Icefield and Cordillera Darwin. The monthly precipitation is distributed throughout the year, with mean values higher in March-April (102 mm in April) and the monthly temperature lowest value in

**Table 1**

Topo-climatic values for the thirteen glacier clusters across Chile. * Indicates between 25 to 75% of the latitudinal concentration of glaciers.

| Cluster | Latitude quartile Q1-Q3* [°S] | Mean Elevation [m a.s.l.] | Glacier Area [km2] Total; mean | Number of glaciers | Annual mean Temperature [°C/yr] 1980-2019 | Annual mean Precipitation [mm/yr] 1980-2019 | Annual mean DSSR [W/m2/yr] 1980-2019 |
|---|---|---|---|---|---|---|---|
| 1 | 18.1-21.6 | 5119 | 44.7; 0.07 | 575 | 1.7 | 207 | 218 |
| 2 | 28.5-30.4 | 4578 | 100.7; 0.08 | 1151 | -1.2 | 159 | 226 |
| 3 | 32.4-33.5 | 4430 | 490; 0.50 | 963 | -5 | 382 | 193 |
| 4 | 32.9-34.2 | 3732 | 341.1; 0.28 | 1185 | -1.2 | 421 | 191 |
| 5 | 33.9-35.6 | 3259 | 175.7; 0.18 | 969 | 3.1 | 574 | 188 |
| 6 | 42-43.8 | 1600 | 227.2; 0.20 | 1097 | 7.9 | 1651 | 133 |
| 7 | 42.3-44.9 | 1612 | 858.8; 0.30 | 2790 | 4.8 | 1314 | 118 |
| 8 | 43.4-47.1 | 1480 | 580; 0.22 | 2570 | 6.2 | 1387 | 118 |
| 9 | 46.4-48.2 | 1450 | 1669.8; 0.57 | 2929 | 3.9 | 1026 | 103 |
| 10 | 46.8-50.8 | 1462 | 14030.5; 4.67 | 3001 | 2 | 983 | 98 |
| 11 | 47.8-51.2 | 1009 | 939; 0.34 | 2764 | 5.4 | 2044 | 94 |
| 12 | 49.2-49.8 | 909 | 108.1; 0.10 | 1013 | 5.9 | 3737 | 91 |
| 13 | 51.9-54.7 | 852 | 2602.7; 0.87 | 2977 | 4.1 | 1341 | 86 |

*Source: self-made.*

July (-2.5°C), with monthly values below 0°C from May to September, and a maximum value in January (6.7°C). The radiation presents a maximum in January (174 W/m²) and a lowest value in June (26 W/m²).

The fifth and southernmost zone, C11:C13 is located between latitude range 49.2.-54.7°S (Q1-Q3) across Aysén fiord (45.1°S) to southern islands of Tierra del Fuego (55°S). It is highly overlapped to C10, and gathers a glacierized surface area of 3,650 km² (6754 glacier bodies) with a mean elevation above 924 m a.s.l. The annual mean temperature is 5.2°C, while annual mean precipitation is the highest of the five studied zones (2374 mm/yr), presenting the low solar radiation (90 w/m²). In this zone, a strong longitudinal distribution is identified from west (coast) to east (Patagonia) of the mountain range, where C12 glacier cluster (49.2-49.8°S) is located between coastal islands (48.8°S) and islands south of the Estrecho de Magallanes (53.8°S) with the lower glacierized area (108 km²) and the highest annual mean temperature (5.9°S) of the zone. Precipitation of 3,737 mm/yr is the highest amount observed in the thirteen glacier clusters studied. To the east of C12, the C11 cluster (47.8-51.2°S) is distributed between the coastal islands at the río Aysén watershed (45.7°S) and islands to the south of the Estrecho de Magallanes (53.8°S). The glacierized surface area in C11 is 939 km² and presents the highest elevation (1,009 m a.s.l.) of the zone C11:C13, while the annual mean precipitation is the second highest amount after C12 with 2044 mm/yr. The last glacier cluster, C13 (51.9-54.7°S) is located between the río Baker watershed (47.4°S) and islands to the south of the Beagle Channel (55.4°S). This glacier cluster has the largest glacierized surface area (2,603 km²) and lowest elevation (852 m a.s.l.) in the zone, as well as the lowest annual mean temperature (4.1°C), precipitation (1341 mm/yr) and solar radiation (86 W/m²). The precipitation is well distributed along the year, showing highest values in March or April (372 mm in March for C12), and the smallest values in September. In this zone the temperature presents a lower amplitude than other zones and the monthly mean is never 0°C. C13 has the lowest radiation value of all clusters with 19 W/m² in June.

## Discussion

In this section we first discuss the results of the thirteen glacier clusters regarding the six glaciological zones currently used to describe the glacier distribution in Chile. Then, we present the benefits in identifying glacier clusters with similar topo-climatic conditions.

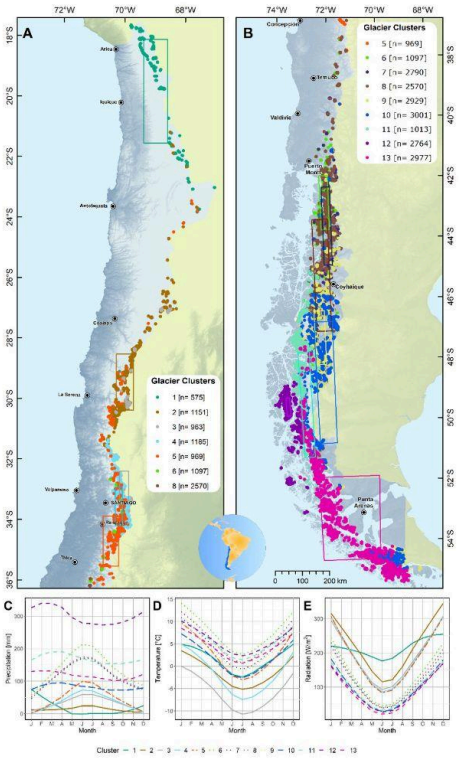


**Figure 3.** Glacier clustering distribution in Chile and climograms. The Chilean glacier's location is associated with a cluster through points (color palette), where the concentration in latitude and longitude ranges (Q1-Q3) of these is represented by rectangles (A). The three plots below show from left to right the average monthly distribution precipitation, temperature and solar radiation associated with each cluster. *Source*: self-made.

a) Performance of the glacier clustering regarding climate conditions across the Andes

The thirteen glacier clusters identified in our study have latitudinal and longitudinal overlaps, which are however limited for C1 (north) and C12 (west of the Patagonian icefields). The most important number of glacier bodies associated with the latitude quartiles (between 25 and 75%) for each glacier cluster, allows identifying a glacier latitudinal distribution with topo-climatic similarities and without overlap to the north of the 31°S. This was used in previous studies to define the glaciological zones across Chile (Barcaza et al., 2017; Dussaillant et al., 2019; Lliboutry, 1998; Masiokas et al., 2009; Sagredo & Lowell, 2012). But, this latitudinal differentiation of the glacier clusters was not clear to the south of the latitude 31°S. Overall, the above mentioned studies identified between four to seven glaciological zones across Chile, even aggregated into two macro zones, the Dry and Wet Andes with a limit between 35-36°S. For instance, Lliboutry (1998) established the first identification of glacial zones in Chile, then Sagredo and Lowell (2012) identified glacial zones using climatic characteristics on a considerable number of glaciers (<234 glacier bodies); from north to south they distinguished: the Desert Andes (17 to 27-32°S), the Central Andes (27-32 to 35-36°S), the Lakes District (35-36 to 41-46°S), the North Patagonia (41-43 to 44-48°S), the South Patagonia (46-48 to 52-53°S) and the Tierra del Fuego (52-53 to -56°S).

In our analysis, for the Dry Andes, five glacier clusters are identified, C1 to C5, with the southernmost cluster observed near 37°S. Here, the Desert Andes gathers the clusters C1 and C2, a zone where Schumacher et al. (2020) observed a higher precipitation between 17-19°S (C1; 207 mm/yr) with respect to the rest of Desert Andes (C2; 159 mm/yr), with precipitation amounts between 100 and 500 mm/yr. These ranges of precipitation in C2 agree with that observed by Kinnard et al. (2020) where the Guanaco glacier mass balance is mostly sensitive to precipitation variations, with precipitation amounts near the glacier between 170 and 240 mm/yr (81% occurring in winter). Glacier clusters C3 to C5 (32.4-35.5°S) are found in the Central Andes, showing a specific elevation distribution with an important precipitation seasonality concentrated during the winter, with higher amounts than observed by Sagredo and Lowell (2012). In this zone, Schumacher et al. (2020) identified a high heterogeneity in the weather records between 30-35°S below 3200 m a.s.l., where C5 (3.1°C; 3259 m a.s.l.) is warmer and wetter with respect to C3 and C4. C3 and C4 clusters showed annual mean temperatures less in C3 with similar precipitation. Measurements on the Bello (C3) and Pirámide (C4) glaciers confirm this behaviour (e.g. similar accumulation amounts), and summer temperatures of -0.8°C in Bello glacier and 1.2°C in Pirámide glacier (DGA, 2015b).

In the Wet Andes, eight glacier clusters are identified (C6 to C13). In the northern Wet Andes, the Lakes District and Northern Patagonia cover a high latitudinal range between 35-36°S and 41-46°S, with the Lakes District being considered up to 41°S. In the Lakes District, six widespread glacier clusters from C5 to C10 can be found. They show a high climatic heterogeneity, with average precipitation (temperature) ranges between 574 mm/yr (3.1°C) in the north to 1651 mm/yr (7.9°C) in the south, accompanied by a decrease in elevation. South from 41°S to 52-53°S in the Patagonian zone and south of 53°S in the Tierra del Fuego, the glaciers show high topo-climatic differences. Studies across the Northern Patagonia Icefield (NPI) and Southern Patagonia Icefield (SPI) observed a large difference in precipitation between the west and the east (Bravo et al., 2019; Warren, 1993), with the San Rafael and San Quintin glaciers variations, to the west to NPI, mainly controlled by changes in winter precipitation (Bertrand et al., 2012; Warren, 1993; Winchester & Harrison, 1996). In the NPI, Barcaza et al. (2017) observed a large difference between records of weather stations located to the west of the NPI compared to those located to the east, where Laguna San Rafael station (46.6°S, 73.9°W; 0 m a.s.l.), in the west, showed warmer and wetter conditions (6.9°C; 3144 mm/yr) than Lago Colonia station (47.3°S, 73.1°W ; 150 m a.s.l.), located to the east (4.9°C; 1649 mm/yr). The same behavior was identified for the C12 cluster extended to the west of the NPI (5.4°C; 2004 mm/yr) and C9 to the east (3.9°C; 1026 mm/yr). High precipitation amounts to the west are likely due to the control by the wet Western air masses from the Pacific Ocean (Langhamer et al., 2018; Warren, 1993). For this latitude range Sagredo and Lowell (2012) identified homogeneous precipitations throughout the year with maximum in summer to the south of 48°S, however Bravo et al. (2019) identified solid precipitation concentrated in winter for NPI and to the west of the SPI. On the other hand, to the east of the SPI the precipitation is homogeneous throughout the year.

b) Implications for the Chilean glaciers monitoring

To understand the glacier response to changes in climate conditions, it is essential to better understand the climate-glaciers relationships. Several studies already focussed on these aspects in the Southern Andes, particularly across the Chilean Andes (Ayala et al., 2016; Ayala et al., 2020; Bravo et al., 2017; Burger et al., 2019; Macdonell et al., 2013; Masiokas et al., 2016; Ragettli et al., 2013; Schaefer et al., 2020). Recently, Schaefer et al. (2020) estimated the energy balance in Bello (33°S), Mocho-Choshuenco (39.5°S) and Tyndall (51°S) glaciers, showing a decrease in the solar radiation importance on the melting processes from north to south, increasing the relevance of the sensible heat fluxes, for which the air temperature is very important. Decrease in solar radiation was observed in our glacier clusters analysis, with solar radiation decreasing from 198 W/m$^2$ (Bello glacier) to 95 W/m$^2$ (Tyndall glacier), and the highest temperatures and precipitation occurring in the Mocho-Choshuenco glacier (7.1°C; 1732 mm/yr), followed by the Tyndall glacier (3.2°C; 1345 mm/yr), and the coldest and driest being Bello glacier (-3.0; 420 mm/yr). Similarly, the Echaurren Norte glacier (33.6°S, 70.1°W) in Central Chile, considered as a reference glacier due to its long time series of mass balance records in the Southern Hemisphere since 1976 (DGA, 2009; Masiokas et al., 2016; Peña et al., 1987; Zemp et al., 2019), has shown a negative accumulated mass balance from 1955. However, this mass loss appears to be larger than other glaciers in the same watershed (Ayala et al., 2020; Farías-Barahona et al., 2019, 2020b).

In addition, it has been shown that 78% of the Echaurren glacier mass balance variance was explained by precipitation variability followed by the temperature (Masiokas et al., 2016). Considering the results of our clustering analysis, the most important mass loss experienced by the Echaurren Norte glacier with regards to the neighbouring glaciers could be explained by the heterogeneity in climate conditions

encountered inside the Maipo watershed (Ayala et al., 2020). In our analysis, the glaciers within the Maipo watershed are distributed between different clusters (C3, C4, and C5), exhibit high precipitation and temperature differences. The C3 glacier cluster with the most important glacierized surface area (64%) displays an annual mean temperature (precipitation) of -5°C (382 mm/yr), followed by C4 that gathers 31% of the glacierized surface area of the Maipo watershed. The 3rd cluster (C5) shows a lower glacierized surface area (5%) but presents the warmer and wetter climate conditions (3.1°C, 574 mm/yr). It is precisely in the C5 cluster where the Echaurren Norte glacier is located. On the other hand, C5 cluster (3259 m a.s.l.) shows the most important surface area of rock glaciers in the Maipo watershed (68%).

## Conclusions

The use of topo-climatic variables from 23,974 glaciers in the Chilean Andes (17.6-55.4°S) allowed the identification of thirteen glacier clusters with a particular climatology, where annual mean temperature, precipitation and solar radiation show variations from north to south and diverse annual regimes.

This new classification of glacierized zones in Chile, using the globally validated TerraClimate product and compared with national studies, demonstrated that a latitudinally based classification made on the basis of a few glaciers is not representative of the Chilean glaciers, due to an observed high latitudinal overlap of climate regimes. For instance, the Central Andes presented various glacier clusters associated with the elevation, meanwhile, the Patagonian glaciers showed longitudinally distributed glacier clusters, where the wet Western air plays a key role in the maritime to continental precipitation regimes.

Finally, the identification of these glacier clusters will contribute regionally to understand the distribution of the dominant meteorological forcing in the glacier mass balance, where the monitored glaciers could be associated with others found in the same glacier cluster, contrary to what was observed in the Echaurren Norte glacier which presents low representativeness in the Maipo watershed and consequently, this better understanding will be useful for hydrological studies in glaciated watersheds.

## Acknowledgments

We thank the Dirección General de Aguas de Chile for providing the glacier national inventory version 2015. The TerraClimate products were obtained freely at http://www.climatologylab.org/terraclimate.html. This work was funded by the National Agency for Research and Development (ANID)/ Scholarship Program/ DOCTORADO BECAS CHILE/2019 – 72200174 and the Secretaría Nacional de Educación Superior, Ciencia, Tecnología e Innovación, SENESCYT/ PhD scholarship. This study was conducted in the framework of the International Joint Laboratory GREAT-ICE, a joint initiative of the IRD and universities and institutions in Bolivia, Peru, Ecuador, and Colombia.

## References

Abatzoglou, J. T., Dobrowski, S. Z., Parks, S. A., & Hegewisch, K. C. (2018). TerraClimate, a high-resolution global dataset of monthly climate and climatic water balance from 1958-2015. *Scientific Data*, *5*, 1–12. https://doi.org/10.1038/sdata.2017.191

Abermann, J., Kuhn, M., & Fischer, A. (2011). A reconstruction of annual mass balances of Austria's glaciers from 1969 to 1998. *Annals of Glaciology*, *52*(59), 127–134. https://doi.org/10.3189/172756411799096259

Ayala, Á., Farías-Barahona, D., Huss, M., Pellicciotti, F., McPhee, J., & Farinotti, D. (2020). Glacier runoff variations since 1955 in the Maipo River Basin, semiarid Andes of central Chile. *The Cryosphere Discussions*, 1–39. https://doi.org/10.5194/tc-2019-233

Ayala, A., Pellicciotti, F., MacDonell, S., McPhee, J., Vivero, S., Campos, C., & Egli, P. (2016). Modelling the hydrological response of debris-free and debris-covered glaciers to present climatic conditions in the semiarid Andes of central Chile. *Hydrological Processes*, *30*(22), 4036–4058. https://doi.org/10.1002/hyp.10971

Ayala, A., Pellicciotti, F., Peleg, N., & Burlando, P. (2017). Melt and surface sublimation across a glacier in a dry environment: Distributed energy-balance modelling of Juncal Norte Glacier, Chile. *Journal of Glaciology*, *63*(241), 803–822. https://doi.org/10.1017/jog.2017.46

Barcaza, G., Nussbaumer, S. U., Tapia, G., Valdés, J., García, J. L., Videla, Y., Albornoz, A., & Arias, V. (2017). Glacier inventory and recent glacier variations in the Andes of Chile, South America. *Annals of Glaciology*, *58*(75), 166–180. https://doi.org/10.1017/aog.2017.28

Bertrand, S., Hughen, K. A., Lamy, F., Stuut, J. B. W., Torrejón, F., & Lange, C. B. (2012). Precipitation as the main driver of Neoglacial fluctuations of Gualas glacier, Northern Patagonian Icefield. *Climate of the Past*, *8*(2), 519–534. https://doi.org/10.5194/cp-8-519-2012

Bolibar, J., Rabatel, A., Gouttevin, I., Galiez, C., Condom, T., & Sauquet, E. (2020). Deep learning applied to glacier evolution modelling. *Cryosphere*, *14*(2), 565–584. https://doi.org/10.5194/tc-14-565-2020

Bown, F., Rivera, A., & Acuña, C. (2008). Recent glacier variations at the Aconcagua basin, central Chilean Andes. *Annals of Glaciology*, *48*, 43–48. https://doi.org/10.3189/172756408784700572

Bown, F., Rivera, A., Zenteno, P., Bravo, C., & Cawkwell, F. (2013). First glacier inventory and recent glacier variation on Isla Grande de Tierra del Fuego and adjacent islands in Southern Chile. In *Global Land Ice Measurements from Space* (pp. 661–674).

Braithwaite, R. J., & Hughes, P. D. (2020). Regional Geography of Glacier Mass Balance Variability Over Seven Decades 1946–2015. *Frontiers in Earth Science*, *8*, 1–14. https://doi.org/10.3389/feart.2020.00302

Bravo, C., Bozkurt, D., Gonzalez-Reyes, Á., Quincey, D. J., Ross, A. N., Farías-Barahona, D., & Rojas, M. (2019). Assessing snow accumulation patterns and changes on the Patagonian Icefields. *Frontiers in Environmental Science*, *7*, 1–18. https://doi.org/10.3389/fenvs.2019.00030

Bravo, C., Loriaux, T., Rivera, A., & Brock, B. W. (2017). Assessing glacier melt contribution to streamflow at Universidad Glacier, central Andes of Chile. *Hydrology and Earth System Sciences*, *21*(7), 3249–3266. https://doi.org/10.5194/hess-21-3249-2017

Burger, F., Ayala, A., Farias, D., Shaw, T. E., MacDonell, S., Brock, B., McPhee, J., & Pellicciotti, F. (2019). Interannual variability in glacier contribution to runoff from a high-elevation Andean catchment: understanding the role of debris cover in glacier hydrology. *Hydrological Processes*, *33*(2), 214–229. https://doi.org/10.1002/hyp.13354

Condom, T., Martínez, R., Pabón, J. D., Costa, F., Pineda, L., Nieto, J. J., López, F., & Villacis, M. (2020). Climatological and Hydrological Observations for the South American Andes: In situ Stations, Satellite, and Reanalysis Data Sets. *Frontiers in Earth Science*, *8*. https://doi.org/10.3389/feart.2020.00092

Davaze, L., Rabatel, A., Dufour, A., Hugonnet, R., & Arnaud, Y. (2020). Region-Wide Annual Glacier Surface Mass Balance for the European Alps From 2000 to 2016. *Frontiers in Earth Science*, *8*, 1–14. https://doi.org/10.3389/feart.2020.00149

DGA. (2009). *Estrategia Nacional de Glaciares*. Valdivia: Technical report: Centro de Estuidos Científicos (CECs).

DGA. (2015a). *Inventario Público de Glaciares de Chile*. Santiago: Technical report: Dirección General de Aguas.

DGA. (2015b). *Modelación de balance de masa y descargas de aguas en glaciares del Norte Chico y Chile Central* (Issue 10945). La Serena: Technical report: Centro de Estudios Avanzados de Zonas Áridas (CEAZA).

Dowson, A. J., Sirguey, P., & Cullen, N. J. (2020). Variability in glacier albedo and links to annual mass balance for the gardens of Eden and Allah, Southern Alps, New Zealand. *The Cryosphere*, *14*(10), 3425–3448. https://doi.org/10.5194/tc-14-3425-2020

Dussaillant, I., Berthier, E., Brun, F., Masiokas, M., Hugonnet, R., Favier, V., Rabatel, A., Pitte, P., & Ruiz, L. (2019). Two decades of glacier mass loss along the Andes. *Nature Geoscience*, *12*(10), 802–808. https://doi.org/10.1038/s41561-019-0432-5

Falaschi, D., Lenzano, M. G., Villalba, R., Bolch, T., Rivera, A., & Lo Vecchio, A. (2019). Six Decades (1958–2018) of Geodetic Glacier Mass Balance in Monte San Lorenzo, Patagonian Andes. *Frontiers in Earth Science*, *7*. https://doi.org/10.3389/feart.2019.00326

Farías-Barahona, D., Ayala, Á., Bravo, C., Vivero, S., Seehaus, T., Vijay, S., Schaefer, M., Buglio, F., Casassa, G., & Braun, M. H. (2020). 60 years of glacier elevation and mass changes in the Maipo River Basin, central Andes of Chile. *Remote Sensing*, *12*(10), 1–19. https://doi.org/10.3390/rs12101658

Farías-Barahona, D., Vivero, S., Casassa, G., Schaefer, M., Burger, F., Seehaus, T., Iribarren-Anacona, P., Escobar, F., & Braun, M. H. (2019). Geodetic mass balances and area changes of Echaurren Norte Glacier (Central Andes, Chile) between 1955 and 2015. *Remote Sensing*, *11*(3). https://doi.org/10.3390/rs11030260

Farías-Barahona, D., Wilson, R., Bravo, C., Vivero, S., Caro, A., Shaw, T. E., Casassa, G., Ayala, Á., Mejías, A., Harrison, S., Glasser, N. F., McPhee, J., Wündrich, O., & Braun, M. H. (2020). A near 90-year record of the evolution of El Morado Glacier and its proglacial lake, Central Chilean Andes. *Journal of Glaciology*, *66*(259), 846–860. https://doi.org/10.1017/jog.2020.52

Fuchs, P., Asaoka, Y., & Kazama, S. (2016). Modelling melt, runoff, and mass balance of a tropical glacier in the Bolivian Andes using an enhanced temperature-index model. *Hydrological Research Letters*, *10*(2), 51–59. https://doi.org/10.3178/hrl.10.51

Fujita, K. (2008). Influence of precipitation seasonality on glacier mass balance and its sensitivity to climate change. *Annals of Glaciology*, *48*, 88–92. https://doi.org/10.3189/172756408784700824

Fujita, K., & Ageta, Y. (2000). Effect of summer accumulation on glacier mass balance on the Tibetan Plateau revealed by mass-balance model. *Journal of Glaciology*, *46*(153), 244–252. https://doi.org/10.3189/172756500781832945

Gerbaux, M., Genthon, C., Etchevers, P., Vincent, C., & Dedieu, J. P. (2005). Surface mass balance of glaciers in the French Alps: Distributed modeling and sensitivity to climate change. *Journal of Glaciology*, *51*(175), 561–572. https://doi.org/10.3189/172756505781829133

Huss, M., & Fischer, M. (2016). Sensitivity of very small glaciers in the swiss alps to future climate change. *Frontiers in Earth Science*, *4*, 1–17. https://doi.org/10.3389/feart.2016.00034

Kaufman, L. & Rousseeuw, P. J. (2008). Partitioning Around Medoids (Program PAM). In L. Kaufman & P. J. Rousseeuw (Eds.), *In Finding Groups in Data* (pp. 68–125). https://doi.org/doi:10.1002/9780470316801.ch2

Kinnard, C., Ginot, P., Surazakov, A., MacDonell, S., Nicholson, L., Patris, N., Rabatel, A., Rivera, A., & Squeo, F. A. (2020). Mass Balance and Climate History of a High-Altitude Glacier, Desert Andes of Chile. *Frontiers in Earth Science*, *8*, 1–20. https://doi.org/10.3389/feart.2020.00040

Langhamer, L., Sauter, T., & Mayr, G. J. (2018). Lagrangian Detection of Moisture Sources for the Southern Patagonia Icefield (1979–2017). *Frontiers in Earth Science*, *6*, 1–17. https://doi.org/10.3389/feart.2018.00219

Liu, L., Jiang, L., Sun, Y., Wang, H., Yi, C., & Hsu, H. (2016). Morphometric controls on glacier mass balance of the puruogangri ice field, central tibetan plateau. *Water (Switzerland)*, *8*(11), 1–18. https://doi.org/10.3390/w8110496

Lliboutry, L. (1998). Glaciers of Chile and Argentina. In J. Williams, Richard & Ferrigno (Ed.), *Satellite Image Atlas of Glaciers of the World; SOUTH AMERICA* (1st ed., pp. 109–206).

Macdonell, S., Kinnard, C., Mölg, T., Nicholson, L., & Abermann, J. (2013). Meteorological drivers of ablation processes on a cold glacier in the semi-arid Andes of Chile. *Cryosphere*, *7*(5), 1513–1526. https://doi.org/10.5194/tc-7-1513-2013

Maćkiewicz, A., & Ratajczak, W. (1993). Principal Components Analysis ( PCA )*. *Computers & Geosciences*, *19*(3), 303–342. https://doi.org/10.1016/0098-3004(93)90090-R

Malmros, J. K., Mernild, S. H., Wilson, R., Yde, J. C., & Fensholt, R. (2016). Glacier area changes in the central Chilean and Argentinean Andes 1955-2013/14. *Journal of Glaciology*, *62*(232), 391–401. https://doi.org/10.1017/jog.2016.43

Manz, B., Buytaert, W., Zulkafli, Z., Lavado, W., Willems, B., Robles, L. A., & Rodríguez-Sánchez, J. P. (2016). High-resolution satellite-gauge merged precipitation climatologies of the tropical andes. *Journal of Geophysical Research*, *121*(3), 1190–1207. https://doi.org/10.1002/2015JD023788

Masiokas, M. H., Christie, D. A., Le Quesne, C., Pitte, P., Ruiz, L., Villalba, R., Luckman, B. H., Berthier, E., Nussbaumer, S. U., González-Reyes, Á., McPhee,

J., & Barcaza, G. (2016). Reconstructing the annual mass balance of the Echaurren Norte glacier (Central Andes, 33.5° S) using local and regional hydroclimatic data. *Cryosphere*, *10*(2), 927–940. https://doi.org/10.5194/tc-10-927-2016

Masiokas, M. H., Rabatel, A., Rivera, A., Ruiz, L., Pitte, P., Ceballos, J. L., Barcaza, G., Soruco, A., Bown, F., Berthier, E., Dussaillant, I., & MacDonell, S. (2020). A Review of the Current State and Recent Changes of the Andean Cryosphere. *Frontiers in Earth Science*, *8*, 1–27. https://doi.org/10.3389/feart.2020.00099

Masiokas, M. H., Rivera, A., Espizua, L. E., Villalba, R., Delgado, S., & Aravena, J. C. (2009). Glacier fluctuations in extratropical South America during the past 1000 years. *Palaeogeography, Palaeoclimatology, Palaeoecology*, *281*(3–4), 242–268. https://doi.org/10.1016/j.palaeo.2009.08.006

Meier, W. J. H., Grießinger, J., Hochreuther, P., & Braun, M. H. (2018). An updated multi-temporal glacier inventory for the patagonian andes with changes between the little ice age and 2016. *Frontiers in Earth Science*, *6*, 62. https://doi.org/10.3389/feart.2018.00062

Ohmura, A., Kasser, P., & Funk, M. (1992). Climate at the equilibrium line of glaciers. *Journal of Glaciology*, *38*(130), 397–411. https://doi.org/10.3189/S0022143000002276

Peña, H., Escobar, F., & Vidal, F. (1987). Estimación de tasas de derretimiento de nieve. *VII Congreso Nacional Sociedad Chilena de Ingeniería Hidraúlica*.

Rabatel, A., Castebrunet, H., Favier, V., Nicholson, L., & Kinnard, C. (2011). Glacier changes in the Pascua-Lama region, Chilean Andes (29° S): recent mass balance and 50 yr surface area variations. *The Cryosphere*, *5*(4), 1029–1041. https://doi.org/10.5194/tc-5-1029-2011

Rabatel, A., Letréguilly, A., Dedieu, J. P., & Eckert, N. (2013). Changes in glacier equilibrium-line altitude in the western Alps from 1984 to 2010: Evaluation by remote sensing and modeling of the morpho-topographic and climate controls. *Cryosphere*, *7*(5), 1455–1471. https://doi.org/10.5194/tc-7-1455-2013

Radić, V., & Hock, R. (2011). Regionally differentiated contribution of mountain glaciers and ice caps to future sea-level rise. *Nature Geoscience*, *4*(2), 91–94. https://doi.org/10.1038/ngeo1052

Ragettli, S., & Pellicciotti, F. (2012). Calibration of a physically based, spatially distributed hydrological model in a glacierized basin: On the use of knowledge from glaciometeorological processes to constrain model parameters. *Water Resources Research*, *48*(3), 1–20. https://doi.org/10.1029/2011WR010559

Ragettli, S., Pellicciotti, F., Bordoy, R., & Immerzeel, W. W. (2013). Sources of uncertainty in modeling the glaciohydrological response of a Karakoram watershed to climate change. *Water Resources Research*, *49*(9), 6048–6066. https://doi.org/10.1002/wrcr.20450

RGI Consortium. (2017). *Randolph Glacier Inventory – A Dataset of Global Glacier Outlines: Version 6.0: Technical Report, Global Land Ice Measurements from Space*. Retrieved from https://www.glims.org/RGI/00_rgi60_TechnicalNote.pdf

Rivera, A., & Bown, F. (2013). Recent glacier variations on active ice capped volcanoes in the southern volcanic zone (37°-46°s), chilean andes. *Journal of South American Earth Sciences*, *45*, 345–356. https://doi.org/10.1016/j.jsames.2013.02.004

Rivera, A., Casassa, G., Acuña, C., & Lange, H. (2000). Variaciones recientes de glaciares en Chile. *Investigaciones Geográficas*, 34, 29. https://doi.org/10.5354/0719-5370.2000.27709

Rivera, A., Casassa, G., Bamber, J., & Kääb, A. (2005). Ice-elevation changes of Glaciar Chico, southern Patagonia, using ASTER DEMs, aerial photographs and GPS data. *Journal of Glaciology*, *51*(172), 105–112. https://doi.org/10.3189/172756505781829557

Rivera, A., Koppes, M., Bravo, C., & Aravena, J. C. (2012). Little Ice Age advance and retreat of Glaciar Jorge Montt, Chilean Patagonia. *Climate of the Past*, *8*(2), 403–414. https://doi.org/10.5194/cp-8-403-2012

Sagredo, E. A., & Lowell, T. V. (2012). Climatology of Andean glaciers: A framework to understand glacier response to climate change. *Global and Planetary Change*, *86–87*(April 2012), 101–109. https://doi.org/10.1016/j.gloplacha.2012.02.010

Sakai, A., & Fujita, K. (2017). Contrasting glacier responses to recent climate change in high-mountain Asia. *Scientific Reports*, *7*(1), 1–8. https://doi.org/10.1038/s41598-017-14256-5

Schaefer, M., Fonseca-Gallardo, D., Farías-Barahona, D., & Casassa, G. (2020). Surface energy fluxes on Chilean glaciers: measurements and models. *The Cryosphere*, *14*(8), 2545–2565. https://doi.org/10.5194/tc-14-2545-2020

Schaefer, M., Rodriguez, J. L., Scheiter, M., & Casassa, G. (2017). Climate and surface mass balance of Mocho Glacier, Chilean Lake District, 40°S. *Journal of Glaciology*, *63*(238), 218–228. https://doi.org/10.1017/jog.2016.129

Schumacher, V., Justino, F., Fernández, A., Meseguer-Ruiz, O., Sarricolea, P., Comin, A., Peroni Venancio, L., & Althoff, D. (2020). Comparison between observations and gridded data sets over complex terrain in the Chilean Andes: Precipitation and temperature. *International Journal of Climatology*, *40*(12), 5266-5288. https://doi.org/10.1002/joc.6518

Seehaus, T., Malz, P., Sommer, C., Lippl, S., Cochachin, A., & Braun, M. (2019). Changes of the tropical glaciers throughout Peru between 2000 and 2016 - Mass balance and area fluctuations. *Cryosphere*, *13*(10), 2537–2556. https://doi.org/10.5194/tc-13-2537-2019

Sevestre, H., & Benn, D. I. (2015). Climatic and geometric controls on the global distribution of surge-type glaciers: Implications for a unifying model of surging. *Journal of Glaciology*, *61*(228), 646–662. https://doi.org/10.3189/2015JoG14J136

Shaw, T. E., Caro, A., Mendoza, P., Ayala, Á., Pellicciotti, F., Gascoin, S., & McPhee, J. (2020). The Utility of Optical Satellite Winter Snow Depths for Initializing a Glacio-Hydrological Model of a High-Elevation, Andean Catchment. *Water Resources Research*, *56*(8), 1–19. https://doi.org/10.1029/2020WR027188

Wang, R., Liu, S., Shangguan, D., Radić, V., & Zhang, Y. (2019). Spatial heterogeneity in glacier mass-balance sensitivity across High Mountain Asia. *Water (Switzerland)*, *11*(4), 1–21. https://doi.org/10.3390/w11040776

Warren, C. R. (1993). Rapid Recent Fluctuations of the Calving San Rafael Glacier , Chilean Patagonia : Climatic or Non-Climatic ? *Geografiska Annaler*, *75*(3), 111–125. https://doi.org/10.2307/521029

Weidemann, S. S., Sauter, T., Malz, P., Jaña, R., Arigony-Neto, J., Casassa, G., & Schneider, C. (2018). Glacier mass changes of lake-terminating grey and tyndall glaciers at the southern patagonia icefield derived from geodetic observations and energy and mass balance modeling. *Frontiers in Earth Science*, *6*, 1–16. https://doi.org/10.3389/feart.2018.00081

Winchester, V., & Harrison, S. (1996). Recent Oscillations of the San Quintin and San Rafael Glaciers , Patagonian Chile. *Geografiska Annaler*, *78*(1), 35–49. https://doi.org/10.1080/04353676.1996.11880450

Zemp, M., Huss, M., Thibert, E., Eckert, N., McNabb, R., Huber, J., Barandun, M., Machguth, H., Nussbaumer, S. U., Gärtner-Roer, I., Thomson, L., Paul, F., Maussion, F., Kutuzov, S., & Cogley, J. G. (2019). Global glacier mass changes and their contributions to sea-level rise from 1961 to 2016. *Nature*, *568*(7752), 382–386. https://doi.org/10.1038/s41586-019-1071-0

**Supplementary information**

Suppementary I. Monthly climatic values between 1980-2019.

| Glacier cluster | Monthly climatic values 1980-2019 | | | | | | | | | | | |
|---|---|---|---|---|---|---|---|---|---|---|---|---|
| | Jan | Feb | Mar | Apr | May | Jun | Jul | Aug | Sep | Oct | Nov | Dec |
| **Precipitation [mm/month]** | | | | | | | | | | | | |
| 1 | 62.8 | 69.7 | 44.7 | 1.4 | 0.1 | 0.3 | 2.1 | 0.1 | 1.6 | 0.6 | 10.2 | 27.3 |
| 2 | 8.2 | 19.0 | 10.6 | 3.8 | 22.2 | 22.8 | 26.1 | 18.9 | 8.8 | 6.7 | 4.2 | 5.7 |
| 3 | 10.4 | 17.9 | 19.6 | 19.4 | 64.0 | 52.1 | 57.6 | 57.5 | 31.8 | 28.2 | 11.1 | 9.4 |
| 4 | 6.1 | 10.6 | 14.8 | 22.9 | 77.0 | 71.2 | 60.8 | 69.9 | 32.8 | 32.4 | 11.0 | 6.4 |
| 5 | 7.9 | 13.5 | 17.8 | 33.9 | 93.0 | 103.7 | 83.7 | 91.4 | 39.2 | 35.8 | 17.6 | 9.2 |
| 6 | 68.1 | 77.7 | 108.4 | 145.7 | 196.6 | 217.5 | 199.2 | 196.8 | 125.4 | 99.7 | 103.4 | 91.2 |
| 7 | 53.9 | 66.4 | 99.4 | 127.4 | 153.0 | 177.9 | 161.0 | 159.4 | 101.6 | 81.8 | 89.4 | 76.9 |
| 8 | 59.2 | 69.8 | 100.5 | 129.4 | 159.9 | 181.6 | 163.2 | 163.6 | 104.9 | 86.2 | 92.1 | 79.8 |
| 9 | 61.2 | 72.0 | 96.2 | 105.3 | 96.3 | 105.0 | 84.5 | 95.0 | 63.8 | 73.0 | 82.7 | 67.1 |
| 10 | 72.7 | 85.2 | 101.3 | 101.8 | 79.7 | 87.2 | 78.4 | 84.7 | 59.1 | 71.3 | 81.1 | 76.4 |
| 11 | 165.4 | 174.9 | 198.9 | 204.4 | 174.3 | 164.6 | 161.5 | 170.9 | 124.5 | 166.3 | 167.7 | 160.2 |
| 12 | 319.4 | 332.0 | 371.6 | 349.3 | 286.0 | 250.1 | 295.5 | 307.2 | 210.4 | 305.9 | 301.6 | 307.8 |
| 13 | 126.9 | 132.6 | 139.0 | 134.2 | 106.4 | 116.3 | 118.2 | 110.2 | 93.9 | 100.8 | 106.9 | 124.1 |
| **Temperature [°C/month]** | | | | | | | | | | | | |
| 1 | 4.7 | 4.4 | 4.1 | 2.8 | 0.2 | -2.3 | -2.5 | -1.7 | 0.6 | 2.1 | 3.5 | 4.6 |
| 2 | 3.1 | 2.6 | 1.6 | -0.5 | -2.6 | -4.9 | -5.3 | -4.7 | -3.5 | -2.3 | 0.2 | 2.0 |
| 3 | -0.4 | -1.0 | -1.9 | -4.3 | -7.1 | -10.4 | -10.8 | -10.1 | -8.9 | -7.1 | -4.3 | -1.7 |
| 4 | 4.5 | 3.8 | 2.6 | -0.1 | -3.5 | -7.1 | -7.4 | -6.6 | -5.4 | -3.1 | -0.1 | 2.9 |
| 5 | 9.1 | 8.4 | 6.8 | 3.8 | 0.4 | -2.7 | -3.0 | -2.2 | -0.8 | 1.7 | 4.6 | 7.4 |
| 6 | 13.4 | 13.0 | 11.0 | 7.9 | 5.3 | 3.2 | 2.3 | 3.5 | 5.3 | 7.7 | 9.7 | 11.9 |
| 7 | 10.2 | 9.9 | 7.9 | 4.7 | 2.1 | -0.1 | -1.0 | 0.3 | 2.1 | 4.4 | 6.6 | 8.7 |
| 8 | 11.5 | 11.1 | 9.2 | 6.1 | 3.4 | 1.3 | 0.4 | 1.6 | 3.5 | 5.9 | 7.9 | 10.1 |
| 9 | 8.9 | 8.6 | 6.8 | 4.1 | 1.4 | -0.8 | -1.2 | -0.4 | 1.6 | 3.9 | 5.7 | 7.8 |
| 10 | 6.7 | 6.4 | 4.9 | 2.3 | -0.3 | -2.3 | -2.5 | -2.0 | -0.1 | 2.1 | 3.6 | 5.6 |
| 11 | 9.7 | 9.5 | 8.1 | 5.9 | 3.4 | 1.7 | 1.5 | 1.9 | 3.7 | 5.6 | 6.9 | 8.7 |
| 12 | 9.5 | 9.5 | 8.1 | 6.2 | 4.0 | 2.7 | 2.5 | 2.6 | 4.1 | 5.8 | 6.8 | 8.6 |
| 13 | 8.0 | 7.8 | 6.8 | 4.6 | 2.5 | 0.8 | 0.8 | 1.2 | 2.8 | 4.6 | 5.5 | 7.2 |

| Glacier cluster | Monthly climatic values 1980-2019 | | | | | | | | | | | |
|---|---|---|---|---|---|---|---|---|---|---|---|---|
| | Jan | Feb | Mar | Apr | May | Jun | Jul | Aug | Sep | Oct | Nov | Dec |
| Solar radiation [W/m2/month] | | | | | | | | | | | | |
| 1 | 224.2 | 199.5 | 224.4 | 210.1 | 182.6 | 175.5 | 179.6 | 206.7 | 233.3 | 251.1 | 258.7 | 248.4 |
| 2 | 307.9 | 275.3 | 258.2 | 204.6 | 136.4 | 112.7 | 119.8 | 156.5 | 216.3 | 275.2 | 311.8 | 334.5 |
| 3 | 284.9 | 251.1 | 223.5 | 157.4 | 103.5 | 93.4 | 100.8 | 131.2 | 173.5 | 228.7 | 270.1 | 297.2 |
| 4 | 291.4 | 264.5 | 223.9 | 157.5 | 100.3 | 84.4 | 94.3 | 123.9 | 167.9 | 221.6 | 268.3 | 300.5 |
| 5 | 294.2 | 263.1 | 216.6 | 154.4 | 99.0 | 81.0 | 91.4 | 119.9 | 168.0 | 217.9 | 266.1 | 297.2 |
| 6 | 232.3 | 206.3 | 146.4 | 95.7 | 61.0 | 40.8 | 48.6 | 76.0 | 107.8 | 156.6 | 194.1 | 221.8 |
| 7 | 208.7 | 185.0 | 130.1 | 82.6 | 56.2 | 34.0 | 41.6 | 64.7 | 91.6 | 132.7 | 162.8 | 194.8 |
| 8 | 218.4 | 193.3 | 136.3 | 87.3 | 56.6 | 35.6 | 43.3 | 68.2 | 97.1 | 143.1 | 175.8 | 206.4 |
| 9 | 185.9 | 159.6 | 110.6 | 69.1 | 44.6 | 27.9 | 34.8 | 55.6 | 82.7 | 127.8 | 158.2 | 181.6 |
| 10 | 173.6 | 148.8 | 102.2 | 62.2 | 40.4 | 26.2 | 32.1 | 53.0 | 79.0 | 121.7 | 151.1 | 172.9 |
| 11 | 162.9 | 143.2 | 98.1 | 64.8 | 43.1 | 29.2 | 34.1 | 59.6 | 82.6 | 123.3 | 150.5 | 167.0 |
| 12 | 154.4 | 137.4 | 93.6 | 61.1 | 40.1 | 24.1 | 27.9 | 51.6 | 76.8 | 117.4 | 147.4 | 160.9 |
| 13 | 151.6 | 131.6 | 87.2 | 51.2 | 31.8 | 18.6 | 22.8 | 43.8 | 70.6 | 114.5 | 149.5 | 160.1 |

*Source: self-made.*

# 5.2 Article n°2

This Article is available at https://doi.org/10.3389/feart.2021.713011

frontiers in Earth Science

ORIGINAL RESEARCH
published: 23 December 2021
doi: 10.3389/feart.2021.713011

## Climatic and Morphometric Explanatory Variables of Glacier Changes in the Andes (8–55°S): New Insights From Machine Learning Approaches

*Alexis Caro*, Thomas Condom and Antoine Rabatel*

*Univ. Grenoble Alpes, CNRS, IRD, Grenoble-INP, Institut des Géosciences de l'Environnement, Grenoble, France*

OPEN ACCESS

**Edited by:**
*Juan-Luis García, Pontificia Universidad Católica de Chile, Chile*

**Reviewed by:**
*Alfonso Fernandez, University of Concepcion, Chile*
*Lucas Ruiz, CONICET Argentine Institute of Nivology, Glaciology and Environmental Sciences (IANIGLA), Argentina*

***Correspondence:**
*Alexis Caro*
*alexis.caro.paredes@gmail.com*

**Specialty section:**
*This article was submitted to Cryospheric Sciences, a section of the journal Frontiers in Earth Science*

**Received:** *21 May 2021*
**Accepted:** *06 December 2021*
**Published:** *23 December 2021*

**Citation:**
*Caro A, Condom T and Rabatel A (2021) Climatic and Morphometric Explanatory Variables of Glacier Changes in the Andes (8–55°S): New Insights From Machine Learning Approaches. Front. Earth Sci. 9:713011. doi: 10.3389/feart.2021.713011*

Over the last decades, glaciers across the Andes have been strongly affected by a loss of mass and surface areas. This increases risks of water scarcity for the Andean population and ecosystems. However, the factors controlling glacier changes in terms of surface area and mass loss remain poorly documented at watershed scale across the Andes. Using machine learning methods (Least Absolute Shrinkage and Selection Operator, known as LASSO), we explored climatic and morphometric variables that explain the spatial variance of glacier surface area variations in 35 watersheds (1980–2019), and of glacier mass balances in 110 watersheds (2000–2018), with data from 2,500 to 21,000 glaciers, respectively, distributed between 8 and 55°S in the Andes. Based on these results and by applying the Partitioning Around Medoids (PAM) algorithm we identified new glacier clusters. Overall, spatial variability of climatic variables presents a higher explanatory power than morphometric variables with regards to spatial variance of glacier changes. Specifically, the spatial variability of precipitation dominates spatial variance of glacier changes from the Outer Tropics to the Dry Andes (8–37°S) explaining between 49 and 93% of variances, whereas across the Wet Andes (40–55°S) the spatial variability of temperature is the most important climatic variable and explains between 29 and 73% of glacier changes spatial variance. However, morphometric variables such as glacier surface area show a high explanatory power for spatial variance of glacier mass loss in some watersheds (e.g., Achacachi with $r^2$ = 0.6 in the Outer Tropics, Río del Carmen with $r^2$ = 0.7 in the Dry Andes). Then, we identified a new spatial framework for hydro-glaciological analysis composed of 12 glaciological zones, derived from a clustering analysis, which includes 274 watersheds containing 32,000 glaciers. These new zones better take into account different seasonal climate and morphometric characteristics of glacier diversity. Our study shows that the exploration of variables that control glacier changes, as well as the new glaciological zones calculated based on these variables, would be very useful for analyzing hydro-glaciological modelling results across the Andes (8–55°S).

**Keywords: climate drivers, morpho-topographic drivers, glacier changes, machine learning, clustering, andes**

## 1 INTRODUCTION

The Andes contain the largest concentration of ice in the southern hemisphere outside the Antarctic and its periphery (RGI Consortium, 2017). Andean glaciers have been affected by an almost continuous negative mass balance and consecutive shrinkage since the middle of the 20th century (Rabatel et al., 2013; Zemp et al., 2019). Despite considerable efforts in recent years regarding quantifications of glacier changes (e.g., Meier et al., 2018; Braun et al., 2019; Dussaillant et al., 2019; Seehaus et al., 2019, 2020), there is still much to investigate in order to analyze the controlling factors of these changes and to determine the hydrological significance of this glacier surface and mass loss on fresh water resources (e.g., Vuille et al., 2018; Masiokas et al., 2020). A better understanding of glacier changes across the Andes could contribute to anticipate and mitigate the related consequences and hazards at watershed scale, for instance in terms of water supply for roughly 45% of the population in Andean countries (Devenish and Gianella, 2012) and for ecosystems (Dangles et al., 2017; Zimmer et al., 2018; Cauvy-Fraunié & Dangles, 2019), primarily during the dry season (Mark et al., 2005; Baraer et al., 2012; Soruco et al., 2015; Guido et al., 2016; Ayala et al., 2020).

Glaciological studies carried out on a limited number of glaciers in the Outer Tropics (8–17°S) have underlined that atmospheric warming is an important control on the current glacier change mainly through the precipitation phases and consecutive albedo effect (Favier et al., 2004; Rabatel et al., 2013). The surface area and elevation of glaciers are morphometric variables that have also been identified to modulate the magnitude of glacier mass loss (e.g., Rabatel et al., 2006, 2013; Soruco et al., 2009). In the Southern Andes (17–55°S), studies focusing on long-term behavior of glaciers (i.e., since the mid-20th century) highlight a high correlation between precipitation and glacier mass balance in the Dry Andes (Rabatel et al., 2011; Masiokas et al., 2016; Kinnard et al., 2020), and with temperature in the Wet Andes (Masiokas et al., 2015; Abdel Jaber et al., 2019; Falaschi et al., 2019). These variables, primarily temperature and precipitation, have been widely used across the Andes to simulate glacier changes and related hydrological contribution through conceptual and physically-based hydro-glaciological models from a local scale to the scale of the Andes (Sicart et al., 2008; Ragettli and Pellicciotti, 2012; Huss and Hock, 2015, 2018; Soruco et al., 2015; Ayala et al., 2016, 2020; Bravo et al., 2017; Mernild et al., 2018; Burger et al., 2019; Shaw et al., 2020).

However, these studies did not quantified the relevance of morphometric variables to estimate glacier changes such as elevation and aspect, or glacier surface area and slope; these variables have already been significantly correlated to glacier changes in studies either dedicated to the Tropical and Southern Andes (e.g., Soruco et al., 2009; Rabatel et al., 2011) or in other mountain ranges (e.g., Rabatel et al., 2016; Brun et al., 2019; Bolibar et al., 2020; Davaze et al., 2020). In addition, simulations of glacier changes are traditionally conducted using geodetic mass balance products and few *in situ* glacier measurements available for calibration/validation purposes. However, glacier surface area changes are not frequently considered in hydro-glaciological simulations (e.g., Ayala et al., 2020; Baraer et al., 2012) and therefore this represents a source of uncertainty in long-term simulations of glacier changes and related impacts.

Currently, several glaciological datasets are available across the Andes thanks to local and international initiatives. Products estimating the geodetic glacier mass balance (GMB) for the whole Andes were recently published (Braun et al., 2019; Dussaillant et al., 2019), while glacier inventories have been made freely available (ANA, 2014; DGA, 2014; IANIGLA-CONICET, 2018; Seehaus et al., 2019, 2020). At the Andes scale, Dussaillant et al. (2019) estimated a negative GMB of $-0.72 \pm 0.22$ m w.e. $yr^{-1}$ (2000–2018), with most negative values in Patagonia ($-0.86 \pm 0.27$ m w.e. $yr^{-1}$) followed by the Outer Tropics ($-0.42 \pm 0.23$ m w.e. $yr^{-1}$), compared to moderate losses in the Dry Andes ($-0.31 \pm 0.19$ m w.e. $yr^{-1}$). Similar results were observed by Braun et al. (2019) for the Patagonian glaciers ($0.91 \pm 0.08$ m w.e. $yr^{-1}$) over a slightly shorter period (2000–2011/2015). Both works used version 6.0 of the Randolph Glacier Inventory (RGI Consortium, 2017) to map glacier outlines for GMB estimations, which includes fewer glaciers compared with national inventories (Zalazar et al., 2020). Conversely to GMB, no product is available for the whole Andes for glacier area variation (GAV). However, many studies have pointed out a negative GAV at a multidecadal time scale across all glacierized regions from the Outer Tropics to Tierra del Fuego (8–55°S). For example, Seehaus et al. (2019, 2020) observed an average GAV of -29% (±1.8% $a^{-1}$) (2000–2016) in the Outer Tropics. In the Dry Andes, an average GAV of -29% (1955–2007) was estimated in the Desert Andes (Rabatel et al., 2011), similar to that observed by Malmros et al. (2016) in the Central Andes (average of $-30 \pm 3$%, 1955–2014). However, a sharp contrast was observed in the Wet Andes, where the Lakes District shows a GAV between -87% (1975–2007) and -20% (1961–2007) on different volcanoes (Rivera and Bown, 2013), in the North Patagonia this reduction was -25% (1985–2011, Paul and Mölg, 2014), and from the Northern Patagonian ice-field to Tierra del Fuego, Meier et al. (2018) estimated an average GAV of -9 ± 5% (1986–2016) including several exceptions of glacier advance, e.g., Glacier Pio XI in the Southern Patagonian ice-field (Hata and Sugiyama, 2021; Rivera and Casassa, 1999; Wilson et al., 2016).

In the present study, our goal is to identify the main climate and morphometric variables that explain the spatial variance of glacier changes across the Andes (8–55°S) using GAV over the 1980–2019 period and GMB over the 2000–2018 period. Our approach is based on machine learning tools. The main explanatory variables of GAV and GMB will be identified at watershed scale using the Least Absolute Shrinkage and Selection Operator (LASSO) linear regression algorithm (Tibshirani, 1996), which has shown good results at glacier scale in the Alps (Bolibar et al., 2020; Davaze et al., 2020). These results will be used to determine new glaciological zones (hereafter named "clusters") across the Andes, composed of glacierized watersheds with similar morphometric and climatic characteristics. This

**TABLE 1 |** List of different glacier inventories is used to generate the multi-temporal glacier surface areas dataset across the Andes between 8–55°S.

| Country | Location, watersheds | Latitude range | Year range | Total glacier surface area [km$^2$] | Glacier number | Type of resource | Delineation technique | References |
|---|---|---|---|---|---|---|---|---|
| Perú | Across Perú | 8.2–15.8°S | 1955–1962 | 2,487 | 3,331 | O | M | Hidrandina (1989) |
| | Across Perú | 8.3–16.2°S | 2005–2012 | 1,299 | 2,679 | S | A + M | ANA (2014) |
| | Across Perú | 8.4–18.4°S | 2000–2016 | 4,901* | 5,835* | S | A | Seehaus et al. (2019) |
| | Across Perú | 8.4–15.9°S | 2016 | 1,118 | 2,259 | S | A + M | INAIGEM (2018) |
| Bolivia | Cordillera Real | 16.1–16.3°S | 2006 | 23 | 86 | S | M | Soruco et al. (2009) |
| | Cordillera Real | 15.8–17.1°S | 2000–2016 | 730* | 976* | S | A | Seehaus et al. (2020) |
| Chile | Maipo | 33.1–34.3°S | 1955–1976 | 626 | 1,466 | O | M | Marangunic (1979) |
| | Cachapoal watershed | 34.3–34.7°S | 1955 | 323 | 273 | O | M | Caviedes (1979) |
| | Tinguiririca watershed | 34.6–34.9°S | 1955 | 166 | 312 | O | M | Valdivia (1984) |
| | Atacama | 18.4–29.8°S | 1955–1976 | 54 | 11 | O | M | Garín (1987) |
| | Isla Riesco | 53.2°S | 1984 | 20 | 17 | S | A + M | Casassa et al. (2002) |
| | Gran Campo Nevado | 52.6–53.1°S | 1998 | 254 | 75 | O + S | A + M | Möller et al. (2007) |
| | Copiapó | 27.7–28.6°S | 2002 | 23 | 92 | O + S | A + M | Vivero (2008) |
| | North and volcanoes | 29.3, 37.9–41.2°S | 1961–2011 | 123* | 103* | O + S | A + M | DGA (2011) |
| | Volcanoes | 35.2–41.1°S | 1961–2011 | 83* | 163* | O + S | A + M | Rivera & Bown (2013) |
| | Across Chile | 17.6–55.4°S | 1996–2009 | 23,641 | 24,109 | O + S | A + M | DGA (2014) Barcaza et al. (2017) |
| | North of Chile | 26.5–29.7°S | Until 2015 | 95 | 884 | S | A + M | García et al. (2017) |
| | Olivares watershed | 32.9–33.5°S | 1955–2013 | 1,289* | 428* | O + S | A + M | Malmros et al. (2016) |
| | Maipo | 33.1–34.3°S | 2018 | 366 | 1,232 | S | A + M | AMTC (2019) |
| AR | Across Argentina | 22.1–54.9°S | 2004–2015 | 5,749 | 17,957 | O + S | A + M | IANIGLA-CONICET (2018) Zalazar et al. (2020) |
| CL and AR | Patagonia and Tierra del Fuego | 45.5–55.5°S | 1984–2017 | 117,216* | 41,062* | S | A | Meier et al. (2018) |
| PE, BO and CL | PE, BO and CL | 8.8–55.3°S | 1955–2011 | 107,245* | 35,950* | O + S | A + M | GLIMS (Raup et al., 2007) |

*Country code: AR, Argentina; CL, Chile; PE, Perú; BO, Bolivia.*
*Type of document: O, Orthophotographs; S, Satellite images. Delineation technique: A, automatic; M, manual.*
**Multitemporal glacier surface area inventory.*

clustering will be performed *via* the Partitioning Around Medoids (PAM) algorithm (Kaufman and Rousseeuw, 2008). We therefore propose an alternative to the glaciological zones used to date (hereafter named "classic zones") based mainly latitudinal ranges (Barcaza et al., 2017; Dussaillant et al., 2019; Lliboutry, 1998; Masiokas et al., 2009; Sagredo and Lowell, 2012; Troll, 1941; Zalazar et al., 2020), and we provide a hydro-glaciological analysis framework based on the explanatory variables of glacier changes spatial variance across the Andes.

**Section 2** presents the material and methods used here. In **Section 3**, we describe glacier changes (GAV and GMB) and show results regarding the controlling factors of glacier change at watershed scale and cluster scale across the Andes. Finally, in **Section 4** we discuss our results and advantages associated with carrying out future glacier change simulations.

## 2 MATERIALS AND METHODS

### 2.1 Glacier Area Variation Across the Andes

#### 2.1.1 Collected Glacier Inventories

Glacier inventories have been published since 1950-60s with several updates in Perú, Bolivia, Chile and Argentina. For this current work, we collected data from national institutions, published studies, and the international GLIMS initiative (Raup et al., 2007). All collected glaciers inventories are listed in **Table 1** (**Supplementary Figure S3**). Glacier outlines were delineated based on aerial photographs and satellite images using visual identification (manual mapping) or by applying an automatic identification for the most recent inventories based on satellite data. In the latter case, automatic delineations were adjusted by visual checks and manual correction whenever needed. In many cases, remote sensing approaches were completed by several field campaigns for *in situ* verifications. These inventories can contain either one glacier outline per glacier (mono-temporal inventories) or several outlines from different years for each glacier (multi-temporal inventories). They have different spatial scales, from specific watersheds to national and multinational extensions.

#### 2.1.2 Glacier Inventories Merging

Based on the most recent glacier inventories made by a government initiative in Perú, Chile and Argentina (ANA, 2014; DGA, 2014; IANIGLA-CONICET, 2018), which are hereafter called the national glacier inventories (NGIs), and the Seehaus et al. (2020) glacier inventory in Bolivia. For Argentina, we do not consider some missing glaciers outlines in the inventory (without polygons), located in the Patagonian ice-field, due to this, the total glacierized area will decrease. It was possible to generate a merged product with glacier outlines from these four Andean countries, where each glacier has an identifier (ID). This ID allows to extract information from each glacier,

such as: coordinates of the centroid, glacier surface areas (and corresponding dates), elevation (maximum, minimum and mean) and aspect (Degree). The slope variable (Degree) was extracted for each glacier from the Shuttle Radar Topography Mission (SRTM) v4.1 product with a pixel size of 100 m (Farr et al., 2007). Here, the surface slope of all glaciers was estimated with the DEM in order to have values quantified in the same way, since no slope data are available for some inventories.

The following procedures and limitations were applied: 1) the glacier inventories were processed in the World Geodetic System (WGS84) and the slope data was extracted using Universal Transverse Mercator (UTM) coordinate system; 2) a glacier is considered to be a polygon found entirely within a single watershed, so that the same glacier cannot be located in two or more watersheds; and 3) rock glaciers and debris-covered glaciers were not considered.

#### 2.1.3 Glacier Area Variation Algorithm

The multi-temporal glacier surface areas dataset (**Table 1**) is used to apply a linear regression for each glacier (surface area = $f$ (time)), where glacier areas per each year until 2018 were used. In order to have a homogeneous dataset across the Andes, we consider the surface area changes over the 1980–2019 period from linear regression of multi-temporal glacier surface areas (glacier outlines) identified in the national glacier inventories. For each glacier, we obtained the slope of linear regression and a coefficient of determination that are both used to evaluate the regressions. After that, we only retain the glaciers that meet the following criteria:

- Glaciers are assumed to show a reduction in the surface area since 1980 up to 2019 (Malmros et al., 2016; Meier et al., 2018; Rabatel et al., 2011; Rivera and Bown, 2013; Seehaus et al., 2019, 2020; Soruco et al., 2009). Therefore, we keep the glaciers for which the linear regression slope between the glacier surface area and date (year) is negative. A positive slope can be found due to differences in the method used to identify glacier outlines, given that all inventories did not use the same criteria to define accumulation zone limits. An example of a positive slope is observed in the Patagonian ice-fields from Meier et al. (2018) in comparison with the Chilean glacier national inventory (Barcaza et al., 2017; DGA, 2014). Another reason for the positive slope is the source date of certain inventories, since discrepancies were observed between the Chilean and Argentine national glacier inventories *versus* the GLIMS inventory data.
- Taking the above information into account, glaciers that show a positive linear regression slope or a negative slope with $r^2 < 0.7$ are removed.
- Subsequently, when looking at the values of the linear regression slope (GAV rates by year), we identified high GAV rates for some glaciers. For example, if a glacier with a surface area of 3 $km^2$ shrinks to 0.01 $km^2$ within a 1-year interval (i.e., a reduction of 99.7%, which is very unlikely) the slope of resulting linear regression is -2.99 $km^2$ $yr^{-1}$. Due to the above, such glaciers with a linear regression slope lower than -1 were considered as outliers and consequently discarded.
- Large glaciers associated with the Patagonian ice-fields that are calving were filtered out. This criterion was chosen because most of the contours of these glaciers show high differences in accumulation zones, where we cannot discriminate if glacier reduction is for differences in accumulation zones or for frontal retreat. In addition, for these glaciers, the water temperature is an important calving process (Sakakibara et al., 2013; Sakakibara and Sugiyama, 2014), that we have not considered in our study.

These filters allowed to obtain GAV data for 4,865 glaciers out of a total of 9,229 glaciers analyzed, where the average number of data used per glacier for estimate GAV was four outlines (polygons). The mean statistical significance (*p-value*) of GAV was < 0.001.

### 2.2 Glacier Mass Balance

The average annual glacier-wide mass balance for each glacier was recalculated for the 2000–2018 period from the glacier change elevation produced by Dussaillant et al. (2019) using ASTER stereo images and applying the ASTERiX methodology. In contrast with Dussaillant et al. (2019), who used the Randoph Glacier Inventory (RGI Consortium, 2017) to calculate the glacier-wide mass balance, we used glacier outlines from the national glacier inventories compiled for Perú, Bolivia, Chile and Argentina (8–55°S). The specific glacier mass balance (mb) was estimated using the glacier surface elevation change by cell (~30 × 30 m) and a glacier ice density of 900 kg/$m^3$ (Cuffey and Paterson, 2010). Finally, in order to obtain a comparative indicator of mass change we calculated the glacier mass balance per glacier ($GMB_n$) as the addition of mb (**Eq. 1**).

$$GMB_n = \sum_{i=1}^{n} mb_i \quad (1)$$

In addition, we did not extrapolate the glacier change elevation for data gaps which occur in some glaciers of the Patagonian ice-fields. The mass balance uncertainty per glacier was estimated using the random error methodology that considers uncertainties on surface elevation change, glacierized area and the volume to mass conversion factor (Brun et al., 2017). In the supplementary material, the GMB derived by Dussaillant et al. (2019) and the ones from the present study are compared considering 1° latitudinal ranges.

### 2.3 Terra Climate Dataset

The TerraClimate dataset comprises a global dataset based on reanalysis data since 1958, with a 4 km grid size at a monthly time scale. This dataset was validated with the Global Historical Climatology Network using 3,230 stations for temperature ($r$ = 0.95; mean absolute error 0.32°C) and 6,102 stations for precipitation ($r$ = 0.90; mean absolute error 9.1%) (Abatzoglou et al., 2018). Here, variables such as the mean temperature, maximum temperature, minimum temperature and precipitation were processed. Based on these four variables, we calculated monthly averages for the periods 1980–2019 and 2000–2018, resulting in 36 (except mean temperature) and 48

climate variables, respectively. These variables were extracted for each grid cell where a glacier was found.

A monthly scale was necessary in order to be able to consider the seasonal differences across the Andes. Most of the glaciers are contained in a single TerraClimate cell, however, for the large glaciers of the Patagonian ice-fields, we only consider cells that encompass the centroid of those glaciers. Mean temperature was estimated from the maximum and minimum monthly temperatures. The mean temperature was not considered for the GAV analysis because the LASSO method should not have more variables than glaciers as samples in linear regression. Below, we show that smallest number of samples by watershed are 35 glaciers for the GAV analysis. For precipitation, we consider snowfall and rainfall together, i.e., we do not perform a phase discrimination using a temperature threshold.

## 2.4 Explanatory Variables of GAV and GMB

### 2.4.1 Data Pre-processing and Watershed Delineation

Morphometric and climate variables extracted from the national glacier inventories and TerraClimate dataset allowed to create two matrices for GAV (1980–2019) and GMB (2000–2018), respectively. The spatial domain at which the GAV and GMB analyses are carried out is the watershed. The watersheds were estimated using the ArcGis v10.6 software. The SRTM v4.1 product with a 100 m resolution (Farr et al., 2007) allowed estimating watershed contours by means of the flow direction and accumulation modules. For the Chilean Patagonian islands, we used the watershed classification provided by the *Dirección General de Aguas* of Chile (Benítez, 1978). Overall, we identified 274 watersheds with a surface area ranging from 260 to 8,095 $km^2$ (mean 2,058 ± 1,271 $km^2$), with a glacierized surface area > 0.01% and hosting at least 10 glaciers. Each watershed has an identification (ID) associated with the glacier central coordinates (centroid).

### 2.4.2 Explanatory Variables Estimation Using the LASSO Method

Correlations between variables with respect to GAV and GMB for each glacier at watershed scale were estimated through LASSO (Tibshirani, 1996) on at least 35 and 50 glaciers by watersheds for GAV and GMB, respectively. This consideration is associated with the existence of glacier change data inside of each watershed, and because LASSO needs a sample minimum greater than a number of predictive variables of GAV and GMB. Recently, Bolibar et al. (2020) and Davaze et al. (2020) have shown satisfactory results using this algorithm in the Alps but at glacier scale and using temporal series. Classical linear regression methods calculate a coefficient values that maximize the $r^2$ value and minimize the error using all available explanatory variables, which results in a high variance and low bias model. The LASSO algorithm trades some of variance with bias to reduce the predictive error and to discard variables that do not explain a sufficient amount of variance in data. To reduce the prediction error, the cross-validation (CV) method is applied, which allows to select an optimal value of lambda penalty parameter. It consists of choosing a set of values for lambda where the error is calculated for each value and lambda value that gives least error is chosen. Afterward, the model is used with a chosen lambda value. We used the package "glmnet" in R to implement the LASSO algorithm (Friedman et al., 2010; Simon et al., 2011), considering 80% of data for training and remaining 20% to evaluate the error at watershed scale. Because no test method exists yet to evaluate the LASSO algorithm performance (Lockhart et al., 2015), we used the root mean square error (RMSE) derived from the LASSO algorithm to evaluate the results and we implemented the *p-value* test from the multiple linear regression method (MLR) to evaluate statistical significance of variables selected by the LASSO algorithm.

Additionally, to analyze the explanatory variables contribution of GAV and GMB at cluster and classic zone scales, we group the monthly climate variables selected by the LASSO algorithm to a single one, where the percentage of variance explained by each monthly variable will be combined. For example, OT3 (with data from seven watersheds for GMB) groups 25 values of morphometric and monthly climate variables, repeating some variables between watersheds, but identifying 15 unique variables for the whole cluster. In each watershed, the sum of each variable's value contributes 100% to the explained variance ($r^2$). Subsequently, the percentages of repeated climatic variables are added where, for example, monthly values of $P_{Jul}$ present in three watersheds (three values) will be added and called $P_{Jul}$. As a result, the 25 variables' value become 15 and when added together contribute 100% of the explained variance. In summary, precipitation variables (composed of 9 monthly values) contribute 82% to the GMB variance in OT3, followed by slope (13%), surface area (2%), and other variables (3%).

## 2.5 Clustering Analysis to Define New Glaciological Zones Derived From the Explanatory Variables of GAV and GMB

A clustering analysis is used to group together glacierized watersheds with similarities by taking the relevant morphometric and climate variables of the GAV and GMB analysis into account. In order to do this, we use the Partitioning Around Medoids (PAM) algorithm (Kaufman and Rousseeuw, 2008), and the Hopkins and Gap statistical methods were used to estimate clustering tendency and optimal number of clusters, respectively (Lawson and Jurs, 1990; Tibshirani et al., 2001). We used the package "cluster" in R to implement the PAM algorithm (Maechler et al., 2021), organizing variables in columns and watersheds in rows to run the PAM algorithm and all subsequent tests. The Hopkins method shows a value of 0 when a dataset is optimal for performing a clustering analysis, whereas a value of 1 shows that data is already clustered. We used this test to show the high diversity between glacierized watersheds across the Andes. In hydrology, homogeneous hydro-meteorological regions are commonly identified using a clustering analysis to transfer information toward ungauged watersheds, assuming a similarity approach. For example, the fuzzy clustering algorithm uses climate variables to determine homogeneous regions (Hall and Minns, 1999; Dikbas et al., 2012; Sahin and Kerem, 2012; Bharath and Srinivas, 2015; Matiu et al., 2020). Sometimes, geomorphological variables are also

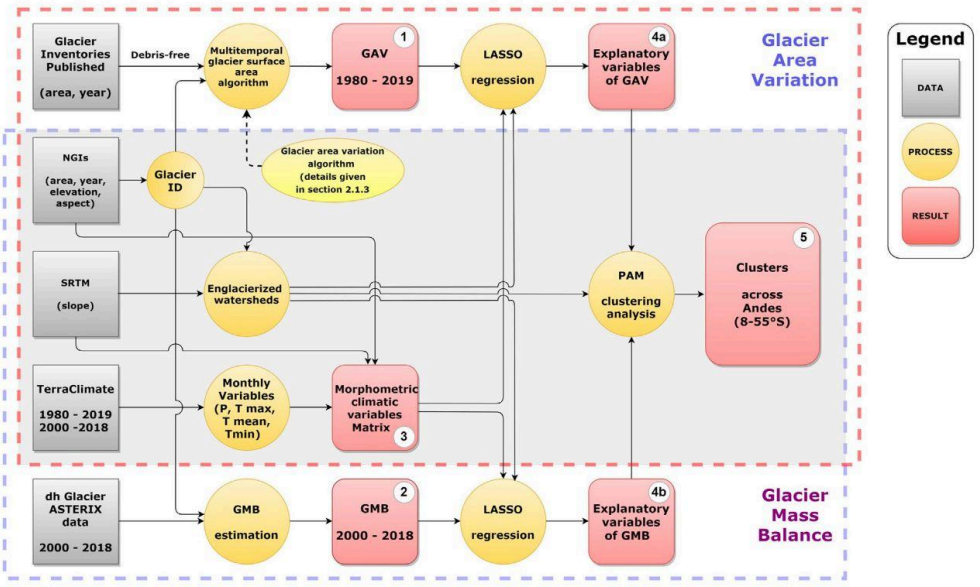


**FIGURE 1 |** The workflow to obtain the explanatory variables of the glacier area variation (GAV) and glacier mass balance (GMB) spatial variances is presented. The final results are used to estimate clusters between 8–55°S using the explanatory variables of glacier changes. The numbers from 1 to 5 refer to the 5 steps described in the text.

considered (e.g., Pagliero et al., 2019). Inside the fuzzy clustering algorithm, the PAM algorithm divides a dataset into groups where each one is represented by one of data points in the group. These points are called a medoids cluster, which is an object within a cluster for which average difference between it and all other clustering members is minimal (Kaufman and Rousseeuw, 2008; Lee et al., 2020). This method, using k-medoids, represents an improvement on the k-means algorithm; it is less sensitive to outliers because it does not use an average as central object (Arora et al., 2016; Lee et al., 2020). Finally, explanatory capacity of each variable in the GAV and GMB represented variances is given for each watershed and then at cluster scale.

Considering the sensitivity of the watersheds to cluster assignment by the PAM algorithm, we performed a sensitivity analysis associated with the removal of variables or group of variables and also by changing the variable values. Considering 1,000 iterations of the PAM algorithm, in each iteration, different variables were removed from the dataset. For example, monthly Tmax, then monthly Tmin and after monthly precipitation were excluded, then morphometric variables were also excluded one by one. On the other hand, in each new iteration the variable values were increased or decreased considering factors between 0.9 and 1.1. Factor values were random for each variable associated with a watershed and were updated for each new iteration. The evaluation was conducted using 274 watersheds and considering comparisons between the PAM runs (the most frequent assignment of a cluster to a watershed) using: 1) only climatic variables, 2) only morphometric variables, and 3) morphometric and climatic variables (removing one variable or a group of variables at each PAM iteration), in relation to each single PAM run removing one morphometric variable or a group of climatic variables. This means that each single PAM run removing one morphometric variable or a group of climatic variables were evaluated with regards to (i), (ii), and (iii) through the coefficient of determination.

## 2.6 Methodological Workflow

This section considered the next overall steps: In step 1) "Glacier area variations 1980–2019", the glacier inventories used to identify each glacier and how its surface area has changed are used. The morphometric variables (surface area, elevation and aspect) are extracted from these inventories and from SRTM data (slope). In step 2) "Glacier mass balance 2000–2018," the procedure used to obtain glacier mass change data based on the ASTERIX product (e.g., Dussaillant et al., 2019) is applied. In step 3) "Morphometric-climatic variables matrix", the monthly climate values (precipitation and temperature) are extracted and implemented in a matrix with the morphometric variables. In step 4) "Explanatory variables of GAV (4a) and GMB (4b)", the matrix of variables is used to derive relationships to explain GAV and GMB through the LASSO algorithm. In step 5) "Clusters", a

clustering analysis is carried out based on the explanatory variables of GAV and GMB.

**Figure 1** illustrates the methodological workflow used in this study. It is composed of five steps that are first used to identify the explanatory variables for GAV over the 1980–2019 period and GMB over the 2000–2018 period. Then, the workflow allows to cluster watersheds based on the explanatory variables of recent glacier changes from the Outer Tropics to Tierra del Fuego (8–55°S).

# 3 RESULTS

## 3.1 Morphometric and Climate Settings

From the national glacier inventories, we considered and identified 44,853 glaciers with a total glacierized area of 29,387 $km^2$ between 8 and 55°S. Of this glacierized surface area, 95% (33,000 glaciers, 27,793 $km^2$) corresponds to free-of-debris glaciers, while 3% (10,881 glaciers, 1,041 $km^2$) are rock glaciers (not considered in this study) and 2% (972 glaciers, 552 $km^2$) are debris-covered glaciers (not considered in this study). Within the studied countries, Chile has the largest glacierized area comprising 78% of the total, followed by Argentina (16%), Peru (5%) and Bolivia (1%). Due to data lacks on glacier outlines of the Southern Patagonian Icefield (on the Argentinean side mainly), these were not considered in this analysis. Therefore, our final sample contains 85% (31,963) of glaciers covering 71% (24,888 $km^2$) of the glacierized surface area across the Andes identified here.

Following the classic zones defined based on former studies (Troll, 1941; Lliboutry, 1998; Masiokas et al., 2009; Sagredo and Lowell, 2012; Barcaza et al., 2017; Dussaillant et al., 2019; Zalazar et al., 2020), 72% of the glacierized area are concentrated in South Patagonia and North Patagonia between 42 and 53°S, where glaciers have a mean elevation of 1,560 m a.s.l. The Tierra del Fuego zone (53–55°S) concentrates 14% of the glacierized area with a mean elevation of 830 m a.s.l. The longest latitudinal extent north of the North Patagonia include zones from the Outer Tropics to the Lakes District (8–42°S) which only contains 14% of the glacierized area. Along this extent (8–42°S), the Outer Tropics (8–17°S) and the Central Andes (30–37°S) zones contain 6% of the glacierized area each. The highest mean elevations of glaciers are found in the Desert Andes (5,575 m a.s.l.) followed by the Outer Tropics (5,177 m a.s.l.).

From a climatic point of view, the mean annual temperature over the 1980–2019 period at glacier elevation tend to decrease from the Outer Tropics (3.2°C) to the Central Andes (-2.7°C). Southward of the Lakes District, the mean annual temperature increases (5.4°C) above the values found in the north and then decreases toward Tierra del Fuego (3.8°S). With regards to precipitation, the mean annual amount decreases from the Outer Tropics (912 mm $yr^{-1}$) to the Dry Andes (151 mm $yr^{-1}$), from where it increases to Southern Patagonia (1,770 mm $yr^{-1}$). Southward, Tierra del Fuego shows a lower amount of precipitation, even less than the Lakes District (1,105 mm $yr^{-1}$). In addition to observed morphometric and climatic differences between the classic zones, it is also possible to identify major differences inside these zones at grid scale (1 × 1°) as shown in the supplementary material (**Supplementary Figure S1** and **Supplementary Figure S2**).

## 3.2 Glacier Surface and Mass Loss

Across the Andes between 8 and 55°S, the mean GAV was estimated to be -31.2 ± 0.6%. This was quantified from data available on 21% (5,160 $km^2$) of the glacierized area across the Andes (**Figure 2A**). The Outer Tropics showed a reduction of −41 ± 0.01% whereas a reduction of −30 ± 0.6% was found for the Southern Andes. For these two regions, these estimates are based on 50 and 19% of the glacierized area, respectively. In the Southern Andes, the Desert Andes (17–30°S) shows the largest shrinkage (−53 ± 0.002%), followed by the Central Andes (30–37°S) with a GAV of −39 ± 0.01%. In the Wet Andes (37–55°S), the Lakes District shows a GAV of −52 ± 0.1%, followed by North Patagonia (−32 ± 1.3%), South Patagonia (−28 ± 1.4%) and Tierra del Fuego (−24 ± 0.4%). For these GAV estimates, the proportion of glacierized area considered varies from one zone to another, comprising 23% of the glacierized area in the Central Andes, 20 and 13% in North and South Patagonia, respectively, and 33% in Tierra del Fuego. In smaller glacierized zones of the Andes (representing 2% of the total), GAV estimates for the Desert Andes and the Lakes District is based on 13% of the glacierized area. Regarding GAV statistical significance, the mean *p-value* was < 0.001. However, 11 of 48 latitudinal ranges from 8 to 55°S showed *p-values* > 0.05. These are located at 12–14°S, 15–16°S, 18°S, 36°S, 38°S, 40°S, and 46–47°S.

Additionally, the GMB is estimated to be -0.82 ± 0.12 m w.e. $yr^{-1}$ when considering 96% (23,978 $km^2$) of the glacierized area of the Andes between 8 and 55°S (**Figure 2B**). The Outer Tropics show a lower mass loss (−0.47 ± 0.03 m w.e. $yr^{-1}$) compared to the southern Andes (−0.84 ± 0.13 m w.e. $yr^{-1}$). In the Dry Andes, the Central Andes show a greater loss (−0.43 ± 0.05 m w.e. $yr^{-1}$) compared to the Desert Andes (−0.22 ± 0.03 m w.e. $yr^{-1}$). In the Wet Andes, North Patagonia presents the greatest loss with −0.96 ± 0.18 m w.e. $yr^{-1}$, followed by South Patagonia (−0.9 ± 0.27 m w.e. $yr^{-1}$), the Lakes District (−0.72 ± 0.08 m w.e. $yr^{-1}$), and Tierra del Fuego (−0.56 ± 0.24 m w.e. $yr^{-1}$). The proportion of glacierized area considered to estimate that GMB is greater than 94% in most of the zones, except in the Central and Desert Andes where these percentages are 72 and 47%, respectively. **Table 2** summarizes GAV and GMB for the classic zones, while differences observed in the GMB estimation by this work, Dussaillant et al. (2019), Braun et al. (2019) and Seehaus et al. (2019, 2020) are shown in the supplementary material (**Supplementary Figure S4** and **Supplementary Table S1**).

Regarding the relationship between GAV and GMB at watershed scale ($n$ = 107; for 3,978 glaciers with a minimum of 10 and maximum of 176 per watershed), **Figure 3** shows that even if the two variables are statistically correlated for several watersheds (mostly located in the Southern Andes between 45 and 50°S), no correlation is found across the Andes. This result justifies identifying separately the morphometric and climate controls for GAV and on the other hand for GMB,

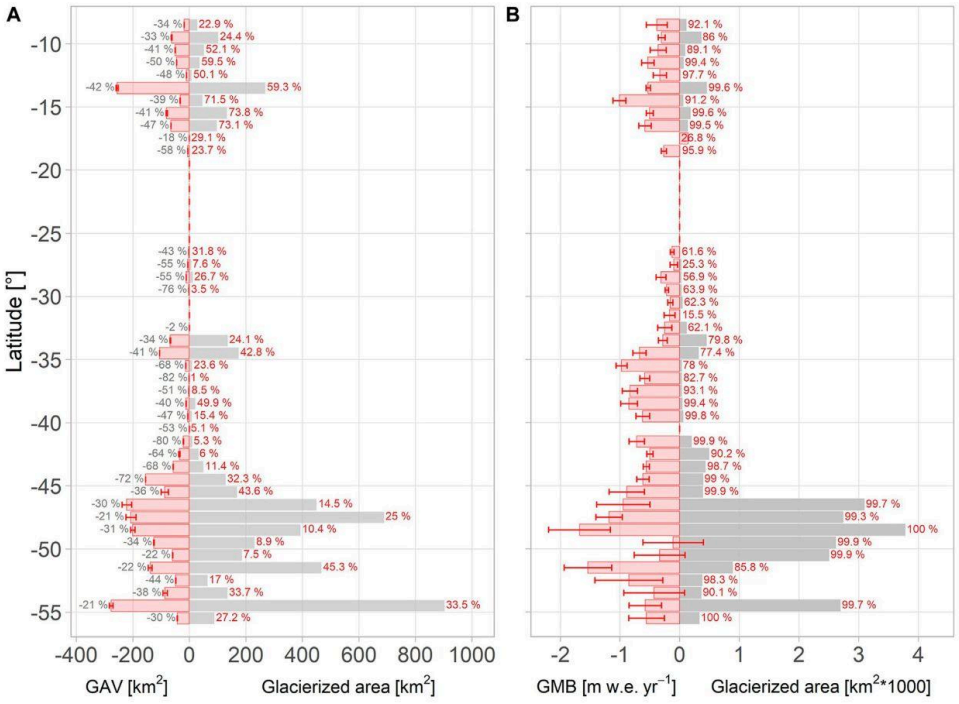


**FIGURE 2 |** The latitudinal GAV (1980–2019) and GMB (2000–2018) across the Andes (8–55°S) are presented in this figure. **(A)** For each 1° latitudinal bar of GAV (red bars) the GAV error (red lines), and percentage of the mean GAV (gray texts) are presented, while the glacierized area used in GAV estimation (gray bars), as well as the percentage of this glacierized area with regards to the total estimated by the national inventories (red text) are shown. **(B)** The GMB (red bars), the GMB error (red lines), and the related glacierized area (gray bars) are presented, indicating the percentage of the glacierized area used in the GMB estimation with regard to the total estimated in the national inventories (gray text). The GMB estimation contains 96% (23,978 km$^2$) of the glacierized area distributed between 26,856 glaciers considered in this study.

considering that the GAV and GMB data include different time ranges with different response times and glacier dynamics.

### 3.3 Explanatory Variables of Glacier Changes Across the Andes

The explanatory capacity of variables on the spatial variance of GAV (1980–2019) and GMB (2000–2018) in Perú, Bolivia, Argentina, and Chile were obtained from 35 watersheds for GAV and from 110 watersheds for GMB (**Figure 4A**) through the LASSO method. The watersheds where the GAV variance was predicted show a mean coefficient of determination of 0.49 (RMSE = 0.85 km$^2$; *p-value* from MLR < 0.05; number of glaciers = 2,484). The lower number of glaciers considered here with regard to the total GAV data (4,865 glaciers) is due to removal of watersheds that do not have a glacierized area > 0.01% of watershed area and a minimum of 35 glaciers. For the remaining 35 watersheds, the LASSO algorithm identified 39 explanatory variables for the GAV dataset. However, this number of explanatory variables differs between watersheds, with a maximum of 21 variables identified by LASSO in some watersheds. Similarly, the GMB analysis considered a minimum of 50 glaciers per watershed, resulting in a mean coefficient of determination of 0.35 for the 110 watersheds (RMSE = 0.35 m w.e. yr$^{-1}$; *p-value* from MLR < 0.05; number of glaciers = 20,740) (**Figure 4B**). The reduction in the number of glaciers (from 31,963 to 20,740) used in the LASSO analysis was due to the smallest number of glaciers considered by watershed. For these 110 watersheds, the LASSO algorithm identified 54 explanatory variables (43 explanatory variables in certain watersheds). These results are presented for the classic zones in the supplementary material (**Supplementary Table S2**), while the coefficient of determination for LASSO and MLR (*p-value*) results are shown in **Supplementary Figure S5**.

Based on the 39 variables that explain the GAV variance, on average for the entire study region (8–55°S), the morphometric

**TABLE 2 |** GAV (1980–2019) and GMB (2000–2018) for the classic zones of the Andes.

| Zones | Latitude (°S) | Glacierized area [%] | Glacierized area [km$^2$] | GAV used area [%] | Mean GAV [%] | GAV st. Dev. [%] | GMB* used area [%] | Mean GMB [m w.e. yr$^{-1}$] | GMB st. Dev. [m w.e. yr$^{-1}$] |
|---|---|---|---|---|---|---|---|---|---|
| Outer Tropics | 8–17 | 6 | 1,555 | 50 | −41.0 ± 0.01 | 25 | 94 | −0.47 ± 0.03 | 0.49 |
| Desert Andes | 17–30 | 1 | 217 | 13 | −53.3 ± 0.002 | 27 | 47 | −0.22 ± 0.03 | 0.17 |
| Central Andes | 30–37 | 6 | 1,398 | 23 | −39.0 ± 0.01 | 27 | 72 | −0.43 ± 0.05 | 0.31 |
| Lakes District | 37–42 | 1 | 351 | 13 | −51.7 ± 0.1 | 30 | 98 | −0.72 ± 0.08 | 0.40 |
| North Patagonia | 42–48 | 31 | 7,638 | 20 | −32.2 ± 1.3 | 27 | 99 | −0.96 ± 0.18 | 0.34 |
| South Patagonia | 48–53 | 41 | 10,303 | 13 | −27.6 ± 1.4 | 25 | 98 | −0.90 ± 0.27 | 0.82 |
| Tierra del Fuego | 53–55 | 14 | 3,426 | 33 | −23.9 ± 0.4 | 24 | 98 | −0.56 ± 0.24 | 0.81 |
| Southern Andes | 17–55 | 94 | 23,333 | 19 | −29.5 ± 0.6 | 26 | 96 | −0.84 ± 0.13 | 0.56 |
| Andes | 8–55 | 100 | 24,888 | 21 | −31.2 ± 0.6 | 27 | 96 | −0.82 ± 0.12 | 0.56 |

*This "GMB, used area" comprises glacier surface area of each glacier where GMB, data is available.

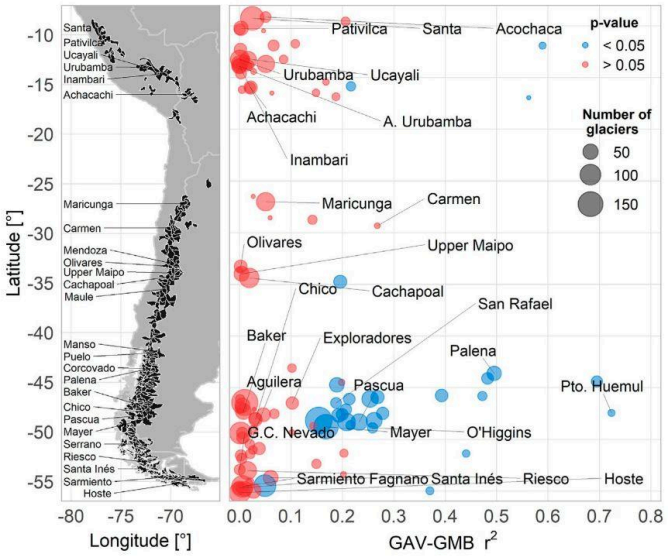


**FIGURE 3 |** The distribution of the 274 glacierized watersheds (glacier cover > 0.01%) across the Andes (8–55°S) and the GAV (1980–2019) and GMB (2000–2018) correlation at watershed scale for 107 watersheds are presented, with its statistical significance and number of glaciers considered in each watershed.

variables such as surface area (16%) and elevation (7%) are those that contribute most, whereas highest contribution of a climate variable is only 5% ($Tmax_{Jan}$). However, if we combine the contribution of monthly climate variables to the GAV variance, the order of explanatory variables changes (e.g., the contribution of monthly climate variables are combined in a single percentage for precipitation, Tmax and Tmin). As such, the climate variables explain 65% of the GAV variance (with temperature and precipitation contributing 35 and 30%, respectively), whereas surface area and elevation explain 16 and 15% of variance, respectively, followed by slope (4%) and aspect (1%). Looking at the GMB variance, on average across the Andes, surface area of glaciers (26%) is the variable that contributes highest percentage, followed by $Tmax_{Nov}$ (5%)

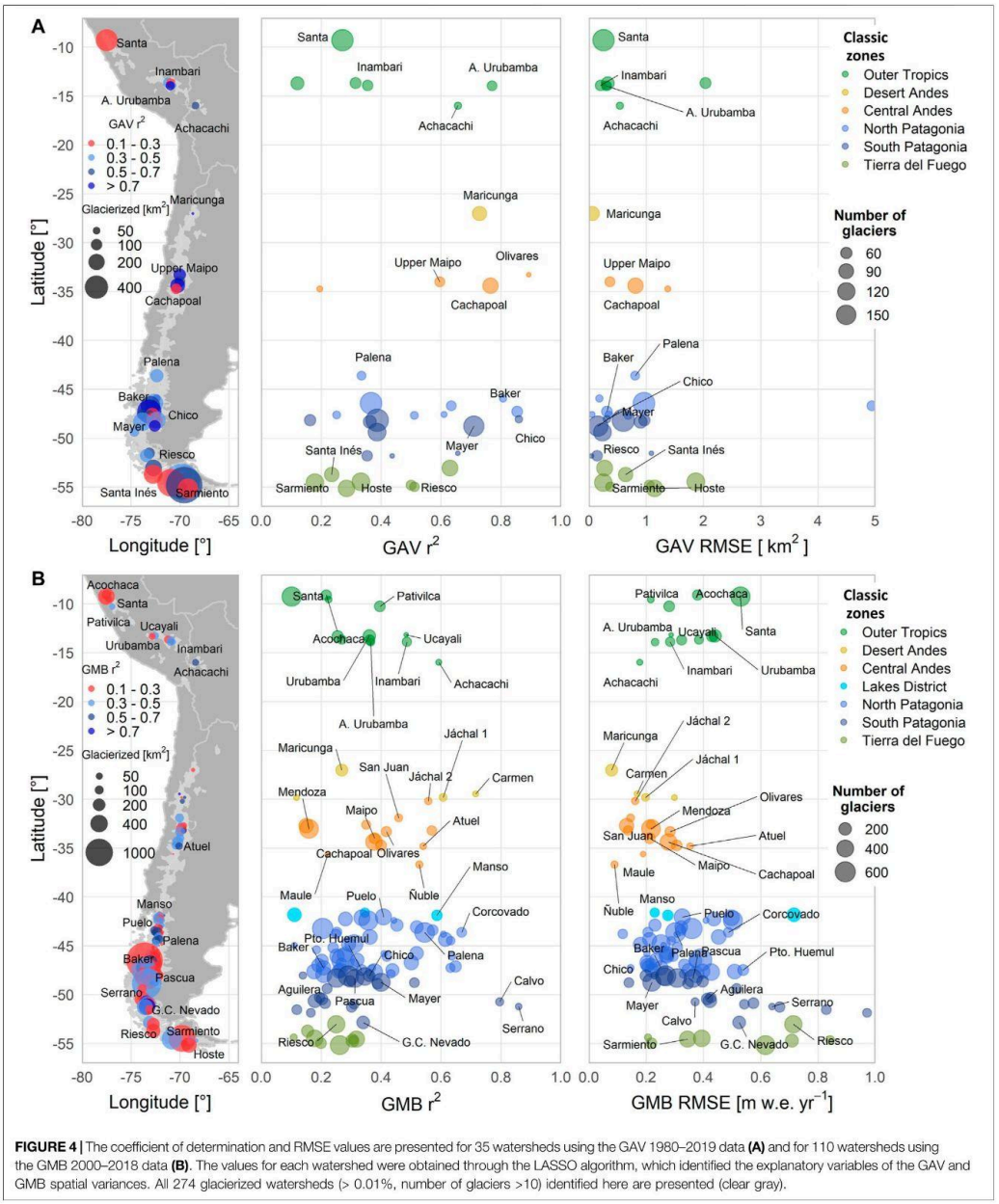


**FIGURE 4 |** The coefficient of determination and RMSE values are presented for 35 watersheds using the GAV 1980–2019 data **(A)** and for 110 watersheds using the GMB 2000–2018 data **(B)**. The values for each watershed were obtained through the LASSO algorithm, which identified the explanatory variables of the GAV and GMB spatial variances. All 274 glacierized watersheds (> 0.01%, number of glaciers >10) identified here are presented (clear gray).

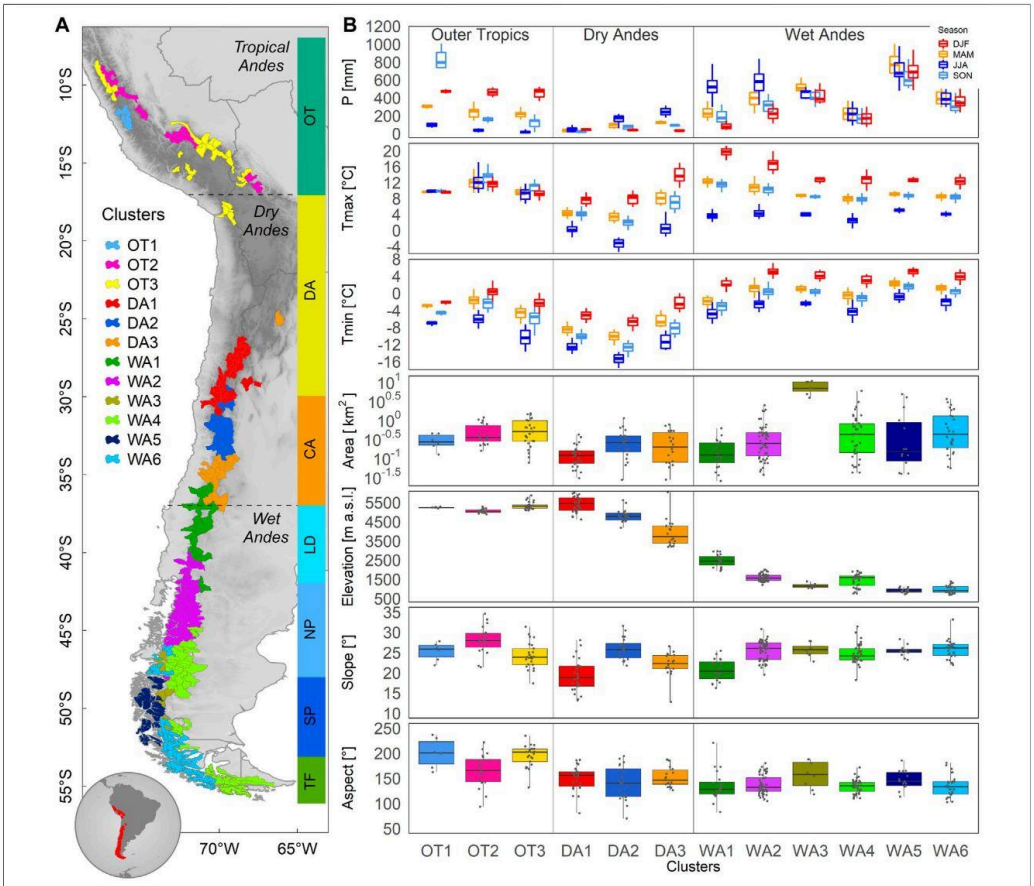


**FIGURE 5 |** The 12 clusters of the glacierized watersheds across the Andes (8–55°S) and the behavior of climatic and morphometric variables. The average values of variables (for 274 watersheds and using 31,963 glaciers) are presented for the 12 clusters identified (PAM algorithm) using the GAV and GMB explanatory variables (LASSO algorithm). These clusters are found in three regions: Outer Tropics (OT; 8–17°S), Dry Andes (DA; 17–37°S) and Wet Andes (WA; 37–55°S). **(A)** shows the cluster distribution across the Andes and the classic zones, from north to south are: Outer Tropics (OT; 8–17°S), Desert Andes (DA; 17–30°S), Central Andes (CA; 30–37°S), Lakes District (LD; 37–42°S), North Patagonia (NP; 42–48°S), South Patagonia (SP; 48–53°S) and Tierra del Fuego (TF; 53–55°S). **(B)** presents the climatic variables (1980–2019) which are grouped into the summer (DJF), autumn (MAM), winter (JJA), and spring (SON) seasons for the Southern Hemisphere. The sum of the precipitation and the extreme temperatures averages are shown here. Additionally, morphometric variables associate with the glacierized area (*i.e.*, surface area, elevation, slope, and aspect) are shown.

and slope (3.5%), with $P_{Apr}$ contributing only 3.3%. As observed for GAV, when monthly explanatory variables are combined, the order of explanatory variables with regards to the GMB variance changes. Therefore, the climate variables explain most of the GMB represented variance with 66% compared to the morphometric variables, with temperature contributing 37% and precipitation contributing 29% of the represented variance. Surface area is the morphometric variable that contributes highest percentage to the GMB variance (26%), followed by elevation (4%), slope (4%) and aspect (0.2%).

### 3.3.1 New Classification Zones of Andean Glaciers

We performed a cluster analysis based on 274 watersheds (31,963 glaciers) using the explanatory variables selected by the LASSO algorithm. Considering the assumption that variables that explain the glacier change spatial variance in 35 watersheds for GAV and in 110 watersheds for GMB can explain glacier change in rest of

Andean watersheds, we use 42 relevant variables selected by LASSO for the GAV and GMB datasets. These 42 variables are 12 monthly values for three climate variables (precipitation, Tmax and Tmin) and six values for morphometric variables (area, slope, aspect, max. elevation, min elevation and mean elevation). Tmean variable was not considered because it showed lowest explanatory capacity of the glacier changes spatial variance. According to the Hopkins method, our dataset shows a high potential to form clusters (the Hopkins test result is equal to 0.1), while the GAP statistic method allowed to quantify the cluster optimal number as 12. Concerning to the PAM algorithm sensitivity, PAM runs using climatic variables and morphometric-climatic variables showed a lower explained variance by the predictors if precipitation or Tmax variables are removed (see **Supplementary Figure S6** in the supplementary material). This means that the cluster assignment of each watershed changes more if these two variables are not present in the cluster analysis. In comparison, the removal of morphometric variables and Tmin showed PAM runs with greater explained variances, meaning that the cluster assignment of each watershed is less sensitive to the removal of these variables. In contrast, PAM runs using only morphometric variables showed a lower explanatory capacity of the variance, associated with an increase of the change to the cluster assignment of each watershed. About increase and decrease of the variable values between 0 and 10%, a way to add uncertainty to variable values, it was not observed any change in the cluster assignment of each watershed.

One cluster in the Outer Tropics (OT1) does not have data of GAV and GMB in some watersheds for estimating the explanatory variables of glacier changes. However, this zone is different from the two others in the Outer Tropics (i.e., OT2 and OT3) due to lower extreme temperature and mean glacier size values, for example. These numeric results are presented in the supplementary material (**Supplementary Table S3**).

**Figure 5A** shows the map that results from the clustering. A clear latitudinal distribution can be seen between 25°S and 40°S, with some overlaps resulting from similar morphometric and climatic configurations between watersheds located on eastern and western sides of the Andes. Here, one interesting latitudinal overlap example can be observed in Dry Andes. A watershed located in DA3 (id = 25,001; $p$ = 185 mm yr$^{-1}$; elevation = 6,039 m a.s.l.) close to DA1 watersheds (id = 26,426; $p$ = 79 mm yr$^{-1}$; elevation = 5,753 m a.s.l.) shows higher precipitation and elevation. However, in the Outer Tropics and the Wet Andes the clusters in general are not delimited with respect to latitude. An exception is the WA2 cluster, which covers watersheds west and east of the mountain range. Watersheds that show similar morphometric and climatic configurations are clustered even if they are not contiguous to one another. An example of this can be seen from watersheds inside W5 and W6 clusters, where they present close values of aspect, slope, and elevation, even the temperature values are close, but the precipitation presents high differences within the clusters even higher than between the two clusters. In addition, Tierra del Fuego is longitudinally split into two clusters (WA4 and WA6).

**Figure 5B** provide more details about the 12 clusters and their relevant morphometric and climatic characteristics. Considering the glacierized surface area in this work, which comprises 71% of the total surface area of the inventoried glaciers in the Andes, the Outer Tropics (8–17°S) comprise three clusters (OT1, OT2, OT3) concentrating 5.7% of the total glacierized area. OT3 contributes to 67% of the glacierized area in the Outer Tropics (3.8% in the Andes; 921 km$^2$). OT3 includes glaciers in Peru, Bolivia and volcanoes in northern Chile and western Bolivia. Within the Outer Tropics, the three clusters show an annual precipitation range between 782 mm yr$^{-1}$ (OT3) and 1,654 mm yr$^{-1}$ (OT1), concentrated during the DJF season (up to 500 mm) in all of the clusters and with a marked dry season in JJA (less than 100 mm). Tmax shows similar values throughout the year for all three clusters, and is slightly higher in OT2 (13.1°C), whereas Tmin shows a seasonal variation with higher values in DJF (OT2; 0.3°C) than in JJA (OT3; -10.3°C). With regards to the morphometric variables, cluster OT3 shows the largest mean glacier surface area (0.6 km$^2$), an average glacier elevation (5,335 m a.s.l.), and the lowest slope (24°). The Dry Andes (17–37°S) gather three clusters (DA1, DA2, DA3) which represent 6.7% of the total glacierized area. In this region, many glaciers (19–26°S) inside watersheds with a lower glacierized areas (glacierized watershed < 0.01%) were excluded. DA2 contains the most extensive glacier coverage with 52% (3.4% of the total for the Andes; 807 km$^2$). Within these three clusters, the annual amount of precipitation increases southward, with 150 mm yr$^{-1}$ in DA1 and 483 m yr$^{-1}$ in DA3. Precipitation is mainly concentrated during JJA in DA2-DA3 and is more evenly distributed in DA1. The extreme temperatures show the highest values in the DJF season (both for Tmax which reaches a maximum of 14°C and Tmin which reaches a minimum of -2.3°C) and lowest values in JJA (Tmax < 0.5°C; Tmin < -11°C). The largest average glacier surface area is found in DA2 (0.3 km$^2$) and the smallest is in DA1 (0.1 km$^2$) where glaciers are also found at the highest elevation (5,389 m a.s.l.) and have the lowest slope (19°) of all the Andes.

The Wet Andes (37–55°S) comprise 87.7% of the total glacierized area of the Andes, distributed in six clusters (WA1 to WA6), where WA3 contains 34% (30.1% in the Andes; 7,205 km$^2$) and WA4 29% (25.9% in the Andes; 6,194 km$^2$) of the glacierized area in the Wet Andes. The annual amount of precipitation differs considerably between the clusters ranging from 2,858 mm yr$^{-1}$ (WA5) to 784 mm yr$^{-1}$ (WA4). Precipitation is concentrated in JJA in WA1 and WA2 (approximately 580 mm) and MAM-JJA in WA3 to WA6 (approximately 800 mm). Extreme temperatures in the Wet Andes present maximum values in DJF (Tmax of roughly 20°C and Tmin of roughly 5°C) and minimum values during JJA (Tmax of roughly 5°C and Tmin of roughly -0.8°C). With regards to morphometric variables, the largest mean glaciers size is found in WA3 (8 km$^2$), and a decrease in the glacier mean elevation is observed from WA1 to WA6, with an average difference of 1,500 m. The slope is similar in all of the Wet Andes (25–26°) clusters although it is slightly lower in WA1 (21°).

### 3.3.2 Explanatory Variables at Cluster and Watershed Scale

The explanatory variables of the GAV and GMB represented variances at watershed scale are presented in detail for GAV (**Figure 6**) and GMB (**Figure 7**), using the 12 clusters. In the

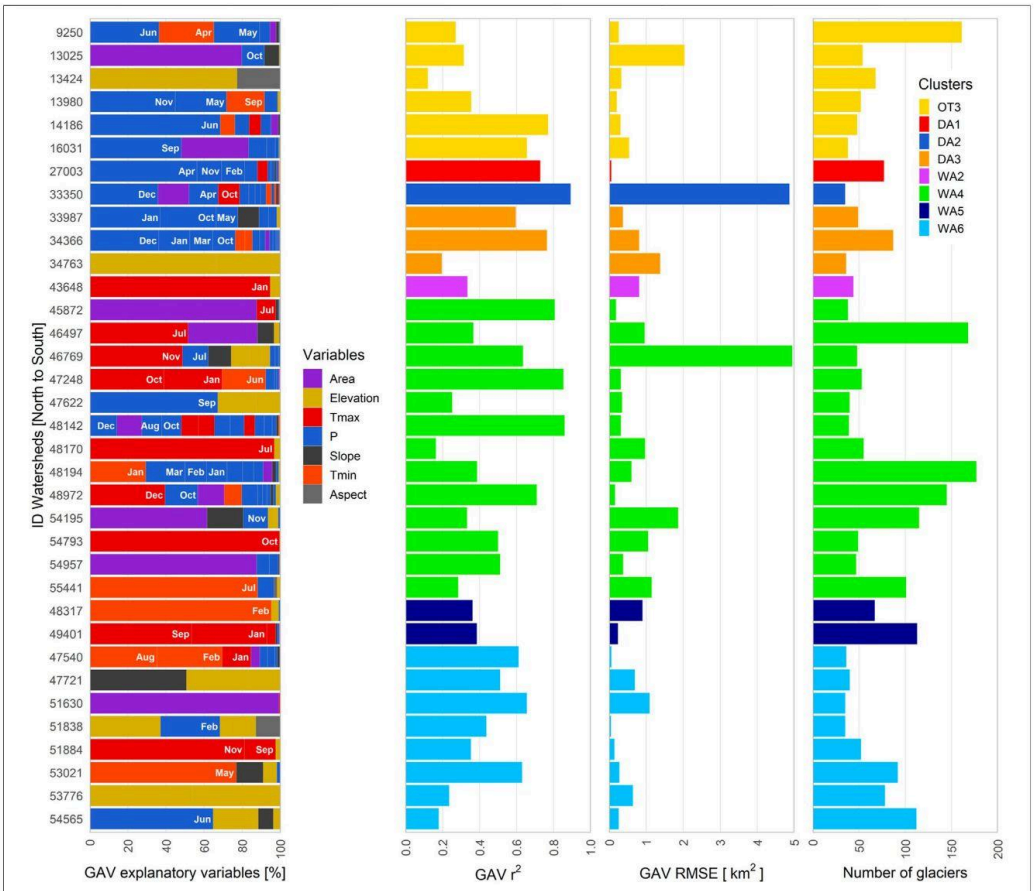


**FIGURE 6 |** Relevance of the morphometric and climatic variables identified by LASSO algorithm to the spatial variance of GAV (1980–2019) across the Andes (8–55°S). The GAV explanatory variables, at watershed scale, is added to represent the 100% associate to each GAV $r^2$ (variance by watershed). Other relevant data as RMSE and the number of glaciers used in estimations are showed. Due to data limitation, the results are available for 8 of the 12 clusters.

Outer Tropics, the explanatory variables of the GMB variance in cluster OT2 are precipitation (71%, $P_{Aug}$ and $P_{Dec}$ mainly) and temperature (19%). In cluster OT3, on average, the GAV variance is explained by precipitation (50%) and temperature (10%), with an increased explanatory power for precipitation (82%, mainly $P_{Sep}$ and $P_{Oct}$) in the GMB variance. In OT3, for the Achacachi watershed (id = 16,031; GAV $r^2 = 0.7$; GMB $r^2 = 0.6$) $P_{Oct}$ and $P_{Sep}$ are most relevant for the GMB and GAV variances, followed by the surface area and slope.

In the Dry Andes, the explanatory variables in cluster DA1 are precipitation (93%) and temperature (5%) for GAV. The variance of GMB is mainly explained by precipitation (49%) and surface area (49%). In DA1, the Río del Carmen watershed (id = 29,516; GMB $r^2 = 0.7$) shows that precipitation and surface area have a similar contribution to the GMB variance. In cluster DA2, the explanatory variables of the GAV and GMB variances are precipitation (> 67%) followed by temperature (> 16%). One of the most glacierized watersheds of the Dry Andes is the Olivares watershed (id = 33,350; GAV $r^2 = 0.9$; GMB $r^2 = 0.4$) for which $P_{Dec}$ and $P_{Apr}$ and surface area explain most of the GAV variance, and $P_{Oct}$, $P_{Aug}$ and $P_{Jun}$ explain most of the GMB variance. In cluster DA3, the explanatory variables of the GAV and GMB variances are precipitation (> 57%), followed by elevation (34%) for GAV and temperature (37%) for GMB. In this cluster, for the Upper Maipo (id = 33,987; GAV $r^2 = 0.6$; GMB $r^2 = 0.4$) and Cachapoal (id = 34,366; GAV $r^2 = 0.8$; GMB $r^2 = 0.4$)

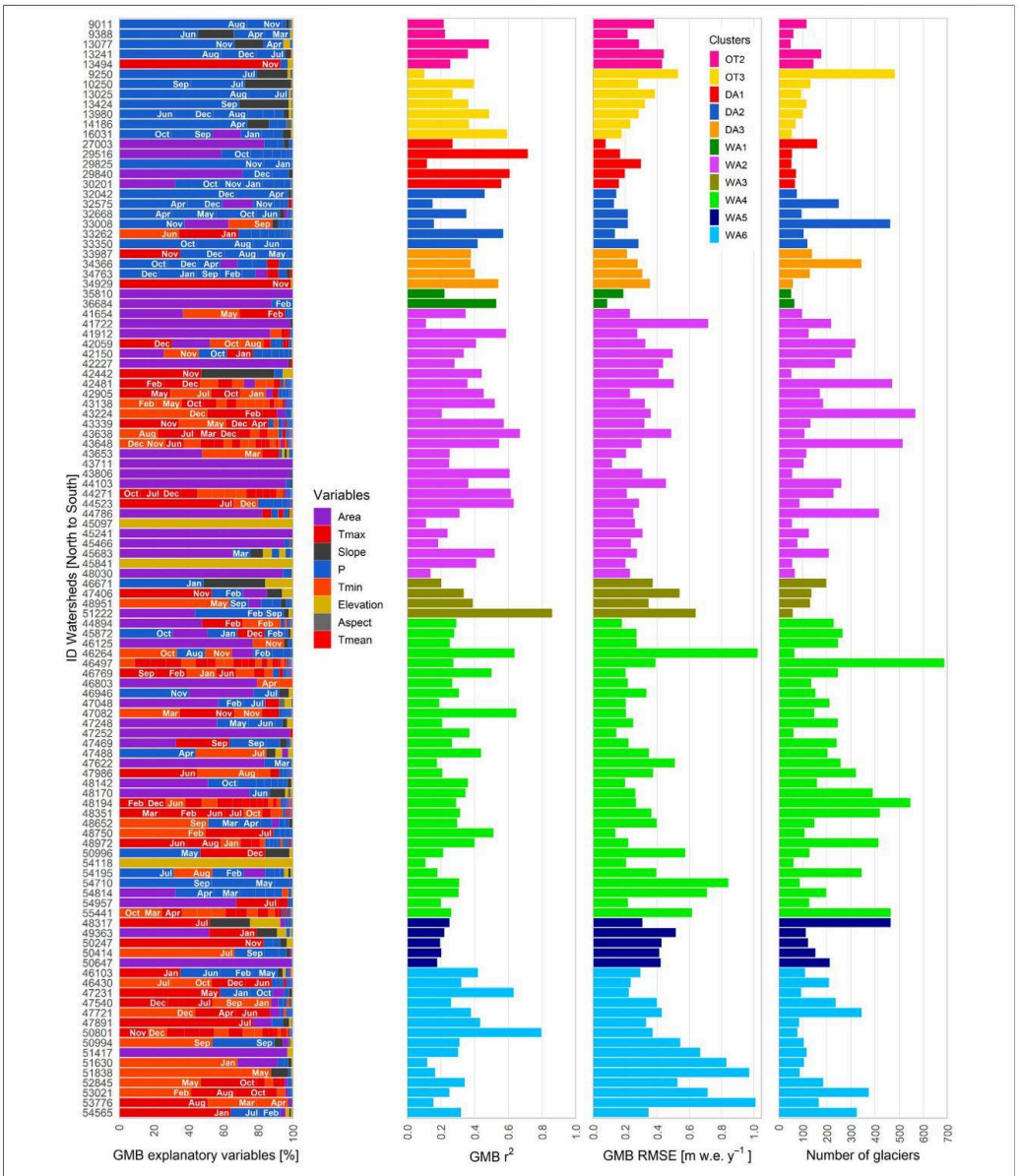


**FIGURE 7 |** Relevance of the morphometric and climatic variables identified by LASSO algorithm to the spatial variance of GMB (2000–2018) across the Andes (8–55°S). The GMB explanatory variables, at watershed scale, is added to represent the 100% associate to each GMB $r^2$ (variance by watershed). Other relevant data as RMSE and the number of glaciers used in estimations are showed. Due to data limitation, the results at watershed scale are available for 11 of the 12 clusters.

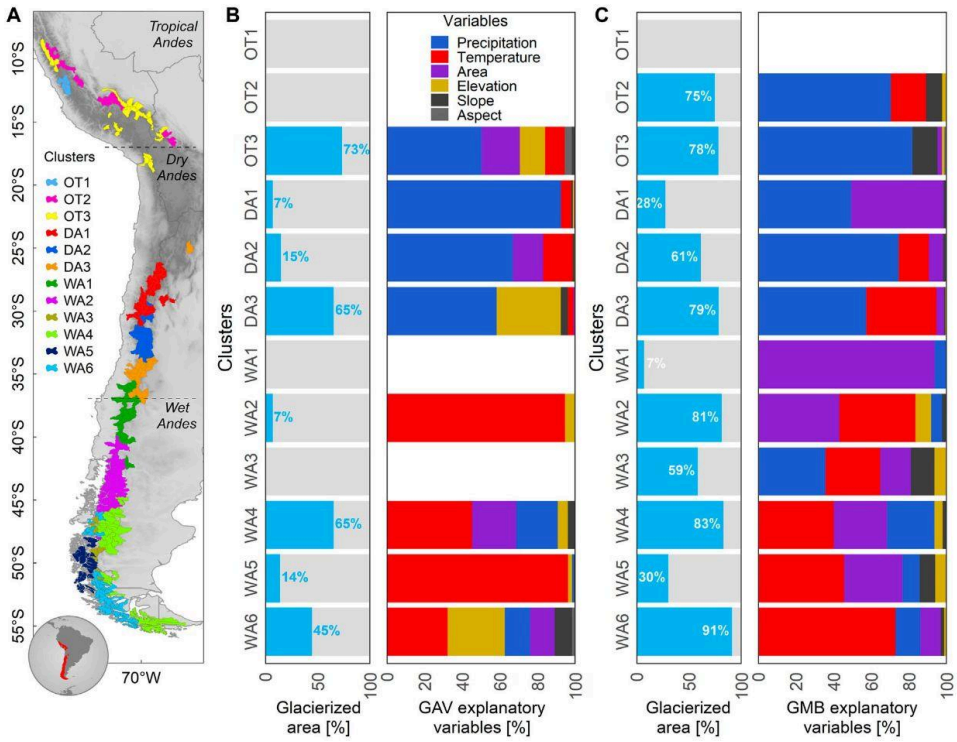


**FIGURE 8 |** Explanatory variables of glacier changes across the Andes (8–55°S) since 1980 at watershed scale. **(A)** The 274 glacierized watersheds inside 12 clusters are shown on the map of South America. The glacierized area considered in estimates of the **(B)** GAV (1980–2019) and **(C)** GMB (2000–2018) explanatory variables (light blue bars) are shown with regard to the percentage of explanatory variables for the GAV and GMB spatial variances (blank spaces are due to a lack of data in that cluster).

watersheds, $P_{Dec}$ (GMB) and $P_{Oct}$ (GAV) are the most relevant. Whereas in the Atuel watershed (id = 34,929; GMB $r^2$ = 0.5), $Tmax_{Nov}$ explains most of the GMB variance.

In the Wet Andes, the WA1 and WA2 clusters are located to the north of the Patagonian ice-fields. In WA1, the GMB variance is mainly explained by the surface area (94%) followed by precipitation (6%). Meanwhile, in WA2, the variable that mainly explains the GAV variance is temperature (95%), whereas the GMB variance is mainly explained by area (43%) and temperature (40%). The GMB variance in the Río Ñuble watershed (id = 26,684; GMB $r^2$ = 0.5), in WA1, is explained by surface area followed by $P_{Feb}$. In cluster WA2, the glacier surface area explains most of the GMB variance in the Río Manso watershed (id = 41,912; GMB $r^2$ = 0.6), and $Tmax_{Dec}$ and surface area are the dominant variables in the Río Puelo watershed (id = 42,059; GMB $r^2$ = 0.4).

Clusters WA3 to WA6 are found between the Northern Patagonian ice-field and the Cordillera Darwin. Cluster WA3 comprises the largest glacierized area in the Andes (30%). Precipitation and temperature (36 and 29%) explained most of the GMB variance, followed by surface area and slope (16–13%). Close to the Southern Patagonian ice-field, in the Río Serrano watershed (id = 51,222; GMB $r^2$ = 0.9), the glacier surface area, $P_{Feb}$ and $P_{Sep}$ are the most statistically significant explanatory variables. In WA4, the variables that explain most of the GAV and GMB variances are temperature (40–45%), followed by surface area (24–38%) and precipitation (22–25%). This cluster contains watersheds that are primarily located to the east of the Patagonian ice-fields, and in the Cordillera Darwin to the east of Monte Sarmiento. To the east of the Southern Patagonian ice-field, the Lago O'Higgins watershed (id = 48,652; GMB $r^2$ = 0.3) shows the statistical importance of $Tmin_{sep}$ and $P_{Mar}$ and $P_{Apr}$. On the southern side of Cordillera Darwin (id = 54,793; GAV $r^2$ = 0.5) the main explanatory variable is $Tmax_{Oct}$, whereas on the northern side, it was found that morphometric and

climatic variables had a very limited explanatory capacity (id = 54,195; GAV $r^2$ = 0.3; GMB $r^2$ = 0.2).

The WA5 and WA6 clusters are located on the western side of the Patagonian Andes. Watersheds in WA5 are mainly found to the west of the Southern Patagonian ice-field, in the coastal region where the highest amount of precipitation in the Andes was identified. For these watersheds, temperature is the most relevant variable. For example, in Río Pascua watershed (id = 48,317; GAV $r^2$ = 0.4; GMB $r^2$ = 0.3) $Tmax_{Jul}$ and $Tmin_{Feb}$ are important in the spatial variance of the glacier changes and in Isla Wellington (id = 50,401; GAV $r^2$ = 0.4) are $Tmax_{Sep}$ and $Tmax_{Jan}$. Whereas in WA6, the explanatory variables strongly differ between GAV and GMB. The morphometric variables (30% elevation) explain 54% of the GAV variance and climate variables (73% temperature) explain 86% of the GMB variance. This cluster comprises watersheds that are primarily distributed around the Northern Patagonian ice-field and the south of the Southern Patagonian ice-field down to Monte Sarmiento, where the largest ice concentration outside the Patagonian ice-fields and Cordillera Darwin is found.

#### 3.3.3 Explanatory Variables at the Regional Scale

**Figure 8** shows the explanatory variables of GAV and GMB spatial variances at cluster scale. At first glance, it can be observed that precipitation explains the highest percentage of GAV and GMB variances for clusters located within the Outer Tropics (OT1, OT2, OT3) and the Dry Andes (D1, D2, D3), whereas temperature is most relevant variable in the Wet Andes (WA1 to WA6). Within the Outer Tropics and the Dry Andes clusters, precipitation explains between 49–93% of the GAV and GMB variances, whereas temperature only explains between 3 and 37%. In the Wet Andes, the explanatory variables of GAV and GMB variances are inverted, with temperature contributing between 29 and 73% of variation and precipitation between 1 and 36%.

In further detail, this explanatory power of precipitation in the Outer Tropics and the Dry Andes clusters and of temperature in the Wet Andes clusters is clear for seven clusters that concentrate 77% of the Andean glacierized area (OT2, OT3, DA2, DA3, WA9, WA10 and WA11). Other clusters show differences in the main explanatory variables for the GAV and GMB variances.

For instance, the DA1 cluster shows that climate variables (98%) predominantly explain the GAV variance, manly for precipitation (93%). On the other hand, GMB is explained in similar proportion by climate (49%) and morphometric (51%) variables, where the most important variables are precipitation and surface area with 49% each. For cluster WA1, without GAV variables identified, morphometric (94%) variables explain the GMB variance through surface area (93.9%). In WA2, temperature (95%) explain the GAV variance while the GMB variance is dominated by morphometric variables (54%) being more relevant surface area (43%) followed by temperature (40%). In WA6, 54% of the GAV variance is explained by morphometric variables (elevation alone explains 30%), and 86% of the GMB variance is explained by climate variables, where temperature explains 73%.

Finally, differences in explanatory power of morphometric and climate variables for the GAV and GMB spatial variances when considering the classic zones or the clusters can be observed in the supplementary material (**Supplementary Table S4** and **Supplementary Table S5**).

## 4 SUMMARY AND CONCLUDING REMARKS

This study is the first to explore climatic and morphometric variables of the spatial variance of glacier changes through a machine learning method across the Andes (8–55°S), in terms of surface area variations since 1980 and mass balance changes since 2000. Overall, we found that the spatial variability of glacier changes is primarily controlled by spatial variability of precipitation from the Outer Tropics to the Dry Andes (8–37°S) and of temperature in the Wet Andes (40–55°S). These results, obtained at watershed scale, allowed to identify 12 new glaciological zones via a clustering analysis that depicts more details compared with the classic zones based on latitude ranges.

### 4.1 Overall Glacier Area and Mass Balance Variations

At the scale of the entire study region, the mean GAV and GMB were calculated at −31.2 ± 2% (1980–2019) and −0.82 ± 0.12 m w.e. $yr^{-1}$ (2000–2018), respectively. Our GMB estimation is close to the one obtained by Dussaillant et al. (2019) of -0.72 ± 0.22 m w.e. $yr^{-1}$ (2000–2018), and more negative in comparison with Braun et al. (2019) estimate (-0.61 ± 0.07 m w.e. $yr^{-1}$; 2000–2015), in both cases at the scale of the entire Andes. Differences between the estimates are related to the use of different glacier inventories to quantify the mass balance from glacier surface elevation differencing data and mass balance calculations. In fact, some glaciers found in the Patagonian ice-fields do not have elevation difference information in the accumulation zone, therefore our results may overestimate the negative mass balance here as we did not extrapolate the glacier change elevation data to fill the gaps, as done by Dussaillant et al. (2019). Our error estimations are lower in comparison with Dussaillant et al. (2019), possibly due to the outlines precision of glaciers identified from the national glacier inventories compared to RGI v6.0. Despite the above, and as shown in **Supplementary Figure S4**, considering ranges of 1° latitude between 8–55°S, we did not observe relevant differences in terms of average mass balance (< 0.3 m w.e.) in comparison with the mass balance estimated in Dussaillant et al. (2019), except between 48–49°S where we estimated a less negative mass balance.

Regarding GAV, the Desert Andes (-53 ± 0.002%) and the Lakes District (-52 ± 0.1%), which include the smallest glacierized surface areas, showed highest glacier shrinkage. The glacier shrinkage estimated here is higher than the one estimated by Rabatel et al. (2011) at -29% over the 1955–2007 period in the Desert Andes and that the one reported by Paul and Mölg (2014) at -25% over the 1985–2011 period in the Lake District, but it is

worth noting that the study period are different and that we consider in the overall study period used here the decade 2010–2020 during which glacier loss in these regions has strongly increased (Dussaillant et al., 2019). Southward of 42°S, the mean GAV estimated here (-24 ± 0.4% to -32 ± 1.3%) was higher than that observed by Meier et al. (2018) (-9 ± 5%, 1986–2016): this is likely related to differences in the study periods and also because we did not consider the large calving glaciers of the Patagonian ice-fields, where we found glacier outlines inconsistences, particularly in accumulation zones; these glaciers covering an area up to 13% of the total in South Patagonia and 20% in North Patagonia. Overall, we discarded the glacier growth due to methodological limitations, but this should have a limited impact because many studies have described a general glacier shrinking across the Andes (e.g., Malmros et al., 2016; Meier et al., 2018; Paul and Mölg, 2014; Rabatel et al., 2011; Rivera and Bown, 2013; Seehaus et al., 2019, 2020), with few exceptions that have been reported (Rivera and Casassa, 1999; Wilson et al., 2016; Hata and Sugiyama, 2021).

Although our GAV estimates show $r^2 > 0.7$, we identified 11 latitudinal ranges in which there are low statistical significance in the relationship between GAV and morphometric or climatic variables (*p-value* > 0.05), concentrated mainly in the Lakes District (between 38 to 39°S and 40 to 41°S) and North Patagonia (between 42 to 43°S and 46 to 48°S).

We found that the statistical relationship between GAV and GMB is mostly non-significant across the Andes. This is not really surprising as the considered time scales for GAV and GMB are not the same and they are of different length. In addition, GAV is related to glacier response times which depends on glacier dynamics, and is therefore related to its morphometric characteristic and thus specific to each glacier. This response time may largely exceed the study period length, particularly for outlet glaciers of the Patagonian ice-fields where it can be on a secular time scale. One consequence of this absence of a relationship between GAV and GMB is that their explanatory variables were identified separately.

## 4.2 Main Controls of Glacier Changes

In relation to the relevant variables at watershed scale for GAV ($r^2$ = 0.5, $n$ = 35) and GMB ($r^2$ = 0.4, $n$ = 110), we found that, on average for the entire study region (8–55°S), climate variables explain an highest percentage of the GAV and GMB spatial variances with more than 65% (> 35% for temperature), whereas the surface area is the most relevant (> 16%) for morphometric variables. We observe a latitudinal limit from 37.5°S (DA3 in Argentina) to 39.9°S (WA2 in Chile) between the explanatory capacity of precipitation and temperature in GAV and GMB spatial variances across the Andes. Precipitation explains highest percentage of GAV and GMB spatial variances (ranging from 49 to 93% depending on the clusters) for the Outer Tropics and the Dry Andes (8–37°S), whereas temperature is the most relevant climate variable (between 29 and 73% of explained spatial variance depending on the cluster) for the Wet Andes (40–55°S). The importance of precipitation in the GMB variability had already been observed in several studies based on *in situ* glacier monitoring by Favier et al. (2004) and Wagnon et al. (2001) in the Outer Tropics. More specifically, Sicart et al. (2003, 2011) showed that during the transition season (Sep-Dec) when ice melt increases, precipitation frequency and intensity are key to modulating ablation because of the impact on glacier surface albedo. In the Dry Andes, no link was found between GAV or GMB which is in agreement with Rabatel et al. (2011). In addition, Rabatel et al. (2011), Masiokas et al. (2016) and Kinnard et al. (2020) pointed out the sensitivity of GMB to precipitation. For this region, we also found that glacier surface area has significant explanatory power for the GMB variance (49% in DA1), which is in agreement with Rabatel et al. (2011) who showed that small glaciers in the Desert Andes have a very negative GMB in comparison with a moderate mass loss for larger glaciers. With regards to the Wet Andes, in the Patagonian ice-fields, spatial variances of glacier changes are mainly controlled by the temperature (WA3 to WA6). This is in agreement with Abdel Jaber et al. (2019) who found that the mass loss in the Northern Patagonia ice-field is likely due to higher temperatures. Outside the Patagonian ice-fields in east (WA4), the glacier shrinkage could be explained by a temperature increase as no change in precipitation was observed (1979–2002) (Masiokas et al., 2015). In addition, Falaschi et al. (2019) found a high correlation between GMB and temperature in Monte San Lorenzo since 1958 to 2018 (temperature Oct to Mar, $r$ = -0.86, *p-value* = 0.1).

## 4.3 Clusters Without a Latitudinal Distribution Across the Andes

In the present work, we used morphometric and climatic variables associated with GMB data for 20,740 glaciers and GAV data for 2,484 glaciers to propose a new classification that comprises 12 clusters encompassing a total of 274 watersheds and 31,963 glaciers between 8 and 55°S. This regional identification was based on the main explanatory variables of glacier changes (GAV and GMB). Up to now, only one type of classification of the glacier environments based on latitudinal ranges has been used, first by Troll (1941) and Lliboutry (1998), followed by recent studies (e.g., Barcaza et al., 2017; Dussaillant et al., 2019; Masiokas et al., 2009, 2020; Zalazar et al., 2020). Sagredo and Lowell (2012) proposed another glaciological classification with nine zones between 8–55°S; this was based on climate variables only, and with a small number of glaciers ($n$ < 234). Here, the clusters provide a classification with greater detail allowing to better take the regional-scale diversity in the glacier characteristics and evolution into account. For instance, glaciers on volcanoes in northern Chile and western Bolivia are no longer linked to the Dry Andes but clustered with those of the Outer Tropics (OT3). In addition, watersheds located at the same latitude sometimes belong to different clusters. These results are in line with Ayala et al. (2020) who identified significant differences (GMB, runoff contribution and glacier elevation) between the southern (DA2) and northern (DA3) watersheds inside the Río Maipo watershed. With regards to the Outer Tropics and the Wet Andes, our results show that a

latitudinal classification is not possible, which is in agreement with previous studies (e.g., Caro et al., 2020; Sagredo & Lowell, 2012). Southward of 46°S, we found different clusters, from west to east, related to the high contrast in precipitation and temperature amounts (WA3 to WA6) related to the wet western air masses originating from the Pacific Ocean (Langhamer et al., 2018). Studies on the Patagonian ice-fields have demonstrated this large difference in precipitation between the western and eastern sides of the cordillera (Warren, 1993; Barcaza et al., 2017; Bravo et al., 2019).

Despite these results, the sensitivity analysis showed that the absence of the variables Tmax and precipitation causes a rearrangement of the cluster assignment to each watershed, while the absence of the morphometric variables and Tmin does not show a major change in this assignment.

### 4.4 Implications in the Glacier Changes Simulations at the Andes Scale

Results obtained through linear machine learning method provide a new framework for glacier changes simulations across the Andes. The increase in temperature-driven and decrease in precipitation-driven glacier changes from the Outer Tropics to the Wet Andes highlights that:

a) A reduction in annual precipitation and changes in their monthly distribution will have a greater impact on glacier mass loss in the Outer Tropics and the Dry Andes in comparison with the Wet Andes. Conversely, changes in monthly temperature will be more relevant to simulate glacier mass loss in the Wet Andes.
b) The newly defined clusters will allow to orient the glacier change simulations, based on the main variables that control GAV and GMB across the Andes. For example, for regional studies across the Dry Andes to the Wet Andes, precipitation and temperature relevancies presented here can be efficiently used to estimate the mass balance, through the precipitation and ice melt factors that can be derived from numerous studies (e.g., Ayala et al., 2020; Bravo et al., 2017; Caro, 2014; Farías-Barahona et al., 2020; Huss and Hock, 2018; Masiokas et al., 2016). In this context, our results will be able to guide future regional hydro-glaciological simulations at watershed and cluster scales across the Andes.

## DATA AVAILABILITY STATEMENT

The original contributions presented in the study are included in the article/**Supplementary Material**, further inquiries can be directed to the corresponding author.

## AUTHOR CONTRIBUTIONS

AC: data processing, analysis, interpretation, and writing. TC and AR: supervision, interpretation and writing.

## FUNDING

This study was conducted as part of the International Joint Laboratory GREAT-ICE, a joint initiative of the IRD and universities and institutions in Bolivia, Peru, Ecuador and Colombia. This research was funded by the National Agency for Research and Development (ANID)/Scholarship Program/ DOCTORADO BECAS CHILE/2019—72200174.

## ACKNOWLEDGMENTS

We acknowledge the LabEx OSUG@2020 (Investissement d'Avenir,—ANR10 LABX56). The first author would like to thank Francisca Bown (Tambo Austral), Edwin Loarte Cadenas (INAIGEM), Katy Medina Marcos (INAIGEM), Justiniano Alejo Cochacin Rapre (ANA), James McPhee (U. of Chile), Diego Cusicanqui, Jeppe Malmros, David Farías-Barahona and Thorsten Seehaus for providing the glacier inventories between the Outer Tropics and Tierra del Fuego (8–55°S), and Fernando Gimeno, Jean Carlos Ruiz Hernández, Inés Dussaillant and Vanesa Carreño for fruitful discussions on this article. Finally, we acknowledge the numerous and constructive comments and suggestions provided by the two reviewers and the Editor.

## SUPPLEMENTARY MATERIAL

The Supplementary Material for this article can be found online at: https://www.frontiersin.org/articles/10.3389/feart.2021.713011/full#supplementary-material

## REFERENCES

Abatzoglou, J. T., Dobrowski, S. Z., Parks, S. A., and Hegewisch, K. C. (2018). TerraClimate, a High-Resolution Global Dataset of Monthly Climate and Climatic Water Balance from 1958-2015. *Sci. Data* 5, 1–12. doi:10.1038/sdata.2017.191

Abdel Jaber, W., Rott, H., Floricioiu, D., Wuite, J., and Miranda, N. (2019). Heterogeneous Spatial and Temporal Pattern of Surface Elevation Change and Mass Balance of the Patagonian Ice fields between 2000 and 2016. *The Cryosphere* 13 (9), 2511–2535. doi:10.5194/tc-13-2511-2019

AMTC (2019). *Inventario de glaciares de la cuenca río Maipo año 2018*. Santiago: CSIRO.

ANA (2014). *Data from: Inventario de Glaciares en el Perú. 2da Actualización*. Huaraz: Ministerio de Agricultura y Riego. Available at: http://geo2.ana.gob.pe:8080/geonetwork/srv/spa/catalog.search;jsessionid=6E35D3AA343E29DA1447AC04F968932B#/metadata/1099ce9e-bd97-49c1-a32a-2eccb35fcf79.

Arora, P., Deepali and Varshney, S. (2016). Analysis of K-Means and K-Medoids Algorithm for Big Data. *Proced. Comp. Sci.* 78 (12), 507–512. doi:10.1016/j.procs.2016.02.095

Ayala, Á., Farías-Barahona, D., Huss, M., Pellicciotti, F., McPhee, J., and Farinotti, D. (2020). Glacier Runoff Variations since 1955 in the Maipo River Basin, Semiarid Andes of central Chile. *Cryosphere Discuss.* 14, 1–39. doi:10.5194/tc-2019-233

Ayala, A., Pellicciotti, F., MacDonell, S., McPhee, J., Vivero, S., Campos, C., et al. (2016). Modelling the Hydrological Response of Debris-free and

Debris-Covered Glaciers to Present Climatic Conditions in the Semiarid Andes of central Chile. *Hydrol. Process.* 30 (22), 4036–4058. doi:10.1002/hyp.10971

Baraer, M., Mark, B. G., Mckenzie, J. M., Condom, T., Bury, J., Huh, K.-I., et al. (2012). Glacier Recession and Water Resources in Peru's Cordillera Blanca. *J. Glaciol.* 58 (207), 134–150. doi:10.3189/2012JoG11J186

Barcaza, G., Nussbaumer, S. U., Tapia, G., Valdés, J., García, J.-L., Videla, Y., et al. (2017). Glacier Inventory and Recent Glacier Variations in the Andes of Chile, South America. *Ann. Glaciol.* 58 (75), 166–180. doi:10.1017/aog.2017.28

Benítez, A. (1978). *Clasificación de Cuencas Hidrográficas de Chile*. Santiago: Unirioja.

Bharath, R., and Srinivas, V. V. (2015). Delineation of Homogeneous Hydrometeorological Regions Using Wavelet-Based Global Fuzzy Cluster Analysis. *Int. J. Climatol.* 35 (15), 4707–4727. doi:10.1002/joc.4318

Bolibar, J., Rabatel, A., Gouttevin, I., Galiez, C., Condom, T., and Sauquet, E. (2020). Deep Learning Applied to Glacier Evolution Modelling. *The Cryosphere* 14 (2), 565–584. doi:10.5194/tc-14-565-2020

Braun, M. H., Malz, P., Sommer, C., Farías-Barahona, D., Sauter, T., Casassa, G., et al. (2019). Constraining Glacier Elevation and Mass Changes in South America. *Nat. Clim Change* 9 (2), 130–136. doi:10.1038/s41558-018-0375-7

Bravo, C., Bozkurt, D., Gonzalez-Reyes, Á., Quincey, D. J., Ross, A. N., Farías-Barahona, D., et al. (2019). Assessing Snow Accumulation Patterns and Changes on the Patagonian Icefields. *Front. Environ. Sci.* 7 (3), 1–18. doi:10.3389/fenvs.2019.00030

Bravo, C., Loriaux, T., Rivera, A., and Brock, B. W. (2017). Assessing Glacier Melt Contribution to Streamflow at Universidad Glacier, central Andes of Chile. *Hydrol. Earth Syst. Sci.* 21 (7), 3249–3266. doi:10.5194/hess-21-3249-2017

Brun, F., Berthier, E., Wagnon, P., Kääb, A., and Treichler, D. (2017). A Spatially Resolved Estimate of High Mountain Asia Glacier Mass Balances from 2000 to 2016. *Nat. Geosci* 10 (9), 668–673. doi:10.1038/ngeo2999

Brun, F., Wagnon, P., Berthier, E., Jomelli, V., Maharjan, S. B., Shrestha, F., et al. (2019). Heterogeneous Influence of Glacier Morphology on the Mass Balance Variability in High Mountain Asia. *J. Geophys. Res. Earth Surf.* 124 (6), 1331–1345. doi:10.1029/2018JF004838

Burger, F., Ayala, A., Farias, D., Shaw, T. E., MacDonell, S., Brock, B., et al. (2019). Interannual Variability in Glacier Contribution to Runoff from a High-elevation Andean Catchment: Understanding the Role of Debris Cover in Glacier Hydrology. *Hydrological Process.* 33 (2), 214–229. doi:10.1002/hyp.13354

Caro, A. (2014). *Estudios glaciológicos en los nevados de Chillán*. Santiago: University of Chile. [thesis].

Caro, A., Gimeno, F., Rabatel, A., Condom, T., and Ruiz, J. C. (2020). Identificación de clústeres glaciares a lo largo de los Andes chilenos usando variables topoclimáticas. *Investig. Geogr.* 60, 119–133. doi:10.5354/0719-5370.2020.59009

Casassa, G., Smith, K., Rivera, A., Araos, J., Schnirch, M., and Schneider, C. (2002). Inventory of Glaciers in Isla Riesco, Patagonia, Chile, Based on Aerial Photography and Satellite Imagery. *Ann. Glaciol.* 34 (1), 373–378. doi:10.3189/172756402781817671

Cauvy-Fraunié, S., and Dangles, O. (2019). A Global Synthesis of Biodiversity Responses to Glacier Retreat. *Nat. Ecol. Evol.* 3 (12), 1675–1685. doi:10.1038/s41559-019-1042-8

Caviedes, J. (1979). *Inventario de glaciares en la hoya del río Cachapoal y predicción de la escorrentía del deshielo, Andes centrales*. Santiago: Universidad de Chile.

Cuffey, K. M., and Paterson, W. S. B. (2011). *The Physics of Glaciers*. Fourth edi. Academic Press. doi:10.3189/002214311796405906

Dangles, O., Rabatel, A., Kraemer, M., Zeballos, G., Soruco, A., Jacobsen, D., et al. (2017). Ecosystem Sentinels for Climate Change? Evidence of Wetland Cover Changes over the Last 30 Years in the Tropical Andes. *PLoS ONE* 12 (5), e0175814–22. doi:10.1371/journal.pone.0175814

Davaze, L., Rabatel, A., Dufour, A., Hugonnet, R., and Arnaud, Y. (2020). Region-Wide Annual Glacier Surface Mass Balance for the European Alps from 2000 to 2016. *Front. Earth Sci.* 8 (May), 1–14. doi:10.3389/feart.2020.00149

Devenish, C., and Gianella, C. (2012). *Sustainable Mountain Development in the Andes. 20 Years of Sustainable Mountain Development in the Andes - from Rio 1992 to 2012 and beyond*. Lima, Peru: CONDESAN.

DGA (2014). *Data from: Inventario Nacional de Glaciares de Chile*. Dirección General de Aguas. Available at: http://www.geoportal.cl/geoportal/catalog/search/resource/resumen.page?uuid=%7B9C5CBF38-72D5-4489-A745-30AEAF1CDFC2%7D.

DGA (2011). Variaciones recientes de glaciares en Chile según principales zonas glaciológicas. Santiago: Available at: http://bibliotecadigital.ciren.cl/handle/123456789/32678.

Dikbas, F., Firat, M., Koc, A. C., and Gungor, M. (2012). Classification of Precipitation Series Using Fuzzy Cluster Method. *Int. J. Climatol.* 32 (10), 1596–1603. doi:10.1002/joc.2350

Dussaillant, I., Berthier, E., Brun, F., Masiokas, M., Hugonnet, R., Favier, V., et al. (2019). Two Decades of Glacier Mass Loss along the Andes. *Nat. Geosci.* 12 (10), 802–808. doi:10.1038/s41561-019-0432-5

Falaschi, D., Lenzano, M. G., Villalba, R., Bolch, T., Rivera, A., and Lo Vecchio, A. (2019). Six Decades (1958-2018) of Geodetic Glacier Mass Balance in Monte San Lorenzo, Patagonian Andes. *Front. Earth Sci.* 7 (12), 1. doi:10.3389/feart.2019.00326

Farías-Barahona, D., Wilson, R., Bravo, C., Vivero, S., Caro, A., Shaw, T. E., et al. (2020). A Near 90-year Record of the Evolution of El Morado Glacier and its Proglacial lake, Central Chilean Andes. *J. Glaciol.* 66, 846–860. doi:10.1017/jog.2020.52

Farr, T. G., Rosen, P. A., Caro, E., Crippen, R., Duren, R., Hensley, S., et al. (2007). The Shuttle Radar Topography mission. *Rev. Geophys.* 45, 1. doi:10.1029/2005RG000183

Favier, V., Wagnon, P., and Ribstein, P. (2004). Glaciers of the Outer and Inner Tropics: A Different Behaviour but a Common Response to Climatic Forcing. *Geophys. Res. Lett.* 31 (16), 1. doi:10.1029/2004GL020654

Friedman, J., Hastie, T., and Tibshirani, R. (2010). Regularization Paths for Generalized Linear Models via Coordinate Descent. *J. Stat. Soft.* 33 (1), 1–22. doi:10.18637/jss.v033.i01

García, A., Ulloa, C., Amigo, G., Milana, J. P., and Medina, C. (2017). An Inventory of Cryospheric Landforms in the Arid diagonal of South America (High Central Andes, Atacama Region, Chile). *Quat. Int.* 438 (11), 4–19. doi:10.1016/j.quaint.2017.04.033

Garín, C. (1987). Inventario de glaciares de los Andes chilenos desde los 18° a los 23° de latitud sur. *Resvista de Geografía Norte Grande* 14, 15.

Guido, Z., McIntosh, J. C., Papuga, S. A., and Meixner, T. (2016). Seasonal Glacial Meltwater Contributions to Surface Water in the Bolivian Andes: A Case Study Using Environmental Tracers. *J. Hydrol. Reg. Stud.* 8, 260–273. doi:10.1016/j.ejrh.2016.10.002

Hall, M. J., and Minns, A. W. (1999). The Classification of Hydrologically Homogeneous Regions. *Hydrological Sci. J.* 44 (5), 693–704. doi:10.1080/02626669909492268

Hata, S., and Sugiyama, S. (2021). Changes in the Ice-Front Position and Surface Elevation of Glaciar Pío XI, an Advancing Calving Glacier in the Southern Patagonia Icefield, from 2000-2018. *Front. Earth Sci.* 8 (1), 1–12. doi:10.3389/feart.2020.576044

Hidrandina, S. A. (1989). *Inventario de glaciares del Perú.* . Huaraz: CONCYTEC.

Huss, M., and Hock, R. (2015). A New Model for Global Glacier Change and Sea-Level Rise. *Front. Earth Sci.* 3 (9), 1–22. doi:10.3389/feart.2015.00054

Huss, M., and Hock, R. (2018). Global-scale Hydrological Response to Future Glacier Mass Loss. *Nat. Clim Change* 8 (2), 135–140. doi:10.1038/s41558-017-0049-x

IANIGLA-CONICET (2018). Data from: Resultados del Inventario Nacional de Glaciares. Available at: https://www.argentina.gob.ar/ambiente/agua/glaciares/inventario-nacional.

INAIGEM (2018). Data from: Inventario de lagunas y glaciares del Perú. Available at: https://inaigem.maps.arcgis.com/apps/opsdashboard/index.html#/f37b51cf963642c0aca30056b445ef63.

Kaufman, L., and Rousseeuw, P. (2008). "Partitioning Around Medoids (Program PAM)," in *In Finding Groups in Data*. Editors P. J. Kaufman and L. Rousseeuw (John Wiley & Sons), 68–125. doi:10.1002/9780470316801.ch2

Kinnard, C., Ginot, P., Surazakov, A., MacDonell, S., Nicholson, L., Patris, N., et al. (2020). Mass Balance and Climate History of a High-Altitude Glacier, Desert Andes of Chile. *Front. Earth Sci.* 8 (2), 1–20. doi:10.3389/feart.2020.00040

Langhamer, L., Sauter, T., and Mayr, G. J. (2018). Lagrangian Detection of Moisture Sources for the Southern Patagonia Icefield (1979-2017). *Front. Earth Sci.* 6 (11), 1–17. doi:10.3389/feart.2018.00219

Lawson, R. G., and Jurs, P. C. (1990). New Index for Clustering Tendency and its Application to Chemical Problems. *J. Chem. Inf. Comput. Sci.* 30 (1), 36–41. doi:10.1021/ci00065a010

Lee, S., Kim, J., Hwang, J., Lee, E., Lee, K.-J., Oh, J., et al. (2020). Clustering of Time Series Water Quality Data Using Dynamic Time Warping: A Case Study from the Bukhan River Water Quality Monitoring Network. *Water* 12 (9), 2411. doi:10.3390/w12092411

Lliboutry, L. (1998). "Glaciers of Chile and Argentina," in *Satellite Image Atlas of Glaciers of the World* (South America: U.S. Geological Survey), I1–I206.

Lockhart, R., Taylor, J., and Tibshirani, R. (2015). A Significance Test for the Lasso. *Ann. Stat.* 42 (2), 413–468. doi:10.1214/13-AOS1175.A

Maechler, M., Rousseeuw, P., Struyf, A., Hubert, M., and Hornik, K. (2021). *Cluster: Cluster Analysis Basics and Extensions*. version 2.1.2. R package.

Malmros, J. K., Mernild, S. H., Wilson, R., Yde, J. C., and Fensholt, R. (2016). Glacier Area Changes in the central Chilean and Argentinean Andes 1955-2013/14. *J. Glaciol.* 62, 391–401. doi:10.1017/jog.2016.43

Marangunic, C. (1979). *Inventario de glaciares hoya del río Maipo*. Santiago: Snia.

Mark, B. G., McKenzie, J. M., and Gómez, J. (2005). Hydrochemical evaluation of changing glacier meltwater contribution to stream discharge: Callejon de Huaylas, Peru/Evaluation hydrochimique de la contribution évolutive de la fonte glaciaire à l'écoulement fluvial: Callejon de Huaylas, Pérou. *Hydrological Sci. J.* 50 (6), 1. doi:10.1623/hysj.2005.50.6.975

Masiokas, M. H., Christie, D. A., Le Quesne, C., Pitte, P., Ruiz, L., Villalba, R., et al. (2016). Reconstructing the Annual Mass Balance of the Echaurren Norte Glacier (Central Andes, 33.5° S) Using Local and Regional Hydroclimatic Data. *The Cryosphere* 10 (2), 927–940. doi:10.5194/tc-10-927-2016

Masiokas, M. H., Delgado, S., Pitte, P., Berthier, E., Villalba, R., Skvarca, P., et al. (2015). Inventory and Recent Changes of Small Glaciers on the Northeast Margin of the Southern Patagonia Icefield, Argentina. *J. Glaciol.* 61 (227), 511–523. doi:10.3189/2015JoG14J094

Masiokas, M. H., Rabatel, A., Rivera, A., Ruiz, L., Pitte, P., Ceballos, J. L., et al. (2020). A Review of the Current State and Recent Changes of the Andean Cryosphere. *Front. Earth Sci.* 8 (6), 1–27. doi:10.3389/feart.2020.00099

Masiokas, M. H., Rivera, A., Espizua, L. E., Villalba, R., Delgado, S., and Aravena, J. C. (2009). Glacier Fluctuations in Extratropical South America during the Past 1000years. *Palaeogeogr. Palaeoclimatol. Palaeoecol.* 281 (3–4), 242–268. doi:10.1016/j.palaeo.2009.08.006

Matiu, M., Crespi, A., Bertoldi, G., Carmagnola, C. M., Marty, C., Morin, S., et al. (2020). Observed Snow Depth Trends in the European Alps 1971 to 2019. *Cryosphere Discuss.* 10, 1–50. doi:10.5194/tc-2020-289

Meier, W. J.-H., Grießinger, J., Hochreuther, P., and Braun, M. H. (2018). An Updated Multi-Temporal Glacier Inventory for the Patagonian andes with Changes between the Little Ice Age and 2016. *Front. Earth Sci.* 6 (5), 1. doi:10.3389/feart.2018.00062

Mernild, S. H., Liston, G. E., Hiemstra, C. A., Yde, J. C., and Casassa, G. (2018). Annual River Runoff Variations and Trends for the Andes Cordillera. *J. Hydrometeorology* 19, 1167–1189. doi:10.1175/JHM-D-17-0094.1

Möller, M., Schneider, C., and Kilian, R. (2007). Glacier Change and Climate Forcing in Recent Decades at Gran Campo Nevado, Southernmost Patagonia. *Ann. Glaciol.* 46, 136–144. doi:10.3189/172756407782871530

Pagliero, L., Bouraoui, F., Diels, J., Willems, P., and McIntyre, N. (2019). Investigating Regionalization Techniques for Large-Scale Hydrological Modelling. *J. Hydrol.* 570 (9), 220–235. doi:10.1016/j.jhydrol.2018.12.071

Paul, F., and Mölg, N. (2014). Hasty Retreat of Glaciers in Northern Patagonia from 1985 to 2011. *J. Glaciol.* 60 (224), 1033–1043. doi:10.3189/2014JoG14J104

Rabatel, A., Castebrunet, H., Favier, V., Nicholson, L., and Kinnard, C. (2011). Glacier Changes in the Pascua-Lama Region, Chilean Andes (29° S): Recent Mass Balance and 50 Yr Surface Area Variations. *The Cryosphere* 5 (4), 1029–1041. doi:10.5194/tc-5-1029-2011

Rabatel, A., Dedieu, J. P., and Vincent, C. (2016). Spatio-temporal Changes in Glacier-wide Mass Balance Quantified by Optical Remote Sensing on 30 Glaciers in the French Alps for the Period 1983-2014. *J. Glaciol.* 62 (236), 1153–1166. doi:10.1017/jog.2016.113

Rabatel, A., Francou, B., Soruco, A., Gomez, J., Cáceres, B., Ceballos, J. L., et al. (2013). Current State of Glaciers in the Tropical Andes: A Multi-century Perspective on Glacier Evolution and Climate Change. *The Cryosphere* 7, 81–102. doi:10.5194/tc-7-81-2013

Rabatel, A., Machaca, A., Francou, B., and Jomelli, V. (2006). Glacier Recession on Cerro Charquini (16° S), Bolivia, since the Maximum of the Little Ice Age (17th century). *J. Glaciol.* 52 (176), 110–118. doi:10.3189/172756506781828917

Ragettli, S., and Pellicciotti, F. (2012). Calibration of a Physically Based, Spatially Distributed Hydrological Model in a Glacierized basin: On the Use of Knowledge from Glaciometeorological Processes to Constrain Model Parameters. *Water Resour. Res.* 48 (3), 1–20. doi:10.1029/2011WR010559

Raup, B., Racoviteanu, A., Khalsa, S. J. S., Helm, C., Armstrong, R., and Arnaud, Y. (2007). The GLIMS Geospatial Glacier Database: A New Tool for Studying Glacier Change. *Glob. Planet. Change* 56 (1–2), 101–110. doi:10.1016/j.gloplacha.2006.07.018

RGI Consortium (2017). "Randolph Glacier Inventory – A Dataset of Global Glacier Outlines: Version 6.0," in *GLIMS Technical Report* (Collardo: Glaciers contribution to sea level rise). doi:10.7265/N5-RGI-60

Rivera, A., and Bown, F. (2013). Recent Glacier Variations on Active Ice Capped Volcanoes in the Southern Volcanic Zone (37°-46°S), Chilean Andes. *J. South Am. Earth Sci.* 45, 345–356. doi:10.1016/j.jsames.2013.02.004

Rivera, A., and Casassa, G. (1999). Volume Changes on Pio XI Glacier, Patagonia: 1975-1995. *Glob. Planet. Change* 22 (1–4), 233–244. doi:10.1016/S0921-8181(99)00040-5

Sagredo, E. A., and Lowell, T. V. (2012). Climatology of Andean Glaciers: A Framework to Understand Glacier Response to Climate Change. *Glob. Planet. Change* 86-87 (4), 101–109. doi:10.1016/j.gloplacha.2012.02.010

Sahin, S., and Kerem Cigizoglu, H. (2012). The Sub-climate Regions and the Sub-precipitation Regime Regions in Turkey. *J. Hydrol.* 450-451, 180–189. doi:10.1016/j.jhydrol.2012.04.062

Sakakibara, D., and Sugiyama, S. (2014). Ice-front Variations and Speed Changes of Calving Glaciers in the Southern Patagonia Icefield from 1984 to 2011. *J. Geophys. Res. Earth Surf.* 119, 2541–2554. doi:10.1002/2014JF003148

Sakakibara, D., Sugiyama, S., Sawagaki, T., Marinsek, S., and Skvarca, P. (2013). Rapid Retreat, Acceleration and Thinning of Glaciar Upsala, Southern Patagonia Icefield, Initiated in 2008. *Ann. Glaciol.* 54 (63), 131–138. doi:10.3189/2013AoG63A236

Seehaus, T., Malz, P., Sommer, C., Lippl, S., Cochachin, A., and Braun, M. (2019). Changes of the Tropical Glaciers throughout Peru between 2000 and 2016 - Mass Balance and Area Fluctuations. *The Cryosphere* 13 (10), 2537–2556. doi:10.5194/tc-13-2537-2019

Seehaus, T., Malz, P., Sommer, C., Soruco, A., Rabatel, A., and Braun, M. (2020). Mass Balance and Area Changes of Glaciers in the Cordillera Real and Tres Cruces, Bolivia, between 2000 and 2016. *J. Glaciol.* 66 (255), 124–136. doi:10.1017/jog.2019.94

Shaw, T. E., Caro, A., Mendoza, P., Ayala, Á., Pellicciotti, F., Gascoin, S., et al. (2020). The Utility of Optical Satellite Winter Snow Depths for Initializing a Glacio-Hydrological Model of a High-Elevation, Andean Catchment. *Water Resour. Res.* 56 (8), 1–19. doi:10.1029/2020WR027188

Sicart, J. E., Hock, R., Ribstein, P., Litt, M., and Ramirez, E. (2011). Analysis of Seasonal Variations in Mass Balance and Meltwater Discharge of the Tropical Zongo Glacier by Application of a Distributed Energy Balance Model. *J. Geophys. Res.* 116 (13), 1–18. doi:10.1029/2010JD015105

Sicart, J. E., Hock, R., and Six, D. (2008). Glacier Melt, Air Temperature, and Energy Balance in Different Climates: The Bolivian Tropics, the French Alps, and Northern Sweden. *J. Geophys. Res.* 113 (24), 1–11. doi:10.1029/2008JD010406

Sicart, J. E., Ribstein, P., Francou, B., and Gallaire, R. (2003). Etude des précipitations et de la fonte sur un glacier tropical: le glacier du Zongo, Bolivie, 16°S. *Hydrological Sci. J.* 48 (5), 799–808. doi:10.1623/hysj.48.5.799.51453

Simon, N., Friedman, J., Hastie, T., and Tibshirani, R. (2011). Regularization Paths for Cox's Proportional Hazards Model via Coordinate Descent. *J. Stat. Soft.* 39 (5), 1–13. doi:10.18637/jss.v039.i05

Soruco, A., Vincent, C., Francou, B., and Gonzalez, J. F. (2009). Glacier Decline between 1963 and 2006 in the Cordillera Real, Bolivia. *Geophys. Res. Lett.* 36 (3), a–n. doi:10.1029/2008GL036238

Soruco, A., Vincent, C., Rabatel, A., Francou, B., Thibert, E., Sicart, J. E., et al. (2015). Contribution of Glacier Runoff to Water Resources of La Paz City, Bolivia (16° S). *Ann. Glaciol.* 56 (70), 147–154. doi:10.3189/2015AoG70A001

Tibshirani, R. (1996). Regression Shrinkage and Selection via the Lasso. *J. R. Stat. Soc. Ser. B (Methodological)* 58 (1), 267–288. doi:10.1111/j.2517-6161.1996.tb02080.x

Tibshirani, R., Walther, G., and Hastie, T. (2001). Estimating the Number of Clusters in a Data Set via the gap Statistic. *J. R. Stat. Soc.* 63, 1. doi:10.1111/1467-9868.00293

Troll, C. (1941). *Studien zur Vergleichenden Geographie der Hochgebirge der Erde*. Bonner Mit.

Valdivia, P. (1984). *Inventario de glaciares. Andes de Chile central.* . Santiago: Hoyas de los ríos Aconcagua, Maipo, Cachapoal y Tinguiririca.

Vivero, S. (2008). *Inventario de glaciares descubiertos de la cuenca del río Copiapó y variaciones recientes en sus frentes Informe final de práctica profesional.* . Santiago: CSIRO.

Vuille, M., Carey, M., Huggel, C., Buytaert, W., Rabatel, A., and Jacobsen, D. (2018). Rapid decline of snow and ice in the tropical Andes: Impacts, uncertainties and challenges ahead. *Earth Science Reviews* 176, 195–213.

Wagnon, P., Ribstein, P., Francou, B., and Sicart, J. E. (2001). Anomalous Heat and Mass Budget of Glaciar Zongo, Bolivia, during the 1997/98 El Niño Year. *J. Glaciol.* 47 (156), 21–28. doi:10.3189/172756501781832593

Warren, C. R. (1993). Rapid Recent Fluctuations of the Calving San Rafael Glacier, Chilean Patagonia: Climatic or Non-climatic? *Geografiska Annaler: Ser. A, Phys. Geogr.* 75 (3), 111–125. doi:10.1080/04353676.1993.11880389

Wilson, R., Carrión, D., and Rivera, A. (2016). Detailed Dynamic, Geometric and Supraglacial Moraine Data for Glaciar Pio XI, the Only Surge-type Glacier of the Southern Patagonia Icefield. *Ann. Glaciol.* 57 (73), 119–130. doi:10.1017/aog.2016.32

Zalazar, L., Ferri, L., Castro, M., Gargantini, H., Gimenez, M., Pitte, P., et al. (2020). Spatial Distribution and Characteristics of Andean Ice Masses in Argentina: Results from the First National Glacier Inventory. *J. Glaciol.* 66, 938–949. doi:10.1017/jog.2020.55

Zemp, M., Huss, M., Thibert, E., Eckert, N., McNabb, R., Huber, J., et al. (2019). Global Glacier Mass Changes and Their Contributions to Sea-Level Rise from 1961 to 2016. *Nature* 568 (7752), 382–386. doi:10.1038/s41586-019-1071-0

Zimmer, A., Meneses, R. I., Rabatel, A., Soruco, A., Dangles, O., and Anthelme, F. (2018). Time Lag between Glacial Retreat and Upward Migration Alters Tropical alpine Communities. *Perspect. Plant Ecol. Evol. Syst.* 30, 89–102. doi:10.1016/j.ppees.2017.05.003

**Conflict of Interest:** The authors declare that the research was conducted in the absence of any commercial or financial relationships that could be construed as a potential conflict of interest.

**Publisher's Note:** All claims expressed in this article are solely those of the authors and do not necessarily represent those of their affiliated organizations, or those of the publisher, the editors and the reviewers. Any product that may be evaluated in this article, or claim that may be made by its manufacturer, is not guaranteed or endorsed by the publisher.

# 5.3 Article n°3 (in open discussion)

This Article is available at https://doi.org/10.5194/egusphere-2023-888

https://doi.org/10.5194/egusphere-2023-888
Preprint. Discussion started: 23 May 2023


## Hydrological Response of Andean Catchments to Recent Glacier Mass Loss

Alexis Caro[1], Thomas Condom[1], Antoine Rabatel[1], Nicolas Champollion[1], Nicolás García[2], Freddy Saavedra[3]

[1]Univ. Grenoble Alpes, CNRS, IRD, INRAE, Grenoble-INP, Institut des Géosciences de l'Environnement, Grenoble, France

[2]Glaciología y Cambio Climático, Centro de Estudios Científicos (CECs), Valdivia, Chile

[3]Departamento de Ciencias Geográficas, Facultad de Ciencias Naturales y Exactas, Universidad de Playa Ancha, Leopoldo Carvallo 270, Playa Ancha, Valparaíso, Chile

*Correspondence to:* Alexis Caro (alexis.caro.paredes@gmail.com)

**Abstract.** The impacts of the accelerated glacier retreat in recent decades on runoff changes are still unknown in most Andean catchments, thereby increasing uncertainties in estimating and managing water availability. Here, we used a monthly time step to simulate glacier evolution and related runoff changes for 36% of the glacierized surface area of the Andes (11,282 km$^2$ in 786 catchments, 11°N-55°S) using the Open Global Glacier Model (OGGM) and a corrected and evaluated version of the TerraClimate dataset between 2000 and 2019. The glacier mass balance and volume were calibrated glacier-by-glacier. The simulation results were evaluated with in situ data in three documented catchments and 15 glaciers. Our results show that the glacier volume (-8.3%) and surface area (-2.2%) are reduced in 93% of the catchments between the periods 2000-2009 and 2010-2019. This glacier loss is associated with changes in climate conditions (precipitation = -9%; temperature = +0.4 ± 0.1°C) inducing an increase in the mean annual glacier melt of 12% (86.5 m$^3$/s) and a decrease in the mean annual rainfall on glaciers of -2% (-7.6 m$^3$/s). We find a regional pattern in the melt factors showing decreasing values from the Tropical Andes toward the Wet Andes. A negative mass balance trend is estimated in the three documented catchments (glacierized surface area > 8%), showing the largest mean glacier contribution during the transition season (September-November) in La Paz (Bolivia) (45%) followed by Baker (Chile) (43%) and Maipo (Chile) (36%) during the summer season (January-March). In addition, our evaluation in the monitored glaciers indicates an underestimation of the mean simulated mass balance by 185 mm w.e. yr$^{-1}$ and a high mean correlation (r = 0.7). We conclude that the large increases in the simulated glacier melt in the Dry Andes (36%) and the Tropical Andes (24%) have helped to improve our knowledge of the hydro-glaciological characteristics at a much wider scale than previous studies, which focused more on a few select catchments in the Andes.

### 1 Introduction

The largest ice concentration in the southern hemisphere outside the Antarctic ice sheet is found in the Andes (RGI Consortium, 2017). Andean glaciers provide the water supply for roughly 45% of the population in the Andean countries (Devenish and Gianella, 2012) and for ecosystems (Zimmer et al., 2018; Cauvy-Fraunié and Dangles, 2019). They have been affected by a continuous shrinkage since the late 1970s, which has intensified during the last two decades (Rabatel et al., 2013; Dussaillant et al., 2019; Masiokas et al., 2020). Glacier volume loss has

https://doi.org/10.5194/egusphere-2023-888
Preprint. Discussion started: 23 May 2023


helped modulate river discharges, mainly in dry seasons (*e.g.*, Baraer et al., 2012; Soruco et al., 2015; Guido et al., 2016; Ayala et al., 2020).

Several studies have estimated glacier changes and their effects on hydrology using observation or modeling focused on specific Andean catchments. For instance, Huss and Hock (2018) studied 11 Andean catchments (1980-2100) and found an increase in glacier runoff in the Tropical and Dry Andes, but a more contrasted signal in the Wet Andes: no glacier runoff changes were observed in some catchments, whereas others showed a reduction or an increase. In the Tropical Andes, the glacier contribution at the annual scale was estimated to be approximately 12% and 15% in the Río Santa (9°S) and La Paz (16°S) catchments, respectively (Mark and Seltzer, 2003; Soruco et al., 2015). For the La Paz catchment, Soruco et al. (2015) found no change in the glacier runoff contribution for the period 1997-2006 compared with the longer 1963-2006 period. This was attributed to the fact that the glacier surface reduction over the time-period was compensated by their increasingly negative mass balance. In the Dry Andes, the Huasco (29°S), Aconcagua (33°S) and Maipo (34°S) catchments showed a glacier contribution comprised between 3 and 23% for different catchment sizes between 241 and 4843 $km^2$ (Gascoin et al., 2011; Ragettli and Pellicciotti, 2012; Ayala et al., 2020). These catchments had mainly negative glacier mass balances which were slightly interrupted during El Niño episodes (2000-2008 period), thereby reducing glacier runoff. In the Wet Andes, Dussaillant et al. (2012) estimated that some catchments in the Northern Patagonian Icefield are strongly conditioned by glacier melting. Despite this, Hock and Huss (2018) did not identify changes in the glacier runoff of the Baker catchment since 1980-2000. Given that these studies are focused on only a few catchments, these local estimations can hardly be seen as representative across the Andes, especially since glacierized catchments can be characterized by major climatic and topographic differences (Caro et al., 2021).

Nowadays, the availability of global glaciological products such as glacier surface elevation differences and glacier volume estimation (Farinotti et al., 2019; Hugonnet et al., 2021; Millan et al., 2022) allows for large-scale glacio-hydrological simulations with the possibility to accurately calibrate and validate numerical models at the catchment scale. In addition, models such as the Open Global Glacier Model (OGGM, Maussion et al., 2019) have been implemented to simulate the glacier mass balance and glacier dynamics at a global scale. Therefore, OGGM and the glaciological global dataset, in combination with in situ meteorological and glaciological measurements, can be used to precisely quantify the glacier retreat and its hydrological responses at the catchment scale across the Andes, while taking the related uncertainties into account.

Here, using OGGM, we estimate the glacier changes (area and volume) and the consecutive hydrological responses (from glacier melt [ice melt and snow melt] and rainfall on glaciers) for 786 catchments across the Andes (11°N-55°S) with a glacierized surface of at least 0.01% for the period 2000-2019. The model was run with monthly air temperature and precipitation data from the TerraClimate dataset (Abatzoglou et al., 2018) that were corrected using weather station records and mass balances measured on monitored glaciers. Our spatial analysis was performed at the catchment scale using the glaciological zones of the Andes defined in Caro et al. (2021); however, we simulated the glaciological and runoff processes at the glacier scale.

Section 2 presents the data and methods. In Section 3, we describe the glacier changes and hydrological responses at the glaciological zone and catchment scales across the Andes. In Section 4, we discuss our results and the main steps forward compared to previous research.

## 2 Data and methods

https://doi.org/10.5194/egusphere-2023-888
Preprint. Discussion started: 23 May 2023


### 2.1 Data collection and preprocessing

#### 2.1.1 Historical climate data

We used two climate datasets: the TerraClimate reanalysis and in situ measurements from meteorological stations. TerraClimate is based on reanalysis data since 1958, with a 4 km grid size at a monthly time scale, and was validated with the Global Historical Climatology Network (temperature, r = 0.95, MAE = 0.32°C; precipitation, r = 0.9, MEA = 9.1%) (Abatzoglou et al., 2018). The mean temperature was estimated from the maximum and minimum temperature whereas precipitation data is accumulated on a monthly basis. The meteorological records were compiled from Andean organizations and scientific reports (Rabatel et al., 2011; MacDonnell et al., 2013; Schaefer et al., 2017; CECs, 2018; Shaw et al., 2020; Hernández et al., 2021; CEAZA, 2022; DGA, 2022; GLACIOCLIM, 2022; IANIGLA, 2022; Mateo et al., 2022; Senamhi, 2022). The mean monthly air temperature measurements were taken from 35 off-glacier and on-glacier meteorological stations, the latter of which are rare. The location and main properties of the meteorological stations are shown in Supplementary Table S1.

#### 2.1.2 Climatic data correction and evaluation

For the temperature variable, we first quantified the local vertical annual temperature lapse rates using the in situ measurements for 33 sites across the Andes (see Table and Figure S1). Then, the TerraClimate temperature was corrected with these in situ records so that they could be used in the simulations. Last, the corrected TerraClimate temperature was evaluated via a comparison with the 34 situ data. Conversely, the precipitation variable from the TerraClimate reanalysis was scaled using the mass balance measurements for 10 monitored glaciers and was evaluated for 15 glaciers (see Tables S3, S4 and S5).

Vertical temperature lapse rates (temperature LRs) from the in situ records were estimated for each glaciological zone across the Andes as per Gao et al. (2012). The temperature LRs are presented in Figure S1. These gradients were applied to correct the raw TerraClimate temperature on the glaciers ($rTC_t$). The corrected TerraClimate temperature at the mean glacier elevation or in glacier catchments ($cTC_t$) was calculated using the following equation:

$$cTC_t = rTC_t + \Gamma * \Delta h \,, \qquad (1)$$

where $\Gamma$ is the temperature LR estimated here, and $\Delta h$ is the elevation difference between a glacier inside a TerraClimate grid and the mean TerraClimate grid elevation.

Then, we assessed the $cTC_t$ in meteorological station locations (9°S-51°S) on a monthly scale, paying attention to the monthly variability in temperature as well as to the mean temperature for all the periods with data. The $cTC_t$ monthly mean variability was evaluated using the Pearson correlation coefficient, whereas the mean temperature for the whole period considered the mean difference between $cTC_t$ and the observed temperature (biases). These results are available in Table S2 and Figure S2.

In addition, the precipitation was scaled ($cTC_p$) using precipitation factors ($Pf$) for each glaciological zone across the Andes. We ran 31 simulations for 18 glaciers with mass balance measurements across the Andes using $Pf$ values between 1 and 4 taking previous studies into account (Masiokas et al., 2016; Burger et al., 2019; Farías-Barahona et al., 2020). In the end, 10 glaciers were selected (see Table S3). The goal was to find the closest simulated mass balance standard deviation in comparison with the measured mass balance standard deviation using

https://doi.org/10.5194/egusphere-2023-888
Preprint. Discussion started: 23 May 2023


different *Pf* values (Equation 2). A similar methodology was proposed by Marzeion et al. (2012) and Maussion et al. (2019). The results of the closest simulated mass balance standard deviations and associated *Pf* are presented in Supplementary Table S3. The simulated annual mass balance was evaluated on 15 monitored glaciers using a similar methodology as that for the $cTC_t$ evaluation. In addition, details such as snow/rainfall partitioning are described hereafter and in the model implementation (2.2. section).

$$Pf = \{ 1 \leq Pf \leq 4 \ : simSD_{mb} \approx obsSD_{mb} \} , \quad (2)$$

#### 2.1.3 Glacier data

**Glacier inventory**

We used version 6.0 of the Randolph Glacier Inventory (RGI Consortium, 2017) to extract the characteristics of each glacier, *e.g.*, location, area, glacier front in land or water. The RGI v6.0 was checked using the national glacier inventories compiled by Caro et al. (2021), filtering every RGI glacier that was not found in the NGI, to obtain a total glacierized surface area of 30,943 $km^2$ (filtering 633 $km^2$). The glacier extent in the RGI v6.0 is representative of the early 2000s.

**Glacier mass balance**

The mass balance datasets were comprised of the global glacier surface elevation change product of Hugonnet et al. (2021) and in situ measurements of the glacier surface mass balance since 2000 from different institutions (e.g., Marangunic et al., 2021; WGMS, 2021). Hugonnet et al.'s (2021) product was quantified for each glacier using the OGGM toolbox. Then, the geodetic mass balance estimates were obtained for every glacier of the RGI v6.0. In situ measurements of the glacier surface mass balance available for all glaciological regions (Tropical Andes, Dry Andes and Wet Andes) were collected at the hydrological year scale (dates vary according to the latitude). The location and main characteristics of the 18 monitored glaciers are shown in Supplementary Table S4.

**Glacier volume**

The global glacier ice thickness product of Farinotti et al. (2019) was used for calibrated each glacier of the RGI v6.0 in OGGM. Farinotti et al. (2019) pooled the outputs of five different models to determine the distribution of the ice thickness on 215,000 glaciers outside the Greenland and Antarctic ice sheets.

#### 2.1.4 Glaciological zones and catchments

Eleven glaciological zones across the Andes were compiled from Caro et al. (2021) and all glaciers northward of the Outer Tropics were considered as zone number 12, called the Inner Tropics. To identify the glacierized area in each catchment, a spatial intersection was made between the glaciers identified in the filtered RGI v6.0 and the Level 9 HydroSHEDS catchments (Lehner et al., 2006). Then, we considered catchments with a glacierized surface area >= 0.01% (max = 62%, mean = 5%). We selected 786 catchments with a surface area between 3,236 and 20 $km^2$ across the Andes (11°N-55°S), including 13,179 glaciers with a total surface area of 11,282 $km^2$ (36% of the total glacierized surface area in the Andes).

https://doi.org/10.5194/egusphere-2023-888
Preprint. Discussion started: 23 May 2023


Calving glaciers (fresh and tide terminating, 15,444 km$^2$), primarily located in the Northern and Southern Patagonian Icefields and in the Cordillera Darwin, were not considered as the calving process is not currently implemented in this OGGM version. The glaciers that were not simulated for the internal model inconsistencies account for less than 1% of the total glacierized surface area. The other remaining 4,514 km$^2$ filtered glacierized surface area corresponds to glacierized catchments that present contradictory variations in terms of glacier volume and surface area. Only 59 km$^2$ was associated with glaciers filtered in the OT1 zone.

We selected the La Paz (Soruco et al., 2015), Maipo (Ayala et al., 2020) and Baker (Dussaillant et al., 2012) catchments located in glaciological regions with different climatic and morphometric characteristics (Caro et al., 2021). In these catchments, previous hydro-glaciological studies have quantified the impact of glacier changes and its hydrological contribution. In addition, river discharge records were collected from Soruco et al. (2015) and the CAMELS-CL project (Alvarez-Garreton et al., 2018) for Bolivia and Chile, respectively. In Bolivia, we considered the four glacierized head catchments providing water to the La Paz catchment: Tuni-Condoriri, Milluni, Hampaturi and Incachaca (discharge records from 2001 to 2007) with a total surface area of 227 km$^2$ and 7.5% of the glacierized surface area (mean elevation of 5,019 m a.s.l.). In Chile, for the Maipo catchment, we compiled records from Río Maipo at the El Manzano station (id = 5710001; 4839 km$^2$; discharge records from 1990 to 2019) and Río Mapocho at the Los Almendros catchments (id = 5722002; 638 km$^2$; discharge records from 1990 to 2019) with a glacierized surface area of 7.5% (mean elevation of 4,259 m a.s.l.). For the Baker catchment, we used the Río Baker Bajo Ñadis records (id = 11545000; 27403 km$^2$; discharge records from 2004 to 2019), considering a glacierized surface area of 8.2% (mean elevation of 1,612 m a.s.l.). Note that only the glacier contribution will be simulated.

### 2.2 Short description of the OGGM

We used the OGGM model (Maussion et al., 2019) across the Andes. OGGM is a modular and open-source numerical workflow implemented in Python that contains enough default input data to simulate the glacier mass balance and ice dynamics using calibrated parameter values for each glacier entity individually. The spatio-temporal configuration used in this study is the glacierized catchment and the monthly time step.

The required input data for running the model are as follows: air temperature and precipitation time series, and glacier outlines and surface topography for specific years. From these input data, it is possible to obtain annual outputs such as the surface mass balance, glacier volume and area and monthly glacier melt (snow and ice) and rainfall on glaciers (Figure 1). The geodetic mass balance rate and the glacier volume parameters were calibrated. First, using a glacier outline and topography, OGGM estimates the flow lines and catchments per glacier, and then the flow lines are calculated using a geometrical algorithm (adapted from Kienholz et al., 2014). Assuming a bed shape, it estimates the ice thickness based on mass conservation and shallow-ice approximation (Farinotti et al., 2017). After these numerical steps, it is possible to determine the area and volume per glacier. The mass balance is implemented using a precipitation phase partitioning and a temperature index approach (Braun and Renner, 1992; Hock, 2003; Marzeion et al., 2012). The monthly mass balance $mb_i$ at an elevation z is calculated as follows:

$$mb_i(z) = TC_{p\,i}^{snow}(z) * P_f - M_f * max(cTC_{t\,i}(z) - T_{melt}, 0), \quad (3)$$

https://doi.org/10.5194/egusphere-2023-888
Preprint. Discussion started: 23 May 2023


Where $TC_{p\,i}^{snow}$ is the TerraClimate solid precipitation before being scaled by the precipitation correction factor ($P_f$), $M_f$ is the glacier's temperature melt factor, $cTC_{t\,i}$ is the monthly corrected TerraClimate temperature, and $T_{melt}$ is the monthly air temperature above which ice melt is assumed to occur (from 0°C to 2.1 °C). $TC_{p\,i}^{snow}$ is calculated as a fraction of the total precipitation ($cTC_p$ ) where 100% is obtained if $cTC_{t\,i} <= T_i^{snow}$ (between 0-2.1°C) and 0% if $cTC_{t\,i} >= T_i^{rain}$ (between 2-4.1 °C), using a linear regression between these temperature thresholds to obtain the solid/liquid precipitation fraction. Here, $M_f$ was calibrated for each glacier individually using the previously described glacier volume change datasets (Hugonnet et al., 2021). The calibrated parameter values are summarized by glaciological zone in Table 1.

**Table 1. Calibrated parameter values used in the glacier mass balance and volume simulations across the Andes (11°N-55°S) during the period 2000-2019**

| Region | Zone | Mass balance parameter values | | | | | | Volume parameter |
|---|---|---|---|---|---|---|---|---|
| | | Temperature LR [°C/m a.s.l.] | Precipitation factor [-] | Mean melt factor [mm mth$^{-1}$ °C$^{-1}$] | Temperature for melt onset [°C] | Temperature at start of snowfall [°C] | Temperature at start of rainfall [°C] | Glen A inversion |
| Tropical Andes | IT | -0.0066 | 1 | 434 | 2.1 | 2.1 | 4.1 | 2.4 $10^{-23}$ |
| | OT2 | | | 284 | | | | 6.3 $10^{-24}$ |
| | OT3 | | | 432 | | | | 1.2 $10^{-23}$ |
| Dry Andes | DA1 | -0.0082 | 2.8 | 418 | 0 | 0 | 2 | 2.4 $10^{-25}$ |
| | DA2 | -0.0065 | 1.9 | 479 | | | | 1.3 $10^{-23}$ |
| | DA3 | -0.0063 | 4 | 299 | | | | 2 $10^{-24}$ |
| Wet Andes | WA1 | -0.0051 | 4 | 103 | | | | 1.7 $10^{-23}$ |
| | WA2 | | 4 | 118 | | | | 1.9 $10^{-23}$ |
| | WA3 | -0.0063 | 2.3 | 152 | | | | 6 $10^{-24}$ |
| | WA4 | | | 128 | | | | 1.3 $10^{-23}$ |
| | WA5 | | | 179 | | | | 1 $10^{-23}$ |
| | WA6 | | | 139 | | | | 1.5 $10^{-23}$ |

#### 2.2.1 Model setup, calibration and validation

We ran the model for each glacier and then the results per catchment were aggregated for each of the 786 catchments along the Andes (including the three selected test catchments for a detailed analysis).

The input data are as follows: the corrected monthly TerraClimate precipitation ($cTC_p$ ) and temperature ($cTC_t$ ), glacier outlines from RGI v6.0 (RGI Consortium, 2017) and surface topography from NASADEM (Crippen et al., 2016). Model outputs such as the surface mass balance and glacier volume were calibrated (Table 1 and Figure 2). The calibration procedure was applied per glacier to match the simulated mass balance 2000-2019 to the geodetic mass balance product from Hugonnet et al. (2021). The simulated glacier volume was calibrated using Farinotti et al.'s (2019) product at a glaciological zone scale to fit the Glen A parameter. In addition, it was assumed that the glacier outlines of all glaciers were made for the year 2000. For instance, in the case of glaciers for which the

https://doi.org/10.5194/egusphere-2023-888
Preprint. Discussion started: 23 May 2023


outline was delimited based on data acquired before or after 2000, this area was considered for the simulations starting in 2000.

Last, the simulated mass balance was evaluated in comparison with in situ mass balance observations (Marangunic et al., 2021; WGMS, 2021). Although the OGGM outputs are in calendar years and the observations are in hydrological years, we consider it essential to evaluate the interannual performance (Pearson correlation, p-value, variance, RMSE and bias from average difference) and the cumulative mass balance since the year 2000.

Figure 1 summarizes the simulation workflow, as well as the results obtained for each glacier in each catchment.

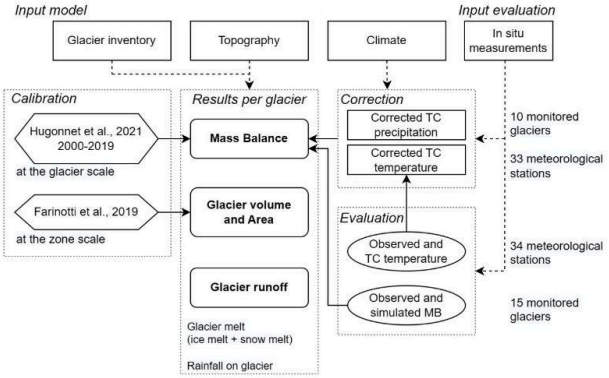


**Figure 1. Workflow per glacier simulation using OGGM between 2000 and 2019. Two groups of input data were used: one to run the model and the second to correct/evaluate the TerraClimate temperature (cTCt) and precipitation (cTCp). Then, the mass balance and glacier volume were calibrated. Lastly, results such as the cTCt and glacier mass balance were evaluated at 34 meteorological stations and on 15 glaciers with mass balance observations.**

## 3 Results

### 3.1 Climatic changes on glaciers across the Andes during the period 2000-2019

The climate associated with 786 Andean glacierized catchments (11°N-55°S) presents a mean corrected TerraClimate temperature (cTCt) of -0.2 ± 2.2°C and a mean annual corrected TerraClimate precipitation (cTCp) of 2699 ± 2006 mm $yr^{-1}$ between 2000 and 2019. The various glaciological regions show significant climatic differences, with contrasting extreme values between the Tropical Andes and Wet Andes in terms of mean annual precipitation (939 ± 261 mm $yr^{-1}$ and 3751 ± 1860 mm $yr^{-1}$, respectively) and mean annual temperature between the Dry Andes and Tropical Andes (-3.7 ± 1.4°C and 1.3 ± 0.8°C, respectively). Certain glaciological zones highlight very negative and positive mean annual temperature values such as DA2 (-4.8°C) and WA2 (1.9°C) and lower and higher cumulative precipitation values such as DA1 (447 mm $yr^{-1}$) and WA5 (6075 mm $yr^{-1}$). Meanwhile, the climate change between the periods 2000-2009 and 2010-2019 across the Andes shows a

https://doi.org/10.5194/egusphere-2023-888
Preprint. Discussion started: 23 May 2023


cumulative precipitation decrease of -9% (-234 mm $yr^{-1}$) and a mean annual temperature increase of 0.4 ± 0.1°C. Precipitation is decreasing primarily in the Dry Andes (-256 mm $yr^{-1}$; -23%) and Wet Andes (-337 mm $yr^{-1}$; -9%), and increasing in the Tropical Andes (44 mm $yr^{-1}$; 5%), whereas the temperature is increasing between 0.3-0.4°C in all regions. At the glaciological zone scale, only the Tropical Andes and DA1 (12%) show a cumulative increase in precipitation, whereas a larger decrease in precipitation is found in DA2 (-32%) and DA3 (-27%). The mean annual temperature increases in all zones, especially the Inner Tropics (+0.6°C) followed by WA3 (+0.5°C). A summary of the climate changes by glaciological zone is presented in Table 2.

Our cTCt evaluation is statistically significant (p-value < 0.01) at 32 meteorological stations with a mean temperature bias of 0.4°C and a mean correlation of 0.96. The regional results show a larger bias in the Tropical Andes (mean = 2.1°C, four stations) with a meteorological station mean elevation of 4,985 m a.s.l., where cTCt cannot represent the mean monthly temperature amplitude. However, cTCt well represents the maximum temperatures in spring/summer and the minimum temperatures in winter. The lowest bias is observed in the Wet Andes and Dry Andes. The Wet Andes, with a meteorological station mean elevation of 813 m a.s.l., shows good results in terms of reproducing the mean monthly temperature amplitude in most stations, with a minimum correlation higher than 0.86. In the Dry Andes, with a meteorological station mean elevation of 3,753 m a.s.l. (18 stations) and bias of 0.2°C, the cTCt reproduces the mean monthly temperature amplitude very well. However, in some stations such as La Frontera and Estrecho Glacier (29°S), the mean cTCt is warmer than 6°C, whereas in other stations such as El Yeso Embalse (33.7°S) and Cipreses glacier (34.5°S), the mean cTCt is colder than 6°C. The detailed cTCt evaluation can be found in Tables S1 and S3 and Figure S2 of the Supplementary Materials.

### 3.2 Glaciological changes across the Andes during the period 2000-2019

The annual mass balance and glacier dynamics per glacier are simulated by taking 36% of the total glacierized surface area across the Andes (11°N-55°S) into account to obtain the glacier area and glacier volume at an annual time scale, as well as the glacier runoff (glacier melting and rainfall on glaciers) at a monthly time scale. In more detail, over 85% of the glacierized surface area in the Dry Andes (18°S-37°S) and 79% in the Tropical Andes (11°N-18°S) is considered, which corresponds to 11% (3,377 $km^2$, in 321 catchments) of the total glacierized area of the Andes. For the Wet Andes (37°S-55°S), 29% of the glacierized surface area in the region is considered, which corresponds to 26% (7,905 $km^2$, in 465 catchments) of the total area in the Andes (see the distribution of the catchments in Figure 2a). The simulated lower glacierized surface area in the Wet Andes results from the filtering out of the numerous calving glaciers found there.

Between the periods 2000-2009 and 2010-2019, the glacier volume and area in the Andean catchments decreases by -8.3% (-59.1 $km^3$) and -2.2% (-245 $km^2$), respectively, associated with a negative mean annual mass balance of -0.5 ± 0.3 m w.e. $yr^{-1}$ (Figure 2d). A decrease in glacier volume and surface is seen in 93% of the catchments (n = 724) whereas 7% of the catchments (n = 65) present an increase in glacier volume and surface. The loss in glacier volume (Figure 2b) is largest (-47.8 $km^3$, -9%) in the Wet Andes, followed by the Tropical Andes (-5.9 $km^3$, -7%) and Dry Andes (-5.4 $km^3$, -6%). Similarly, a larger decrease in the glacier surface area (Figure 2c) is observed in the Wet Andes (-144.4 $km^2$, -2%), followed by the Tropical Andes (-55.5 $km^2$, -4%) and lastly the Dry Andes (-45.2 $km^2$, -3%). As expected, the correlation between both glacier change variables is consistent at the zone scale, showing a positive correlation between the changes in area and volume (r = 0.9).

https://doi.org/10.5194/egusphere-2023-888
Preprint. Discussion started: 23 May 2023


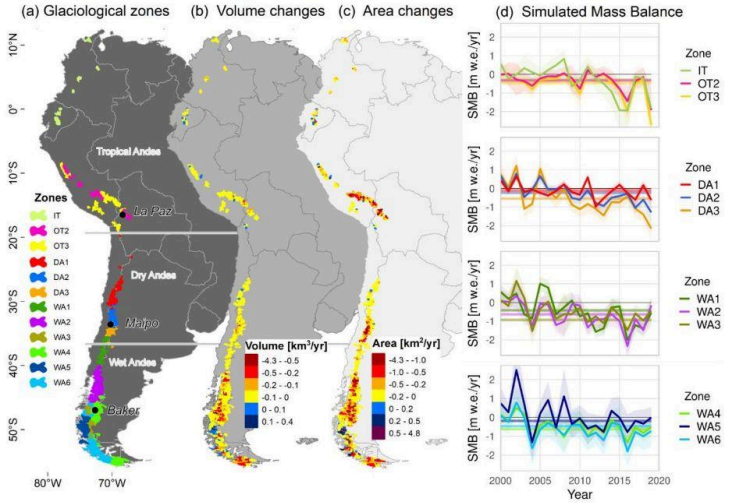


**Figure 2. Recent glacier changes across the Andes. The glacier changes are comprised of the mean annual differences between the periods 2000-2009 and 2010-2019 per catchment (n = 786). (a) It shows the distribution of the glaciological zones (11°N-55°S), followed by the (b) volume and (c) area changes at the catchment scale. The (d) annual simulated mass balances are presented in each glaciological zone (the shaded areas are the standard deviation), where the straight lines correspond to the mean geodetic mass balance (2000-2019) estimated by Hugonnet et al. (2021).**

When estimating the mass balance, it is interesting to check the calibrated melt factors ($M_f$) of the temperature index model in order to evaluate its possible regionalization, i.e., to evaluate the spatial coherence (see Figure 3). We obtain very similar values in contiguous zones, with the lowest values found in the Wet Andes (mean below 179 mm $mth^{-1}$ $°C^{-1}$), followed by the Tropical Andes (mean below 434 mm $mth^{-1}$ $°C^{-1}$), and the Dry Andes (mean below 479 mm $mth^{-1}$ $°C^{-1}$). The largest melt factor values are found in the Dry Andes where the DA2 zone (mean = 479 mm $mth^{-1}$ $°C^{-1}$) presents the lowest mean temperatures across the Andes (-4.8°C between 2000-2019). The lowest melting factor values are calibrated in the Wet Andes where zone WA1 (mean = 103 mm $mth^{-1}$ $°C^{-1}$) shows high mean temperatures (1.8°C between 2000-2019). Despite this, a lower correlation between the melt factors and mean temperature for the 2000-2019 period is estimated (r = -0.5; p-value = 0.08). Conversely, the correlation between the melt factors and mean precipitation for the 2000-2019 period is high (r = -0.8; p-value = 0.002).

To test our results we evaluated the simulated mass balance in 15 monitored glaciers (Tables S4 and S5 and Figure S3). The in situ data show a mean negative mass balance (-832 ± 795 mm w.e. $yr^{-1}$) between 2000 and 2019 greater than our mean simulated mass balance (-647 ± 713 mm w.e. $yr^{-1}$) in the same glaciers. The evaluation results give a mean Pearson correlation of 0.67 (except for Agua Negra, Ortigas 1, Guanaco and Amarillo glaciers, which shows either no correlation or a negative correlation) with an underestimation of the mean simulated mass balance

https://doi.org/10.5194/egusphere-2023-888
Preprint. Discussion started: 23 May 2023


of 185 mm w.e. $yr^{-1}$ (bias); 40% of the glaciers present a correlation equal to or greater than 0.7. In terms of the best results by glaciological region, in the Tropical Andes, the Conejeras glacier has a high correlation (r = 0.9) and bias (1104 mm w.e. $yr^{-1}$), whereas in the Dry Andes, the Piloto Este, Paula, Paloma Este and Del Rincón glaciers display a high correlation (r >= 0.8) and a mean bias of 351 mm w.e. $yr^{-1}$. In the Wet Andes, the Mocho-Choshuenco and Martial Este glaciers show a moderate correlation (r = 0.5) and a lower overestimation of the simulated mass balance (-118 mm w.e. $yr^{-1}$). Model limitations are observed in the Zongo glacier (r = 0.3 and bias = -224 mm w.e. $yr^{-1}$) in the Tropical Andes. In the Dry Andes, no correlation is observed in the three monitored glaciers (Guanaco, Amarillo and Ortigas 1); this is mainly because sublimation, an ablation process that is not represented in the model, is dominant for these glaciers.

The details of the glacier changes in the 786 Andean catchments, which are larger in the Wet Andes followed by the Tropical Andes and then the Dry Andes, are available in the Supplementary Materials. The simulated mass balance evaluation for the 15 glaciers can be found in Figures S4 and S5 of the Supplementary Materials.

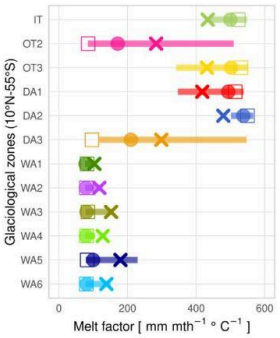


**Figure 3. Statistics for the calibrated melt factors per glacier at the glaciological zone scale across the Andes. This figure shows the mean (x), median (circle), mode (square), and percentile 25 and 75 (lines) values for 13,179 glaciers.**

### 3.3 Changes in glacier runoff across the Andes during the period 2000-2019

Due to glacier changes across the Andes, high glacier runoff variations are observed from glacier melt and rainfall on glaciers (Figure 4). The mean annual glacier melt in all catchments for the period 2000-2019 was 696 $m^3/s$. At the regional scale, the Wet Andes shows the largest mean annual glacier melt in the Andes (583.5 $m^3/s$), followed by the Dry Andes (59.9 $m^3/s$) and then the Tropical Andes (52.7 $m^3/s$). However, if we look at the mean annual glacier melt changes between the periods 2000-2009 and 2010-2019, we see an increase of 12% (86.5 $m^3/s$) across the Andes, where 84% (n = 661) of catchments show an increase and 12% (n = 95) of them present a decrease. As Table S6 shows, an increase in glacier melt is observed in catchments with a higher glacier elevation, larger glacier size, lower mean temperature and higher mean precipitation compared with catchments that show either a decrease

https://doi.org/10.5194/egusphere-2023-888
Preprint. Discussion started: 23 May 2023


in glacier melt or no changes at all. These latter catchments also show the largest decrease in precipitation (-10 to -14%).

The mean annual glacier melt changes show the largest percentage increase in the Tropical Andes (40%, 21 $m^3/s$), followed by the Dry Andes (36%, 21.7 $m^3/s$), and the Wet Andes (8%, 4.8 $m^3/s$). In addition, significant differences are observed for the different zones: for instance, the Inner Tropics in the Tropical Andes presents the largest increase (73% with only 4.1 $m^3/s$), followed by DA1 (62% with only 1.8 $m^3/s$) in the Dry Andes. In the Wet Andes, the larger percentage of increase in the mean annual glacier melt changes is observed in WA5 (14% with 4.1 $m^3/s$), showing a lower percentage in comparison with the Inner Tropics and DA1 zones, however, its absolute increase in glacier melt is equal to or greater than 4.1 $m^3/s$. These results per glaciological zone are summarized in Table 2. Related to the previously described glacier changes (see Section 3.2) between the periods 2000-2009 and 2010-2019, at the glaciological zone scale, we logically find a high negative correlation between the glacier melt and glacier volume changes in the Tropical Andes and Dry Andes ($r = -0.9$) and the Wet Andes ($r = -1$).

In addition, the mean annual rainfall on glaciers across the Andes is 387 $m^3/s$ for the period 2000-2019. The Wet Andes has the largest amount of annual rainfall (372.7 $m^3/s$), followed by the Tropical Andes (10.5 $m^3/s$) and Dry Andes (4.2 $m^3/s$) with the lowest contribution of rainfall. In terms of the changes in the mean annual rainfall on glaciers between the periods 2000-2009 and 2010-2019, we observe a reduction of -2% (-7.6 $m^3/s$) across the Andes, showing a reduction in 41% of the catchments ($n = 322$) whereas the largest proportion of the catchments (51%, $n = 403$) show an increase. Table S6 shows that the catchments with the larger increase of rainfall on glaciers are concentrated in the same latitude range as the catchments with an increase in glacier melt. These catchments have similar glacier elevations and glacier sizes. The catchments that do not show changes in rainfall on glaciers are concentrated in the Dry Andes region, where the rainfall contributes less to the glacier runoff volume.

At the glaciological region scale, the mean annual rainfall on glaciers decreases in the Wet Andes (-3%, 10.1 $m^3/s$), but increases in the Tropical Andes (23%, 2.4 $m^3/s$) and Dry Andes (3%, 0.1 $m^3/s$). In addition, large differences are observed in the glaciological zones (Table 2): e.g. DA1 in the Dry Andes has the largest percentage increase (106% with only 0.2 $m^3/s$), followed by IT (74% with only 0.4 $m^3/s$) in the Tropical Andes. In the Wet Andes, the larger increase (in percent) in the mean annual rain on the glaciers is observed in WA5 (6.6% with 2.1 $m^3/s$). Other zones such as WA2 and WA6 show large absolute reductions (-11.7 $m^3/s$ and -4.5 $m^3/s$, respectively).

The changes in glacier melt and rainfall on glaciers observed in the Tropical Andes, Dry Andes and Wet Andes are summarized in Table 2, and are available for the 786 Andean catchments in the Supplementary Materials.

https://doi.org/10.5194/egusphere-2023-888
Preprint. Discussion started: 23 May 2023


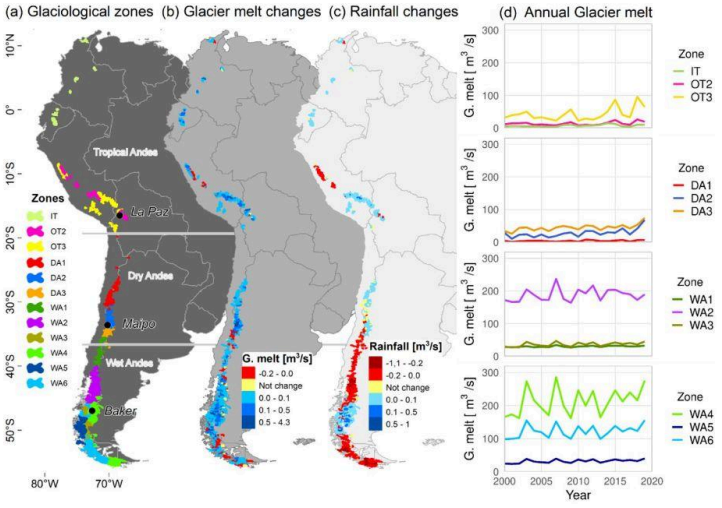


**Figure 4. Recent glacier runoff components across the Andes. The total glacier melt and rainfall on glaciers are comprised of the mean differences between the periods 2010-2019 and 2000-2009 per catchment (n = 786). (a) It shows the distribution of the glaciological zones (11°N-55°S), followed by (b) glacier melt and (c) rainfall on glaciers at the catchment scale. The (d) total annual glacier melt is presented in each glaciological zone.**

**Table 2. Mean annual changes in glacier area and volume, glacier runoff and climate between periods 2000-2009 and 2010-2019 at the glaciological zones scale across the Andes (11°N-55°S)**

| Region | Zone | Change in surface area [km$^2$] (%) | Change in volume [km$^3$] (%) | Change in glacier melt [m$^3$/s] (%) | Change in rainfall on glaciers [m$^3$/s] (%) | Simulated area [km$^2$] and percentage in total glacierized area (%) | cTCt change [°C] | cTCp change [mm yr$^{-1}$ (%)] |
|---|---|---|---|---|---|---|---|---|
| Tropical Andes | IT | -5.8 (-3) | -0.7 (-8) | 4.1 (73) | 0.4 (74) | 191 (88) | 0.6 | 81 (7.1) |
| | OT2 | -19.3 (-4) | -1.2 (-8) | 2.8 (23) | 0.3 (10) | 437 (77) | 0.3 | 19 (2) |
| | OT3 | -30.4 (-3) | -4 (-7) | 14.1 (40) | 1.6 (25) | 1149 (81) | 0.4 | 43 (5.2) |
| Dry Andes | DA1 | -5.2 (-2) | -0.4 (-4) | 1.8 (62) | 0.2 (106) | 218 (93) | 0.3 | 50 (11.9) |
| | DA2 | -7.4 (-1) | -2 (-4) | 11.3 (59) | 0.1 (14) | 770 (76) | 0.3 | -269 (-32) |
| | DA3 | -32.6 (-5) | -3 (-8) | 8.5 (23) | -0.1 (-3) | 613 (97) | 0.3 | -629 (-27.2) |

https://doi.org/10.5194/egusphere-2023-888
Preprint. Discussion started: 23 May 2023


| | | | | | | | | |
|---|---|---|---|---|---|---|---|---|
| Wet Andes | WA1 | -7 (-3) | -1.1 (-8) | 1.7 (6) | -1.6 (-13) | 237 (93) | 0.3 | -937 (-18.3) |
| | WA2 | -41.2 (-3) | -11.6 (-13) | 10.7 (6) | -11.7 (-9) | 1550 (91) | 0.4 | -454 (-8) |
| | WA3 | -4.9 (-1) | -3 (-7) | 4.4 (14) | 1.1 (5) | 469 (4) | 0.5 | -161 (-4.4) |
| | WA4 | -72 (-2) | -21.4 (-9) | 15.3 (8) | 4.4 (5) | 3746 (57) | 0.4 | -96 (-5.1) |
| | WA5 | 4.5 (1) | -0.3 (-1) | 4.1 (14) | 2.1 (7) | 378 (15) | 0.4 | -407 (-6.5) |
| | WA6 | -23.9 (-2) | -10.5 (-8) | 7.7 (7) | -4.5 (-5) | 1524 (32) | 0.3 | -382 (-10) |

### 3.4 Hydro-glaciological behavior at the catchment scale during the period 2000-2019

In this section, we focus on three Andean catchments: La Paz (16°S, Tropical Andes), Maipo (33°S, Dry Andes) and Baker (47°S, Wet Andes) (see locations in Figure 2 or 4), where previous glaciological observations and simulations of glacier evolution and water production have been carried out, and in situ records are also available. Detailed results for each of the 786 catchments and glaciers included are available in the dataset provided in the Supplementary Material.

#### 3.4.1 Glaciological variations in the selected catchments: La Paz (16°S), Maipo (33°S) and Baker (47°S)

Figure 5 shows the annual mass balance in the three catchments (2000-2019). The mean over the study period is negative, and there is a negative trend for the annual values toward 2019. For instance, for the Maipo catchment, we estimate a mean annual mass balance of -0.29 ± 0.14 m w.e. $yr^{-1}$, a slightly more negative balance in the Baker catchment (-0.47 ± 0.19 m w.e. $yr^{-1}$), whereas the glaciers in the La Paz catchment show a greater loss of -0.56 ± 0.19 m w.e. $yr^{-1}$. In addition, when considering the annual mass balance values, it is possible to note differences between the catchments. The La Paz catchment shows mostly negative annual mass balance values over the whole period, while in the Baker and Maipo catchments the mass balances are predominantly negative after 2004 and 2009, respectively. Considering the total area and volume changes per catchment in the periods 2000-2009 and 2010-2019, an overall reduction is observed in each of the three catchments. For the La Paz catchment, considering 86% (14 $km^2$) of glacierized area in 2000 (mean glacierized elevation of 5,019 m a.s.l.) and 20 glaciers, the glacierized surface area and volume decrease by -7% (-1 $km^2$) and -11% (-0.1 $km^3$), respectively. For the Maipo catchment, with a larger percentage of simulated glacierized surface area in 2000 (99%, with mean elevation of 4,259 m a.s.l.) and a greater number of glaciers (n = 225), the area and volume decrease by -1% (-4.2 $km^2$) and -5% (-1 $km^3$), respectively. For the Baker catchment, which contains the largest glacierized surface area of the three catchments in 2000, we simulated 66% of this glacierized area (1514 $km^2$, with mean elevation of 1,612 m a.s.l.) and 1805 glaciers: this area shrank by approximately -2% (-36.7 $km^2$), losing close to -11% (-9.3 $km^3$) of its volume. These results are summarized in Table 3.

https://doi.org/10.5194/egusphere-2023-888
Preprint. Discussion started: 23 May 2023


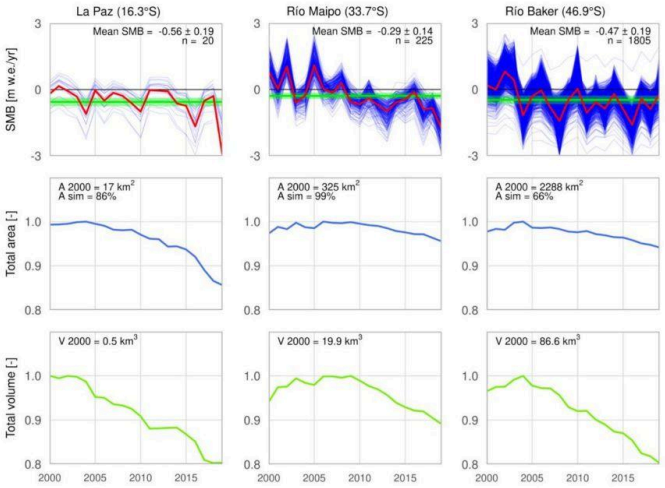


**Figure 5. Recent specific mass balance, surface area, and volume variations in the La Paz, Maipo, and Baker catchments from 2000 to 2019. The first row shows the mass balance for each simulated glacier (blue line), as well as the weighted mean mass balance per catchment (red line). The mean geodetic mass balance and its error for the period 2000-2019 are also presented (green bar). The second row presents the total glacierized area per catchment (blue line). The total area from RGI v6.0 and the simulated area percentage are also presented. The last row exhibits the total volume per catchment (green line). The surface area and volume have both been normalized to make it easier to compare the evolution between the catchments.**

### 3.4.2 Hydrological contribution of glaciers in the selected catchments: La Paz (16°S), Maipo (33°S) and Baker (47°S)

The La Paz, Maipo, and Baker catchments display large climatic and glaciological differences over the period 2000-2019. For instance, contrasting cumulative precipitation amounts can be found between the Baker and La Paz catchments (2224 ± 443 mm $yr^{-1}$ and 791 ± 100 mm $yr^{-1}$, respectively), while the La Paz and Maipo catchments present the maximum difference in mean annual temperature (1.4 ± 0.5°C and -4.1 ± 0.5°C, respectively) (Figure 6). At a seasonal scale, precipitation in the Maipo and Baker catchments is concentrated in autumn and winter (April-September), even if the latter catchment also has a significant amount of precipitation in summer. Conversely, precipitation in the La Paz catchment mainly occurs in spring and summer (October to March). In addition, the La Paz and Baker catchments are characterized by the warmest temperatures (>0°C) in spring and summer; the warmest temperatures for the Maipo catchment occur in summer. Changes in the climatic conditions are observed between 2000-2009 and 2010-2019. For instance, a decrease in cumulative precipitation is observed in the Maipo (-30%, -454 mm $yr^{-1}$) and Baker catchments (-2%, -52 mm $yr^{-1}$), but an increase can be seen in the

https://doi.org/10.5194/egusphere-2023-888
Preprint. Discussion started: 23 May 2023


La Paz catchment (4%, 30 mm $yr^{-1}$). The mean annual temperature increases in the three catchments (+0.5°C in La Paz and Baker, +0.4°C in Maipo).

The glacier runoff simulation, which considers the glacier melt (ice and snow melt) and rainfall on glaciers (liquid precipitation), shows strong differences between the catchments (Figure 6). Over the period 2000-2019, the glaciers in the Baker catchment have the highest mean annual glacier melt (94 ± 19.6 $m^3/s$), followed by those in the Maipo (15.1 ± 4.2 $m^3/s$) and La Paz catchments (0.5 ± 0.2 $m^3/s$). The rainfall on glaciers contributes 30% to glacier runoff in the Baker catchment (41 ± 10.1 $m^3/s$); a lower value is found in the La Paz catchment with 17% (0.1 $m^3/s$) followed by the Maipo catchment with 5% (0.8 ± 0.3 $m^3/s$), which is the lowest contribution of rainfall on glaciers in these catchments. The simulations of glacier runoff changes between the periods 2000-2009 and 2010-2019 for the three catchments show an increase in glacier melt and rainfall on glaciers. The largest relative increase in mean annual glacier melt is observed in the Maipo with 37% (4.7 $m^3/s$), followed by the La Paz with 21% (0.09 $m^3/s$) and the Baker catchments with 10% (9 $m^3/s$). Meanwhile, the largest relative increase in the mean annual rainfall on glaciers is observed in the La Paz catchment (15%, 0.01 $m^3/s$), followed by the Baker catchment (11%, 4.3 $m^3/s$) and lastly the Maipo catchment (2%, 0.02 $m^3/s$). The results for the glacier melt and rainfall on glaciers are summarized in Table 3.

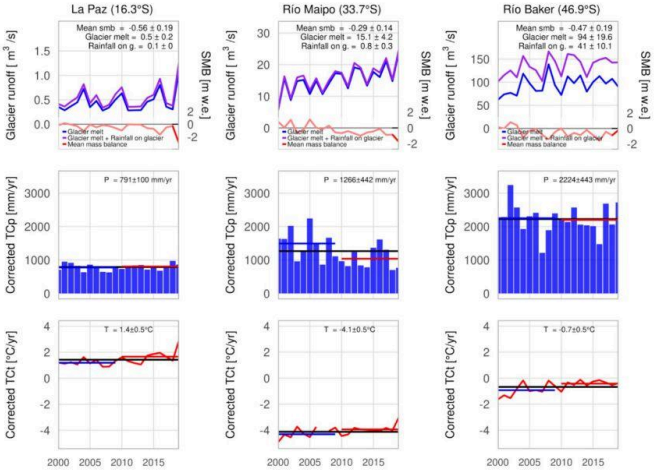


**Figure 6. Hydro-glaciological responses and climate variations in the La Paz, Maipo and Baker catchments from 2000 to 2019. The first row presents the mean annual glacier runoff (purple line = ice melt+snow melt+rainfall on glaciers), the mean annual glacier melt (blue line = ice melt+snow melt), and the annual mass balance (red line). The other rows show the mean total annual precipitation and mean annual temperature with the mean annual amount for the periods 2000-2019 (black line), 2000-2009 (blue line) and 2010-2019 (red line).**

https://doi.org/10.5194/egusphere-2023-888
Preprint. Discussion started: 23 May 2023


In Figure 7, at a mean monthly temporal scale for the period 2000-2019, the glacier melt simulation presents a short maximum during summer (January-February) in the Maipo and Baker catchments. In contrast, peaks in the La Paz catchment are extended during spring and summer (November-March) highlighting the so-called transition season (between September and November) where there is a low amount of rainfall on glaciers and glacier melt progressively increases. In the Baker catchment, melting begins earlier in September while in Maipo it begins later (November). The interannual variability of glacier melt over the periods 2000-2009 and 2010-2019 shows a larger contribution from the glacier in the period 2010-2019 for the Maipo catchment. Furthermore, the simulated rainfall on glaciers is larger mainly during the summer season in all catchments, with more rainfall in the La Paz catchment (December to February) after the transition season.

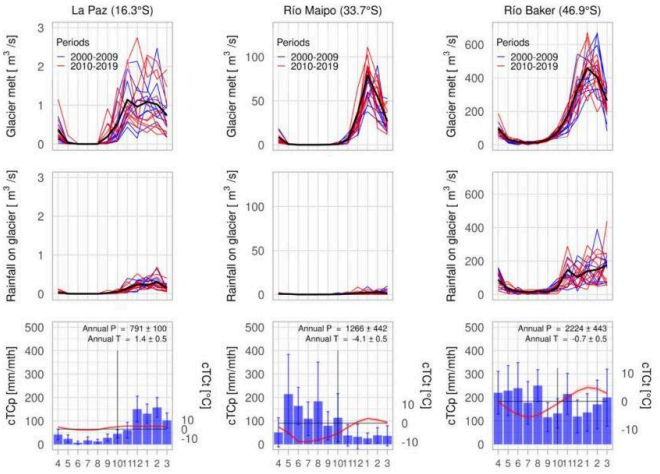


**Figure 7. Monthly hydro-glaciological responses and climate variations in the La Paz, Maipo and Baker catchments from 2000 to 2019. The first and second rows present the mean monthly glacier melt and rainfall on glaciers (black line) and the mean amounts per year during the periods 2000-2009 (red lines) and 2010-2019 (blue lines). In the last row, the climographs show the mean monthly precipitation (blue bars) and temperature (red line) for the period 2000-2019.**

For the mean annual discharge measurements in each catchment and the mean annual simulated glacier runoff (glacier melt and rainfall on glaciers) between 2000-2019 (Figure 8), we estimate that the largest glacier contribution is in the Baker catchment (24%), followed by the La Paz (22%) and Maipo catchments (14%), where all catchments present a similar proportion of glacierized surface area (7.5% to 8.2%). If we consider the summer season only (January to March), the glacier contribution is highest in the Baker catchment (43%), followed by the Maipo (36%) and La Paz catchments (18%), where the larger percentage of glacier melt is found in the Maipo catchment (34%) and the larger percentage of rainfall on glaciers is displayed in the Baker catchment (12%).

https://doi.org/10.5194/egusphere-2023-888
Preprint. Discussion started: 23 May 2023


Unlike the Maipo and Baker catchments, which present a maximum glacier contribution in the summer season, the La Paz catchment shows the largest glacier contribution (45%) in the transition season (September to November).

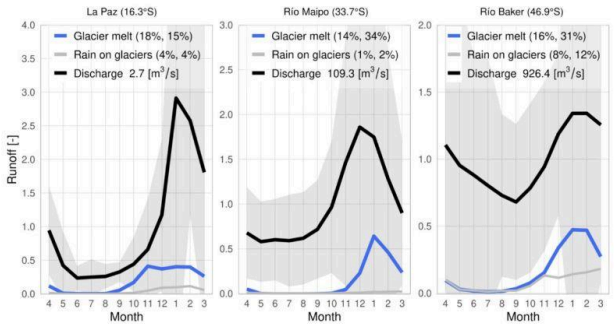


**Figure 8. Monthly simulated glacier runoff (glacier melt + rainfall on glaciers) and discharge measurements in the La Paz, Maipo, and Baker catchments from 2000 to 2019. The results for the glacier melt (blue lines) and rainfall on glaciers calculations (gray) are presented, as well as the discharge measurement (black line) and its standard deviation (gray area). The mean annual glacier contribution (as a percentage) and the mean glacier contribution (as a percentage) from January to March are shown in parentheses. The values are normalized by the mean river discharge.**

415

**Table 3. Hydro-glaciological and climatic changes between the periods 2000-2009 and 2010-2019 for the three selected catchments**

| Region | Catchment | Change in surface area [$km^2$] (%) | Change in volume [$km^3$] (%) | Contribution of the annual glacier melt [$m^3/s$] (%) | Contribution of the annual rainfall on glaciers [$m^3/s$] (%) | Total simulated glacierized area [$km^2$] (%) | cTCt change [°C] | cTCp change [mm $yr^{-1}$] (%) |
|---|---|---|---|---|---|---|---|---|
| TA | La Paz | -0.96 (-6.7) | -0.1 (-11.5) | 0.09 (21.3) | 0.01 (15.3) | 14.4 (86) | 0.5 | 30 (4) |
| DA | Maipo | -4.2 (-1.3) | -1 (-5) | 4.7 (37) | 0.02 (2.2) | 353.9 (99) | 0.4 | -454 (-30) |
| WA | Baker | -36.7 (-2.4) | -9.3 (-10.7) | 9 (10) | 4.3 (11.2) | 1514 (66) | 0.5 | -52 (-2) |

## 4 Discussion

In this section we will discuss the relevance of the results obtained at the regional- to glacier-scale across the Andes. We will also discuss the main methodological advantages and limitations of the simulations.

420 ### 4.1 Comparison with previous studies across the Andes

Hock and Huss (2018) studied 11 Andean catchments across the Andes (1980-2000 and 2010-2030) and estimated an increase in glacier runoff in the Tropical Andes (Santa and Titicaca catchments) and the Dry Andes (Rapel and

https://doi.org/10.5194/egusphere-2023-888
Preprint. Discussion started: 23 May 2023


Colorado catchments). Our results are consistent with these estimates. We show an increase in glacier melt by 40% and 36% in both regions, respectively, between the periods 2000-2009 and 2010-2019. However, in the Wet Andes, Hock and Huss (2018) did not estimate any changes in glacier runoff on the western side of the Andes (Biobio catchment), and instead found a decrease (Río Negro catchment) and an increase (Río Santa Cruz catchment) in glacier runoff on the eastern side of the Andes. Our results for this region show an increase in glacier melt by 8% and a decrease in rainfall on glaciers by -3%.

Based on local reports in the Tropical Andes, the catchment associated with the Los Crespos glacier (id = 6090223080) on the Antisana volcano shows a small decrease in the glacier area of -1% between the periods 2000-2009 and 2010-2019, which is in agreement with Basantes-Serrano et al. (2022). Their study estimated that almost half of the glacier area (G1b, G2-3, G8, G9 and G17) had a positive mass balance during the period 1998-2009 with the largest glacier presenting a mass balance of 0.36 ± 0.57 m w.e. $yr^{-1}$, in agreement with our mass balance estimation at the catchment scale of 0.2 ± 0.5 m w.e. $yr^{-1}$ (2000-2009). However, in this region, the corrected TerraClimate temperature cannot reproduce the magnitude of the monthly temperature variation (see Figure S2). This limits the effectiveness of the parameter values used in the model to accurately simulate the melting onset and the amount of solid/liquid precipitation. Furthermore, the mass balance simulation is performed through the temperature index model which does not take the sublimation process into account; and in addition, it runs at a monthly time step thereby limiting the relevant processes that occur hourly. On the other hand, the catchments that contain the Zongo glacier (id = 6090629570) and the Charquini glacier (id = 6090641570) display results that are consistent with the observations (Rabatel et al., 2012; Seehaus et al., 2020; Autin et al. 2022). In addition, our simulated mass balance evaluation on the Zongo glacier shows a low bias (-0.2 m w.e. $yr^{-1}$) with regard to the observations. In the Dry Andes, the catchments associated with the Pascua Lama area (id = 6090836550 and id = 6090840860), the Tapado glacier (id = 6090853340) and the glaciers of the Olivares catchment (id = 6090889690) show consistent results in terms glaciological variations in comparison with the observations (Rabatel et al., 2011; Malmros et al., 2016; Farías-Barahona et at., 2020; Robson et al., 2022). In the Wet Andes, the catchments associated with the Chilean side of the Monte Tronador (id = 6090945100) and the Martial Este and Alvear glaciers in Tierra del Fuego (id = 6090037770) show results that are consistent with previous reports (Rabassa 2010; Ruiz et al., 2017). Despite this, it is possible that our methodology could overestimate precipitation in some catchments; for example, the cumulative precipitation associated with the Nevados de Chillán catchment (id = 6090916140) was estimated at 4023 mm $yr^{-1}$.

At the glaciological region scale, previous studies have reported a large decrease in the percentage of glacier area in the Tropical Andes by -29% (2000-2016) (Seehaus et al., 2019; 2020), followed by the Dry Andes between -29 and -30% (Rabatel et al., 2011; Malmros et al., 2016) although for a longer time-period. In the Wet Andes, Meier et al. (2018) reported a -9% decrease in the glacier area (1986–2016). Our simulations are consistent with these observed glacier area reductions. In addition, Caro et al. (2021) estimated a similar trend across the Andes between 1980-2019 (Tropical Andes = -41%, Dry Andes = -39%, Wet Andes = -24%). On the other hand, we found high correlations between the mean annual climatic variables and annual mass balance. In the Dry Andes, this correlation was high with precipitation (r = 0.8 ± 0.1) and in the Wet Andes, temperature was correlated with mass balance (r = -0.7 ± 0.1) as previously observed by Caro et al. (2021). These correlations between precipitation or temperature with the annual mass balances for each catchment across the Andes can be reviewed in Table S7 and Figure S5 of the Supplementary Materials.

https://doi.org/10.5194/egusphere-2023-888
Preprint. Discussion started: 23 May 2023


### 4.2. Comparison of our results with previous studies in the three selected catchments

In the La Paz catchment, Soruco et al. (2015) evaluated the mass balance of 70 glaciers (1997-2006) and their contribution to the hydrological regime. In the present study, we simulated a less negative mass balance (-0.56 ± 0.19 m w.e. $yr^{-1}$ *vs.* -1 m w.e. $yr^{-1}$) considering a largest glacierized area due to the use of RGI v6.0 (with 14.1 $km^2$ in comparison to 8.3 $km^2$). Our estimation of the mean annual glacier runoff (22%) is larger than the previous estimation close to 15% (Soruco et al., 2015). This may be due to the fact that we have considered a warmer 2010-2019 period than the one observed in Soruco et al. (2015). Unlike the previous report, we estimated a larger glacier contribution during the wet season (26%, October to March) and increasing in the transition season (45%, September to November). This increase in glacier contribution given by the model agrees with the larger glacier mass loss observed by Sicart et al. (2007) and Autin et al. (2022) during this season. In the Maipo catchment, we identified a slightly smaller glacierized area (325 $km^2$ for the year 2000, -14%) compared with Ayala et al. (2020) because they considered rock glaciers from the Chilean glacier inventory. In addition, we observed a more negative mass balance after 2008, coinciding with the mega-drought period characterized by a decrease in precipitation and an increase in temperature (Garreaud et al., 2017). The hydrological response to this negative mass balance trend is an increase in glacier runoff since 2000 that is concentrated between December and March. Our mean annual glacier contribution estimation close to 15%, reaching 36% in summer (January-March), is close to Ayala et al.'s (2020) estimation (16% at the annual scale for the period 1955-2016). It is difficult to compare our results given here with previous studies in the Maipo and La Paz catchments, as any comparison is limited by the use of different input data and models, as well as spatial resolution, time step and calibration processes. Lastly, in the Baker catchment, Dussaillant et al. (2012) stated that catchments associated with the Northern Patagonian Icefield (NPI) are strongly conditioned by glacier melting. In this respect, Hock and Huss (2018) did not identify glacier runoff changes between the periods 1980-2000 and 2010-2030, they only considered 183 $km^2$ of the glacierized area (-12% until 2020), whereas we estimated a 10% and 11% increase in glacier melt and rainfall on glaciers, respectively, taking a larger glacierized area (1514 $km^2$; -2% until 2020) into account. The relevance of the rainfall on glaciers with regards to the glacier runoff estimated here is close to 30% (including glaciers from east of NPI to the east) which is confirmed by Krogh et al. (2014), who estimated that over 68% of the total precipitation at the catchment scale in east NPI (León and Delta catchments) corresponds to rainfall.

### 4.3 Melt factor values distributed across the Andes

Several reconstructions of the glacier surface mass balance have been performed across the Andes (9-52°S) using a temperature index with higher mean values in the Tropical Andes (0.3-0.5 mm $h^{-1}$ $ºC^{-1}$), than in the Dry Andes (0.3-0.4 mm $h^{-1}$ $ºC^{-1}$) and Wet Andes (0.1-0.5 mm $h^{-1}$ $ºC^{-1}$) (e.g., Fukami & Naruse, 1987; Koisumi and Naruse, 1992; Stuefer et al., 1999, 2007; Takeuchi et al., 1995; Rivera, 2004; Sicart et al., 2008; Condom et al., 2011; Caro, 2014; Huss and Hock, 2015; Bravo et al., 2017). However, these studies considered different scales, both spatially (from stakes to a catchment scale) and temporally (from hourly to monthly), as well as different in situ and fixed (literature) melt factor values for the snow and ice temperature index. Taking these differences into account, we found a regional pattern for the melt factor using the same methodology at a monthly time step. The mean calibrated melt factor values decrease from the Tropical Andes toward the Wet Andes (TA = 0.5 ± 0.3 mm $h^{-1}$ $ºC^{-1}$, DA = 0.6 ± 0.2 mm $h^{-1}$ $ºC^{-1}$, WA = 0.2 ± 0.1 mm $h^{-1}$ $ºC^{-1}$) (see Table 1 and Figure 3). This geographical distribution aligns with our evaluation of the TerraClimate dataset. The lowest mean temperatures estimated in the

https://doi.org/10.5194/egusphere-2023-888
Preprint. Discussion started: 23 May 2023


Dry Andes imply higher factor values to reach the calibrated mass loss in the few months in which the temperatures exceed 0°C. The opposite can be observed in the Wet Andes, where low factor values are associated with a greater number of months with temperatures exceeding 0°C.

### 4.4 Simulation limitations

Limitations in the simulations result from different sources: (1) the quality/accuracy of the input data; (2) the calibration of the precipitation and melt factors; and (3) the model itself, including its structure and the processes that are not represented. Regarding the evaluation of the corrected TerraClimate temperature using meteorological observations in the Tropical Andes, the corrected TerraClimate data do not reproduce either the low monthly temperature amplitude or the higher temperature in specific months which have a mean bias of 2.1°C (e.g. Llan_Up-2 9°S, Zongo at glacier station 16°S). These differences found in the corrected TerraClimate limit the capacity of the ice/snow melting module to accurately simulate the months in which melting can occur. To account for this, the values of the thresholds used for the melting onset and for the solid/liquid precipitation phase have been adjusted. On the contrary, in the Dry Andes and Wet Andes, the corrected TerraClimate temperatures are closer to the in situ observations (mean bias = 0.2ºC) and present a reliable monthly distribution. This results in model parameter values that are in better agreement with the values used in other studies. Other limitations come from RGI v6.0 because some glaciers are considered as only one larger glacier. For example, in the Dry Andes (id = 6090889690) two large glaciers, the Olivares Gamma and the Juncal Sur, form one (even larger) glacier. These glaciers could underestimate the simulated change in glacier area, limiting the performance of the volume module which depends on the glacier geometry and bedrock shape.

Furthermore, we applied different precipitation factor values in the Tropical Andes (1), Dry Andes (1.9 to 4) and Wet Andes (2.3 to 4), in order to increase the annual amplitude of the simulated mass balance. These values are in agreement with former studies, for example, similar values were used in the Dry Andes (Masiokas et al., 2016; Burger et al., 2019; Farías-Barahona et al., 2020). Values that are too high could lead to an overestimation of precipitation on some glaciers. However, to confirm that the precipitation factor produces realistic precipitation values, we adjusted the standard deviation of the simulated mass balance to the observed mass balance, a method similar to that proposed in Marzeion et al. (2012) and Maussion et al. (2019). On the other hand, the uncertainty of the calibrated melt factors come from the climate and geodetic mass balance datasets used to run and calibrate the model, respectively. Because of the monthly temperature variability, the upper threshold defines the melting onset and determines the number of months in which it occurs. Meanwhile, the geodetic mass balance defined the maximum melting per glacier in a given period. Based on our evaluation of the corrected TerraClimate temperature and simulated mass balance, we found a true seasonal melting distribution, associated with a mean underestimated mass balance of 185 mm w.e. $yr^{-1}$ that was highly correlated with the in situ data ($r = 0.7$).

With regards to the structural limitations of the model, it would be relevant to distinguish between ice and snow melt when simulating the glacier melt with two melt factors. In addition, the sublimation on the glacier surface is very relevant in the Tropical Andes and DA1 (Rabatel et al., 2011; MacDonnell et al., 2013). However, the OGGM model does not incorporate these processes in glacier runoff and mass balance simulations.

## 5 Conclusion

https://doi.org/10.5194/egusphere-2023-888
Preprint. Discussion started: 23 May 2023


In this study, we present a detailed quantification of the glacio-hydrological evolution across the Andes (11°N-55°S) over the period 2000-2019 using OGGM. Our simulations rely on a glacier-by-glacier calibration of the changes in glacier volume. Simulations cover 36% (11,282 km$^2$) of their glacierized surface area across the Andes where 50% of the area corresponds to the Patagonian icefields and Cordillera Darwin that were not simulated due to specific processes such as calving and which are not accounted for in the version of glaciological model used here. In addition, we used corrected climate forcing and evaluated our simulation results at both the glacier and catchment scale using in situ observations, which are uncommon practices in regional simulations. From our results we can highlight the following:

- 93% of the studied glacierized catchments show a decrease in glacier area between the periods 2000-2009 and 2010-2019, displaying a high coherence with previous reports based, in particular, on glaciers in the Tropical Andes (Rabatel et al., 2012; Seehaus et al., 2020), Wet Andes (Rabassa 2010; Ruiz et al., 2017) and Dry Andes (Rabatel et al., 2011; Malmros et al., 2016; Farías-Barahona et at., 2020).
- The glacier runoff response to this glacier reduction has the largest percentage increase in the Tropical Andes and Dry Andes. Despite this, the largest percentage increase of glacier runoff (> 62%) estimated in the Inner Tropic and Dry Andes 1 zones corresponds to the lowest absolute glacier runoff amounts across the Andes.
- The three selected catchments, located in contrasted climatic zones, are used to evaluate the simulations. They display consistent results with previous studies and in situ observations. The larger glacier contributions to the catchment water flows are quantified for the Baker (43%) and Maipo (36%) catchments during the summer season (January-March). On the contrary, the larger glacier contribution to the La Paz catchment (45%) was estimated during the transition season (September to November).

Lastly, our results help to improve knowledge about the hydrological responses of glaciers in a large part of the Andes through the correction of climate data, the use of the same input data and the same simulation processes as well as a strong glacier calibration applied to the glaciers. The implementation of this calibrated and evaluated model in the historical period is a prerequisite for simulating the future evolution of the Andean glaciers.

**Code and data availability**

Data per glacier in this study is available at https://doi.org/10.5281/zenodo.7890462

**Supplement link**

xxx

**Author contributions**

AC, TC and AR were involved in the study design. AC wrote the model implementation and produced the figures, tables and first draft of the manuscript. NC contributed to the model implementation. AC and NG carried out the data curation and TerraClimate temperature evaluation. AC performed the first level of analysis, which was improved by input from TC, AR, NC, FS. All authors contributed to the review and editing of the manuscript.

https://doi.org/10.5194/egusphere-2023-888
Preprint. Discussion started: 23 May 2023


**Acknowledgments**

We acknowledge LabEx OSUG@2020 (Investissement d'Avenir, ANR10 LABX56). The first author would like to thank Dr. Shelley MacDonell (University of Canterbury - CEAZA), Ashley Apey (Geoestudios), Dr. Marius Schaefer (U. Austral de Chile), and Claudio Bravo and Sebastián Cisterna (CECs, Centro de Estudios Científicos de Valdivia) for the data provided. In addition, the first author thanks the OGGM support team, especially Patrick Schmitt, Lilian Schuster, Larissa van der Laan, Anouk Vlug, Rodrigo Aguayo and Fabien Maussion. Lastly, the first author greatly appreciates discussing the results for specific glaciers or catchments with Dr. Ezequiel Toum (IANIGLA, Argentina), Dr. Álvaro Ayala (CEAZA, Chile), Dr. Lucas Ruiz (IANIGLA, Argentina), Dr. Gabriella Collao (IGE, U. Grenoble Alpes, France), Dr. Diego Cusicanqui (IGE-ISTerre, U. Grenoble Alpes, France), and Dr. David Farías-Barahona (FAU, U. de Concepción, Chile).

**Financial support**

This study was conducted as part of the International Joint Laboratory GREAT-ICE, a joint initiative of the IRD, universities/institutions in Bolivia, Peru, Ecuador and Colombia, and the IRN-ANDES-C2H. This research was funded by the National Agency for Research and Development (ANID)/Scholarship Program/DOCTORADO BECAS CHILE/2019-72200174.

**References**

Abatzoglou, J. T., Dobrowski, S. Z., Parks, S. A., and Hegewisch, K. C. TerraClimate, a High-Resolution Global Dataset of Monthly Climate and Climatic Water Balance from 1958-2015. Sci. Data 5, 1–12. https://doi:10.1038/sdata.2017.191, 2018.

Alvarez-Garreton, C., Mendoza, P. A., Boisier, J. P., Addor, N., Galleguillos, M., Zambrano-Bigiarini, M., Lara, A., Puelma, C., Cortes, G., Garreaud, R., McPhee, J., and Ayala, A.: The CAMELS-CL dataset: catchment attributes and meteorology for large sample studies – Chile dataset, Hydrol. Earth Syst. Sci., 22, 5817–5846, https://doi.org/10.5194/hess-22-5817-2018, 2018.

Autin, P., Sicart, J. E., Rabatel, A., Soruco, A., and Hock, R. Climate Controls on the Interseasonal and Interannual Variability of the Surface Mass and Energy Balances of a Tropical Glacier (Zongo Glacier, Bolivia, 16° S): New Insights From the Multi-Year Application of a Distributed Energy Balance Model. Journal of Geophysical Research: Atmospheres, 127(7), https://doi.org/10.1029/2021JD035410, 2022.

Ayala, Á., Farías-Barahona, D., Huss, M., Pellicciotti, F., McPhee, J., and Farinotti, D. Glacier Runoff Variations since 1955 in the Maipo River Basin, Semiarid Andes of central Chile. Cryosphere Discuss. 14, 1–39. https://doi:10.5194/tc-2019-233, 2020.

Baraer, M., Mark, B. G., Mckenzie, J. M., Condom, T., Bury, J., Huh, K.-I., et al. Glacier Recession and Water Resources in Peru's Cordillera Blanca. J. Glaciol. 58 (207), 134–150. https://doi:10.3189/2012JoG11J186, 2012.

Basantes-Serrano, R., Rabatel, A., Francou, B., Vincent, C., Soruco, A., Condom, T., and Ruíz, J. C.: New insights into the decadal variability in glacier volume of a tropical ice cap, Antisana (0°29′ S, 78°09′ W), explained by the morpho-topographic and climatic context, The Cryosphere, 16, 4659–4677, https://doi.org/10.5194/tc-16-4659-2022, 2022.

https://doi.org/10.5194/egusphere-2023-888
Preprint. Discussion started: 23 May 2023


Bravo, C., Loriaux, T., Rivera, A., & Brock, B. W. Assessing glacier melt contribution to streamflow at Universidad Glacier, central Andes of Chile. Hydrology and Earth System Sciences, 21(7), 3249-3266. https://doi.org/10.5194/hess-21-3249-2017, 2017.

Braun, L. N. and Renner, C. B. Application of a conceptual runoff model in different physiographic regions of Switzerland. Hydrol. Sci. J. 37(3), 217-231. 1992.

Burger, F., Ayala, A., Farias, D., Shaw, T. E., MacDonell, S., Brock, B., et al. Interannual Variability in Glacier Contribution to Runoff from a High-elevation Andean Catchment: Understanding the Role of Debris Cover in Glacier Hydrology. Hydrological Process. 33 (2), 214–229. https://doi:10.1002/hyp.13354, 2019.

Caro A, Condom T and Rabatel A. Climatic and Morphometric Explanatory Variables of Glacier Changes in the Andes (8–55°S): New Insights From Machine Learning Approaches. Front. Earth Sci. 9:713011. https://doi: 10.3389/feart.2021.713011, 2021.

Caro, A. Estudios glaciológicos en los nevados de Chillán. Santiago: University of Chile. [thesis], 2014

Cauvy-Fraunié, S., and Dangles, O. A Global Synthesis of Biodiversity Responses to Glacier Retreat. Nat. Ecol. Evol. 3 (12), 1675–1685. https://doi:10.1038/s41559-019-1042-8, 2019.

CEAZA, datos meteorológicos de Chile [data set], http://www.ceazamet.cl/, 2022.

CECs. Meteorological data measured by Centro de Estudios Científicos, 2018.

Condom. T., Escobar, M., Purkey, D., Pouget J.C., Suarez, W., Ramos, C., Apaestegui, J., Zapata, M., Gomez, J. and Vergara, W. Modelling the hydrologic role of glaciers within a Water Evaluation and Planning System (WEAP): a case study in the Rio Santa watershed (Peru). Hydrol. Earth Syst. Sci. Discuss., 8, 869–916. https://doi:10.5194/hessd-8-869-2011, 2011.

Crippen, R., Buckley, S., Agram, P., Belz, E., Gurrola, E., Hensley, S., Kobrick, M., Lavalle, M., Martin, J., Neumann, M., Nguyen, Q., Rosen,P., Shimada, J., Simard, M., Tung, W. NASADEM Global Elevation Model: Methods and Progress. The International Archives of thePhotogrammetry, Remote Sensing and Spatial Information Sciences XLI-B4, 125–128. (20), 2016.

Devenish, C., and Gianella, C. Sustainable Mountain Development in the Andes. 20 Years of Sustainable Mountain Development in the Andes - from Rio 1992 to 2012 and beyond. Lima, Peru: CONDESAN, 2012.

DGA, datos de estudios hidroglaciológicos de Chile [data set], https://snia.mop.gob.cl/BNAConsultas/reportes, 2022.

Dussaillant A., Buytaert W., Meier C. and Espinoza F. Hydrological regime of remote catchments with extreme gradients under accelerated change: the Baker basin in Patagonia. Hydrological Sciences Journal,Volume 57, https://doi.org/10.1080/02626667.2012.726993, 2012.

Dussaillant, I., Berthier, E., Brun, F., Masiokas, M., Hugonnet, R., Favier, V., et al. Two Decades of Glacier Mass Loss along the Andes. Nat. Geosci. 12 (10), 802–808. https://doi:10.1038/s41561-019-0432-5, 2019.

Farías-Barahona, D., Wilson, R., Bravo, C., Vivero, S., Caro, A., Shaw, T. E., et al. A Near 90-year Record of the Evolution of El Morado Glacier and its Proglacial lake, Central Chilean Andes. J. Glaciol, 66, 846–860. https://doi:10.1017/jog.2020.52, 2020.

Farinotti, D., Huss, M., Fürst, J. J., Landmann, J., Machguth, H., Maussion, F., et al. A consensus estimate for the ice thickness distribution of all glaciers on Earth. Nat. Geosci. 12, 168–173. https://doi: 10.1038/s41561-019-0300-3, 2019.

https://doi.org/10.5194/egusphere-2023-888
Preprint. Discussion started: 23 May 2023


Farinotti, D., Brinkerhoff, D. J., Clarke, G. K., Fürst, J. J., Frey, H., Gantayat, P., ... & Andreassen, L. M. How accurate are estimates of glacier ice thickness? Results from ITMIX, the Ice Thickness Models Intercomparison eXperiment. The Cryosphere, 11(2), 949-970, https://doi.org/10.5194/tc-11-949-2017, 2017.

Fukami, H. and Naruse, R. Ablation of ice and heat balance on Soler glacier, Patagonia. Bull. Glacier Res. 4, 37–42, 1987.

Gao L., Bernhardt M. and Schulz K. Elevation correction of ERA-Interim temperature data in complex terrain. Hydrol. Earth. Syst. Sci. 16(12): 4661–4673, https://doi: 10.5194/hess-16-4661-2012, 2012.

Garreaud, R. D., Alvarez-Garreton, C., Barichivich, J., Boisier, J. P., Christie, D., Galleguillos, M., LeQuesne, C., McPhee, J., and Zambrano-Bigiarini, M.: The 2010–2015 megadrought in central Chile: impacts on regional hydroclimate and vegetation, Hydrol. Earth Syst. Sci., 21, 6307–6327, https://doi.org/10.5194/hess-21-6307-2017, 2017.

Gascoin, S., Kinnard, C., Ponce, R., Lhermitte, S., MacDonell, S., and Rabatel, A.: Glacier contribution to streamflow in two headwaters of the Huasco River, Dry Andes of Chile, The Cryosphere, 5, 1099–1113, https://doi.org/10.5194/tc-5-1099-2011, 2011.

GLACIOCLIM, Données météorologiques [data set], https://glacioclim.osug.fr/Donnees-des-Andes, 2022.

Guido, Z., McIntosh, J. C., Papuga, S. A., and Meixner, T. Seasonal Glacial Meltwater Contributions to Surface Water in the Bolivian Andes: A Case Study Using Environmental Tracers. J. Hydrol. Reg. Stud. 8, 260–273. https://doi:10.1016/j.ejrh.2016.10.002, 2016.

Hernández, J., Mazzorana, B., Loriaux, T., and Iribarren, P. Reconstrucción de caudales en la Cuenca Alta del Río Huasco, utilizando el modelo Cold Regional Hydrological Model (CRHM), AAGG2021, 2021

Hock, R. Temperature index melt modelling in mountain areas. Journal of Hydrology, 282(1-4), 104-115. https://doi.org/10.1016/S0022-1694(03)00257-9, 2003.

Hugonnet, R., McNabb, R., Berthier, E. et al. Accelerated global glacier mass loss in the early twenty-first century. Nature 592, 726–731. https://doi.org/10.1038/s41586-021-03436-z, 2021.

Huss, M. and Hock, R. A new model for global glacier change and sea-level rise, Front. Earth Sci., 3, 54, https://doi.org/10.3389/feart.2015.00054, 2015.

Huss, M. and Hock, R. Global-scale hydrological response to future glacier mass loss, Nature Climate Change, 8, 135–140, https://doi.org/10.1038/s41558-017-0049-x, 2018.

IANIGLA, datos meteorológicos [data set], https://observatorioandino.com/estaciones/, 2022.

Kienholz, C., Rich, J. L., Arendt, A. A., and Hock, R.: A new method for deriving glacier centerlines applied to glaciers in Alaska and northwest Canada, The Cryosphere, 8, 503–519, https://doi.org/10.5194/tc-8-503-2014, 2014.

Koizumi, K. and Naruse R. Measurements of meteorological conditions and ablation at Tyndall Glacier, Southern Patagonia, in December 1990. Bulletin of Glacier Research, 10, 79-82, 1992.

Krögh, S.A., Pomeroy, J.W., McPhee, J. Physically based hydrological modelling using reanalysis data in Patagonia. J. Hydrometeorol. http://dx.doi.org/10.1175/JHM-D-13-0178.1, 2014.

Lehner B, Verdin K, Jarvis A. Hydrological data and maps based on Shuttle elevation derivatives at multiple scales (HydroSHEDS)-Technical Documentation, World Wildlife Fund US, Washington, DC, Available at http://hydrosheds.cr.usgs.gov, 2016.

https://doi.org/10.5194/egusphere-2023-888
Preprint. Discussion started: 23 May 2023


MacDonell, S., Kinnard, C., Mölg, T., Nicholson, L., and Abermann, J. Meteorological drivers of ablation processes on a cold glacier in the semi-arid Andes of Chile, The Cryosphere, 7, 1513–1526, https://doi.org/10.5194/tc-7-1513-2013, 2013.

Malmros, J. K., Mernild, S. H., Wilson, R., Yde, J. C., and Fensholt, R. Glacier Area Changes in the central Chilean and Argentinean Andes 1955-2013/14. J. Glaciol. 62, 391–401. https://doi:10.1017/jog.2016.43, 2016.

Marangunic C., Ugalde F., Apey A., Armendáriz I., Bustamante M. and Peralta C. Ecosistemas de montaña de la cuenca alta del río Mapocho, Glaciares en la cuenca alta del río Mapocho: variaciones y características principales. AngloAmerican - CAPES UC, 2021.

Mark, B. and Seltzer, G. Tropical glacier meltwater contribution to stream discharge: A case study in the Cordillera Blanca, Peru. J. Glaciol, 49(165), 271-281. https://doi:10.3189/172756503781830746, 2003.

Marzeion, B., Jarosch, A. H., and Hofer, M.: Past and future sea-level change from the surface mass balance of glaciers, The Cryosphere, 6, 1295–1322, https://doi.org/10.5194/tc-6-1295-2012, 2012.

Masiokas, M. H., Christie, D. A., Le Quesne, C., Pitte, P., Ruiz, L., Villalba, R., et al. Reconstructing the Annual Mass Balance of the Echaurren Norte Glacier (Central Andes, 33.5° S) Using Local and Regional Hydroclimatic Data. The Cryosphere 10 (2), 927–940. https://doi:10.5194/tc-10-927-2016, 2016.

Masiokas, M. H., Rabatel, A., Rivera, A., Ruiz, L., Pitte, P., Ceballos, J. L., et al. A Review of the Current State and Recent Changes of the Andean Cryosphere. Front. Earth Sci. 8 (6), 1–27. doi:10.3389/feart.2020.00099, 2020.

Mateo, E. I., Mark, B. G., Hellström, R. Å., Baraer, M., McKenzie, J. M., Condom, T., Rapre, A. C., Gonzales, G., Gómez, J. Q., and Encarnación, R. C. C.: High-temporal-resolution hydrometeorological data collected in the tropical Cordillera Blanca, Peru (2004–2020), Earth Syst. Sci. Data, 14, 2865–2882, https://doi.org/10.5194/essd-14-2865-2022, 2022.

Maussion, F., Butenko, A., Champollion, N., Dusch, M., Eis, J., Fourteau, K., et al. The open global glacier model (OGGM) v1.1. Geoscientific Model. Develop. 12, 909–931. https://doi:10.5194/gmd-12-909-2019, 2019

Millan, R., Mouginot, J., Rabatel, A. et al. Ice velocity and thickness of the world's glaciers. Nat. Geosci. 15, 124–129. https://https://doi.org/10.1038/s41561-021-00885-z, 2022.

Rabassa, J. El cambio climático global en la Patagonia desde el viaje de Charles Darwin hasta nuestros días. Revista de la Asociación Geológica Argentina, 67(1), 139-156, 2010.

Rabatel, A., Bermejo, A., Loarte, E., Soruco, A., Gomez, J., Leonardini, G., Vincent, C., and Sicart, J. E.: Relationship between snowline altitude, equilibrium-line altitude and mass balance on outer tropical glaciers: Glaciar Zongo – Bolivia, 16◦ S and Glaciar Artesonraju – Peru, 9◦ S, J. Glaciol., 58, 1027–1036, https://doi:10.3189/2012JoG12J027, 2012.

Rabatel, A., Castebrunet, H., Favier, V., Nicholson, L., and Kinnard, C. Glacier Changes in the Pascua-Lama Region, Chilean Andes (29° S): Recent Mass Balance and 50 Yr Surface Area Variations. The Cryosphere 5 (4), 1029–1041. https://doi:10.5194/tc-5-1029-2011, 2011.

Rabatel, A., Francou, B., Soruco, A., Gomez, J., Cáceres, B., Ceballos, J. L., et al. Current State of Glaciers in the Tropical Andes: A Multi-century Perspective on Glacier Evolution and Climate Change. The Cryosphere 7, 81–102. https://doi:10.5194/tc-7-81-2013, 2013.

Ragettli, S., and Pellicciotti, F. Calibration of a Physically Based, Spatially Distributed Hydrological Model in a Glacierized basin: On the Use of Knowledge from Glaciometeorological Processes to Constrain Model Parameters. Water Resour. Res. 48 (3), 1–20. https://doi:10.1029/2011WR010559, 2012.

https://doi.org/10.5194/egusphere-2023-888
Preprint. Discussion started: 23 May 2023


RGI Consortium. Randolph Glacier Inventory - A Dataset of Global Glacier Outlines, Version 6. Boulder, Colorado USA. NSIDC: National Snow and Ice Data Center, https://doi.org/10.7265/4m1f-gd79, 2017.

Rivera, A. Mass balance investigations at Glaciar Chico, Southern Patagonia Icefield, Chile. PhD thesis, University of Bristol, UK, 303 pp, 2004.

Robson, B. A., MacDonell, S., Ayala, Á., Bolch, T., Nielsen, P. R., and Vivero, S. Glacier and rock glacier changes since the 1950s in the La Laguna catchment, Chile, The Cryosphere, 16, 647–665, https://doi.org/10.5194/tc-16-647-2022, 2022.

Ruiz, L., Berthier, E., Viale, M., Pitte, P., and Masiokas, M. H. Recent geodetic mass balance of Monte Tronador glaciers, northern Patagonian Andes, The Cryosphere, 11, 619–634, https://doi.org/10.5194/tc-11-619-2017, 2017.

Schaefer M., Rodriguez J., Scheiter M., and Casassa, G. Climate and surface mass balance of Mocho Glacier, Chilean Lake District, 40°S. Journal of Glaciology, 63(238), 218-228, https://doi:10.1017/jog.2016.129, 2017.

Seehaus, T., Malz, P., Sommer, C., Soruco, A., Rabatel, A., and Braun, M. Mass balance and area changes of glaciers in the Cordillera Real and Tres Cruces, Bolivia, between 2000 and 2016. J. Glaciol, 66(255), 124-136. https://doi:10.1017/jog.2019.94, 2020.

SENAMHI, datos hidrometeorológicos de Perú [data set], https://www.senamhi.gob.pe/?&p=descarga-datos-hidrometeorologicos, 2022.

Shaw, T. E., Caro, A., Mendoza, P., Ayala, Á., Pellicciotti, F., Gascoin, S., et al. The Utility of Optical Satellite Winter Snow Depths for Initializing a Glacio-Hydrological Model of a High-Elevation, Andean Catchment. Water Resour. Res. 56 (8), 1–19. doi:10.1029/2020WR027188. 2020.

Sicart, J. E., P. Ribstein, B. Francou, B. Pouyaud, and T. Condom. Glacier mass balance of tropical Zongo Glacier, Bolivia, comparing hydrological and glaciological methods, Global Planet. Change, 59(1), 27– 36, 2007.

Stuefer, M. Investigations on Mass Balance and Dynamics of Moreno Glacier Based on Field Measurements and Satellite Imagery. Ph.D. Dissertation, University of Innsbruck, Innsbruck, 1999.

Stuefer, M., Rott, H. and Skvarca, P. Glaciar Perito Moreno, Patagonia: climate sensitivities and glacier characteristics preceding the 2003/04 and 2005/06 damming events. J. Glaciol., 53 (180), 3–16. https://doi: 10.3189/172756507781833848, 2007.

Soruco, A., Vincent, C., Rabatel, A., Francou, B., Thibert, E., Sicart, J. E., et al. Contribution of Glacier Runoff to Water Resources of La Paz City, Bolivia (16° S). Ann. Glaciol. 56 (70), 147–154. https://doi:10.3189/2015AoG70A001, 2015.

Takeuchi, Y., Naruse R. and Satow K. Characteristics of heat balance and ablation on Moreno and Tyndall glaciers, Patagonia, in the summer 1993/94. Bulletin of Glacier Research, 13, 45-56, 1995.

WGMS. Global Glacier Change Bulletin No. 4 (2018-2019). Michael Zemp, Samuel U. Nussbaumer, Isabelle Gärtner-Roer, Jacqueline Bannwart, Frank Paul, and Martin Hoelzle (eds.), ISC (WDS) / IUGG (IACS) / UNEP / UNESCO / WMO, World Glacier Monitoring Service, Zurich, Switzerland, 278 pp. Based on database version https://doi.org/10.5904/wgms-fog-2021-05, 2021.

Zimmer, A., Meneses, R. I., Rabatel, A., Soruco, A., Dangles, O., and Anthelme, F. Time Lag between Glacial Retreat and Upward Migration Alters Tropical alpine Communities. Perspect. Plant Ecol. Evol. Syst. 30, 89–102. https://doi:10.1016/j.ppees.2017.05.003, 2018.

# 5.4 Article n°4 (in progress)

To be submitted to the Earth's Future journal https://agupubs.onlinelibrary.wiley.com/journal/23284277

## Glacio-hydrological changes along the Andes over the first half of the 21st Century

Alexis Caro[1], Thomas Condom[1], Antoine Rabatel[1], Rodrigo Aguayo[2], Nicolas Champollion[1]

[1]Univ. Grenoble Alpes, CNRS, IRD, INRAE, Grenoble-INP, Institut des Géosciences de l'Environnement, Grenoble, France
[2]Facultad de Ciencias Ambientales, Centro EULA-Chile, Universidad de Concepción, Concepción, Chile

**Abstract**

Documenting how much water will come from the glaciers during the 21st century is key for anticipating proper management of water resources. However, the role of glaciers at the catchment scale across the Andes has not been fully addressed. Focusing on a glacierized area of 27,669 km$^2$, we analyze the evolution of glaciers forced by eight Global Circulation Models (GCMs) from CMIP6 during the period 1990-2049. Additionally, glacier runoff simulations are performed individually by glacier, utilizing a validated and calibrated version of the Open Global Glacier Model (OGGM) as well as the filtered set of GCMs (scored considering the precipitation and temperature) and the whole GCMs ensemble. We delve into the glacier runoff projections in 778 catchments throughout the 21st century, specifically during 2030-2049, considering two climate scenarios (SSP1-2.6 and SSP5-8.5). The peak water was estimated by catchment considering the annual glacier runoff from simulated glaciers. Our results reveal variations in GCMs performance, with specific GCMs showing higher scores in different glaciological regions. Between 1990-2019 and 2020-2049 warming trends are observed over the entire Andes, with the most significant mean annual temperature increase expected in the Tropical Andes (above 0.7°C between the two periods). Conversely, precipitation is anticipated to change in a lower amount, decreasing in all regions (-1 to -3%) except the Tropical Andes (+0.6%). These variables are key in the glacier dynamics and consequent estimate of glacier runoff. Between 2000-2019 and 2030-2049 glacier runoff estimates demonstrate most significant cumulative loss, in terms of percentage regarding the historical period, in the Tropical Andes (-43%, 25.8 m$^3$ s$^{-1}$ in SSP1-2.6), followed by the Dry Andes (-37%, 14.4 m$^3$ s$^{-1}$ in SSP1-2.6), and the Wet Andes (-32%, 177.2 m$^3$ s$^{-1}$ in SSP1-2.6). Notably, some catchments in the Dry Andes exhibit the largest negative and positive changes in the mean annual glacier runoff in the Andes. The Atuel catchment (35°S) shows a reduction of -62% (2.4 m$^3$ s$^{-1}$), whereas the Tupungato catchment (34°S) exhibits an increase of 32% (0.9 m$^3$ s$^{-1}$) in mean annual glacier runoff, showing large differences that can exist in close catchments. Most catchments are expected to reach peak water before the first half of the 21st century (percentiles 25-75 in 2010 and 2028), albeit with variations depending on the

glaciological regions. Our study underlines the critical importance of considering seasonal variations when analyzing GCMs in glaciological simulations and emphasizes regional disparities in glacier runoff volume across the Andes for future water resources management.

**1. Introduction**

In the Andes, most of the knowledge regarding future glacier changes is derived from global simulations (e.g., Marzeion et al., 2012; Radic and Hock, 2014; Huss and Hock, 2015; Rounce et al., 2023). The recent study by Rounce et al. (2023) stands out as it incorporates geodetic mass balance measurements obtained at the scale of individual glaciers by Hugonnet et al. (2021) to calibrate the glacier mass balance during the historical period. It is important to note that these global-scale studies have not been specifically evaluated for the Andes, even though simulating current observations is a crucial prerequisite for predictive models (Aschwanden et al., 2013). The reported glacier volume changes projected throughout the 21st century by the above mentioned studies demonstrate consistent results in the Tropical Andes, with an approximate loss of around -98 ± 13% under the RCP 8.5 scenario based on CMIP5 models. However, in the southern Andes, which encompasses the largest glacierized area, there is a wider range of mass loss estimates, ranging from -44 ± 14% to -68 ± 20% (Huss and Hock, 2015; Rounce et al., 2023). Even under the most optimistic scenarios (*i.e.* RCP 2.6), the reduction in glacier volume remains significant. Furthermore, a global study by Huss and Hock (2018) focused on 12 Andean catchments and estimated that glacier runoff, which includes ice and snow melt as well as rainfall on glaciers, is projected to increase in most of the catchments until 2050. However, after 2050, it is expected to decrease in all catchments except for the Santa Cruz catchment (49°S, Argentina).

Local simulations of future glacier changes across the Andes have been conducted, encompassing glaciers in Colombia, Ecuador, Peru, Bolivia, and Chile (Frans et al., 2015; Réveillet et al., 2015; Yarleque et al., 2018; Vuille et al., 2018; Rabatel et al., 2018; Scheiter et al., 2021) as well as the Patagonian icefield (Schaefer et al., 2013; Bravo et al., 2021). These studies focus on different objectives (*e.g.*, surface mass balance, glacier dynamic, glacier runoff) and use different CMIP5 models. In the tropical Andes, Vuille et al. (2018) estimated that the Antizana Glacier (0°S, inner tropics) is more vulnerable to warming throughout the 21st century in comparison with the Zongo Glacier (16°S, outer tropic). For Zongo Glacier, projected volume losses range from -40 ± 7% to -89 ± 4% between 2010 and 2100 depending on the considered RCP (Réveillet et al., 2015) and a discharge reduction in 2100 was estimated by 25% at the annual scale and by 57% during the dry season for RCP RCP4.5 (Frans et al., 2015).

In the southern Andes, no study was performed in the Dry Andes, but for the Wet Andes, Scheiter et al. (2021) projected an ice volume loss between -56 and -97% depending on the RCP for the Mocho

Choshuenco glacier in 2100. Two other studies reported future glacier changes in the Patagonian icefields. In the Northern Patagonian Icefield (NPI) a strong increase in ablation is estimated from 2050 onward with a reduction of solid precipitation from 2080 onward due to higher temperatures, with uncertainties arising from future climate and ice dynamics (Schaefer et al., 2013). Bravo et al. (2021) compared simulations for the period 2005-2050 with the historical period 1976-2005 and estimated a larger reduction in mass balance between -1.5 to -1.9 m w.e. for the NPI compared to the Southern Patagonian Icefield (SPI) (-1.1 to -1.5 m w.e).

The influence of uncertainties in future climate scenarios on future glacier changes has been a subject of investigation, as discussed by Marzeion et al. (2020). Their study indicates that both at the global and Andean scales, the impacts of uncertainties in future climate scenarios increase over the course of the 21st century. However, in contrast, the uncertainties related to the glacier model parameterization decrease over time. Furthermore, Hausfather et al. (2022) found that more than one-quarter of the models in the Coupled Model Intercomparison Project 6 (CMIP6) (Eyring et al., 2016) have higher variability in temperature compared to the CMIP5 models. This higher variability in temperature projections could introduce additional uncertainty in the estimates of future glacier changes. Similarly, Tokarska et al. (2020) highlighted that certain CMIP6 models with high climate sensitivity (i.e., beyond the AR5 likely range of 1.5°-4.5°C by the end of the 21st century) tend to overestimate historical warming trends. Consequently, this bias might lead to future warming projections being biased towards higher temperatures in these CMIP6 models. Conversely, CMIP6 models with climate sensitivity values within the likely range exhibit warming trends consistent with observations over the historical period, providing more reliable estimates for future climate scenarios and their impact on glaciers.

As glaciers continue to reduce under projected climate change scenarios, it becomes imperative to ascertain the timing of peak water - the period when glacier runoff increases before eventually declining - throughout the Andes. This knowledge holds paramount importance as it enables stakeholders to anticipate when glacier contributions to river flows will cease in the future.

This study aims to address the lack of specific estimates regarding future glacier changes and their hydrological implications in the Andean glacierized catchments, which are not typically based on calibrated/validated models. Additionally, as uncertainties in climate projections grow towards the latter half of the 21st century, we have two main objectives. Firstly, we evaluate the performance of eight GCMs and two climate change scenarios (SSP1-2.6 and SSP5-8.5) sourced from CMIP6 across the Andes (11°N-55°S) for both historical (1990-2019) and future periods (2020-2049). Secondly, we utilize an ensemble of evaluated GCMs (complete ensemble) and a filtered ensemble throughout the first half of the

21st century to simulate glacier runoff (including ice and snowmelt) since 2000. For this purpose, we employed a calibrated/evaluated version of the Open Global Glacier Model (OGGM), as implemented by Caro et al. (2023, under review) for the Andes. To address the limitations in glacier volume knowledge for the Andes (Vuille et al., 2018; Masiokas et al. 2020), we adopted the dataset provided by Farinotti et al. (2019), implemented in OGGM, for calibrating the initial volume of Andean glaciers.

## 2. Data and Methodology

### 2.1. Analysis of the GCMs in the historical and future periods

In this study, we analyze temperature and precipitation data from two scenarios and eight GCMs simulations sourced from CMIP6 (see Table S1). Our analysis takes into account the Almazroui et al. (2021) assessment for TerraClimate in South America and the global evaluation of warmer models from Hausfather et al. (2022) and Tokarska et al. (2020). To establish a basis for comparison, we scale the GCMs simulations and compare them with the corrected TerraClimate data (cTC, temperature, and precipitation) (Abatzoglou et al., 2018; Caro et al., 2023, under review) during the historical period of 1990-2019 across the Andes on a glacierized area of 27,668 $km^2$ (considering glaciers with a surface area > 1 $km^2$). Meanwhile, we also perform comparisons between GCMs during both the historical and future periods (2020-2049). The analysis involves three main steps: Our analysis comprises three steps: 1) statistical downscaling of GCMs data for the historical period; 2) calculation of annual, seasonal, and monthly metrics to compare the GCMs data with the corrected TerraClimate data for the historical period; and 3) Identification of changes in climate variables between the historical and future periods.

The GCMs output data were gathered for each glacier, however, the analysis was performed at the glaciological region scale, where climate characteristics vary substantially (Caro et al., 2021). Going into detail, these three steps consist in:

- Step 1. Temperature and precipitation values of the GCMs were adjusted at the mean elevation of each glacier using a statistical downscaling approach for two future scenarios, namely SSP1-2.6 and SSP5-8.5. The mean monthly and annual values of GCMs variables were corrected on the basis of the historical climate (1990-2019) given by the monthly corrected TerraClimate. The TerraClimate dataset at the mean glacier elevation was corrected and compared with 34 meteorological stations by Caro et al. (2023, under review).
- Step 2. Correlation pattern analyses were based on monthly and seasonal (OND, JFM, AMJ, JAS) correlations between the eight GCMs and the corrected TerraClimate data in the period 1990-2019. We chose seasons as OND and JFM, because in these months the larger surface mass loss occurs in the Outer Tropics (transition season, Autin et al., 2022) and in the Dry Andes zones

(austral summer). Because statistical downscaling does not scale specific months, we used the Pearson coefficient of correlation and the root mean square error (RMSE) (McSweeney et al., 2015) as metrics to score the GCMs performance during the historical period.

- Step 3. We identified climate likely ranges through the GCMs ensemble considering the mean differences between the historical and future periods for temperature and precipitation at annual and seasonal (OND, JFM, AMJ, JAS) time-steps in each glacier. The climate change likely ranges are estimated by the percentiles 10 and 90 of these differences using all GCMs and glaciers (modified from DRIAS project, 2023). In addition, we estimate the median of these differences. A similar method is used by the DRIAS project of the *Ministère de la Transition Écologique* of the French government (see Table S4, DRIAS project, 2023, and Sørland et al., 2018). The annual analysis between the historical and future periods (2020-2049 and 2070-2099) is considered to test our results with previous reports of climate change (e.g., IPCC, 2022; Olmo et al., 2022; Agudelo et al., under review). The estimation of the climate change likely ranges allows us to identify the hot/cold and dry/wet models.

**2.2. Short description of the Open Global Glacier Model (OGGM)**

OGGM is a modular and open-source workflow that simulates glacier mass balance and ice dynamics using calibrated parameter values for each glacier (Maussion et al., 2019). The required input data are: air temperature and precipitation time series, glacier outlines and surface topography. From these inputs, annual (e.g. surface mass balance, glacier volume and area) and monthly (glacier melt [snow + ice] and rainfall on glaciers) outputs can be simulated.

Using a glacier outline and topography, OGGM estimates flow lines using a geometrical algorithm (adapted from Kienholz et al., 2014). Assuming a bed shape, it estimates the ice thickness based on mass conservation and shallow ice approximation (Maussion et al., 2019). After these numerical steps, area and volume per glacier can be simulated. Mass balance is implemented using a precipitation phase partitioning and a temperature-index approach (Braun and Renner, 1992; Hock, 2003; Marzeion et al., 2012). The monthly mass balance $mb_i$ at an elevation z is computed as follows:

$$mb_i(z) = TC_{p\,i}^{snow}(z) * P_f - M_f * max\left(cTC_{t\,i}(z) - T_{melt}, 0\right) \quad (3),$$

where $TC_{p\,i}^{snow}$ is the TerraClimate solid precipitation before being scaled by the precipitation correction factor ($P_f$), $M_f$ is the glacier's temperature sensitivity parameter, $cTC_{t\,i}$ is the monthly corrected TerraClimate temperature, and $T_{melt}$ is the monthly air temperature above which ice melt is assumed to

occur (from 0°C to 2.1 °C). $TC_{p\,i}^{snow}$ is computed as a fraction of the total precipitation ($cTC_p$) where 100% is getting if $cTC_{t\,i}$ <= $T_i^{snow}$ (between 0-2.1°C) and 0% if $cTC_{t\,i}$ >= $T_i^{rain}$ (between 2-4.1 °C); and linearly interpolated in between. Here, the $M_f$ was calibrated for each glacier individually using glacier volume change datasets previously described (Hugonnet et al., 2021).

**2.2.1. Model setup in the period 2000-2050**

The OGGM model was previously calibrated and evaluated during the period 2000-2019 across the Andes (10°N-55°S) in a former study by Caro et al. (2023 under review). They evaluated and corrected temperature and precipitation input data, and evaluated the simulated glacier mass balances outputs from the model using *in situ* mass balance measurements available for 15 monitored glaciers along the Andes, and also the model performance at the level of three Andean catchments (La Paz 17°S, Maipo 33°S and Baker 45°S).

The model was run for each glacier and then results were analyzed for each glaciological zone identified by Caro et al. (2021) across the Andes. During the historical (2000-2019) and future (2020-2050) periods the input data are: glacier outlines from RGI v6.0 (RGI Consortium, 2017) and surface topography from NASADEM (Crippen et al., 2016). The corrected monthly TerraClimate precipitation ($cTC_p$) and temperature ($cTC_t$) were used in the historical period, meanwhile the same variable from eight GCMs were used as input for the future simulations. The calibration procedure was applied for each individual glacier to adjust the simulated mass balance of the 2000-2019 period to the geodetic mass balance product from Hugonnet et al. (2021). The simulated glacier volume was calibrated using Farinotti et al. (2019) product at a glaciological zone scale fitting the A parameter of the Glen flow law. In addition, glacier outlines of all glaciers were associated with the year 2000. The main corrected and calibrated parameters to run OGGM across the Andes are summarized in Table S2.

**2.3. Glacier runoff analysis**

Glacier runoff changes were estimated by adding the annual melt from each glacier by catchment. From this annual glacier runoff time series, the difference of the mean annual glacier runoff between the periods 2000-2019 and 2030-2049 was estimated for 778 glacierized catchments. Meanwhile, peak water refers to the annual glacier runoff that will initially increase and after declining in response to glacier retreat due to changes in climate conditions (Huss and Hock, 2018), which can be for example a long-term response of catchments to sustained warming (Hock et al., 2005). We calculate the peak water inspired by Huss and Hock (2018) through the following procedure by glacier and after by catchment: i) A maximum of eight

time series of the simulated glacier runoff from each glacier are compiled. Each time series comes from the different OGGM runs using different GCMs (the number of GCMs varies between the filtered and complete ensembles in each glaciological region); ii) Then, the time series were averaged, getting one time series of glacier runoff per glacier; iii) these were summed annually by catchment, allowing us to obtain the annual glacier runoff in each catchment between 2000-2099; iv) The glacier runoff was smoothed using a moving average comprising 11 years, from which 20 years related to maximum glacier runoff were identified; v) finally, the peak water year corresponds to the median of these years with a fixed uncertainty range of 10 years.

## 3. Results

### 3.1. GCMs analysis for the historical and future periods

#### 3.1.1. GCMs analysis for the historical period

This section analyzes the correlations and errors between downscaled Global Climate Models (GCMs) and corrected TerraClimate data (cTC) across the Andes region, focusing on a monthly and seasonal scale during the historical period (1990-2019) for 3,213 glaciers (covering 27,669 $km^2$). At the monthly scale, GCMs' temperature ($r = 0.9 \pm 0.1$) and precipitation ($r = 0.4 \pm 0.1$) exhibit statistically significant correlations on all glaciers (Figure S1E). The mean monthly temperature error is $1.1 \pm 0.1$°C, and the monthly total precipitation error is $106 \pm 68$ mm, considering both climate change scenarios from GCMs. When considering glaciological regions, the Dry and Wet Andes show the largest errors in temperature and precipitation, followed by the Tropical Andes (Figure S2). At a seasonal scale, there are significant correlations for temperature and precipitation on a moderate proportion of glaciers (above 30%) during specific seasons (Table S3). For example, in the Tropical Andes, correlations are significant in JFM and AMJ for precipitation, and in OND for temperature. In the Dry Andes, a considerable number of glaciers show significant correlations in all seasons. Meanwhile, in the Wet Andes, significant correlations are observed in JFM and AMJ for temperature and during JAS and OND for precipitation. The statistical error of the seasonal series of GCMs shows a temperature difference lower than 1°C, and the maximum errors for precipitation are found in the Tropical Andes (JAS), followed by the Dry (AMJ) and Wet Andes (JAS).

Considering that the largest glacier mass loss occurs through the transition season (OND) in the Tropical Andes and during the summer season (JFM) in the Dry and Wet Andes, we scored the eight GCMs regarding their temperature and precipitation variables performance in these seasons (see Figure S1A-D). In the Tropical Andes, the largest number of glaciers is better correlated with INM-CM5, GFDL,

NorESM2 (for temperature) and FGOALS and INM-CM5 (for precipitation). For the Dry Andes, high performance was estimated from CAMS, NorESM2 (for temperature) and MPI, CESM2 (for precipitation). Regarding the Wet Andes, the models INM-CM4 (for temperature) and GFDL, INM-CM4, FGOALS, and MPI (for precipitation) exhibit the highest correlations in the majority of glaciers. Conversely, the models MPI and INM-CM4 in the Tropical Andes, INM-CM4 in the Dry Andes, and MPI, INM-CM5 and FGOALS in the Wet Andes are relevant for only a very small number of glaciers. These findings provide valuable insights into the GCMs' performance in relation to temperature and precipitation variables during the critical seasons of glacier mass loss across the Andes.

**3.1.2. Future climate change on glaciers**

We analyze the differences in mean temperature and precipitation during the periods 1990-2019 and 2020-2049 for each individual glacier considering the eight GCMs. The differences led us to define the likely range by glaciological region (climate likely ranges) considering the percentiles 10 and 90. The objective is to identify models found outside of the regional climate change likely ranges at the annual and seasonal scales, which will be called hot/cold and dry/wet models.

At an annual scale, both scenarios (SSP1-2.6 and SSP5-8.5) exhibit the most significant temperature increase in the Tropical Andes (median = 0.7 and 0.9°C, respectively), followed by the Dry (median = 0.6 and 0.9°C) and Wet Andes (median = 0.4 and 0.6°C). Notably, SSP5-8.5 depicts a warmer outcome. In contrast, precipitation is projected to decrease in all glaciological regions and scenarios, except for the Tropical Andes under the SSP1-2.6 scenario (median = +0.6%). The Dry Andes show the most considerable precipitation reduction (median = -2.8 and -1.9%), trailed by the Wet Andes (median = -2.6 and -0.8%) and the Tropical Andes (median = -0.8, SSP5-8.5). At a seasonal scale, the largest increase in temperature is observed in the SSP5-8.5 scenario, particularly in the Tropical Andes (JAS), followed by the Dry (OND and JFM = +1.0°C) and Wet Andes (JFM = +0.7°C). Regarding precipitation changes, the Tropical Andes (JFM) are estimated to experience the most significant increase, while the Dry Andes show lower negative median total precipitation during OND. Detailed percentile values can be found in Table S4 and Figure 1.

Seasonal temperature and precipitation play a crucial role in glacier mass loss during the transition (OND) and wet seasons (JFM) in the Tropical Andes. The largest glacier ablation occurs during the transition season, and any delay in precipitation during the wet season can lead to a significant increase in ablation rates. In the Tropical Andes, the models project a median temperature increase of 0.7°C (SSP1-2.6) and 0.9°C (SSP5-8.5) during both seasons. Precipitation is expected to decrease during the transition season by -0.9 to -0.8% and increase during the wet season by 1.4 to 1.7%. Conversely, in the Southern Andes,

glacier accumulation is concentrated in autumn/winter (AMJ and JAS), although significant precipitation also occurs in spring and summer in the Wet Andes (OND and JFM). During summer, the increased precipitation contributes to reducing the strong glacier ablation rates due to an increase in albedo. In the Dry Andes, the models indicate a median temperature increase of 0.6°C (SSP1-2.6) and 1°C (SSP5-8.5) during spring and summer. However, the scenarios differ significantly in terms of precipitation. Under the SSP5-8.5 scenario, median precipitation is projected to decrease by 8.8% during spring and remain unchanged (0%) during summer. On the other hand, the SSP1-2.6 scenario shows an increase in median precipitation during spring (1.2%) and a reduction during summer (-2.7%). As for the Wet Andes, both scenarios of climate change exhibit a reduction in median precipitation, with the largest impact observed during summer (precipitation reduction of -2.4 to -4.5%) compared to spring (precipitation reduction of -1.9 to -4%). Additionally, the median temperature increase is more significant in summer (temperature rise of 0.5-0.7°C) than in spring (temperature rise of 0.4-0.5°C). For detailed values, please refer to Table S4.

From the regional temperature and precipitation likely ranges (Figure 1A-B for annual and Figure 1C for seasonal), we identified hot/cold and dry/wet models. Annually, for the Tropical Andes, GCMs' median values remain within likely ranges for both climate change scenarios. However, in the Dry Andes, FGOALS exhibits hot/dry characteristics and CAMS is a wet model. Moving to the Wet Andes, CESM2 and GFDL models are dry and cold, respectively, while FGOALS is a hot model. At the seasonal scale, FGOALS and CECSM2 display mean values outside the likely ranges. Specifically, in the Tropical Andes, CESM2 is a hot model during (OND). In the Dry Andes, FGOALS (OND) and CESM2 (JFM) are hot models, whereas CAMS (OND) and FGOALS (JFM) are wet models. In the Wet Andes, the FGOALS model is hot/dry (OND).

In summary, we estimated that MPI INM-CM4 and CESM2 present a lower score in the Tropical Andes, INM-CM4, CESM2, FGOALS and CAMS do it in the Dry Andes, and the models MPI, INM-CM5, FGOALS, CESM2 and GFDL show low scores in the Wet Andes. Because of that, we performed the analysis of changes in glacier runoff even excluding these GCMs (filtered ensemble) or considering all the GCMs (complete ensemble).

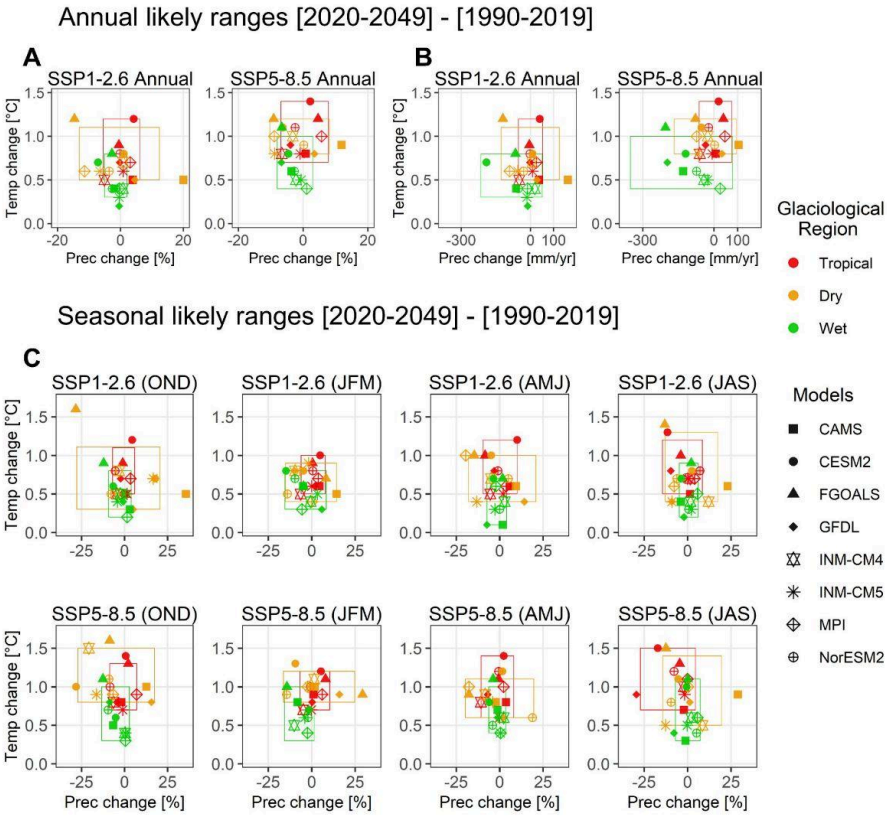


Figure 1. Temperature and precipitation changes between the historical (1990-2019) and future periods (2020-2049) across the glaciological Andean regions in two climate change scenarios. Percentiles 10 and 90 (boxes, likely ranges) from mean differences in both periods are estimated considering all glaciers in the complete ensemble of GCMs. Annual climate change likely ranges are exhibited in terms of absolute (A) and relative values (B) for precipitation considering SSP1-2.6 and SSP5-8.5 scenarios. C) show these differences by seasons considering both scenarios. Estimations are performed using 3,213 glaciers (27,668 km$^2$) (TA = 598, DA = 370, WA = 2245). Models situated into the boxes formed the filtered ensemble.
The Annual climate change likely ranges for the periods 1990-2019 and 2070-2099 can be checked in Figure S3. of the Supplementary materials.

### 3.2. Future glacier evolution

#### 3.2.1. Changes in glacier runoff for the period 2030-2049

This section focuses on analyzing the mean annual change of glacier runoff between two distinct periods: 2000-2019 and 2030-2049. To estimate these changes, we employ the filtered ensemble of GCMs. The

analysis is conducted at both the glaciological region and catchment scales, taking into consideration the cumulative volumes of glacier runoff by catchment. Additionally, we have computed the changes in mean annual glacier runoff using the complete ensemble of GCMs. For more detailed information, including specific numerical data, please refer to the Supplementary Information (Tables S5 and S6, and Figure S4).

Figure 2 illustrates the mean annual changes in glacier runoff by comparing the historical and future periods for each of the 778 catchments analyzed in the Andes. Within the glaciological regions, comparing the two periods 2000-2019 and 2030-2049, the filtered ensemble reveals a median reduction in glacier runoff of -0.1 $m^3 s^{-1}$ for both scenarios in the Tropical Andes. This reduction is observed in the majority of catchments up to the 90th percentile. In the Dry Andes, variations in glacier runoff are observed between the two scenarios. The SSP1-2.6 scenario displays the highest number of catchments with reduced glacier runoff (median = -0.01 $m^3 s^{-1}$), indicating a decrease in overall melt rates. Conversely, the SSP5-8.5 scenario shows that a significant number of catchments exhibit minimal changes in glacier runoff (median = -0.003 $m^3 s^{-1}$). However, until the 90th percentile of these catchments, an increase in glacier runoff (0.72 $m^3 s^{-1}$) is observed in the SSP5-8.5 scenario. For the Wet Andes, both scenarios indicate a median reduction in glacier runoff of -0.2 $m^3 s^{-1}$, suggesting decreased glacier runoff rates. Negative values persist until the 90th percentile of catchments, indicating a consistent reduction in glacier runoff for this region.

At the regional scale, changes in the glacier runoff using the filtered ensemble show similar amounts than the simulations from the complete ensemble (Figure S6), whereas, at the catchment scale lower changes are estimated from the filtered ensemble. These statistics detailed by glaciological regions in both ensembles can be seen in Tables S5 and S6.

Three distinct types of behavior in glacier runoff changes are observed across catchments for the SSP1-2.6 and SSP5-8.5 scenarios (Table S7). These behaviors include positive changes, negative changes, and catchments exhibiting positive changes under SSP5-8.5 and negative changes under SSP1-2.6. The largest volume changes in glacier runoff are consistently negative across all regions and time periods (2000-2019 and 2030-2049) for both scenarios. The Tropical Andes exhibit the most significant annual cumulative loss in terms of percentage regarding the historical period, with a reduction of 43% (-25.8 $m^3 s^{-1}$ in SSP1-2.6). The Dry Andes follow, with a cumulative loss of 37% (-14.4 $m^3 s^{-1}$ in SSP1-2.6), and the Wet Andes, with a cumulative loss of 32% (-177.2 $m^3 s^{-1}$ in SSP1-2.6). However, a smaller number of catchments (n = 22) show an increase in glacier runoff, predominantly in the Dry Andes. However, a smaller number of catchments (n = 22) show an increase in glacier runoff, mainly in the Dry Andes, experiencing a 38% increase (+3.5 $m^3 s^{-1}$ in SSP5-8.5). Some catchments demonstrate both increases and

reductions in glacier runoff depending on the scenario. In the Dry Andes (Figure S4), these catchments show a 6% increase (+1.1 $m^3 s^{-1}$) in the SSP5-8.5 scenario and a 7% reduction (-1.4 $m^3 s^{-1}$) in the SSP1-2.6 scenario. Notably, the Olivares catchment (id = 6090889690) and Cipreses catchment (id = 6090897370) in Chile are among these catchments exhibiting contrasting behavior. Regarding the spatial distribution of catchments, positive changes are predominantly observed in Argentine catchments, such as the Tupungato catchment (id = 6090891240). Conversely, the negative changes, which constitute the majority of the volume changes, are distributed evenly between Chile and Argentina. Noteworthy catchments in this category include the Azufre catchment (id = 6090904960) and Atuel catchment (id = 6090900470).

Table 1 displays simulations of extreme glacier runoff changes in catchments using the SSP5-8.5 scenario, categorized by glaciological regions. These results provide insights into significant variations in glacier runoff. Across all regions, the Acodado catchment in the Wet Andes experiences the most substantial reduction in glacier runoff, with a decrease of -8.4 $m^3 s^{-1}$. Meanwhile, the Atuel catchment exhibits the largest reduction in percentage terms in the Dry Andes, with a reduction of -62% (-2.4 $m^3 s^{-1}$). These changes represent a considerable decline compared to their historical annual glacier runoff (2000-2019).

Conversely, the Huemules, Tupungato, and Olivares catchments show the most substantial increases in glacier runoff. It is noteworthy that the eastern side of the Andes (Argentina) estimates the most pronounced reductions and increases in glacier runoff, indicating potential impacts on water resources and hydrological systems in the Dry Andes. Comparatively, the Tropical Andes experience smaller extreme changes in glacier runoff compared to other glaciological regions, which can be attributed to relatively lower mean glacier runoff during the historical period. Notably, catchments such as Chawpi Urqu and Quelccaya display average volumes below 2.3 ± 1.3 $m^3 s^{-1}$.

Table 1. Maximum reductions and increases in glacier runoff identified using scenario 8.5 between the periods 2000-2019 and 2030-2019 across the Andes

| Catchment name | Mean annual Glacier runoff in the reference 2000-2019 [$m^3 s^{-1}$] | Change of glacier runoff between 2030-2049 and 2000-2019 [$m^3 s^{-1}$] | Change of glacier runoff between 2030-2049 and 2000-2019 [%] | Glaciological region | Country | Catchment id | Latitude |
|---|---|---|---|---|---|---|---|
| Negative changes | | | | | | | |
| Acodado | 18.8 ± 2.1 | -8.4 | -45 | Wet Andes | Chile | 6090024320 | 47°S |
| Atuel | 4.0 ± 0.6 | -2.4 | -62 | Dry Andes | Argentina | 6090900470 | 35°S |
| Chawpi Urqu | 2.3 ± 1.3 | -1.2 | -45 | Tropical Andes | Perú-Bolivia | 6090601720 | 15°S |
| Positive changes | | | | | | | |
| Huemules | 7.2 ± 2 | 1.3 | 18 | Wet Andes | Chile | 6090965210 | 48°S |
| Tupungato | 2.7 ± 1.0 | 0.9 | 32 | Dry Andes | Argentina | 6090891240 | 34°S |
| Olivares | 2.7 ± 1.1 | 0.5 | 16 | Dry Andes | Chile | 6090889690 | 33°S |
| Quelccaya | 0.8 ± 0.4 | 0.3 | 45 | Tropical Andes | Perú | 6090582670 | 15°S |

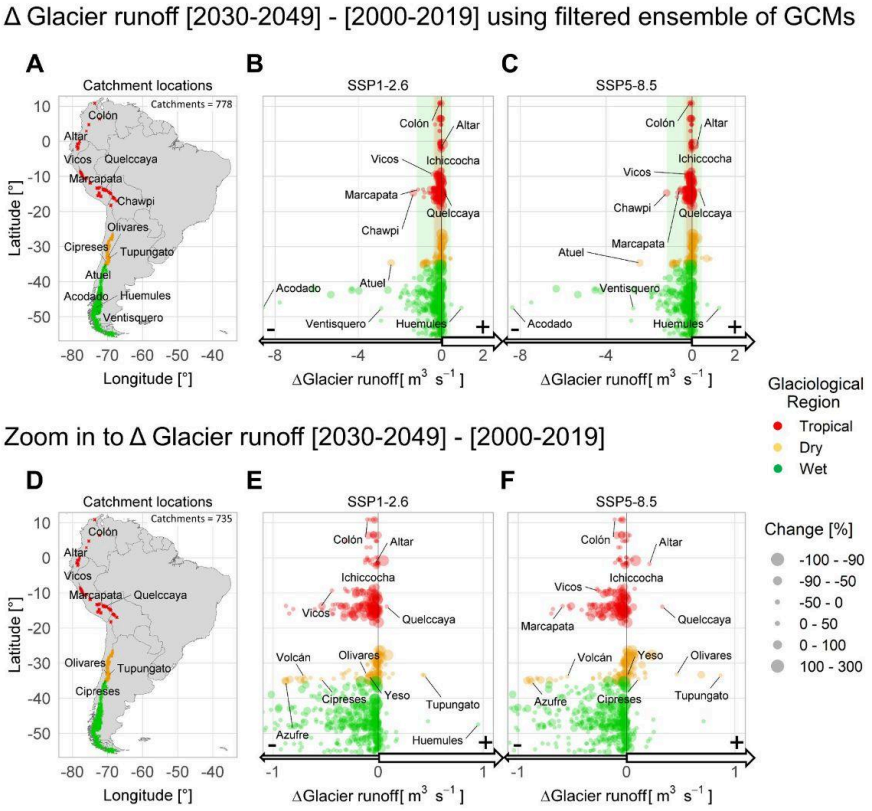


Figure 2. Mean annual changes in glacier runoff between the periods 2000-2019 and 2030-2049 at the catchment scale using the filtered ensemble of GCMs. In the period 2000-2019 is considered the cTC running whereas in the period 2030-2049 is an ensemble of evaluated GCMs. A) and D) show the location of all catchments and the other ones considered in the zoom in, respectively. In B) the glacier runoff differences are present in percentage across the Andes (778 catchments) and in absolute values of changes ($m^3$ $s^{-1}$) in the SSP1-2.6 and C) SSP5-8.5 scenarios. E) and F) represent catchments in a zoom in between glacier runoff changes of -0.15 and 0.15 $m^3$ $s^{-1}$. Shadows in B and C display the standard deviation of glacier runoff changes by the Tropical, Dry and Wet Andes.
These glacier runoff changes can be seen for the complete ensemble in Figure S5 of the Supplementary information.

### 3.2.2. Peak water throughout 21st century along the Andes

The expected peak water (PW) estimation for 778 Andes catchments, considering the filtered ensemble of General Circulation Models (GCMs), indicates that the maximum contribution of glacier runoff to river discharge will likely occur before the first half of the 21st century. Figure 3 illustrates the distribution of

PW years (percentiles 25 and 75 in both scenarios), with a concentration between 2010 and 2028 across the Andes. The closest PW years to the present occur first in the Wet Andes (2010-2024, n = 465 catchments), followed by the Tropical Andes (2014-2030, n = 183 catchments), and finally in the Dry Andes (2021-2046, n = 130 catchments). Notably, PW years were observed only in the past period (2000-2025), where all three regions exhibit similar peak water years between 2010 and 2022. In the future period (2026-2099), the PW years are concentrated between 2026 and 2049. The Tropical Andes experience PW years first (2026-2040, 50 to 86 catchments), followed by the Wet Andes (2030-2038, 40 to 30 catchments), and finally the Dry Andes (2030-2048, 82 to 110 catchments). Interestingly, in the Dry Andes, most catchments show PW years in the future (2026-2099) when the SSP5-8.5 scenario is employed, which can be compared with the results obtained using the SSP1-2.6 scenario. More details regarding the distribution of PW years by glaciological regions can be found in Figure S6, while Figure S7 provides the results of PW using the complete ensemble of GCMs.

Specific locations in Figure 3 and catchments in Table 2 provide a detailed view of the changes in peak water year and the associated amounts of glacier runoff. These details allow for an examination of glacier runoff at the catchment scale within the SSP5-8.5 scenario.

In the Tropical Andes region, the Pico Cristóbal Colón catchments in Colombia display PW years spanning from 2020 to 2028, with a maximum glacier runoff of 0.3 $m^3 s^{-1}$. Moving to Ecuador, the PW years are projected to occur later in the second half of the 21st century, specifically from 2022 to 2084. Notably, the Altar catchment in Ecuador stands out, with a PW year estimated at 2052 ± 10 and a glacier runoff of 1.0 $m^3 s^{-1}$. Meanwhile, in Perú, the cordilleras with significant glacierized areas experience their PW year before the first half of the 21st century. The Cordillera Blanca shows PW years ranging from 2018 to 2064, while the Cordillera Vilcanota exhibits PW years from 2024 to 2050. The Marcapata catchment, located in the Cordillera Vilcanota, holds the largest estimated glacier runoff volume in the Tropical Andes at 3.0 $m^3 s^{-1}$, with a PW year projected in 2030 ± 10. It is noteworthy that this maximum value is only one-third of the maximum identified in the central zone of Chile and Argentina (CL-AR box) within the Dry Andes region. The Dry Andes shows a PW year range from 2010 to 2062. The largest glacier runoff is simulated in the Cipreses catchment (9.3 $m^3 s^{-1}$), followed by the Volcán catchment (4.0 $m^3 s^{-1}$), and the Olivares catchment (3.6 $m^3 s^{-1}$). For PW years simulated after 2049, larger glacier runoff volumes are observed in the Tupungato catchment (4.0 $m^3 s^{-1}$) and the Yeso catchment (1.2 $m^3 s^{-1}$). In contrast to the Tropical and Dry Andes, the Wet Andes region exhibits significant amounts of glacier runoff. Catchments in the Wet Andes, particularly in the latitudinal range of 46-48°S, including the Northern Patagonian Icefield and surrounding glaciers, show a PW year range before the first half of the 21st century, from 2010 to 2048. The Acodado catchment stands out with the highest maximum glacier

runoff of 17.8 $^{3}$ $s^{-1}$ and a PW year of 2010 ± 10, situated on the west side of the Andes. On the eastern side of the Northern Patagonian Icefield, catchments related to the Baker basin are estimated to experience PW years before 2030. Among these catchments, the Soler catchment (in the NPI) exhibits a larger PW volume of 8.5 $^{3}$ $s^{-1}$ compared to those found east of the NPI, like Maitenes, with a runoff of 0.9 $^{3}$ $s^{-1}$. From this analysis, we conclude that the calculation of the PW for each catchment is crucial in characterizing the local differences and spatial variability observed in the Andes. These diverse behaviors are attributed to the distinct morphometric characteristics of glaciers and local climates in each catchment.

The annual and monthly temporal series of glacier runoff for each glacier and catchment are available in the Supplementary data. For more in-depth information and specific examples, refer to Figures S8, S9, and S10 in the Supplementary information. These figures present the detailed temporal variations in glacier runoff for the respective glaciers and catchments.

Table 2. Catchments highlighted by glacier runoff during the identified peak water year between 2000-2099 across the Andes

| Catchment name | PW year | PW glacier runoff [$m^3$ $s^{-1}$] | Location | Country | Catchment id |
|---|---|---|---|---|---|
| Pico Cristóbal Colón | 2024 ± 10 | 0.3 | Colombia | Colombia | 6090000970 |
| Altar | 2052 ± 10 | 1.0 | Ecuador | Ecuador | 6090249220 |
| Vicos | 2020 ± 10 | 1.5 | Co. Blanca | Perú | 6090461650 |
| Ichiccocha | 2030 ± 10 | 1.2 | Co. Blanca | Perú | 6090449220 |
| Marcapata | 2030 ± 10 | 3.0 | Co.Vilcanota | Perú | 6090571030 |
| Cipreses | 2010 ± 10 | 9.3 | CL-AR box | Chile and Argentina | 6090897370 |
| Volcán | 2040 ± 10 | 4.0 | CL-AR box | Chile and Argentina | 6090892940 |
| Olivares | 2040 ± 10 | 3.6 | CL-AR box | Chile and Argentina | 6090889690 |
| Tupungato | 2058 ± 10 | 4.0 | CL-AR box | Chile and Argentina | 6090891240 |
| Yeso | 2054 ± 10 | 1.2 | CL-AR box | Chile and Argentina | 6090892710 |
| Acodado | 2010 ± 10 | 17.8 | NPI | Chile | 6090024320 |
| Soler | 2026 ± 10 | 8.5 | NPI | Chile | 6090963530 |
| Maitenes | 2010± 10 | 0.9 | East of NPI | Chile | 6090962900 |

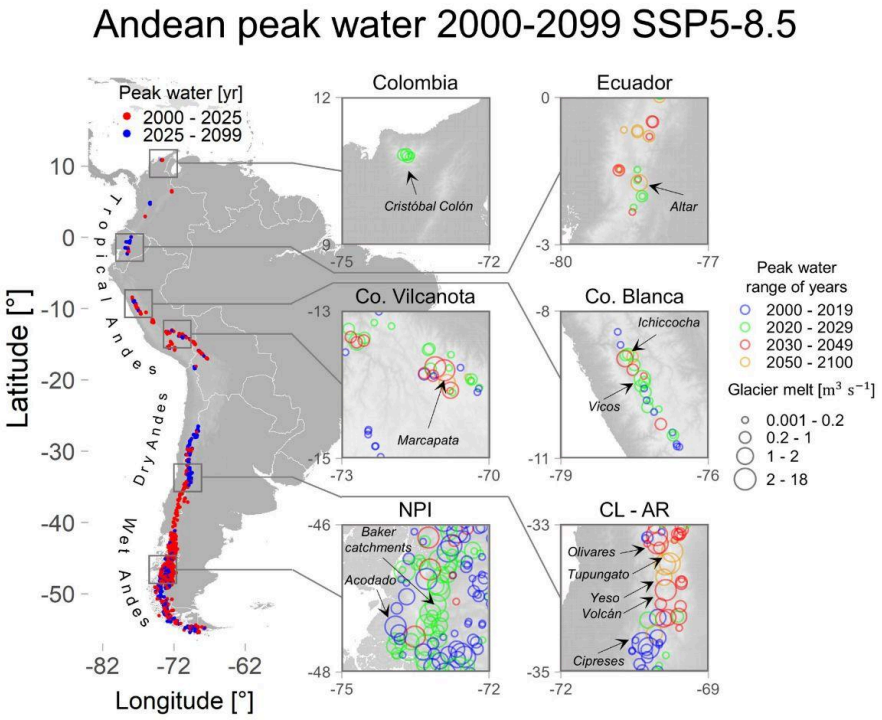


Figure 3. Peak water year and related mean annual glacier runoff across the Andes for the SSP5-8.5 scenario throughout the 21st century. In the South American maps, the peak waters per catchment are exhibited before (2000-2025) and after today (2026-2099), using simulations forced by the filtered ensemble of GCMs. Details can be seen in six locations from Colombia to NPI (Northern Patagonian Icefield). The CL-AR location shows central Chile and Argentina.
The same maps for the SSP1-2.6 scenario can be checked in Figure S7 of the Supplementary material.

## 4 Discussion

### 4.1. Climate projections analysis

Presently, a comprehensive evaluation of GCMs outputs in glacierized catchments across the Andes is notably lacking, encompassing both CMIP6 and earlier datasets. Consequently, the prevailing reference source has been the IPCC AR6 report (IPCC, 2022), which examined climate variations in the Andes utilizing over 30 CMIP6 GCMs. Nevertheless, a key distinction between our simulations, focused on glaciers, and the IPCC report is the treatment of regional extension, wherein the latter considers a broader land area beyond the glacierized surfaces and situated at lower elevations. IPCC (2022) indicate an overall temperature increase across all scenarios, with the northern half of the continent experiencing

more substantial warming, gradually decreasing southward. Additionally, precipitation is anticipated to decrease over the Southern Andes while increasing over the Northern Andes during the period 2041-2060, taking 1995-2014 as a reference period (under the SSP5-8.5 scenario). This pattern is consistent with the findings of Almazroui et al. (2021), who evaluated an ensemble of CMIP6 models across South America. Moreover, the GCM ensemble exhibits a tendency to underestimate precipitation during the rainiest months while overestimating it during the drier months in the southern Andes, particularly in the Southwest region (Almazroui et al., 2021). In comparison to observations in the Southern region, all models portray wetter conditions, indicating a potential limitation in the model's performance in accurately simulating precipitation patterns in this area. In agreement with the IPCC, our results confirm a maximum temperature increase in the Tropical Andes (1.9°C), followed by the Dry (1.5°C), and Wet Andes (1.1°C, southward of NPI). For precipitation, the IPCC reports a reduction in the Dry Andes (-8%) and Wet Andes (-0.1%), alongside an increase in the Tropical Andes (4.5%). However, our findings diverge, showing a negative trend in the Tropical and Wet Andes. Notably, precipitation only exhibits an increase in the SSP1-2.6 scenario for the Tropical Andes.

Regarding the Tropical Andes and the northern area of the Dry Andes, Olmo et al. (2022) conducted a study focusing on the representation of precipitation variability in the July-October season (1979-2014) by using the CESM2, CMCC-CM2-HR4, and MPI-ESM1-2-HR models from CMIP6. The authors found that these models effectively capture the underlying physical mechanisms governing precipitation patterns in the specified period. Our analysis revealed that both the CESM2 and MPI-ESM1-2-HR models exhibit a high monthly correlation but a poor seasonal correlation for the OND season. On the other hand, in the Dry Andes region (18-37°S), these same GCMs exhibit a robust seasonal correlation, which holds significant importance for glacier mass balance simulations.

Turning our attention to future projections, we observed that under the SSP1-2.6 and SSP5-8.5 scenarios, there is a median reduction in precipitation during the JAS and OND seasons (as projected by MPI, CESM2, and NorESM2-MM). These results are in line with the estimations made by Agudelo et al. (under review), which indicate an increase in the occurrence of dry days (19.4%) during the austral winter (JAS) and a higher frequency of dry circulation patterns during the July-October period. Notably, the CESM2 model demonstrated the most favorable outcomes concerning precipitation variability over the southwestern region during the historical period (1901-2014), as indicated by Rivera and Arnould (2020).

**4.2. Glacier volume and runoff simulations toward 2049**

Three critical aspects in the glacier dynamics considered in the simulations using OGGM need to be discussed to account for the likelihood of the presented results:

i) The approach based on the SIA, implemented in OGGM, lacks longitudinal/transverse stress gradients and other complex mechanisms (Le Meur et al., 2004). As a consequence, glaciers' response to climate forcing is nearly immediate, making higher-order ice flow models (Oerlemans, 2008) more suitable for accurately representing ice flow. However, the use of these high-order models presents computational challenges (Jouvet, 2022), currently limiting their application in regional and global simulations.

ii) The ice thickness calibration in this study relies on data from Farinotti et al. (2019), which employs an ensemble of up to five models to estimate the ice thickness distribution. Unfortunately, this approach leads to an overestimation of approximately 20% (median) of the measured ice thickness. Moreover, our calibration parameter values for ice thickness align with values from Cuffey and Paterson (2010) and Millan et al. (2022). The simulations predict lower Glen A parameter values for glaciers with lower internal temperatures, such as those found in the glaciological zone DA1 ($2.4\ 10^{-25}$ $s^{-1}$ $Pa^{-3}$), which represents the coldest zone in the Andes. Additionally, Millan et al. (2022) estimated Glen A parameters in the Andes ranging between $5.6\ 10^{-25}$ and $2.4\ 10^{-24}$ $s^{-1}$ $Pa^{-3}$, while the calibrated values used in this study range from $2.4\ 10^{-25}$ and $2.4\ 10^{-23}$ $s^{-1}$ $Pa^{-3}$.

iii) Due to the limitations mentioned in (i) and (ii), our simulations of future glacier runoff changes carry uncertainties arising from the ice thickness simulation and its calibration. Moreover, the climate performance in the historical period and the various climate models and scenarios considered contribute to this uncertainty. Estimating melt factor values is critical, and we derive them from the calibration, using Hugonnet et al. (2021) data of geodetic mass balance. However, we must acknowledge that our historical climate dataset, which was corrected in Caro et al. (2023, under review), and combined with Hugonnet et al. (2021) data, could introduce errors in the calibrated melt factor. Consequently, this error could affect the simulated mass balance of glaciers and the related ice thickness estimation. Furthermore, the future climate data from each GCM (temperature and precipitation) was corrected relative to the historical climate dataset.

**4.3. Peak Water estimation across the Andes: comparison with former studies**

Our 21st century peak water estimates partially align with Huss and Hock (2018) findings. They identified peak water in 12 Andean basins with a glacierized surface area of 9,544 $km^2$, representing different proportions in the Tropical Andes (23%), Dry Andes (20%), and Wet Andes (57%). Their research revealed a peak water already passed in the inner tropics (2 catchments) and projected a peak water occurrence between 2011-2046 in the outer tropics (4 catchments). In the Dry Andes, the estimated peak water was around 2010 ± 24 (2 catchments on the western side), while the Wet Andes showed a broader range from 2003 ± 11 to 2096 ± 24 (4 catchments). Interestingly, they found evidence of past peak water in the northern area of the Wet Andes.

In contrast, our estimations considered a larger glacierized surface area (11,282 $km^2$), filtering glaciers not accounted for in glacier national inventories and calving glaciers in the Patagonian icefields. Our results suggest that the peak water will occur before the first half of the 21st century across the Andes. According to our results, the peak water has already occurred in most of the Tropical Andes catchments and will occur before 2049 in most of the Dry Andes catchments. We took into account over 85% of the glacier surface in the Dry Andes on both sides of the Andes, as glacier contribution is the most significant across the entire Andean region. In the Wet Andes, the majority of catchments experienced peak water before the present day. Furthermore, our estimation of peak water presents different ranges of years across the Andes, tied too to varying climate change scenarios. Generally, an earlier peak water occurrence is associated with less warm scenarios, which aligns with observations in the Himalayan mountains and specific Andean catchments (Huss and Hock, 2018; Laha et al., 2021).

**5 Conclusions**

In this article, we conducted an analysis of eight GCMs from CMIP6 to determine the climate models that demonstrate the highest performance in reproducing the corrected TerraClimate data for the period 1990-2019 and between them in the period 2020-2049 across the Andes, covering a total glacierized surface of 27,669 $km^2$. These results were used to run the Open Global Glacier Model (OGGM) and to estimate the changes in glacier runoff throughout the 21st century from Colombia and Tierra del Fuego.

- Among the GCMs analyzed, we identified those that exhibit the best scores in the Andes, specifically for the Tropical Andes (CAMS, FGOALS, GFDL, INM-CM5, and NorESM2), in the Dry Andes (GFDL, INM-CM5, MPI, and NorESM2) and for the Wet Andes (CAMS, INM-CM4, and NorESM2). With these models (filtered ensemble), as well as, all analyzed GCMs (complete ensemble), we were able to analyze the changes in glacier runoff.

- For the first time, we conducted a comprehensive simulation of glacier dynamics and glacier runoff in 778 Andean catchments, utilizing a calibrated and validated model with a specific focus on the Andes region. Our findings revealed a notable reduction in glacier runoff across the Andes during the periods 2000-2019 and 2030-2049, particularly when considering the filtered ensemble of GCMs. In the Tropical and Wet Andes regions, we observed a negative median change in glacier runoff (-0.1 $m^3 s^{-1}$ and -0.2 $m^3 s^{-1}$, respectively), while the Dry Andes exhibited a relatively lower median reduction in glacier runoff (-0.003 $m^3 s^{-1}$). Interestingly, within these regions, we identified certain catchments that displayed significant increases in glacier runoff, notably Tupungato and Olivares in the Dry Andes, exceeding 16%. The Dry Andes region demonstrated a cumulative increase of 38% in glacier runoff compared to the historical period (3.5 $m^3 s^{-1}$ for SSP5-8.5 in 34 catchments). Conversely, the Chawpi Urqu catchment in the Tropical Andes, situated on the Bolivia-Peru border, experienced a substantial reduction of 45% in glacier runoff. Overall, the Tropical Andes experienced the most significant cumulative loss, with a reduction of 43% compared to the historical period.
- The projection indicates that peak water from glacier runoff will occur across the Andes before the first half of the 21st century, specifically between 2010 and 2028. Nevertheless, the distribution of peak water years exhibits significant variations along the Andes and locally at the mountain range scale. The Wet Andes region is expected to experience the earliest peak water years (2010 to 2024), followed by the Tropical Andes (2014 to 2030). In contrast, the Dry Andes region is projected to experience peak water years later, primarily in 130 catchments, occurring between 2021 and 2046. During the future period of 2026-2099, the occurrence of peak water years is anticipated to be lower in number across the Andes. Notably, the Dry Andes region comprises the largest number of catchments, ranging from 82 to 110 (2030 to 2048). Within this region, specific attention should be given to catchments that contribute the highest amounts of glacier runoff, such as the Cipreses (peak water in 2010 ± 10 with 9.3 $m^3 s^{-1}$), Volcán (peak water in 2040 ± 10 with 4.0 $m^3 s^{-1}$), and the Olivares catchment (peak water in 2040 ± 10 with 3.6 $m^3 s^{-1}$).

This simulation approach provides a comprehensive understanding of the variations in glacier runoff using the GCMs with coherent behavior in the historical and future periods. We highlight the temporal and spatial variations in peak water from glacier runoff across the Andes, emphasizing the importance of considering regional and catchment differences in water resource adaptation strategies, especially in the most affected region by a long drought in the Andes as the central zone of Chile and Argentina.

**References**

Abatzoglou, J. T., Dobrowski, S. Z., Parks, S. A., and Hegewisch, K. C. (2018). TerraClimate, a High-Resolution Global Dataset of Monthly Climate and Climatic Water Balance from 1958-2015. Sci. Data 5, 1–12. https://doi:10.1038/sdata.2017.191

Agudelo, A., et al. (2023). Future projections of low-level atmospheric circulation patterns over South Tropical South America: Impacts on precipitation and Amazon dry season length. Journal of Geophysical Research: Atmospheres [in review]

Almazroui, M., Ashfaq, M., Islam, M. N., et al. (2021). Assessment of CMIP6 Performance and Projected Temperature and Precipitation Changes Over South America. Earth Syst Environ 5: 155–183. https://doi.org/10.1007/s41748-021-00233-6

Aschwanden, A., Aðalgeirsdóttir, G., and Khroulev, C. (2013). Hindcasting to measure ice sheet model sensitivity to initial states, The Cryosphere, 7. https://doi.org/10.5194/tc-7-1083-2013

Autin, P., Sicart, J. E., Rabatel, A., Soruco, A., & Hock, R. (2022). Climate Controls on the Interseasonal and Interannual Variability of the Surface Mass and Energy Balances of a Tropical Glacier (Zongo Glacier, Bolivia, 16° S): New Insights From the Multi‐Year Application of a Distributed Energy Balance Model. Journal of Geophysical Research: Atmospheres, 127(7). https://doi.org/10.1029/2021JD035410

Braun, L. N. and Renner, C. B. (1992). Application of a conceptual runoff model in different physiographic regions of Switzerland. Hydrol. Sci. J. 37(3), 217-231. https://doi.org/10.1080/02626669209492583

Bravo, C., Bozkurt, D., Ross, A.N. et al. (2021). Projected increases in surface melt and ice loss for the Northern and Southern Patagonian Icefields. Sci Rep 11, 16847. https://doi.org/10.1038/s41598-021-95725-w

Caro, A, Condom, T. and Rabatel, A. (2021). Climatic and Morphometric Explanatory Variables of Glacier Changes in the Andes (8–55°S): New Insights From Machine Learning Approaches. Front. Earth Sci. https://doi.org/10.3389/feart.2021.713011

Caro, A., Condom, T., Rabatel, A., Champollion, N., García, N., and Saavedra, F. (2023). Hydrological Response of Andean Catchments to Recent Glacier Mass Loss, EGUsphere [preprint]. https://doi.org/10.5194/egusphere-2023-888

Crippen, R., Buckley, S., Agram, P., Belz, E., Gurrola, E., Hensley, S., Kobrick, M., Lavalle, M., Martin, J., Neumann, M., Nguyen, Q., Rosen,P., Shimada, J., Simard, M., Tung, W. (2016). NASADEM Global Elevation Model: Methods and Progress. The International Archives of thePhotogrammetry, Remote Sensing and Spatial Information Sciences XLI-B4, 125–128. (20). https://doi.org/10.5194/isprs-archives-XLI-B4-125-2016

Cuffey, K. and Paterson, W. (2010). The Physics of Glaciers, 4th edn., Academic Press.

DRIAS project 2023, DRIAS, futures of climate - Education (drias-climat.fr).

Eyring, V., Bony, S., Meehl, G. A., Senior, C. A., Stevens, B., Stouffer, R. J., and Taylor, K. E. (2016). Overview of the Coupled Model Intercomparison Project Phase 6 (CMIP6) experimental design and organization, Geosci. Model Dev., 9, 1937–1958, https://doi.org/10.5194/gmd-9-1937-2016

Farinotti, D., Huss, M., Fürst, J. J., Landmann, J., Machguth, H., Maussion, F., et al. (2019). A consensus estimate for the ice thickness distribution of all glaciers on Earth. Nat. Geosci. 12, 168–173. https://doi.org/10.1038/s41561-019-0300-3

Frans, C., Istanbulluoglu, E., Lettenmaier, D. P., Naz, B., Clarke, G., Condom, T., et al. (2015). Predicting glacio-hydrologic change in the headwaters of the Zongo River, Cordillera Real, Bolivia. Water Resour. Res. 51, 9029–9052. https://doi.org/10.1002/2014WR016728

Hausfather, Z., Marvel, K., Schmidt, G. A., Nielsen-Gammon, J. W., and Zelinka, M. (2022). Climate simulations: recognize the 'hot model' problem, Nature, 605, 26–29, https://doi.org/10.1038/d41586-022-01192-2

Hock, R. (2003). Temperature index melt modelling in mountain areas. Journal of Hydrology, 282(1-4), 104-115. https://doi.org/10.1016/S0022-1694(03)00257-9

Hugonnet, R., McNabb, R., Berthier, E. et al. (2021). Accelerated global glacier mass loss in the early twenty-first century. Nature 592, 726–731. https://doi.org/10.1038/s41586-021-03436-z

Huss, M., and Hock, R. (2015). A new model for global glacier change and sea-level rise. Front. Earth Sci. 3:54. https://doi.org/10.3389/feart.2015.00054

Huss, M., and Hock, R. (2018). Global-scale hydrological response to future glacier mass loss. Nat. Clim. Change 8, 135–140. https://doi.org/10.1038/s41558-017-0049-x

IPCC. IPCC WGI Interactive Atlas: Regional information (Advanced), 2022.

Jouvet, G., Cordonnier, G., Kim, B., Lüthi, M., Vieli, A., & Aschwanden, A. (2022). Deep learning speeds up ice flow modelling by several orders of magnitude. Journal of Glaciology, 68(270), 651–664. https://doi.org/10.1017/jog.2021.120

Kienholz, C., Rich, J. L., Arendt, A. A., and Hock, R.(2014). A new method for deriving glacier centerlines applied to glaciers in Alaska and northwest Canada, The Cryosphere, 8, 503–519, https://doi.org/10.5194/tc-8-503-2014

Laha, S., Banerjee, A., Singh, A., Sharma, P., & Thamban, M. (2021). The control of climate sensitivity on variability and change of summer runoff from two glacierised Himalayan catchments preprint. Hydrology and Earth System Sciences Discussions. https://doi.org/10.5194/hess-2021-499

Le Meur, E., Gagliardini, O., Zwinger, T. and Ruokolainen, J. (2004). Glacier flow modelling: a comparison of the shallow ice approximation and the Full-Stokes solution. Comptes Rendus Physique 5(7), 709–722. https://doi.org/10.1016/j.crhy.2004.10.001

Marzeion, B., Hock, R., Anderson, B., Bliss, A., Champollion, N., Fujita, K., Huss, M., Immerzeel, W. W., Kraaijenbrink, P., Malles, J., Maussion, F., Radić, V., Rounce, D. R., Sakai, A., Shannon, S., van de Wal, R., and Zekollari, H. (2020). Partitioning the Uncertainty of Ensemble Projections of Global Glacier Mass Change, Earth's Future, 8, https://doi.org/10.1029/2019EF001470

Marzeion, B., Jarosch, A. H., and Hofer, M.(2012). Past and future sea-level change from the surface mass balance of glaciers, The Cryosphere, 6, 1295–1322, https://doi.org/10.5194/tc-6-1295-2012

Masiokas, M. H., Rabatel, A., Rivera, A., Ruiz, L., Pitte, P., Ceballos, J. L., et al. (2020). Current state and recent changes of the cryosphere in the Andes. Front Earth Sci. 8:99. https://doi.org/10.3389/feart.2020.00099

Maussion, F., Butenko, A., Champollion, N., Dusch, M., Eis, J., Fourteau, K., et al. (2019). The open global glacier model (OGGM) v1.1. Geoscientific Model. Develop. 12, 909–931. https://doi:10.5194/gmd-12-909-2019

McSweeney, C. F., Jones, R. G., Lee, R. W., and Rowell, D. (2015). Selecting CMIP5 GCMs for downscaling over multiple regions. Climate Dynamics, 44(11-12), 3237–3260. https://doi.org/10.1007/s00382-014-2418-8

Millan, R., Mouginot, J., Rabatel, A. et al. (2022) Ice velocity and thickness of the world's glaciers. Nat. Geosci. 15, 124–129. https://https://doi.org/10.1038/s41561-021-00885-z

Oerlemans, J., 2008. Minimal Glacier Models. Utrecht Publishing and Archiving Services: Igitur, 90 pp.

Olmo, M. E., Espinoza, J., Bettolli, M. L., Sierra, J. P., Junquas, C., Arias, P. A. Moron V and Balmaceda-Huarte R (2022). Circulation patterns and associated rainfall over south tropical South America: GCMs evaluation during the dry-to-wet transition season. J. Geophys. Res. Atmos. 127. https://doi.org/10.1029/2022JD036468

Rabatel, A., Ceballos, J. L., Micheletti, N., Jordan, E., Braitmeier, M., Gonzalez, J., et al. (2018). Toward an imminent extinction of Colombian glaciers? Geografiska Annaler: Series A. Phys. Geogr. 100, 75–95. https://doi.org/10.1080/04353676.2017.1383015

Radic, V., and Hock, R. (2014). Glaciers in the Earth's hydrological cycle. Assessments of glacier mass and runoff changes on global and regional scales. Surv. Geophys. 35, 813–837. https://doi.org/10.1007/s10712-013-9262-y

Réveillet, M., Rabatel, A., Gillet-Chaulet, F., and Soruco, A. (2015). Simulations of changes to Glacier Zongo, Bolivia (16S), over the 21st century using a 3-D full-Stokes model and CMIP5 climate projections. Ann. Glaciol. 56, 89–97. https://doi.org/10.3189/2015aog70a113

RGI Consortium. Randolph Glacier Inventory. (2017). A Dataset of Global Glacier Outlines, Version 6. Boulder, Colorado USA. NSIDC: National Snow and Ice Data Center, https://doi.org/10.7265/4m1f-gd79

Rivera, J.A., Arnould, G. (2020). Evaluation of the ability of CMIP6 models to simulate precipitation over Southwestern South America: climatic features and long-term trends (1901–2014). Atmos Res 241:104953. https://doi.org/10.1016/j.atmosres.2020.104953

Rounce, D. et al. (2023). Global glacier change in the 21st century: Every increase in temperature matters. Science 379,78-83. https://doi.org/10.1126/science.abo1324

Schaefer, M., MacHguth, H., Falvey, M., and Casassa, G. (2013). Modeling past and future surface mass balance of the Northern Patagonia icefield. J. Geophys. Res. Earth Surf. 118, 571–588. https://doi.org/10.1002/jgrf.20038

Scheiter, M., Schaefer, M., Flández, E., Bozkurt, D., and Greve, R. (2021). The 21st-century fate of the Mocho-Choshuenco ice cap in southern Chile, The Cryosphere, 15, 3637–3654, https://doi.org/10.5194/tc-15-3637-2021

Sørland, S. L., Schär, C., Lüthi, D. and Kjellström, E. (2018). Bias patterns and climate change signals in GCM-RCM model chains. Environ. Res. Lett., 13, 074017. https://doi.org/10.1088/1748-9326/aacc77

Tokarska, K. B., Stolpe, M. B., Sippel, S., Fischer, E. M., Smith, C. J., Lehner, F., and Knutti, R. (2020). Past warming trend constrains future warming in CMIP6 models, Science Advances, 6, eaaz9549, https://doi.org/10.1126/sciadv.aaz9549

Vuille, M., Carey, M., Huggel, C., Buytaert, W., Rabatel, A., Jacobsen, D., et al. (2018). Rapid decline of snow and ice in the tropical Andes–Impacts, uncertainties and challenges ahead. Earth Sci. Rev. 176, 195–213. https://doi.org/10.1016/j.earscirev.2017.09.019

Yarleque, C., Vuille, M., Hardy, D. R., Timm, O. E., De la Cruz, J., Ramos, H., et al. (2018). Projections of future disappearance of the Quelccaya, the largest tropical ice cap on Earth. Nat. Sci. Rep. 8:15564. https://doi.org/10.1038/s41598-018-33698-z

# Part III: Glaciological and climate data

The data from the statistical analysis, as well as, of simulations on glaciers carry on in this thesis are described in Table 7.

Table 7. Data of glaciers across the Andes generated in the thesis available to be downloaded.

| Data Name | Description | Espatial extension | Link |
|---|---|---|---|
| Glacier Clusters identification across Chilean Andes using Topo-Climatic variables: DATA | Shapefile related to the Chilean glacier which are related to each estimated cluster | Chile between 17-55°S | Glacier Clusters identification across Chilean Andes using Topo-Climatic variables: DATA \| Zenodo |
| Hydrological Response of Andean Catchments to Recent Glacier Mass Loss (data) | - Annual time series of simulated glacier area, glacier volume, glacier runoff and corrected temperature and precipitation by glacier. Period 2000-2019.<br><br>- Summary by catchments of simulated glacier area, glacier volume, glacier runoff and corrected temperature and precipitation for periods 2000-2019, 2000-2009 and 2010-2019. | Acros the Andes 11°N-55°S | Hydrological Response of Andean Catchments to Recent Glacier Mass Loss (data) \| Zenodo |

# Part IV: Appendixes

## 5.5 Conference Proceedings

2023

**Alexis Caro**, Thomas Condom, Antoine Rabatel, Nicolas Champollion, Nicolás García, Freddy Saavedra. Respuesta hidrológica a la reducción de masa glaciar en las cuencas Andinas (11°N-55°S). Simposio Internacional de Cambio Climático y Resiliencia, September, 2023

**Alexis Caro**, Thomas Condom, Antoine Rabatel, Nicolas Champollion, Nicolás García. Respuesta hidrológica a la reducción de masa glaciar en las cuencas Andinas (11°N-55°S). SOCHICRI meeting 2023.

**Alexis Caro**, Thomas Condom, Antoine Rabatel. Andean catchments hydrological response to recent glacier mass loss. Programme de Recherche Agence Française pour le Développement / IRD : Cycle de l'Eau et Changement Climatique (CECC) Programme Réunion – CECC ANDES - ANDEX project. Santiago of Chile, 02 may 2023.

2022

**Alexis Caro**, Álvaro Ayala, Thomas Condom, Antoine Rabatel. (2022). Contribución hídrica de los glaciares a las cuencas hidrográficas con mayor densidad poblacional de Chile central (33-35°S) durante los periodos pre-Megasequía y Megasequía. Annual meeting SOCHIGEO, Chile.

**Alexis Caro**, Thomas Condom, Antoine Rabatel. (2022). Variables explicatorias de la reducción glaciar entre Perú y Tierra del Fuego. Annual meeting SOCHICRI, Chile.

Daniela González, Yael Aguirre, Freddy Saavedra, Valentina Contreras, **Alexis Caro**, Ana Hernández and Carlos Romero. (2022). Visualización de resultados de base de datos de nieves con nubes reducidas, en la cuenca del Aconcagua, a partir de datos MODIS, a través de la plataforma Google Earth Engine. Annual meeting SOCHICRI, Chile.

Freddy Saavedra, Carlos Romero, Daniela Gonzalez, Yael Aguirre, **Alexis Caro**, Valentina Contreras, Ana Hernández-Duarte. (2022). Producto MODIS mejorado de cobertura nival diaria a lo largo de los Andes: Aplicación de algoritmos de extracción de nubes a través de Google. Annual meeting SOCHICRI, Chile.

Freddy Saavedra, Ana Hernández-Duarte, Daniela Gonzalez, Yael Aguirre, Valentina Contreras, **Alexis Caro**, Carlos Romero (2022). Validation of Cloud Reduction Algorithms Over MODIS Snow Products on Andes Mountain. EGU General Assembly Conference 2022.

2021

**Alexis Caro**, Thomas Condom, Antoine Rabatel. (2021). Controladores climáticos y morfo-topográficos de la reducción de los glaciares andinos. Seminario Universidad de Playa Ancha y Gobierno regional de Valaparaíso, Chile.

Freddy Saavedra, Carlos Romero, Daniela Gonzalez, Yael Aguirre, **Alexis Caro**, Valentina Contreras, and Ana Hernández-Duarte. (2021). Validation of Cloud Reduction Algorithms Over MODIS Snow Products on Andes Mountain. AGU Fall Meeting 2021.

**Alexis Caro**, Fernando Gimeno, Antoine Rabatel, Thomas Condom, and Jean Carlos Ruiz. (2021) Glacier Clusters identification across Chilean Andes using Topo-Climatic variables. EGU General Assembly Conference 2021.

**Alexis Caro**, Thomas Condom, Antoine Rabatel. (2021). Controladores climáticos y morfo-topográficos de la reducción de los glaciares andinos desde algoritmos de machine learning. Seminarios Glaciología del Centro de Estudios Científicos de Valdivia (CECs), Chile.

## 5.6 Workshops

2023. Tropospheric lapse rate: observations and modeling of past, present and future variations July 6-7, 2023 Sorbonne Université, Campus Jussieu, France

2021. 5th OGGM workshop 20-24 September 2021, Neuharlingersiel, Germany.

2021. Fundamentals of DeepLearning workshop. NVIDIA, GRICAD Laboratory and the Data Stewarship of UGA.

## 5.7 Summer school

CHESS Summer School on Cryospheric Monitoring (3 ECTS). Course of 150 hours. La Serena, 5-15th December 2022.

## 5.8 Classes

Teacher in Curso Google Earth Engine enfocado en nieve. AndeSnow project (CLIMAT-AmSud). 5-7 January 2022, Valparaíso, Chile.

## 5.9 Related projects

2019-2023 : Chilean scholarship for PhD project. Funded by the Chilean research agency (ANID).

2022-2023 : Strategic Research Fund in Drought project funded by the Chilean research agency (ANID). Glaciological simulation in Drought and water security platform for catchment planning: historical evolution and future trajectories under global change project.

2022-2023 : GLASI project funded by the LabEx OSUG@2020 (UGA). Réponses hydrologiques passée et future (2000-2100) au retrait des glaciers dans les Andes (10°N-55°S).

2021-2022 : Andesnow (CLIMAT-AmSud) project funded by the CNRS. Collaboration project between France,Chile (UPLA), Argentina (IANIGLA-CONICET) and Perú (Univ. La Molina).

# References

Abatzoglou, J. T., Dobrowski, S. Z., Parks, S. A., and Hegewisch, K. C. (2018). TerraClimate, a High-Resolution Global Dataset of Monthly Climate and Climatic Water Balance from 1958-2015. Sci. Data 5, 1–12. https://doi.org/10.1038/sdata.2017.191

Aceituno, P., et al. (1993). Stability analysis of the relationship between the Southern Oscillation and rainfall in South America. Bull. Inst. fr. études Andines.

Almazroui, M., Ashfaq, M., Islam, M. N. et al. (2021). Assessment of CMIP6 Performance and Projected Temperature and Precipitation Changes Over South America. Earth Syst Environ 5: 155–183. https://doi.org/10.1007/s41748-021-00233-6

Alvarez-Garreton, C., Mendoza, P. A., Boisier, J. P., Addor, N., Galleguillos, M., Zambrano-Bigiarini, M., Lara, A., Puelma, C., Cortes, G., Garreaud, R., McPhee, J., and Ayala, A. (2018). The CAMELS-CL dataset: catchment attributes and meteorology for large sample studies – Chile dataset, Hydrol. Earth Syst. Sci., 22, 5817–5846. https://doi.org/10.5194/hess-22-5817-2018

ANA (2014). Data from: Inventario de Glaciares en el Perú. 2da Actualización. Huaraz: Ministerio de Agricultura y Riego.

Arnold, N. S., Willis, I. C., Sharp, M. J., Richards, K. S. and Lawson, W.J. (1996). A distributed surface energy-balance model for a small valley glacier. I. Development and testing for Haut Glacier d'Arolla, Valais, Switzerland. J. Glacial, 42(140),77–89. https://doi.org/10.3189/S0022143000030549

Autin, P., Sicart, J. E., Rabatel, A., Soruco, A., Hock, R. (2022). Climate controls on the interseasonal and interannual variability of the surface mass and energy balances of a tropical glacier (Zongo Glacier, Bolivia, 16°S): new insights from the multi-year application of a distributed energy balance, J. Geophys. Res. Atmos., Volume 127. https://doi.org/10.1029/2021JD035410

Ayala, Á., Farías-Barahona, D., Huss, M., Pellicciotti, F., McPhee, J., and Farinotti, D. (2020). Glacier Runoff Variations 600 since 1955 in the Maipo River Basin, Semiarid Andes of central Chile. Cryosphere Discuss. 14, 1–39. https://doi:10.5194/tc-2019-233

Ayala, Á., Pellicciotti, F., MacDonell, S., McPhee, J., Burlando, P. (2017). Patterns of glacier ablation across North-Central Chile: Identifying the limits of empirical melt models under sublimation-favorable conditions. Water Resources Research, 53(7), 5601– 5625. https://doi.org/10.1002/2016WR020126

Barcaza, G., Nussbaumer, S. U., Tapia, G., Valdés, J., García, J.-L., Videla, Y., et al. (2017). Glacier inventory and recent glacier variations in the Andes of Chile, South America. Ann. Glaciol. 58, 166–180. https://doi.org/10.1017/aog.2017.28

Basantes-Serrano, R., Rabatel, A., Francou, B., Vincent, C., Soruco, A., Condom, T., and Ruíz, J. C. (2022). New insights into the decadal variability in glacier volume of a tropical ice cap, Antisana (0°29' S, 78°09' W), explained by the morpho-topographic and climatic context. The Cryosphere, 16, 4659–4677, https://doi.org/10.5194/tc-16-4659-2022

Bergström, S. (1991). Principles and Confidence in Hydrological Modelling. Hydrology Research, 22(2):123–136. ISSN 0029-1277. https://doi.org/10.2166/nh.1991.0009

Bindschadler, R., 1983. The importance of pressurized subglacial water in separation and sliding at the glacier bed. Journal of Glaciology, 29(101), 3–19. https://doi.org/10.3189/S0022143000005104

Blatter, H. (1995). Velocity and stress fields in grounded glaciers: a simple algorithm for including deviatoric stresses. J Glaciol, 41:333–344. https://doi.org/10.3189/S002214300001621X

Boulton, G. S., and Hindmarsh, R. C. A. (1987). Sediment deformation beneath glaciers: rheology and geological consequences. Journal of Geophysical Research, 92(B(9)), 9059–9082. https://doi.org/10.1029/JB092iB09p09059

Bown, F., Rivera, A., & Acuña, C. (2008). Recent glacier variations at the Aconcagua basin, central Chilean Andes. Annals of Glaciology, 48, 43–48. https://doi.org/10.3189/172756408784700572

Bown, F., Rivera, A., Pêtlicki, M., Bravo, C., Oberreuter, J., and Moffat, C. (2019). Recent ice dynamics and mass balance of Jorge Montt Glacier, Southern Patagonia Icefield. J. Glaciol. 65, 732–744. https:// doi.org/10.1017/jog.2019.47

Braithwaite, R.J. (1995). Aerodynamic stability and turbulent sensible-heat flux over a melting ice surface, the Greenland ice sheet. J. Glacial, 41(139), 562–571. https://doi.org/10.3189/S0022143000034882

Braithwaite, R.J. and Olesen, O. B. (1990). A simple energy-balance model to calculate ice ablation at the margin of the Greenland ice sheet. J. Glaciol., 36(123), 222–228. https://doi.org/10.3189/S0022143000009473

Braun, L. N. and Renne, C. B. (1992). Application of a conceptual runoff model in different physiographic regions of Switzerland. Hydrological Sciences Journal, 37(3):217–231. https://doi.org/10.1080/02626669209492583

Braun, M. H., Malz, P., Sommer, C., Farías-Barahona, D., Sauter, T., Casassa, G., et al. (2019). Constraining Glacier Elevation and Mass Changes in South America. Nat. Clim Change 9 (2), 130–136. https://doi.org/10.1038/s41558-018-0375-7

Bravo, C., Bozkurt, D., Ross, A.N. et al. (2021). Projected increases in surface melt and ice loss for the Northern and Southern Patagonian Icefields. Sci Rep 11, 16847. https://doi.org/10.1038/s41598-021-95725-w

Bravo, C., Loriaux, T., Rivera, A., and Brock, B. W. (2017). Assessing glacier melt contribution to streamflow at Universidad Glacier, central Andes of Chile. Hydrology and Earth System Sciences, 21(7), 3249-3266. https://doi.org/10.5194/hess-21-3249-2017

Bravo, C., Quincey, D. J., Ross, A. N., Rivera, A., Brock, B., Miles, E., and Silva, A. (2019). Air temperature characteristics, distribution, and impact on modeled ablation for the South Patagonia Icefield. Journal of Geophysical Research: Atmospheres, 124. https://doi.org/10.1029/2018JD028857

Brock, B. W., Willis, I. C., Sharp, M. J., & Arnold, N. S. (2000). Modelling seasonal and spatial variations in the surface energy balance of Haut Glacier d'Arolla, Switzerland. Annals of Glaciology, 31, 53–62. https://doi.org/10.3189/172756400781820183

Brun, F., Berthier, E., Wagnon, P., Kääb, A., and Treichler, D. (2017). A Spatially Resolved Estimate of High Mountain Asia Glacier Mass Balances from 2000 to 2016. Nat. Geosci 10 (9), 668–673. https://doi.org/10.1038/ngeo2999

Caceres, B. (2010). Actualización del Inventario de Tres Casquetes Glaciares del Ecuador. Master Thesis, University of Nice, France.

Caro, A. (2014). Estudios glaciológicos en los nevados de Chillán. University of Chile. [thesis].

Caro, A., Condom, T. and Rabatel, A. (2021). Climatic and Morphometric Explanatory Variables of Glacier Changes in the Andes (8–55°S): New Insights From Machine Learning Approaches. Front. Earth Sci. 9:713011. https://doi.org/10.3389/feart.2021.713011

CEAZA. (2022). datos meteorológicos de Chile [data set], http://www.ceazamet.cl/

CECs. (2018). Meteorological data measured by Centro de Estudios Científicos.

Collao-Barrios, G., Gilliet-Chaulet, F., Favier, V., Casassa, G., and Berthier, E.(2018). Ice flow modelling to constrain the surface mass balance and ice discharge of San Rafael Glacier, Northern Patagonia Icefield. J. Glaciol. 64, 568–582. https://doi.org/10.1017/jog.2018.46

Condom. T., Escobar, M., Purkey, D., Pouget J.C., Suarez, W., Ramos, C., Apaestegui, J., Zapata, M., Gomez, J. and Vergara, W. (2011). Modelling the hydrologic role of glaciers within a Water Evaluation and Planning System (WEAP): a case study in the Rio Santa watershed (Peru). Hydrol. Earth Syst. Sci. Discuss., 8, 869–916. https://doi:10.5194/hessd-8-869-2011

Cuffey, K. and Paterson, W. (2010). The Physics of Glaciers, 4th edn., Academic Press.

Daanen et al. (2011). Encyclopedia of Snow, Ice and Glaciers (eds Singh, V. P., Singh, P. & Haritashya, U. K.) 672–679 (Springer, 2011).

Dangles, O., Rabatel, A., Kraemer, M., Zeballos, G., Soruco, A., Jacobsen, D., et al. (2017). Ecosystem sentinels for climate change? Evidence of wetland cover changes over the last 30 years in the high Bolivian Andes. PLoS One 12:e0175814. https://doi.org/10.1371/journal.pone.0175814

Davies, B. J., et al. (2020). The evolution of the Patagonian Ice Sheet from 35 ka to the present day (PATICE). Earth-Science Rev. 204, 103152. https://doi.org/10.1016/j.earscirev.2020.103152

De Angelis, H. (2014). Hypsometry and sensitivity of the mass balance to changes in equilibrium-line altitude: the case of the Southern Patagonia Icefield. J. Glaciol. 60, 14–28. https://doi.org/10.3189/2014JoG13J127

DGA (2014). Data from: Inventario Nacional de Glaciares de Chile. Dirección General de Aguas. Available at http://www.geoportal.cl

DGA (2015). Technical report SIT 382. Modelación del Balance de Masa y descarga de agua en glaciares de Chile Central. CEAZA.

DGA (2022). Datos de estudios hidroglaciológicos de Chile [data set], https://snia.mop.gob.cl/BNAConsultas/reportes

Dussaillant, I., Berthier, E., Brun, F., Masiokas, M., Hugonnet, R., and Favier, V. (2019). Two decades of glacier mass loss along the Andes. Nat. Geosci. 12, 802–808. https://doi.org/10.1038/s41561-019-0432-5

Dussaillant, J. A., W. Buytaert, C. Meier, and F. Espinoza. (2012). Hydrological regime of remote catchments with extreme gradients under accelerated change: The Baker basin in Patagonia. Hydrol. Sci. J., 57, 1530–1542, https://doi.org/10.1080/02626667.2012.726993

Espinoza, J. C., Garreaud, R., Poveda, G., Arias, P. A., Molina-Carpio, J., Masiokas, M., et al. (2020). Hydroclimate of the andes part I: main climatic features. Front. Earth Sci. 8:64. https://doi.org/10.3389/feart.2020.00064

Falaschi, D., Bravo, C., Masiokas, M. H., Villalba, R., and Rivera, A. (2013). First glacier inventory and recent changes in glacier area in the Monte San Lorenzo region (47°S), southern Patagonian Andes, South America. Arctic Antarctic Alpine Res. 45, 19–28. https://doi.org/10.1657/1938-4246-45.1.19

Farías-Barahona, D., Vivero, S., Casassa, G., Schaefer, M., Burger, F., Seehus, T., et al. (2019). Geodetic Mass Balances and Area Changes of Echaurren Norte Glacier (Central Andes, Chile) between 1955 and 2015. Remote Sens. 11:260. https://doi.org/10.3390/rs11030260

Farinotti, D., Huss, M., Bauder, A., Funk, M., and Truffer, M. (2009). A method to estimate the ice volume and icethickness distribution of alpine glaciers, J. Glaciol., 55, 422–430. https://doi.org/10.3189/002214309788816759

Farinotti, D., Huss, M., Fürst, J. J., Landmann, J., Machguth, H., Maussion, F., et al. (2019). A consensus estimate for the ice thickness distribution of all glaciers on Earth. Nat. Geosci. 12, 168–173. https://doi.org/10.1038/s41561-019-0300-3

Favier, V., Wagnon, P., Chazarin, J.-P., Maisincho, L., and Coudrain, A. (2004). One-year measurements of surface heat budget on the ablation zone of Antizana glacier 15, Ecuadorian Andes, J. Geophys. Res., 109, D18105, https://doi.org/10.1029/2003JD004359

Francou, B., and Vincent, C., 2015. Quoi de neuf sur la planète blanche? Comprendre le déclin des glaces et ses conséquences. Glénat, Grenoble: 143 pp.

Francou, B., Vuille, M., Favier, V., and Cáceres, B. (2004). New evidence for an ENSO impact on low-latitude glaciers: Antizana 15, Andes of Ecuador, 0°28'S. J. Geophys. Res. 109:D18106. https://doi.org/10.1029/2003JD004484

Francou, B., Vuille, M., Wagnon, P., Mendoza, J., and Sicart, J. E. (2003). Tropical climate change recorded by a glacier in the central Andes during the last decades of the twentieth century: Chacaltaya. Bolivia, 16°S. J. Geophys. Res. 108:4154. https://doi.org/10.1029/2002JD002959

Frans, C., Istanbulluoglu, E., Lettenmaier, D. P., Naz, B., Clarke, G., Condom, T., et al. (2015). Predicting glacio-hydrologic change in the headwaters of the Zongo River, Cordillera Real, Bolivia. Water Resour. Res. 51, 9029–9052. https://doi.org/10.1002/2014WR016728

Fujiyoshi, Y., Kondo, H., Inoue, J., and Yamada, T. (1987). Characteristics of precipitation and vertical structure of air temperature in northern Patagonia, Bull. Glacier Res., 4, 15–24.

Fukami, H. and Naruse, R. (1987). Ablation of ice and heat balance on Soler glacier, Patagonia. Bull. Glacier Res. 4, 37–42.

Gantayat P, Kulkarni AV and Srinivasan J. (2014). Estimation of ice thickness using surface velocities and slope: case study at Gangotri Glacier, India. Journal of Glaciology 60(220), 277–282. https://doi.org/10.3189/2014JoG13J078

Garreaud, R. D. (2009). The Andes climate and weather. Adv. Geosci. 22, 3–11. https://doi.org/10.5194/adgeo-22-3-2009

Garreaud, R. D., Camila, A. G., Jonathan, B., Juan, P. B., Duncan, C., Carlos, L., et al. (2017). The 2010–2015 megadrought in central Chile: impacts on regional hydroclimate and vegetation. Hydrol. Earth Syst. Sci. 21, 6307–6327. https://doi.org/10.5194/hess-21-6307-2017

Gascoin, S., Kinnard, C., Ponce, R., Lhermitte, S., MacDonell, S., and Rabatel, A. (2011). Glacier contribution to streamflow in two headwaters of the Huasco River, Dry Andes of Chile, The Cryosphere, 5, 1099–1113, 660. https://doi.org/10.5194/tc-5-1099-2011

Gillett, N. P., Kell, T. D., & Jones, P. D. (2006). Regional climate impacts of the Southern Annular Mode. Geophysical Research Letters, 33(23), L23704. https://doi.org/10.1029/2006GL027721

GLACIOCLIM. (2022). Données météorologiques [data set], https://glacioclim.osug.fr/Donnees-des-Andes

Glen, J. W. (1955). The creep of polycrystalline ice. Proceeding of the Royal Society of London. Series A, 228, 519–538. https://www.jstor.org/stable/99642

Glen, J. W., (1952). Experiments on the deformation of ice. Journal of Glaciology, 2(12), 111–114. https://doi.org/10.3189/S0022143000034067

Goelzer, H., et al. (2018). Design and results of the ice sheet model initialisation experiments Initmip-Greenland: an ISMIP6 intercomparison. The Cryosphere 12(4), 1433–1460. https://doi.org/10.5194/tc-12-1433-2018

Goldberg, D. and Heimbach, P. (2013). Parameter and state estimation with a time-dependent adjoint marine ice sheet model. The Cryosphere 7(6),1659–1678. https://doi.org/10.5194/tc-7-1659-2013

Gualco, L. F., Maisincho, L., Villacís, M., Campozano, L., Favier, V., Ruiz-Hernández, J. C., & Condom, T. (2022). Assessing the contribution of glacier melt to discharge in the tropics: the case of study of the Antisana glacier 12 in Ecuador. Frontiers in Earth Science, 568. https://doi.org/10.3389/feart.2022.732635

Gupta, H. V., Kling, H., Yilmaz, K. K., and Martinez, G. F. (2009). Decomposition of the mean squared error and NSE performance criteria: Implications for improving hydrological modelling, J. Hydrol., 377, 80–91. https://doi.org/10.1016/j.jhydrol.2009.08.003

Haeberli, W., and Hoelzle, M. (1995). Application of inventory data for estimating characteristics of and regional climate-change effects on mountain glaciers: a pilot study with the European Alps. Annals of Glaciology, 21, 206–212. https://doi.org/10.3189/S0260305500015834

Hata, S., and Sugiyama, S. (2021). Changes in the Ice-Front Position and Surface Elevation of Glaciar Pío XI, an Advancing Calving Glacier in the Southern Patagonia Icefield, From 2000-2018. Front. Earth Sci. 8, 576044. https://doi.org/10.3389/feart.2020.576044

Hausfather, Z., Marvel, K., Schmidt, G. A., Nielsen-Gammon, J. W., and Zelinka, M. (2022). Climate simulations: recognize the 'hot model' problem, Nature, 605, 26–29, https://doi.org/10.1038/d41586-022-01192-2

Hay, J. E. and Fitzharris, B. B. (1988). A Comparison of the Energy-Balance and Bulk-aerodynamic Approaches for Estimating Glacier Melt. Journal of Glaciology, vol. 34(117), 145–153. https://doi.org/10.3189/S0022143000032172

Hernández, J., Mazzorana, B., Loriaux, T., and Iribarren, P. (2021). Reconstrucción de caudales en la Cuenca Alta del Río Huasco, utilizando el modelo Cold Regional Hydrological Model (CRHM), AAGG2021.

Hock, R. (2003). Temperature index melt modelling in mountain areas. Journal of Hydrology, 282(1-4), 104-115. https://doi.org/10.1016/S0022-1694(03)00257-9

Hock, R. and Holmgren, B. (2005). A distributed surface energy-balance model for complex topography and its application to Storglaciären, Sweden, J. Glaciol., 51, 25–36. https://doi.org/10.3189/172756505781829566

Hooke, R. L., (2005). Principles of Glacier Mechanics, 2nd edn. Cambridge: Cambridge University Press, 448 pp.

Houston, J. and Hartley, A. (2003). The central Andean west-slope rain-shadow and its potential contribution to the origin of hyper-aridity in the Atacama Desert, Int. J. Climatol., 23(12), 1453–1464. https://doi.org/10.1002/joc.938

Hugonnet, R., McNabb, R., Berthier, E. et al. (2021). Accelerated global glacier mass loss in the early twenty-first century. Nature 592, 726–731. https://doi.org/10.1038/s41586-021-03436-z

Huss, M. and Hock, R. (2018). Global-scale hydrological response to future glacier mass loss, Nature Climate Change, 8, 135–140, https://doi.org/10.1038/s41558-017-0049-x

Huss, M. and Hock, R. (2015). A new model for global glacier change and sea-level rise. Front. Earth Sci. 3:54. https://doi.org/10.3389/feart.2015.00054

Hutter, K. (1981). The effect of longitudinal strain on the shear stress of an ice sheet: in defence of using streched coordinates, J. Glaciol., 27, 39–56. https://doi.org/10.3189/S0022143000011217

Hutter, K. (1983). Theoretical glaciology: material science of ice and the mechanics of glaciers and ice sheets.

Ianigla-Conicet, and Mayds (2018). Resumen ejecutivo de los resultados del Inventario Nacional de Glaciares. Mendoza: IANIGLA-CONICET, 27.

IANIGLA (2022). Datos meteorológicos [data set], https://observatorioandino.com/estaciones/

INAIGEM (2018). Inventario Nacional de Glaciares. Huaraz: INAIGEM.

Jiskoot, H. (2011). Dynamics of Glaciers. In Singh, V. P., Singh, P. & Haritashya, U. K. (eds.) Encyclopedia of Snow, Ice and Glaciers, 245–256. https://doi.org/10.1007/978-90-481-2642-2_127

Jordan, E., Ungerechts, L., Caceres, B., Penafiel, A., and Francou, B. (2005). Estimation by photogrammetry of the glacier recession on the Cotopaxi Volcano (Ecuador) between 1956 and 1997. Hydrol. Sci. J. 50:94. https://doi.org/10.1623/hysj.2005.50.6.949

Jouvet, G. (2023). Inversion of a Stokes glacier flow model emulated by deep learning. Journal of Glaciology, 69(273), 13–26. https://doi.org/10.1017/jog.2022.41

Jouvet, G., Cordonnier, G., Kim, B., Lüthi, M., Vieli, A., & Aschwanden, A. (2022). Deep learning speeds up ice flow modelling by several orders of magnitude. Journal of Glaciology, 68(270), 651–664. https://doi.org/10.1017/jog.2021.120

Kamb, B. (1987). Glacier surge mechanisms based on linked cavity configuration of the basal water conduit system. Journal of Geophysical Research, 92(B9), 9083–9100. https://doi.org/10.1029/JB092iB09p09083

Kamb, B., and Echelmeyer, K. A. (1986). Stress-gradient coupling in glacier flow: I Longitudinal averaging of the influence of ice thickness and surface slope. Journal of Glaciology, 32(111), 267–284. https://doi.org/10.3189/S0022143000015604

Kaser, G. (1995). How do tropical glaciers behave? Some comparisons between tropical and mid-latitude glaciers. In: Ribstein, P., Francou, B. (Eds.), Aguas Glaciares y Cambios en los Andes Tropicales. Conferencias y Posters. Seminaro Internacional, La Paz, 13-16 Junio, pp 207-218.

Kaser, G. (1999). A review of the modern fluctuations of tropical glaciers, Glob. Planet. Change, 22, 93–103. https://doi.org/10.1016/S0921-8181(99)00028-4

Kaser, G. (2001). Glacier-climate interaction at low latitudes. J. Glaciol., 47, 195–204. https://doi.org/10.3189/172756501781832296

Kaser, G., and Osmaston, H. (2002). Tropical Glaciers. New York, NY: Cambridge University Press, 207.

Kaufman, L., and Rousseeuw, P. (2008). Partitioning Around Medoids (Program PAM), In Finding Groups in Data. Editors P. J. Kaufman and L. Rousseeuw (John Wiley & Sons), 68–125. https://doi.org/10.1002/9780470316801.ch2

Kinnard, C., Larouche, O., Demuth, M. N., and Menounos, B. (2022) Modelling glacier mass balance and climate sensitivity in the context of sparse observations: application to Saskatchewan Glacier, western Canada, The Cryosphere, 16, 3071–3099, https://doi.org/10.5194/tc-16-3071-2022

Kondo, H. and Yamada, T. (1988). Some remarks on the mass balance of the terminal-lateral fluctuations of San Rafael Glacier, the Northern Patagonia Icefield, Bull. Glacier Res., 6, 55–63.

Koppes, M., Conway, H., Rasmussen, L., and Chernos, M. (2011). Deriving calving variations from reanalysis data and sparse observations, Glaciar San Rafael, northern Patagonia, 1950–2005. Cryosphere 5, 791–808. https://doi.org/10.5194/tc-5-791-2011

Krogh S.A., Pomeroy J.W., and McPhee J. (2014). Physically based mountain hydrological modeling using reanalysis data in patagonia. J. Hydrometeorol. 16: 172–193. https://doi.org/10.1175/JHM-D-13-0178.1

Kuhn, M., 1987: Micro-meteorological conditions for snow melt. J. Glaciol., 33 (113), 24–26. https://doi.org/10.3189/S002214300000530X

Le Meur, E., Gagliardini, O., Zwinger, T. and Ruokolainen, J. (2004). Glacier flow modelling: a comparison of the shallow ice approximation and the Full-Stokes solution. Comptes Rendus Physique 5(7), 709–722. https://doi.org/10.1016/j.crhy.2004.10.001

Lehner, B., Verdin, K., Jarvis, A. (2006). Hydrological data and maps based on Shuttle elevation derivatives at multiple scales 685 (HydroSHEDS)-Technical Documentation, World Wildlife Fund US, Washington, DC, Available at http://hydrosheds.cr.usgs.gov

Lliboutry, L., 1958. Contribution à la théorie du frottement du glacier sur son lit. Comptes rendus Hebdomadaires des Séances de l'Académie des Sciences. Paris, 247(3), 318–320.

Lliboutry, L., 1968. General theory of subglacial cavitation and sliding of temperate glaciers. Journal of Glaciology, 7(49), 21–58. https://doi.org/10.3189/S0022143000020396

Lo Vecchio, A. et al. (2019). MODIS Image-derived ice surface temperature assessment in the Southern Patagonian icefield. Prog. Phys. Geogr. 43(6), 754–776. https://doi.org/10.1177/0309133319851022

Lopez, P., Chevallier, P., Favier, V., Pouyaud, B., Ordenes, F., and Oerlemans, J. (2010). A regional view of fluctuations in glacier length in southern South America. Glob. Planet. Change 71, 85–108. https://doi.org/10.1016/J.GLOPLACHA.2009.12.009

MacDonell, S., Kinnard, C., Mölg, T., Nicholson, L., Abermann, J. (2013). Meteorological drivers of ablation processes on a cold glacier in the semi-arid Andes of Chile. Cryosphere 7:1513–1526. https://doi.org/10.5194/tc-7-1513-2013

Malmros, J. K., Mernild, S. H., Wilson, R., Yde, J. C., and Fensholt, R. (2016). Glacier Area Changes in the Central Chilean and Argentinean Andes 1955-2013/14. J. Glaciol. 62, 391–401. https://doi.org/10.1017/jog.2016.43

Marangunic, C., Ugalde, F., Apey, A., Armendáriz, I., Bustamante, M. and Peralta, C. Ecosistemas de montaña de la cuenca alta del río Mapocho, Glaciares en la cuenca alta del río Mapocho: variaciones y características principales. Anglo American - CAPES UC, 2021

Mark, B. and Seltzer, G. (2003).Tropical glacier meltwater contribution to stream discharge: A case study in the Cordillera Blanca, Peru. J. Glaciol, 49(165), 271-281. https://doi.org/10.3189/172756503781830746

Marzeion, B., Jarosch, A. H., and Hofer, M. (2012). Past and future sea-level change from the surface mass balance of glaciers. Cryosphere 6, 1295–1322. https://doi.org/10.5194/tc-6-1295-2012

Masiokas, M. H., Christie, D. A., Le Quesne, C., Pitte, P., Ruiz, L., Villalba, R., et al. (2016). Reconstructing the annual mass balance of the Echaurren Norte glacier (Central Andes, 33.5° S) using local and regional hydroclimatic data. Cryosphere 10, 927–940. https://doi.org/10.5194/tc-10-927-2016

Masiokas, M. H., Rabatel, A., Rivera, A., Ruiz, L., Pitte, P., Ceballos, J. L., et al. (2020). Current state and recent changes of the cryosphere in the Andes. Front Earth Sci. 8:99. https://doi.org/10.3389/feart.2020.00099

Masiokas, M. H., Villalba, R., Luckman, B. H., Montaña, E., Betman, E., Christie, D., et al. (2013). Recent and historic Andean snowpack and streamflow variations and vulnerability to water shortages in central-western Argentina. Climate Vulnerability: Understanding and Addressing Threats to Essential Resources, Vol. 5, eds R. A. Pielke, J. Adegoke, D. Niyogi, G. Kallos, T. R. Seastedt, and F. Hossain (Amsterdam: Elsevier Inc), 213–227. https://doi.org/10.1016/b978-0-12-384703-4.00522-0

Mateo, E. I., Mark, B. G., Hellström, R. Å., Baraer, M., McKenzie, J. M., Condom, T., Rapre, A. C., Gonzales, G., Gómez, J. Q., and Encarnación, R. C. C. (2022). High-temporal-resolution hydrometeorological data collected in the tropical Cordillera Blanca, Peru (2004–2020), Earth Syst. Sci. Data, 14, 2865–2882. https://doi.org/10.5194/essd14-2865-2022

Maussion. F, et al. (2019). The open global glacier model (OGGM) v1.1. Geoscientific Model Development 12(3), 909–931. https://doi.org/10.5194/gmd-12-909-2019

Meier, W. J. H., Grießinger, J., Hochreuther, P., and Braun, M. H. (2018). An updated multi-temporal glacier inventory for the Patagonian Andes with changes between the Little Ice Age and 2016. Front. Earth Sci. 6:62. https://doi.org/10.3389/feart.2018.00062

Melkonian, A. K., Willis, M. J., Pritchard, M. E., Rivera, A., Bown, F., and Bernstein, S. A. (2013). Satellite-derived volume loss rates and glacier speeds for the Cordillera Darwin Icefield, Chile. Cryosphere 7, 823–839. https://doi.org/10.5194/tc-7-823-2013

Michel-Griesser, L., Picasso, M., Farinotti, D., Funk, M. and Blatter, H. (2014). Bedrock topography reconstruction of glaciers from surface topography and mass-balance data. Computational Geosciences 18(6), 969–988. https://doi.org/10.1007/s10596-014-9439-6

Millan, R., Mouginot, J., Rabatel, A. et al. (2022). Ice velocity and thickness of the world's glaciers. Nat. Geosci. 15, 124–129. https://https://doi.org/10.1038/s41561-021-00885-z

Minowa, M., Sugiyama, S., Sakakibara, D., and Sawagaki, T. (2015). Contrasting glacier variations of Glaciar Perito Moreno and Glaciar Ameghino, Southern Patagonia Icefield. Ann. Glaciol. 56, 26–32. https://doi.org/10.3189/2015AoG70A020

Minowa, M., Schaefer, M., Sugiyama, S., Sakakibara, D., and Skvarca, P. (2021). Frontal ablation and mass loss of the Patagonian icefields, Earth Planet. Sc. Lett., 561, 116811, https://doi.org/10.1016/j.epsl.2021.116811

Monnier, S., and Kinnard, C. (2015). Reconsidering the glacier to rock glacier transformation problem: new insights from the central Andes of Chile. Geomorphology 238, 47–55. https://doi.org/10.1016/j.geomorph.2015.02.025

Monnier, S., and Kinnard, C. (2017). Pluri-decadal (1955–2014) evolution of glacier–rock glacier transitional landforms in the central Andes of Chile (30–33°S). Earth Surf. Dyn. 5, 493–509. https://doi.org/10.5194/esurf-5-493-2017

Moreno, P.I., Videla, J., Valero-Garcés, B., Alloway, B.V., Heusser, L.E. (2018a). A continuous record of vegetation, fire-regime and climatic changes in northwestern Patagonia spanning the last 25,000 years. Quat. Sci. Rev., 198 (2018), pp. 15-36. https://doi.org/10.1016/j.quascirev.2018.08.013

Moreno, P.I., Vilanova, I., Villa-Martínez, R. et al. (2018). Onset and Evolution of Southern Annular Mode-Like Changes at Centennial Timescale. Sci Rep 8, 3458. https://doi.org/10.1038/s41598-018-21836-6

Morris, J. N., Poole, A. J., and Klein, A. G. (2006). Retreat of tropical glaciers in Colombia and Venezuela from 1984 to 2004 as measured from ASTER and Landsat images. Proceeding of the 63rd Eastern Snow Conference, Newark, 181–191.

Mössner, M., Innerhofer, G., Schindelwig, K., Kaps, P., Schretter, H., Nachbauer, W. (2013). Measurement of mechanical properties of snow for simulation of skiing. J. Glaciol, 59, 1170–1178. https://doi.org/10.3189/2013JoG13J031

Munro, D S. 1990. Comparison of melt energy computations and ablatometer measurements on melting ice and snow. Arct. Alp. Res., 22(2), 153–162.

Nash, J. E. and Sutcliffe, J. V. (1970). River flow forecasting through conceptual models part I-A discussion of principles. J. Hydrol. 10, 282–290. https://doi.org/10.1016/0022-1694(70)90255-6

Nicholson, L., Marín, J., Lopez, D., Rabatel, A., Bown, F., Rivera, A. (2009). Glacier inventory of the upper Huasco valley, Norte Chico, Chile: glacier characteristics, glacier change and comparison to central Chile. Ann. Glaciol. 50, 111–118. https://doi.org/10.3189/172756410790595787

Nye, J. F. (1951). The flow of glaciers and ice-sheets as a problem in plasticity. Proceedings of the Royal Society of London. Series A, 207, 554–572

Nye, J. F. (1957). The distribution of stress and velocity in glaciers and ice-sheets. Proceedings of the Royal Society of London. Series A, 239, 113–133.

Nye, J. F. (1965). The Flow of a Glacier in a Channel of Rectangular, Elliptic or Parabolic Cross-Section. Journal of Glaciology, 5(41), 661–690. Cambridge University Press.

Oerlemans, J. (1997). A flowline model for Nigardsbreen, Norway: projection of future glacier length based on dynamic calibration with the historic record. Journal of Glaciology, 24, 382–389. https://doi.org/10.3189/S0260305500012489

Oerlemans, J. (2008). Minimal Glacier Models. Utrecht Publishing and Archiving Services: Igitur, 90 pp.

Ohata, T., Kondo, H., and Enomoto, H. (1985). Meteorological observations at San Rafael Glacier. Glaciological Studies in Patagonia Northern Icefield 1983–1984. Edited by: Nakajima, C., Data Center for Glacier Research, Japanese Society of Snow and Ice, Nagoya, 22–31.

Paul, F., and Moelg, N. (2014). Hasty retreat of glaciers in northern Patagonia from 1985 to 2011. J. Glaciol. 60, 1033–1043. https://doi.org/10.3189/2014JoG14J104

Pellicciotti, F., Brock, B., Strasser, U., Burlando, P., Funk, M., Corripio, J. (2005). An enhanced temperature-index glacier melt model including the shortwave radiation balance: development and testing for Haut Glacier d'Arolla, Switzerland. Journal of Glaciology 51 (175): 573-587. https://doi.org/10.3189/172756505781829124

Perego, M., Price, S. and Stadler, G. (2014). Optimal initial conditions for coupling ice sheet models to earth system models. Journal of Geophysical Research: Earth Surface 119(9), 1894–1917. https://doi.org/10.1002/2014JF003181

Pope, A.: GLOSSARY OF GLACIER MASS BALANCE AND RELATED TERMS, Cogley, J. G., Hock, R., Rasmussen, L. A., Arendt, A. A., Bauder, A., Braithwaite, R. J., Jansson, P., Kaser, G., Möller, M., Nicholson, L., and Zemp, M. (2012). International Hydrological Programme (IHP) of the United Nations Educational, Scientific and Cultural Organization (UNESCO), UNESCO, Paris, IHP-VII Technical Documents in Hydrology No. 86, IACS Contribution No. 2, vi 114 p., 2011, Polar Rec., 48, e15. https://doi.org/10.1017/S0032247411000805

Proksch, M., Rutter, N., Fierz, C., and Schneebeli, M. (2016). Intercomparison of snow density measurements: bias, precision, and vertical resolution, The Cryosphere, 10, 371–384, https://doi.org/10.5194/tc-10-371-2016

Rabatel, A. (2015). Apports d'une approche combinant mesures in situ et télédétection optique pour le suivi des glaciers de montagne: cas des Andes tropicales et des Alpes occidentales (Doctoral dissertation, Université Grenoble Alpes).

Rabatel, A., Castebrunet, H., Favier, V., Nicholson, L., and Kinnard, C. (2011). Glacier changes in the Pascua-Lama region, Chilean Andes (29° S): recent mass balance and 50 yr surface area variations. Cryosphere 5, 1029–1041. https://doi.org/10.5194/tc-5-1029-2011

Rabatel, A., Ceballos, J. L., Micheletti, N., Jordan, E., Braitmeier, M., Gonzalez, J., et al. (2018). Toward an imminent extinction of Colombian glaciers? Geografiska Annaler: Series A. Phys. Geogr. 100, 75–95. https://doi.org/10.1080/04353676.2017.1383015

Rabatel, A., Francou, B., Soruco, A., Gomez, B., Caceres, J. L., Ceballos, R., et al. (2013). Current state of glaciers in the tropical Andes: a multi-century perspective on glacier evolution and climate change. Cryosphere 7, 81–102. https://doi.org/10.5194/tc-7-81-2013

Radić, V. and Hock, R. (2014). Glaciers in the Earth's hydrological cycle: assessments of glacier mass and runoff changes on global and regional scales. Surv. Geophys. 35, 813–837. https://doi.org/10.1007/s10712-013-9262-y

Ragettli, S. and Pellicciotti, F. (2012). Calibration of a physically based, spatially distributed hydrological model in a glacierized basin: On the use of knowledge from glaciometeorological processes to constrain model parameters, Water Resour. Res., 48, W03509. https://doi.org/10.1029/2011WR010559

Ramallo, C. (2013). Caractérisation du régime pluviométrique et sa relation à la fonte du Glacier Zongo (Cordillère Royale), (Doctoral dissertation). Retrieved from https://tel.archives-ouvertes.fr/tel-01548283

Réveillet, M., Rabatel, A., Gillet-Chaulet, F., and Soruco, A. (2015). Simulations of changes to Glacier Zongo, Bolivia (16S), over the 21st century using a 3-D full-Stokes model and CMIP5 climate projections. Ann. Glaciol. 56, 89–97. https://doi.org/10.3189/2015aog70a113

RGI Consortium (2017). Randolph Glacier Inventory – A Dataset of Global Glacier Outlines: Version 6.0, in GLIMS Technical Report (Collardo: Glaciers contribution to sea level rise). https://doi.org/10.7265/N5-RGI-60

Rigsby, G. P. (1958). Effect of hydrostatic pressure on the velocity of shear deformation of single ice crystals. Journal of Glaciology, 3(24), 261–272. https://doi.org/10.3189/S0022143000023911

Rivera, A. (2004). Mass balance investigations at Glaciar Chico, Southern Patagonia Icefield, Chile. PhD thesis, University of Bristol, UK, 303 pp.

Rivera, A. and Bown, F. (2013). Recent glacier variations on active ice capped volcanoes in the Southern Volcanic Zone (37º-46ºS), Chilean Andes. Journal of South American Earth Sciences, 45: 345-356. https://doi.org/10.1016/j.jsames.2013.02.004

Rivera,A., and Casassa,G. (1999). Volume Changes on Glaciar Pio XI, Patagonia: 1975-1995. Global and Planetary Change , 22(1-4):233-244. https://doi.org/10.1016/S0921-8181(99)00040-5

Rothlisberger, H. and Lang, H. (1987). Glacial hydrology. In Gurnell, A. M. and Clark, M.J., eds. Glacio-flumal sediment transfer: an alpine perspective. Chichester, etc., John Wiley and Sons, 207–284.

Rounce, D. R., et al. (2023). Global glacier change in the 21st century: Every increase in temperature matters. Science379,78-83(2023). https://doi.org/10.1126/science.abo1324

Schaefer, M., MacHguth, H., Falvey, M., and Casassa, G. (2013). Modeling past and future surface mass balance of the Northern Patagonia icefield. J. Geophys. Res. Earth Surf. 118, 571–588. https://doi.org/10.1002/jgrf.20038

Schaefer, M., MacHguth, H., Falvey, M., Casassa, G., and Rignot, E. (2015). Quantifying mass balance processes on the Southern Patagonia icefield. Cryosphere 9, 25–35. https://doi.org/10.5194/tc-9-25-2015

Schaefer, M.; Rodriguez, J.; Scheiter, M.; Casassa, G. (2017). Climate and surface mass balance of Mocho Glacier, Chilean Lake District, 40°S. J. Glaciol. 63, 218–228. https://doi.org/10.1017/jog.2016.129

Scheiter, M., Schaefer, M., Flández, E., Bozkurt, D., and Greve, R. (2021). The 21st-century fate of the Mocho-Choshuenco ice cap in southern Chile, The Cryosphere, 15, 3637–3654, https://doi.org/10.5194/tc-15-3637-2021

Schneider, C., Schnirch, M., Acuña, C., Casassa, G., and Kilian, R. (2007). Glacier inventory of the Gran Campo Nevado Ice Cap in the Southern Andes and glacier changes observed during recent decades. Glob. Planet. Change 59, 87–100. https://doi.org/10.1016/j.gloplacha.2006.11.023

Schoolmeester, T., Johansen, K. S., Alfthan, B., Baker, E., Hesping, M., and Verbist, K. (2018). The Andean Glacier and Water Atlas – The Impact of Glacier Retreat on Water Resources. Arendal: UNESCO and GRID-Arendal. Available online at: https://unesdoc.unesco.org/ark:/48223/pf0000265810

Seehaus, T., Malz, P., Sommer, C., Lippl, S., Cochachin, A., and Braun, M. (2019). Changes of the Tropical Glaciers throughout Peru between 2000 and 2016 - Mass Balance and Area Fluctuations. The Cryosphere 13 (10), 2537–2556. https://doi.org/10.5194/tc-13-2537-2019

Seehaus, T., Malz, P., Sommer, C., Soruco, A., Rabatel, A., and Braun, M. (2020). Mass Balance and Area Changes of Glaciers in the Cordillera Real and Tres Cruces, Bolivia, between 2000 and 2016. J. Glaciol. 66 (255), 124–136. https://doi.org/10.1017/jog.2019.94

SENAMHI. (2022). datos hidrometeorológicos de Perú [data set], https://www.senamhi.gob.pe/?&p=descarga-datoshidrometeorologicos

Sharp, R. P. (1988). Living Ice: Understanding Glaciers and Glaciation. Cambridge: Cambridge University Press, 248 pp.

Shaw, T. E., Caro, A., Mendoza, P., Ayala, Á., Pellicciotti, F., Gascoin, S., et al. (2020). The Utility of Optical Satellite Winter Snow Depths for Initializing a Glacio-Hydrological Model of a High-Elevation, Andean Catchment. Water Resour. Res. 56 (8), 1–19. https://doi.org/10.1029/2020WR027188

Sicart, J. E., Hock, R., Ribstein, P., Litt, M., and Ramirez, E. (2011). Analysis of seasonal variations in mass balance and meltwater discharge of the Tropical Zongo Glacier by application of a distributed energy balance model. J. Geophys. Res. 116:D13105. https://doi.org/10.1029/2010JD015105

Sicart, J. E., Wagnon, P., and Ribstein, P. (2005). Atmospheric controls of heat balance of Zongo Glacier (16°S. Bolivia). J. Geophys. Res. 110:D12106. https://doi.org/10.1029/2004JD005732

Soruco, A., Vincent, C., Francou, B., Ribstein, P., Berger, T., Sicart, J. E., et al. (2009). Mass balance of Glaciar Zongo, Bolivia, between 1956 and 2006, using glaciological, hydrological and geodetic methods. Ann. Glaciol. 50:2009. https://doi.org/10.3189/172756409787769799

Soruco, A., Vincent, C., Rabatel, A., Francou, B., Thibert, E., Sicart, J. E., et al. (2015). Impacts of glacier shrinkage on water resources of La Paz city, Bolivia (16°S). Ann. Glaciol. 56, 147–154. https://doi.org/10.3189/2015AoG70A001

Stuefer, M. (1999). Investigations on Mass Balance and Dynamics of Moreno Glacier Based on Field Measurements and Satellite Imagery. Ph.D. Dissertation, University of Innsbruck, Innsbruck.

Takeuchi, Y., Naruse R. and Satow K. (1995). Characteristics of heat balance and ablation on Moreno and Tyndall glaciers, Patagonia, in the summer 1993/94. Bulletin of Glacier Research, 13, 45-56.

Thompson, D. W. J., and J. M. Wallace, (2000). Annular modes in the extratropical circulation. Part I: Month-to-month variability. J. Climate, 13, 1000–1016. https://doi.org/10.1175/1520-0442(2000)013%3C1000:AMITEC%3E2.0.CO;2

Tibshirani, R. (1996). Regression Shrinkage and Selection via the Lasso. J. R. Stat. Soc. Ser. B (Methodological) 58 (1), 267–288. https://doi.org/10.1111/j.2517-6161.1996.tb02080.x

Tokarska, K. B., Stolpe, M. B., Sippel, S., Fischer, E. M., Smith, C. J., Lehner, F., and Knutti, R. (2020). Past warming trend constrains future warming in CMIP6 models, Science Advances, 6, eaaz9549. https://doi.org/10.1126/sciadv.aaz9549

Toum, E., Masiokas, M. H., Villalba, R., Pitte, P. & Ruiz, L. (2021). The HBV.IANIGLA Hydrological Model. The R Journal. https://doi.org/10.32614/RJ-2021-059

Troll, C. (1941). Studien zur Vergleichenden Geographie der Hochgebirge der Erde. Bonn: Bonner Mitteilungen, 1941.

Valex, T. (2015). Etude approfondie de la phase des précipitations par comparaison de spectro-pluviomètre optique (disdromètres) sur trois sites andins contrastés climatiquement (Bolivie, Pérou et Equateur). Stage assistant ingenieur Anne 2014-2015. Maître de Stage Condom Thomas. LTHE, Grenoble.

Vincent, C., Soruco, A., Azam, F., Basantes-Serrano, R., Jackson, M., Kjollmoen, B., et al. (2018). A non-linear statistical model for extracting a climatic signal from glacier mass-balance measurements. J. Geosphys. Res. Earth Surf. 123, 2228–2242. https://doi.org/10.1029/2018JF004702

Vuille, M., Carey, M., Huggel, C., Buytaert, W., Rabatel, A., Jacobsen, D., et al. (2018). Rapid decline of snow and ice in the tropical Andes–Impacts, uncertainties and challenges ahead. Earth Sci. Rev. 176, 195–213. https://doi.org/10.1016/j.earscirev.2017.09.019

Weertman, J., 1957. On the sliding of glaciers. Journal of Glaciology, 3(21), 33–38. https://doi.org/10.3189/S0022143000024709

Weidemann, S., Sauter, T., Schneider, L., and Schneider, C. (2013). Impact of two conceptual precipitation downscaling schemes on mass-balance modeling of Gran Campo Nevado ice cap, Patagonia. J. Glaciol. 59, 1106–1116. https://doi.org/10.3189/2013JoG13J046

WGMS. (2021). Global Glacier Change Bulletin No. 4 (2018-2019). Michael Zemp, Samuel U. Nussbaumer, Isabelle Gärtner-Roer, Jacqueline Bannwart, Frank Paul, and Martin Hoelzle (eds.), ISC (WDS) / IUGG (IACS) / UNEP / UNESCO / WMO, World Glacier Monitoring Service, Zurich, Switzerland, 278 pp. Based on database version. https://doi.org/10.5904/wgms-fog-2021-05

Winkelmann, R., Martin, M. A., Haseloff, M., Albrecht, T., Bueler, E., Khroulev, C., and Levermann, A. (2011). The Potsdam Parallel Ice Sheet Model (PISM-PIK) – Part 1: Model description, The Cryosphere, 5, 715–726. https://doi.org/10.5194/tc-5-715-2011

Yamada, T. (1987). Glaciological characteristics revealed by 37.6 m deep core drilled at the accumulation area of San Rafael Glacier, the Northern Patagonia Icefield, Bull. Glacier Res., 4, 59–67.

Yarleque, C., Vuille, M., Hardy, D. R., Timm, O. E., De la Cruz, J., Ramos, H., et al. (2018). Projections of future disappearance of the Quelccaya, the largest tropical ice cap on Earth. Nat. Sci. Rep. 8:15564. https://doi.org/10.1038/s41598-018-33698-z

Zalazar, L., Ferri Hidalgo, L., Castro, M., Gargantini, H., Giménez, M., Pitte, P., et al. (2017). Glaciares de Argentina: Resultados Preliminares del Inventario Nacional de Glaciares. Rev. Glac. Ecosist. Montaña 2, 13–22.

Zemp, M., Huss, M., Thibbert, E., and Cogley, J. G. (2019). Global glacier mass changes and their contributions to sea-level rise from 1961 to 2016. Nature 568:E9. https://doi.org/10.1038/s41586-019